INFRARED SPECTROSCOPY OF MOLECULAR IONS AND ION-SOLVENT CLUSTERS

Thesis by
Jong-Ho Choi

In Partial Fulfillment of the Requirements
for the Degree of
Doctor of Philosophy

California Institute of Technology
Pasadena, California

1995
(Submitted February 15, 1995)

I would like to dedicate this thesis to my wife and son

for their patience, devotion, affection and love.

ACKNOWLEDGMENTS

It was my great fortune to meet and work with a variety of people at Caltech. They all have particular personalities and qualities, which have been essential to learning and executing research throughout my graduate school years.

First, I would like to thank my research advisor, Professor Mitchio Okumura, for all the generous support he provided through his constant enthusiasm for research, motivation, financial backing, and friendship. Also, I was really touched by the enormous patience he showed to me and other group members during his tenure-track period. The time I spent with him will be invaluable to my future career. Simply, it was my *privilege* to work with him.

A few Okumura group people were instrumental in the success of much of what I have done here. I wish to thank my labmate Keith Kuwata, the first pious Christian I met at Caltech. He demonstrated the wonders of *ab initio* theory and helped me do some of the experiments presented in this thesis. Yibin Cao was very helpful to understanding the nonlinear optics and China, where he is starting a new career. My colleague and officemate, Matt Johnson, was a mentor in the laboratory. He taught me electronics and other practical skills which have been formative experiences. I also thank Jim Spotts, Teresa Moore, ex-postdoc Bermi Haas, Christine Nelson and Alex Wong for their help and kindness.

I have to thank my committee members, Harry Gray, Jack Beauchamp and Vincent McKoy for their encouragement and insightful discussion. Harry, my former advisor, especially cared about my well being and career.

I am grateful to several Caltech people. Seung Koo Shin and his wife were helpful during my early stay. *Mon Ami Monsieur.* Guy Durenberg demonstrated the wonderful machining skills and helped me get used to the machines. Tom Dunn was generous in teaching how to solve the tricky problems of electronics.

I would like to express my gratitude to my mentor, Professor Youngsang Choi at my alma mater. He has given me considerate advice and words of encouragement, which have been indispensable during my stay at Caltech. I should thank Sangwon Lee and his family for their friendship and affection. I wish him great progress and the best of luck.

I would like to thank a few special people, my parents and family. Without their support my life as a graduate student would have been too trying. My parents have always shown constant affection and devotion to me. My sister and brother-in-law in Germany, and two brothers in Korea have understood my student life in America and have been on my side. My son, Paul, has been the biggest barrier to my research since he was born in 1991. He has been tirelessly trying to stay with me and pulled my trousers at the door when it was time to go to the lab. I felt really sorry to see his sorrowful look with tears. I love you, Paul. And finally, there is one who deserves more than I could express my gratitude; she has been patient and understanding through sacrificing herself; she has shown me an unfailing love and has helped to overcome my deficiencies. I thank my wife, Kyung-Ae, for all that she has done for me throughout these years. *This is for you.*

ABSTRACT

Studies to elucidate details of ion-molecule interactions at the molecular level are of extreme importance for understanding the solvation process and ion-molecule reactions in clusters and in the condensed phase. In the quest of this purpose, infrared predissociation spectroscopy has been applied to three ionic systems.

Infrared spectra of mass-selected clusters $NO^+(H_2O)_n$ showed that the smaller clusters (n = 1-3) were complexes of H_2O ligands bound to a nitrosonium ion (NO^+) core. In the n = 4 cluster, we found evidence for the onset of an intracluster reaction that formed HONO. From an analysis of the spectrum, we concluded that the n = 5 cluster rearranged to form $H_3O^+(H_2O)_3$ (HONO), *i.e.*, an adduct of the reaction products. This study provides clear evidence for the intracluster rearrangement reaction

$$NO^+(H_2O)_n \rightarrow H_3O^+(H_2O)_{n-2}\,(HONO) \text{ at } n \geq 4.$$

Infrared spectroscopic results on $NO_2^+(HOX)$ (X = H, D, ^{35}Cl, ^{37}Cl) clusters showed a remarkable similarity in the chemistry of protonated nitric acid and chlorine nitrate, and two types of isomers were observed. The structure of the ground-state isomer is an ion-molecule complex, $NO_2^+(HOX)$, and the second most stable isomer is a covalently bound species, $(OH)(OX)NO^+$. We found evidence for an IR photon-induced isomerization reaction. These spectroscopic results were quite consistent with the predictions of *ab initio* theory, and may provide important clues to the heterogeneous reaction mechanism involved in the depletion of stratospheric ozone.

The first infrared spectroscopic observations of gas-phase hydrated chloride clusters, $Cl^-(H_2O)_n$, led to crucial suggestions concerning the structures of halide-water systems. In

$Cl^-(H_2O)$, the water forms a nearly linear hydrogen bond with the chloride ion, and in $Cl^-(H_2O)_2$ and $Cl^-(H_2O)_3$, the water ligands hydrate the chloride ion asymmetrically, but do not form a hydrogen bond with each other. The observed results for $n = 1$ and 2 showed good agreement with correlated *ab initio* calculations. In the $n = 4$ cluster, the probed structure was the one in which one Cl^--bonded water ligand forms a hydrogen bond to an adjacent water ligand. In $Cl^-(H_2O)_5$, a liquid-phase-like broad spectrum was observed with several peaks still apparent.

TABLE OF CONTENTS

CHAPTER 1

Introduction to Infrared Spectroscopy of Ions and Ionic Clusters

1.1 IONS AND IONIC CLUSTERS

Ions in the gas phase are transient species which have attracted enormous attention in the last two decades. The observation of ions in planetary atmospheres, interstellar space, plasmas, and flames is indicative of their crucial roles in many chemical environments. Molecular ion spectroscopy is presently a field of remarkable vitality, in which important discoveries are being made at a truly impressive rate. Furthermore, new technological innovations, such as the advent of tunable, high-power, narrow-band lasers, and the rapid development of quantum optics and electronics, have built up a foundation for the development of new spectroscopic methods to investigate charged molecules.[1,2]

The first laboratory microwave absorption experiment on a molecular ion was made by Dixon and Woods, who studied CO^+.[3-5] Woods and co-workers demonstrated that a plasma-discharge source built in their laboratory could be employed to produce sufficiently high densities of molecular ions to execute high resolution absorption measurements. Their experiments have had a great impact on the subsequent development of molecular ion spectroscopy. The first laboratory infrared spectrum was observed by Wing and co-workers using a fast ion beam (of several thousand eVs) to generate the HD^+ ion.[6] They obtained the absorption spectrum indirectly through measurement of changes in the charge exchange cross-section between the ion and a suitable collision partner induced by the absorption of an infrared photon. Although fast ion beams usually generate hot ionic species resulting in complicated spectra, their scheme of using fast ion beams and an indirect detection method, such as charge

exchange, photofragmentation, or photodetachment, has evolved into one of the principal techniques for studying molecular ion spectroscopy.

The first direct observation of an infrared absorption spectrum was made by Oka.[7] He employed a dc discharge of hydrogen to generate H_3^+ ion and observed the v_2 band using a tunable infrared difference frequency laser. The more general application of direct infrared absorption spectroscopy was, however, restricted by the fact that the weak ionic signals are masked by the presence of immensely stronger neutral molecular absorption. This problem was overcome with the introduction of velocity modulation laser spectroscopy, developed by Gudeman *et al.*[8,9] This technique takes advantage of the Doppler shifts in the infrared absorption frequencies of ions resulting from their acceleration in the electric fields of plasmas. Velocity modulation laser spectroscopy has been successfully employed in studies of some of the most fundamental molecular ions, e.g., H_3O^+, NH_3^+ and CH_3^+.[9] However, such discharges can lead to the co-existence of several ionic species, making the analysis of spectra complicated and provide harsh environments for larger ions such as ionic clusters.

For ionic clusters, early research was focused on determining the thermodynamics of clustering reactions. The first experimental method was high pressure mass spectrometry. The development and applications of the technique were pioneered by Kebarle and co-workers and extensively employed by several groups, including the groups of Castleman, Hiraoka, and Meot-ner.[10-13] They obtained the enthalpy, entropy and free energy ($\Delta H°$, $\Delta S°$ and $\Delta G°$) of stepwise formation for a wide range of ion-molecule complexes and ionic clusters. In spite of the wealth of thermodynamic data,[14]

however, very few spectroscopic investigations have been performed on ionic clusters due to the low number densities of clusters from conventional cluster ion sources.

One of the dramatic developments in the field of ionic cluster chemistry has come from combining laser spectroscopy with mass spectrometry using molecular beams.[15] Due to the facility of production and mass selection, properties of ionic clusters can be studied as a function of size. In addition, clusters themselves are unique. Novel chemical species with remarkable stability have been observed in the mass spectra. Such observations have been explained in terms of novel geometries with so-called "magic number." Two well-known examples are the soccer-ball-like C_{60}^+ and the hydrated hydronium ion, $H_3O^+(H_2O)_{20}$.[16,17] The stability of protonated water cluster is ascribed to the strong attractive interaction between the central H_3O^+ ion and the surrounding 20 water molecules forming a pentagonal dodecahedral cage.

The major advantage of cluster research is that ionic clusters can be used to explore specific ion-molecule interactions and the effects of solvation on chemical reactions normally masked by the inherent averaging within bulk samples.[18-20] The following examples illustrate the breadth of approaches that have been developed. Bowers and co-workers investigated photofragmentation of $(CO_2)_3^+$ and showed that photodissociation proceeds by sequential loss of CO_2 monomers.[21] Lineberger and co-workers examined solvent effects on the spectroscopy and photodissociation dynamics of $(CO_2)_n^+$ and $Br_2^-(CO_2)_n$ clusters.[18,22] The Brucat and Duncan groups separately employed a laser vaporization technique to generate various metal ion-molecule clusters, such as Mg^+X ($X = H_2O$, rare gas, N_2), and $V^+(H_2O)$.[23-25] From the vibronic spectra due to electronic

transitions of the metal ion chromophore, considerable structural information about clusters was obtained. Farrar and co-workers obtained predissociation spectra for bound-bound transitions in $Sr^+(H_2O)_n$ and $Sr^+(NH_3)_n$ by monitoring the photofragments.[26,27] Assuming that the electronic excitations are localized on Sr^+, they could deduce information on the electronic structure of the Sr^+-ligand systems. Recently Neumark and co-workers applied the zero-kinetic energy (ZEKE) technique to several anion-molecule complex systems such as $I^-(CO_2)$ and their vibrationally resolved spectra provide reliable potential parameters for *ab initio* calculations.[28]

For ionic cluster systems without bound-bound electronic transitions in the visible or near UV region, infrared spectroscopy is a promising approach. However, there are a number of serious difficulties with obtaining traditional absorption vibrational spectra: a) partition functions are large, b) it is difficult to produce sufficiently high densities of these ionic species to be useful for spectroscopy, and c) the spectroscopy is complicated due to the existence of large amplitude motions. One of the successful approaches to overcoming such obstacles is to take advantage of "consequence" techniques. These techniques are based upon direct observation of the "action" spectrum resulting from a direct consequence of photon absorption event rather than attenuation of the incident radiation due to absorption. One powerful method is the vibrational predissociation spectroscopy developed by the Y.T. Lee group.

1.2 VIBRATIONAL PREDISSOCIATION SPECTROSCOPY

The general process underlying vibrational predissociation spectroscopy for ionic clusters can be expressed as follows:

$$M^{\pm}(S)_n + m\,h\nu_{IR} \rightarrow M^{\pm}(S)_{n-p} + pS$$

Here, $M^{\pm}$ designates a positive or negative ion core, S, the clustering neutral solvent (ligand), and m, number of infrared photons of frequency ν_{IR}. In some cases, infrared photons of two or more different frequencies might be involved. The process above requires that the parent cluster ion has absorbed sufficient energy from the infrared laser to cause the evaporation of p ligand molecules and produce a daughter ion of smaller mass.

In the case of weakly bound ionic clusters, absorption of a single photon of a high frequency stretch provides sufficient energy to the system, leading to the continuum levels of the dissociating products (Figure 1). For an ionic cluster system with a binding energy larger than the energy of a single infrared photon, a multiphoton excitation scheme is required to induce dissociation unless there are large amounts of internal excitation already present. Multiphoton excitation has been widely used in the study of neutral polyatomic molecules as a probe of both reaction dynamics and spectroscopy.[29] Although exact quantitative theories to describe the behavior of a molecule in a strong IR field are not yet available, a generally accepted qualitative picture exists which describes many of the observed phenomena.[30] An important feature of this process is that the first photon absorbed excites a resonant transition to a well defined vibrational level and that all subsequent excitation follows the resonant absorption of the first photon. After

accumulating enough energy via a multiphoton process, energy is quickly redistributed throughout the system, and if there is sufficient energy in the weakest bond of the cluster, predissociation can take place.

This method has been successfully applied to several ionic cluster systems by Lee and co-workers.[31-33] They applied tunable IR laser radiation to mass-selected ions in an octupole ion trap while monitoring the intensity of photodissociated product ions with a quadrupole mass spectrometer. In contrast to traditional direct absorption methods, this technique provides high sensitivity. For typical experimental conditions, the fractional absorption is on the order of 10^{-12}, at least five orders of magnitude more sensitive than the detection limit of the best direct absorption experiments. (For a typical infrared absorption cross section $\sigma \approx 10^{-17}$ cm^2, an absorption pathlength $l \approx 100$ cm, and an ion beam density $n \approx 10^3$ cm^{-3}, the fractional absorption, given by $n\sigma l$, is ca. 10^{-12}).

The first infrared predissociation experiments were performed by Okumura *et al.*[31] on $H_3^+(H_2)_n$, which could be dissociated with a single IR photon. For systems which would not dissociate with a single IR photon, such as $H_3O^+(H_2O)_n$, two approaches were attempted. One was to attach a "spy" molecule such as H_2 to the system forming $H_3O^+(H_2O)_nH_2$. The underlying idea was that the spy molecule would not perturb properties of the ionic clusters very seriously, and dissociate more readily. Although the clusters were interesting in their own right, the observed perturbation in the spectra was sometimes found to be quite substantial. The other approach, developed by Yeh *et al.*,[32] was to employ a multiphoton dissociation process. Since for $H_3O^+(H_2O)_n$ clustered systems, the density of states in an excited vibrational level is much higher than in the

ground vibrational level, excited vibrational states are more easily dissociated upon sequential absorptions of photons produced by a high power, fixed-frequency IR laser. Lisy and co-workers studied cesium-methanol clusters by pumping the absorption corresponding to the ν_4 C-O stretching mode in methanol with a CO_2 laser and determined the number of methanol ligands in the first solvation shell.[34]

In our group at Caltech, a time-of-flight mass spectrometer based on the design of Lineberger's group[18] has been built. We have successfully applied vibrational predissociation spectroscopy to various ionic cluster systems, such as SiH_7^+ and $NO_2^+(H_2O)_n$ (n = 1 to 5) clusters, to study the structures and reactions occurring within the cluster.[35-37]

1.3 FRAMEWORK OF THESIS

This thesis presents projects I have performed in collaboration with my co-workers during my stay at Caltech and consists of three parts: a) an experimental section (Chapter 2), b) spectroscopic results from three ionic cluster systems (Chapters 3, 4 and 5), and c) previously published papers from the projects I participated in (Appendix).

In Chapter 2, the experimental scheme employed is described. This chapter includes: a) sample preparation, b) the supersonic molecular beam, c) methods of generating molecular ion and ionic clusters, d) the time-of-flight mass-spectrometer, e) the tunable infrared laser system, f) photofragment ion detection and data acquisition, and g) the overall system operation scheme.

In Chapter 3, infrared spectroscopy of mass-selected clusters $NO^+(H_2O)_n$ for n = 1 to 5 is presented. Correlated *ab initio* calculations of vibrational frequencies and intensities for n = 1 and 2 performed by my colleague Keith T. Kuwata are described to aid in the interpretation of the spectra. This study provides the evidence for the intracluster rearrangement reaction

$$NO^+(H_2O)_n \rightarrow H_3O^+(H_2O)_{n-2}\,(HONO) \text{ at } n \geq 4.$$

Chapter 4 presents infrared spectroscopic results on various $NO_2^+(HOX)$ (X = H, D, ^{35}Cl, ^{37}Cl) clusters using glow-discharge and electron-impact sources. The studies of protonated chlorine nitrate, $NO_2^+(HOCl)$, together with earlier mass-spectrometric studies by our group, provide some insight into the reaction mechanism for the depletion of stratospheric ozone observed over Antarctica during the austral spring.

In Chapter 5, the first infrared spectroscopic observations of gas-phase halide clusters, $Cl^-(H_2O)_n$ (n = 1 to 5), are presented, together with correlated *ab initio* calculations. The analysis of the infrared spectra leads to crucial suggestions concerning the structures of halide water systems.

The Appendix presents published papers on two projects in which I participated.[35-37] The experiments were performed together with my co-workers, Dr. Yibin Cao, Dr. Bernd-Michael Haas, and Matthew S. Johnson. The work on SiH_7^+ is the first system we pursued in our laboratory, and the two papers regarding $NO_2^+(H_2O)_n$ clusters provide the first spectroscopic evidence for intracluster rearrangement reactions.

1.4 REFERENCES

1. J.P. Maier (ed), *Ion and Cluster Ion Spectroscopy and Structure*, (Elsevier, Amsterdam, 1989).

2. J.P. Maier, Chem. Soc. Rev. **17**. 45 (1989).

3. T.A. Dixon and R.C. Woods, Phys. Rev. Lett. **34**, 61 (1975).

4. R.C. Woods, T.A. Dixon, R.J. Saykally, and P.G. Szanto, Phys. Rev. Lett. **35**, 1269 (1975).

5. R.J. Saykally, T.A. Dixon, T.G. Anderson, P.G. Szanto, and R.C. Woods, Astrophys. J. 205, L101 (1987).

6. W.H. Wing, G.A. Ruff, W.E. Lamb, and J.J. Spezeski, Phys. Rev. Lett. **36**, 1488 (1976).

7. T. Oka, Phys. Rev. Lett. **45**, 531 (1980).

8. C.S. Gudeman, M.H. Begemann, J. Pfaff, and R.J. Saykally, Phys. Rev. Lett. **50**, 727 (1983).

9. C.S. Gudeman and R.J. Saykally, Annu. Rev. Phys. Chem. **35**, 387 (1987).

10. P. Kebarle and A.M. Hogg, J. Chem. Phys. **42**, 798 (1965).

11. A.W. Castleman, Jr. and R.G. Keese, Acc. Chem. Res. **19**, 413 (1986); *ibid*, Chem. Rev. **86**, 589 (1986).

12. K. Hiraoka, S. Fujimaki, K. Aruga, and S. Yamabe, Chem. Phys. Lett. **208**, 491 (1993) and references therein.

13. M. Meot-ner, J. Am. Chem. Soc. **106**, 1265 (1984).

14. R.G. Keesee and A.W. Castlemann, Jr., J. Phys. Chem. Ref. Data Vol. 15, No. 8 (1986).

15. E.R. Grant and R.G. Cooks, Science. **250**. 61 (1990).

16. H.W. Kroto, J.R. Heath, S.C. Obrien, R.F. Curl, and R.E. Smalley, Nature, **318**,162 (1985).

17. S. Wei, Z. Shi, and A.W. Castleman, Jr., J. Chem. Phys. **94**, 3268 (1991).

18. M.L. Alexander, N.A. Levinger, M.A. Johnson, D.Ray, and W.C. Lineberger, J. Chem. Phys. **88**, 6200 (1988).

19. J.F. Garvey and R.B. Bernstein, Chem. Phys. Lett. **126**, 394 (1986).

20. G. Radhakrishnan, S. Buelow, and C. Wittig, J. Chem. Phys. **84**, 727 (1986).

21. H.-S. Kim, M.F. Jarrold, and M.T. Bowers, J. Chem. Phys. **84**, 4882 (1986).

22. M.A. Johnson, M.L. Alexander, W.C. Lineberger, Chem. Phys. Lett. **112**, 285 (1984).

23. K.F. Wiley, C.S. Yeh, D.L. Robbins, J.S. Pilgrim, and M.A. Duncan, J. Chem. Phys. **97**, 8886 (1992).

24. J.S. Pilgrim, C.S. Yeh, and M.A. Duncan, Chem. Phys. Lett. **210**, 322 (1993).

25. D.E. Lessen, R.L. Asher, and P.J. Brucat, J. Chem. Phys. **93**, 6102 (1990).

26. M.H. Shen and J.M. Farrar, J. Chem. Phys. **94**, 3322 (1991).

27. M.H. Shen and J.M. Farrar, J. Phys. Chem. **93**, 4386 (1989).

28. Y. Zhao, C.C. Arnold, and D.M. Neumark, J. Chem. Soc. Faraday Trans. **89**, 1449 (1993).

29. P.A. Schulz, A.S. Sudbo, D.J. Krajnovich, H.S. Kwok, Y.R. Shen, and Y.T. Lee. Ann. Rev. Phys. Chem. **30**, 379 (1979).

30. J.I. Steinfeld, *Molecules and Radiation* (2nd ed.), MIT press, Cambridge, Massachusetts (1985).

31. M. Okumura, L.I. Yeh, and Y.T. Lee, J. Chem. Phys. **88**, 79 (1988).

32. L.I. Yeh, M. Okumura, J.D. Myers, J.M. Price, and Y.T. Lee. J. Chem. Phys. **91**, 7319 (1989).

33. J.M. Price, M.W. Crofton, and Y.T. Lee, J. Chem. Phys. **91**, 7319 (1989); J.M. Price, Ph.D. thesis, University of California at Berkeley (1990).

34. W.L. Liu and J.M. Lisy, J. Chem. Phys. **89**. 606 (1988).

35. Y. Cao, J.-H. Choi, B.-M. Haas, M.S. Johnson, and M. Okumura, J. Phys. Chem. **97**, 5215 (1993).

36. Y. Cao, J.-H. Choi, B.-M. Haas, M.S. Johnson, and M. Okumura, J. Chem. Phys. **99**, 9307 (1993).

37. Y. Cao, J.-H. Choi, B.-M. Haas, and M. Okumura, J. Phys. Chem. **98**, 12176 (1994).

1.5 FIGURE CAPTION

FIG. 1. Two orthogonal Morse potentials are plotted. X-H coordinate represents a high frequency mode such as O-H, N-H, and C-H. The other coordinate corresponds to a low frequency ion-solvent mode. One photon X-H excitation is enough to dissociate the weakly bound cluster ions. Most of the ionic cluster systems described in this thesis fall under this category.

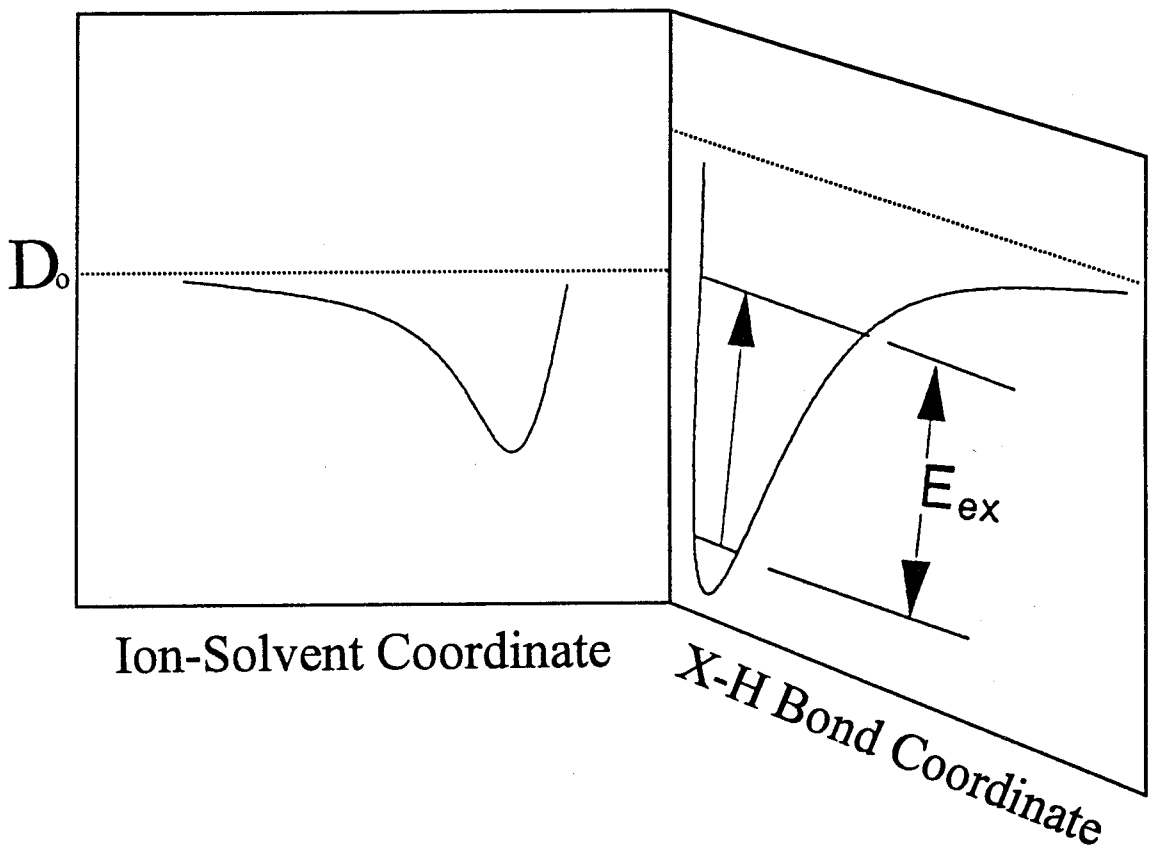

Figure 1.

CHAPTER 2

Infrared Ion Photodissociation Spectrometer

2.1 OVERVIEW

As described in Chapter 1, we utilized infrared predissociation spectroscopy to obtain the vibrational spectra of the following ionic cluster systems: both positively charged $NO^+(H_2O)_n$ (n = 1-5), and $NO_2^+(HOX)$ (X = H, D, ^{35}Cl, ^{37}Cl), and negatively charged $Cl^-(H_2O)_n$, (n = 1-5) systems. The apparatus employed for these investigations was a tandem reflectron time-of-flight (TOF) mass spectrometer, combined with an infrared laser as the spectroscopic probe (see Figure 1). The spectrometer was designed based upon the ionic cluster photodissociation apparatus built by the Lineberger group, which was then modified for our experiments.[1,2]

This chapter is composed of two parts: Part I describes the TOF mass spectrometer and Part II, the overall system operation scheme. The description of the TOF mass spectrometer is subdivided into six sections. Section A describes how the sample concentration was regulated. In section B the generation and characterization techniques of the supersonic molecular beam are presented. Section C shows three schemes for generating molecular ions and ion-solvent clusters. Typical mass distributions from the resulting ion beam were characterized by the time-of-flight mass spectrometer outlined in section D. The general setup for generating tunable infrared radiation from an optical parametric oscillator is in section E. In section F, the photodissociation experiments of vibrationally excited ions, the detection schemes for both positively and negatively charged ionic clusters and the data acquisition system are described.

In the second part of this chapter, the overall system operation is described. Specifically, two synchronization schemes as well as detailed pulsing sequence diagrams

are presented. The first of these describes the scheme employed for the experiments in Chapters 3 to 5. The second outlines a recently designed scheme for use with future experiments that utilizes improved data-collection capabilities.

2.2 TIME-OF-FLIGHT MASS SPECTROMETER

A. Sample Preparation: Concentration Regulation

Preparation of a desired mixture occurred in the stainless steel gas line shown in Figure 2. This line consisted of pressure transducers connected to the readout, two mechanical pumps, one of which backed a diffusion pump, two mass-flow controllers, and two bubblers. To eliminate contamination by ambient air gas into the chamber, the whole system was heliarc-welded to minimize the number of fittings. All fittings were metal-sealed VCR. The residual water, a notorious problem where anhydrous conditions or use of deuterated water are required, was removed by an Edward diffusion pump (Diffstaks 63-150) which was fore-pumped by a mechanical pump. The vacuum pressure was indicated by a thermocouple (Duniway DST-531) and an ionization gauge (Duniway 1-075-N). The stagnation pressure, when the chamber was pressurized, was measured by a Baratron pressure transducer (MKS TYPE-122A) connected to a digital readout (MKS PDR-D-1).

To dilute gas-phase samples, such as NO (Chapter 3), silane, or diborane, the concentration was regulated by a home-built electronic circuit that controlled two mass-flow controllers as shown in Figure 3. One controller (MKS 1159B denoted by Channel 1) regulated the flow speed of carrier gas (100 sccm), the other (denoted by Channel 2), the flow speed of the seed gas (20 sccm). The performance of the controller was based upon a

feed back loop that regulated the flow speed of both controllers. Once the proper mixing ratio between two channels was determined by a pre-set, the mixing ratio and the pressure monitored by transducer were consistently maintained by the feedback circuit. In some cases where very dilute sample was required, a timer circuit that limited the duty cycle of the sample controller reduced the mixing ratio down to one-tenth the initially prepared ratio. This optional circuit is also shown in Figure 3.

For liquid samples, such as HNO_3 (Chapter 4), water or benzene, the concentration was regulated through the use of a leak-tight liquid bubbler immersed in a temperature bath (in this case the two mass-flow controllers were bypassed). The carrier gas passed over the liquid surface of the species of interest. Depending on the vapor pressure and mass spectrum, a suitable bath temperature was selected to obtain the proper concentrations. In cases that required two immiscible liquid samples, for example water and CCl_4 (Chapter 5), two separate bubblers were installed in the middle of the gas line.

B. Supersonic Molecular Beam

When a gas at high stagnation pressure is forced into vacuum through a small-diameter nozzle, it experiences significant adiabatic cooling during the expansion process due to the Joule-Thomson effect. During the expansion that defines a supersonic molecular beam, random thermal motion is converted into a highly directional axial flow. In modern spectroscopy, supersonic molecular beam has been a major advance, providing two principal advantages.[3] First, the molecules of interest that are entrained in a supersonic jet undergo significant translational and rotational cooling through numerous collisions with the carrier gas. Vibrational cooling is also noted but occurs to a lesser extent. Since few

rovibrational states are occupied initially, the cooling results in a dramatic simplification of the spectrum. Second, the expansion process can generate various kinds of clusters, such as van der Waals complexes and ionic clusters, that can provide a deeper understanding of molecular interactions within a weakly bound molecular system.

Our group has chosen to use a pulsed molecular beam rather than a continuous, supersonic jet. The advantages include a higher jet density, better rotational and vibrational cooling and a decreased tendency for condensation. During the last decade, a variety of pulsed valves have been devised. The pulsed valves adopted by our group are either a solenoid valve (General Valve Co.) or a piezoelectric valve designed by Trickl and Proch.[4] The solenoid valve has been used only for the pick-up experiments investigating the entrainment of secondary solvent molecules reduced by the valve into a primary ionic cluster beam. The valve, however, has the disadvantage of a very long gas pulsewidth ($\geq$ 1 ms), which is not suitable for the experiments requiring a high peak beam intensity. Furthermore, long pulses can often result in interference between the tail end of the molecular beam gas pulse and gas reflected back into the beam by the surrounding walls.

All of the experiments described in this thesis utilized the Trickl valve. The valve contained a piezoelectric disk translator (Polytec PI. University model P-286.23), which could flex by as much as 100 μm at a voltage of up to -1 kV with a rise time of 35 μs. High voltage pulses were generated by a home-built driver that provided pulses with 35 μs minimum rising and falling times. The translational motion allowed gas to flow through the nozzle by moving the adjustable plunger to produce gas pulse lengths between 150 to 250 μs at full opening. The piezo element could operate at a maximum repetition rate of 1 kHz,

and its normal temperature range of operation is between 250 K and 350 K. If a remote nozzle was mounted, the valve can be operated from 77 K up to 1000 K. In cases where unwanted side reactions may damage the piezo surface, perfluorinated grease was applied to protect the surface.

The characteristics of the molecular beam profile were measured by a fast ionization gauge (FIG) developed by Gentry and Giese.[5] The gauge built by our group resembled the configuration commonly used in the Bayard-Alpert type of thermionic ionization gauge, and has a rise time of about 1 μs. When measured at a distance of 1.5 cm from the pulsed valve with H_2 carrier gas (backing pressure 700 Torr), the measured beam profile exhibited a pulsewidth of about 100-150 μs FWHM. Such a pulsewidth was rather short compared to the performance of other valves. In addition, the pulsewidth was found to be proportional to the opening duration of the pulsed valve.

C. Generation of Molecular Ions and Ionic Clusters

A number of methods were developed to produce high intensity beams of molecular ions and ionic clusters for various spectroscopic studies. To generate both positively and negatively charged species, we employed three ionization methods coupled with the pulsed supersonic expansion: surface ionization, pulsed glow discharge, and electron impact sources.

Surface ionization is an efficient method for generating alkali metal ions such as K^+, Cs^+ and Rb^+ with almost 100% ionization efficiency.[6,7] The substance (usually in the form of paste) was coated on a spiral tungsten filament (ca. 0.4 mm diameter) and emitted the ionic species of interest. The tungsten spiral was 5 mm in length and 2 mm in diameter, and

was connected to the power supplies through Teflon-covered wires. Due to the heat transfer into the piezoelectric element, we designed a 1-cm-long molecular beam nozzle whose outer surface was in contact with continuously flowing cold water through copper tubing. The coated filament was placed a few mm away from the cold nozzle and heated by a floating power supply. The amount of ion current varies with the wire diameter and length as well as the amount of paste on the wire. Under our experimental conditions, a current of approximately 5 A was required to generate ions such as K^+. The emitted ion current was generally on the order of 10^{-8} A as measured by an electrometer (Keithley Inst. Model 602 picoammeter). A continuous beam of low energy cations was injected transverse to the pulsed supersonic molecular beam. This scheme was quite successful in generating predominantly alkali metal cations and some of their solvated clusters.

Most of positively charged ionic clusters discussed in this thesis were produced by a pulsed high-pressure glow discharge source, shown in Figure 4. The source was composed of three parts: a 2-mm-long, 0.5-mm-diam. stainless-steel nozzle, a 10-mm-long, 1-mm-diam. aluminum discharge cell, and a 5-mm-long, 1-mm-diam. stainless-steel expansion channel. The discharge cell contained two 1-mm-diam Ni electrode holders made of electrically insulating Delrin plastic. The electrodes were placed as close as possible to the nozzle side and were inserted into the cell until separated by 1 mm. The discharge source was mounted directly on the front of the pulsed valve. The valve was operated at a stagnation pressure of 1000 to 1500 Torr and at a repetition rate of 10 Hz (200 μs width). When the pressure inside the cell reaches a maximum (ca. 50 Torr), a high-voltage thyratron switch was triggered to apply -1 to -3 kV pulse across the electrodes. The source conditions

were optimized to produce a glow discharge plasma without initiating an arc discharge. The resulting plasma underwent many thermalizing collisions as the gas flows through the channel and further cooled during the subsequent supersonic expansion.

To generate some of the positively charged clusters and all hydrated chloride clusters to be described in Chapters 4 and 5, we employed a home-built electron impact source based on the design developed by Erdman and Zipf.[8] The source consisted of a filament with a mounting block, a grid plate, an acceleration element followed by an einzel lens, and deflectors. We have used thoriated iridium ribbon filaments with platinum tabs (0.002" x 0.0027" x 3", Electron Tech. Inc. Model 201-998-8100). The source was mounted on the side of the pulsed valve housing, and was heated by a floating external power supply (~6A). A continuous beam of 760 eV electrons was injected transverse to the pulsed supersonic molecular beam and was collected by a Faraday cup mounted on the opposite side of the electron gun. The position alignment of the electron beam was optimized using the fluorescence glow from the Ar molecular beam. Typical emission and Faraday-cup currents were about 1-3 mA and 100-500 μA, respectively.

D. TOF Mass Spectrometer and Mass Spectra

Our TOF mass spectrometer (Figure 1) consisted of three differential vacuum regions: source chamber, TOF chamber and photolysis/detection chamber.

The source chamber (50 × 50 × 75 cm^3) contained the Trickl pulsed valve and ion sources described in Sections B and C, and was pumped by a 10-in. freon-baffled diffusion pump (Varian VHS-10, 5000 *l*/s) which was backed by two mechanical pumps (Welch Co. Duo Seal-1397 500 *l*/s). Without a gas load, the chamber pressure was maintained at ~1 x

10^{-6} Torr. With a gas load produced at a repetition rate of 10 Hz, the pressure was maintained at ~0.5 to 5 x 10^{-4} Torr under typical experimental conditions. The expanding ion plasma was skimmed by a 3-mm-diam. orifice that was placed a few cm away from the ion source to collimate the ion beam. The distance between the source and skimmer was carefully adjusted to obtain an optimized TOF distribution and was typically 3 to 20 cm. When an electron impact source was employed, we attached in some cases a plate with a 1-cm-diameter hole in front of the pulsed valve and biased the plate and skimmer to increase ion intensity (Since both positively and negatively charged ionic clusters were studied in this thesis, polarities of most electric components were simply reverse-biased except some components. Typical values and biasing schemes employed are shown in Table I).

Most of the gas load was removed in the source chamber. Following the skimmer, the ion beam entered a second chamber containing TOF ion optics of a modified Wiley-McLaren type.[9] The TOF region (15-cm diameter x 120-cm long) was divided into two regions by a 1"-diameter hole for further differential pumping. Each region was pumped by freon-baffled 6"- and 4"-in. diffusion pumps (Varian VHS-6, 2400 *l*/s and VHS-4, 1200 *l*/s, respectively) which were backed by two mechanical pumps (Welch Co. Duo Seal-1397, 500 *l*/s and Duo Seal-1422, 160 *l*/s). Without and with a gas load, the pressure was maintained at ~7 x 10^{-7} and ~5 x 10^{-6} Torr, respectively.

The ion beam in the TOF region was extracted at 3° relative to the expansion axis by applying a high voltage pulse to a repeller plate. We adopted the parallel arrangement to pick up all ions in the extraction region. However, this scheme generally showed a lower mass resolution compared to the perpendicular extraction configuration. To improve the

mass resolution, an extra acceleration stage was added to the most commonly used Wiley-McLaren configuration which has an extraction region followed by an acceleration stage. This three-stage arrangement (a 4.4-cm-long extraction region, two consecutive acceleration regions of 3.0 and 4.8 cm) was calculated to result in both simultaneous first- and second-order spatial focusing at one location, the point where the ions were probed by the infrared laser beam. This kind of focusing is not possible for the two-stage scheme.[2] Improved mass resolution was observed by carefully adjusting the two acceleration voltages in our experiments. Recently De Heer *et al.* have also observed an improvement in mass resolution using a similar three-stage TOF mass spectrometer for the special case where the electric field of the central stage is free.[10] After passing the three-stage ion optics, the accelerated ions were focused by a set of an einzel lens and deflectors, and then traveled field-free region where the separation of ions began depending on their mass. The ions were collimated by a second einzel lens and directed by deflectors and entered the photolysis/detection chamber through a 1"-diameter aperture.

The photolysis/detection region was a 35-cm high, 70-cm diameter chamber with a bell-shaped cover. The chamber contained a mass gate, a reflectron, ion detectors and optical windows. To eliminate possible contamination of detectors by the vapor of diffusion pump oil, the region was pumped by a turbomolecular pump (Airco Co. Model 514, 500 *l*/s) which was back-pumped by a diffusion pump (Edward Co. Diffstaks-100/300, 280 *l*/s). The diffusion pump was backed by a mechanical pump (Edward Co. ED-100, 100 *l*/s). Without and with a gas load, the pressure was maintained at ~2 x 10^{-7} and ~4 x 10^{-7} Torr, respectively.

The ions in the photolysis/detection region were further mass-separated and then mass-analyzed by a reflectron which was tilted by 4° with respect to the ion beam axis. The primary function of the reflectron was to separate parent and fragment ions according to their mass (Section F). Another important capability was to refocus divergent ions of the same mass.[1] The ion beam tends to diverge in a field-free region due to the spread of kinetic energies. However, if the retarding field is applied via the reflectron, the ions are, after leaving the reflectron and traveling some field-free region, refocused at the ion detector. We applied a 13-cm long retarding field and the reflected ions traveled a 30-cm-long field-free region to be detected by a chevron microchannel plate detector (Galileo Electro-Optic. FTD 2003, $t_{rise} \leq 1$ *n*s). The biasing of the detector depended upon the polarity of ions (Table I). The resulting ion signal was sent to a preamplifier with a gain of 10 (Comlinear Co. CLC-100). The signal transfer from the detector to the preamplifier was achieved through the circuits shown in Figure 5. In the negative ion mode, capacitative coupling was required since the anode potential was biased up to +2 kV. The preamplified signal was recorded by a transient digitizer/signal averager (LeCroy 8818/6010). The averaged signal (typically after summing 100 scans) was transferred via a GPIB interface to an IBM-AT computer for display and analysis using the program "TOFVIEW2."[2]

E. Tunable Infrared Laser: Optical Parametric Oscillator

The pulsed tunable infrared laser beam utilized in vibrational predissociation experiments was obtained from an angle tuned $LiNbO_3$ optical parametric oscillator (OPO). The parametric oscillation is based on the second-order nonlinear dielectric properties of the $LiNbO_3$ crystal in which the induced polarization has components proportional to the

square of the electric field.[11,12] The generation of an infrared beam in an OPO involves the transfer of power from an intense "pump" beam at ω_p to "signal" and "idler" beams at ω_s and ω_i ($\omega_s \geq \omega_i$), where $\omega_p = \omega_s + \omega_i$. This process is fundamentally similar to that of second-harmonic generation, in which power is provided from the low-frequency optical field at ω to the field at 2ω. The only difference is in the direction of power flow. Detailed discussion on an OPO is presented in the references.[11,12] In this section, only the low-resolution mode is described.

Our OPO cavity configuration was based on the design of Brosnan and Byer.[13,14] Figure 6 shows a schematic diagram of the optical components of our OPO. The cavity whose optical length was 20 cm consisted of 5 components: $LiNbO_3$ crystal (Crystal Tech. 5-cm-long, 1.0-cm^2 cross section, 1-arc-min. wedge on output end, AR coated on both ends at 1.064 μm), a pair of right-angle ZnSe prism beam expanders (Janos, length of hypotenuses: small 2.5 cm, large 4.5 cm, longer normal face AR coated at 1.55 μm with a ThF_4 coating), a 600 lines/mm grating as the rear mirror as well as a line width-narrowing element (Bausch and Lomb, 3 cm x 3 cm, blazed for first order at 1.55 μm), an input coupler (CVI. 1"-diam. 45° reflector for 1.064 μm), and a broadband reflective mirror as the output coupler (CVI. 1"-diam. 3' wedge, 60% at 1.4-1.8 μm). The components were mounted on a 1-cm-thick Super Invar plate (thermal expansion coeff. ca. $3x10^{-7}$ K^{-1}).

The OPO was pumped by a 10-Hz Nd:YAG laser (Spectra Physics. GCR-12S) which generated 350-mJ pulses at 1.06 μm. The YAG beam was multi-passed 9 m in order to have a nominally Gaussian TEM_{00} intensity profile and to remove hot spots, and to eliminate possible back-reflection damaging of the YAG crystal rod (see Figure 7). Q-

switch delay was altered from an optimal setting in order to lengthen the pulse width from 6-7 ns to ~15 ns. The multi-passed pump beam was coupled into the oscillator cavity by a 45° input beam splitter. Our OPO was a singly resonant parametric oscillator, i.e., the cavity was resonant only on the signal wave. A prerequisite for generation of signal and idler beams is satisfaction of the conservation of momentum, leading to the phase-matching relationship

$$\mathbf{k}_p = \mathbf{k}_s + \mathbf{k}_i \qquad (1)$$

where **k** is the wave vector of each beam. In the case of our uniaxial $LiNbO_3$ crystal, the input pump beam corresponds to an extraordinary (*e*) wave, and both signal and idler beams, to ordinary (*o*) waves. This kind of conversion of the *o* wave into two *e* waves is called Type I phase matching. Our OPO was continuously tunable from 2600 to 6800 cm^{-1} by simultaneously adjusting the angles of the crystal and grating mounted on stepping motors (ca. 2×10^{-4} degree per step) along an empirically determined tuning curve (Fig. 8). Pulse energies were measured by a Molectron power meter (Model J25LP). The idler beam had a typical energies of 3-6 mJ/pulse, and a linewidth of 1.5 cm^{-1}. The optical path from the OPO laser to the TOF mass spectrometer was enclosed by Plexiglas and continuously purged with dry air to remove infrared absorption caused by ambient water vapor.

To separate the idler beam from the other two beams, we used non-collinear phase matching. In this scheme, each of the three beams propagates in a different direction. The signal beam vector is fixed, but the vectorial phase matching condition (eq. 1) is still satisfied. In our case, the pump beam was sent into the crystal tilted slightly upwards with respect to the lasing signal beam axis. As the three beams propagated, the spatial separation

was easily achieved. As shown in Figure 7, the idler was the top-most beam, because it had the smallest wave vector. The residual pump YAG beam was reflected by a hemispherical mirror and then scattered away by a graphite block. The idler beam was focused by a BaF_2 lens and sent into the TOF mass spectrometer.

The OPO laser wavelength was calibrated by recording the rovibrational spectrum of a reference gas in a home-built photoacoustic cell.[15] The leak-tight 8.5-cm-long, 1-cm-diameter cell was made of aluminum and contained two CaF_2 infrared windows and one microphone (Knowles, EK-3031). The cell was usually filled with 10-40 Torr of the reference gas. Depending on the spectral region of interest, several reference gases were selected by referring to the IUPAC table.[16] If the reference gas undergoes rovibrational transitions induced by the infrared beam and then collides with other non-excited molecules, energy transfer and subsequent thermalization will occur, leading to an increase of temperature and pressure. This change was detected by a microphone transducer and the resulting signal amplified through an OP-Amp circuit. The amplified signal was sent to an analog-to-digital converter for display and spectrum analysis.

The operation of the OPO laser was controlled by an IBM-AT computer using the program "OPODATA."[2] Two dual-channel stepping motor controller boards (Keithley MSTEP-5) and an integrated data acquisition and control board (Keithley DAS-16) were interfaced with the laser and diagnostics. The OPODATA program controlled and kept track of the angular positions of the crystal and grating, and recorded the power and photoacoustic spectra for analysis and calibration.

F. Detection of Photofragment Ion and Action Spectra

The acquisition of vibrational predissociation spectra involved some additional steps beyond the procedure for obtaining TOF mass spectra described in Section D. First, we used a mass gate for a selection of a single parent ion. Although our pulsed infrared beam traveled perpendicular to the ion beam axis and excited one ionic species, the proximity of several parent ions and the possible appearance of metastables from other parent ions made identification of photofragments ambiguous in some cases. To remove the ambiguity, we placed the mass gate a few cm before the photolysis point. The 1-cm-long mass gate is composed of two deflectors which are separated by 1.5 cm. The whole body was shielded except for the 6-mm-diameter entrance and exit holes. The gate was normally biased up to 400 V, except for the duration when parent ions of interest were passing. Therefore, only the selected ionic species was not deflected and reached the laser interaction region.

Second, the laser timing was adjusted to excite the mass-selected parent cluster. The ion arrival time at the interaction region was obtained by either calculation or by placing a MCP detector at the photolysis point. The laser firing time was monitored by the photodiode signal. The synchronization was achieved by adjusting the delay such that the photodiode signal appeared at the ion arrival time on an oscilloscope. The detailed pulse scheme will be described in section 2.3.

Lastly, the reflectron voltage was adjusted to focus the photofragment ion of interest. Detailed discussion on the photofragment ion detection was presented in the literature,[1] and only a brief account is given here. Upon photodissociation, the photofragments keep almost the same initial velocity (the translational energy release from

vibrational predissociation makes only a small change at the initial parent ion energies used here), regardless of their mass, and their kinetic energy (T_f) is simply reduced to the ratio of the fragment mass (m_f) to the parent mass (m_p) times the parent ion energy (T_p), i.e., (m_f / m_p) T_p. Furthermore, ion trajectories are unchanged if the ratio of kinetic energy to applied reflectron voltage is fixed. Therefore, the photofragment trajectory follows that of the parent when the reflectron voltage is reduced by the factor (m_f / m_p) V_0, where V_0 is the potential applied to detect the parent ion. Since the fragment ions also spend the same amount of time in the reflectron, the photofragments appear at the same time with the parent ion and can be unambiguously identified.

2.3 SYSTEM OPERATION: SYNCHRONIZATION SCHEME

In contrast to the cw mode, the pulse mode of operation required a sophisticated timing scheme to obtain interpretable photofragmentation data. Since the TOF mass spectrometer and the infrared laser in our setup were controlled by two separate digital delay generators (Stanford Research System (SRS) DG-535 and EG&G Co. Model 9650, respectively), a unified synchronization scheme to control both simultaneously was required to obtain infrared predissociation spectra. Two schemes were designed and are shown in Figures 9 and 10. The first one was adopted for all experiments described in this thesis. The second scheme has recently been designed for future experiments with improved data collection capabilities.

In the first scheme, shown in Fig. 9, the overall pulsing sequence was governed by a master delay generator (in this case, the EG&G delay generator). The master EG&G sent three sequential triggering pulses to four components: the flashlamp and the Q-switch of our Nd:YAG laser, the OPO data acquisition, and the slave delay generator (SRS delay generator). Typical delay between EG&G (T_0) and flashlamp (channel A) was 1 msec. The Q-switch and the data acquisitions were simultaneously triggered by the Channel B. The delay between flashlamp and Q-switch determined the energy output of 1.06-μm YAG beam and was 120 to 200 μsec. The slave SRS was externally triggered by the master EG&G and then controlled the pulsing sequence of the TOF components: the pulsed valve, the thyratron, the pulsed ion-repeller, and the LeCroy transient digitizer. When a discharge source was used, the delay between the pulsed valve (A) and the thyratron (B), typically 200-500 μsec, depended upon the distance between the supersonic nozzle and discharge electrodes, and the TOF mass spectrum. The delay between the pulsed valve and the pulsed ion-repeller (in the case of an electron-impact source) also depended upon the distance between two components and was typically 300-700 μsec. The optimum delays were determined by the TOF mass spectrum. The trigger pulse of the ion-repeller was also sent to trigger the oscilloscope and mass-gate. The delay between ion-repeller trigger and the data acquisition trigger was 0 to 50 μsec, depending upon the mass-spectrum region of interest. Once the optimized mass spectrum and ion arrival time at the photolysis point were obtained, the delay (Δ) between master and slave delay generators was adjusted to match the arrival time of the pulsed ion beam with the firing of pulsed laser beam as described in Section 2.2.F.

The above scheme was carried out at a repetition rate of 10 Hz to match our Nd:YAG laser repetition rate. In most cases, the photofragmentation spectra were obtained under the laser-on conditions only. Therefore, the measured intensity is a sum of photofragments and background metastables. To subtract the background metastables, the intensity was measured at the beginning and end of every scan while blocking the laser and averaged. To avoid this unpleasant situation, a new scheme has recently been designed (Fig. 10). The new scheme is performed at the repetition rate of 20 Hz and the main features are a new dual channel transient digitizer (Precision Instrument 9825), a flip/flop circuit (Fig. 11), a master pulse generator and two slave delay generators. The master pulse generator triggers the TOF slave generator and a flip/flop circuit at 20 Hz. The flip/flop circuit converts the 20 Hz into 10 Hz and then triggers the laser slave generator. Therefore, although the laser is fired at 10 Hz, the data acquisition is carried out at 20 Hz, enabling us to measure direct photofragments and background metastables.

2.4 REFERENCES

1. M.L. Alexander, N.A. Levinger, M.A. Johnson, D. Ray, and W.C. Lineberger, J. Chem. Phys. **88**, 6200 (1988); M.A. Johnson, and W.C. Lineberger, in *Techniques for the Study of Ion-Molecule Reactions*, J.M. Farrar and W.H. Saunders, Jr., Eds. (Wiley-Interscience, New York, 1988).

2. Y. Cao, Ph.D. Thesis. California Institute of Technology (1994).

3. G. Scoles, *Atomic and Molecular Beam Methods, Volume 1* (Oxford University Press, New York, 1988).

4. D. Proch and T. Trickl, Rev. Sci. Instrum. **60**, 173 (1989).

5. W.R. Gentry and C.F. Giese, Sci. Instrum. **49**, 595 (1978).

6. J.P. Blewett, Phys. Rev. **50**, 464 (1936).

7. R. Wilson and G. Brewer, *Ion Beam with application to Ion Implantation* (Wiley Interscience, New York, 1973).

8. P.W. Erdman and E.C. Zipf, Rev. Sci. Instrum. **53**, 225 (1982).

9. W.C. Wiley and I.H. McLaren, Rev. Sci. Instrum. **26**, 1150 (1955).

10. W.A. De Heer and P. Milani, Rev. Sci. Instrum. **62**, 670 (1991).

11. Y.R. Shen, *Principles of Nonlinear Optics* (Wiley Interscience, New York, 1984).

12. A. Yariv, *Quantum Electronics* 3rd. Ed. (John Wiley and Sons Inc., New York, 1989).

13. S.J. Brosnan and R.L. Byer, IEEE. J. Quantum Electronics, **15**, 415 (1979).

14. T.K. Minton, S.C. Reid, H.L. Kim, and J.D. McDonald, Optics Communications, **69**, 289 (1989).

15. G.A. West, J.J. Barrett, D.R. Siebert, and K.V. Reddy, Rev. Sci. Instrum. **54**, 797 (1983).

16. *Tables of Wavenumbers for the Calibration of Infrared Spectrometers*, the IUPAC Commission on Molecular Structure and Spectroscopy (Butterworth, Washington, D.C. 1961).

17. C. Manzanares I, A. Brock, J. Peng, and V.M. Blunt, Chem. Phys. Lett. **207**, 159 (1993).

TABLE I. Comparison of detection schemes.

	Positive Ion	Negative Ion
Pulsed Repeller	+ 2.6 kV	- 0.9 kV
Accelerator	+	-
Einzel Lenses 1,2 and 3 (acceleration mode)	-	+
Horizontal and Vertical Deflectors	±	±
Mass Gate (presetted)	+	+
Reflectron	+2.65 kV	-1 kV
Detector Front Plate	ground	-30 V
Detector Configuration	see Fig. 5a	see Fig. 5b
Ion Repeller (optional)	+	-
Skimmer (optional)	-	+

2.5 FIGURE CAPTIONS

FIG. 1. Schematic of the time-of-flight mass spectrometer in tandem with a tunable infrared laser (OPO).

FIG. 2. Schematic diagram of the gas line.

FIG. 3. Electronic circuit of the mass-flow controller. Timing circuit is shown as optional.

FIG. 4. Schematics of the pulsed high-pressure glow discharge source. Two 1-mm-diameter nickel electrodes are insulated from the grounded cell by Delrin. When the pressure inside reaches a maximum, a high voltage pulse (-1.0 ~ -3.0 kV) is applied across the nickel electrodes to initiate the discharge.

FIG. 5. The detection circuits for systems of a) positively charged ions, and b) negatively charged ions. Since the anode is biased up to +2 kV, capacitative coupling is required as in b).

FIG. 6. Schematic diagram of the optical cavity of the OPO. The grating tilts in the plane of the figure, and the $LiNbO_3$ crystal tilts out of the plane. The output coupler is mounted on a piezo translational stage. The components were mounted on a 1-cm-thick Super Invar plate.

FIG. 7. Schematic of the Nd:YAG laser-pumped $LiNbO_3$ OPO. Schemes of multipass setup and beam separation are shown together.

FIG. 8. Angle tuned $LiNbO_3$ OPO tuning curve. The crystal at 25 °C is pumped by a Nd:YAG laser ($\lambda_p = 1.06$ μm).

FIG. 9. Synchronization scheme consisting of two pulse delay generators (PDG), a master and a slave.

FIG. 10. Synchronization scheme consisting of a master pulse generator and two slave pulse delay generators. This scheme shows improved data-collection capabilities.

FIG. 11. A flip/flop circuit utilized in Figure 10.

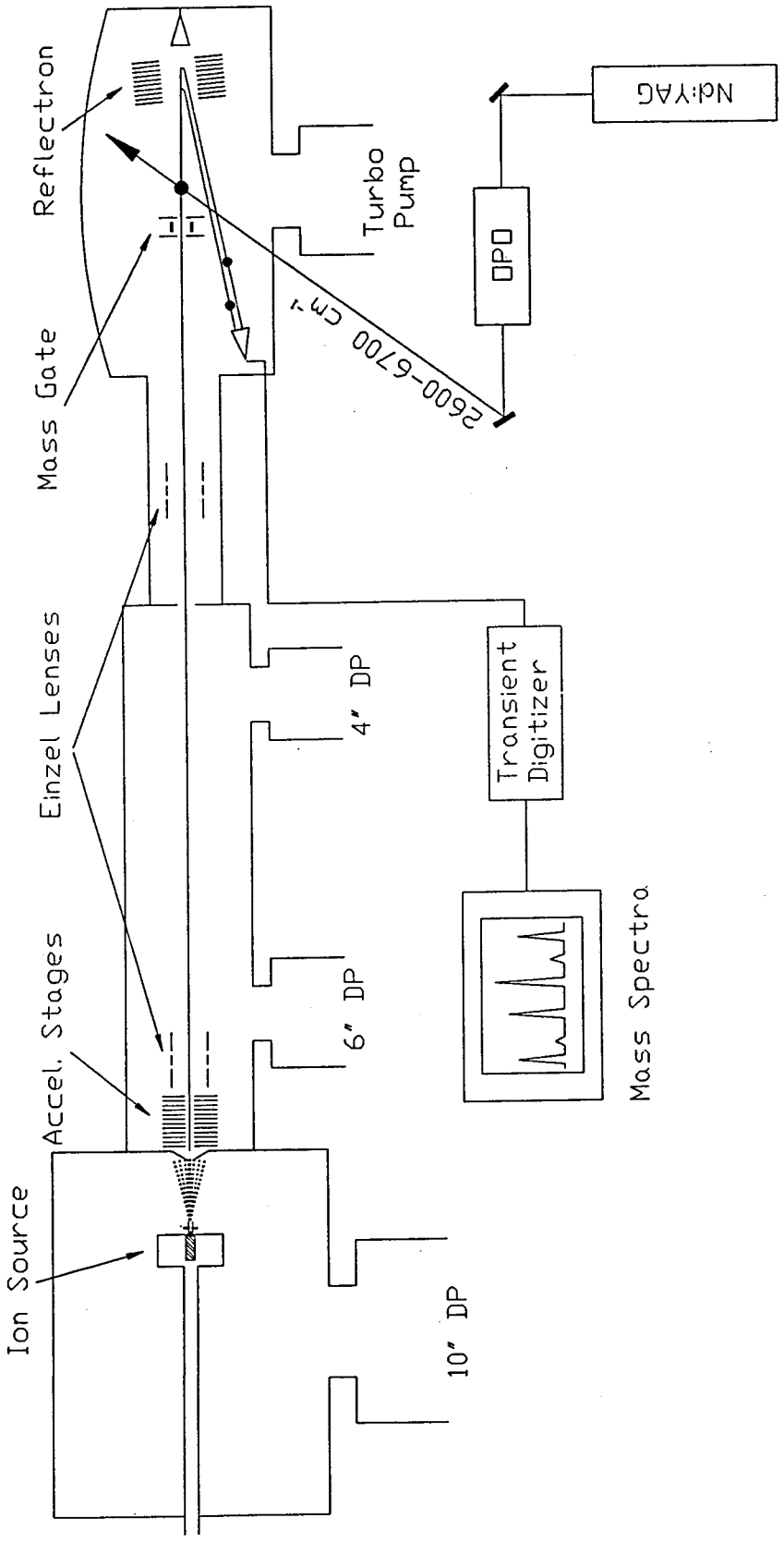
Reflectron
Mass Gate
Einzel Lenses
Accel. Stages
Ion Source
Turbo Pump
Nd:YAG
OPO
2600-6700 cm-1
4" DP
6" DP
10" DP
Transient Digitizer
Mass Spectra

Figure 1.

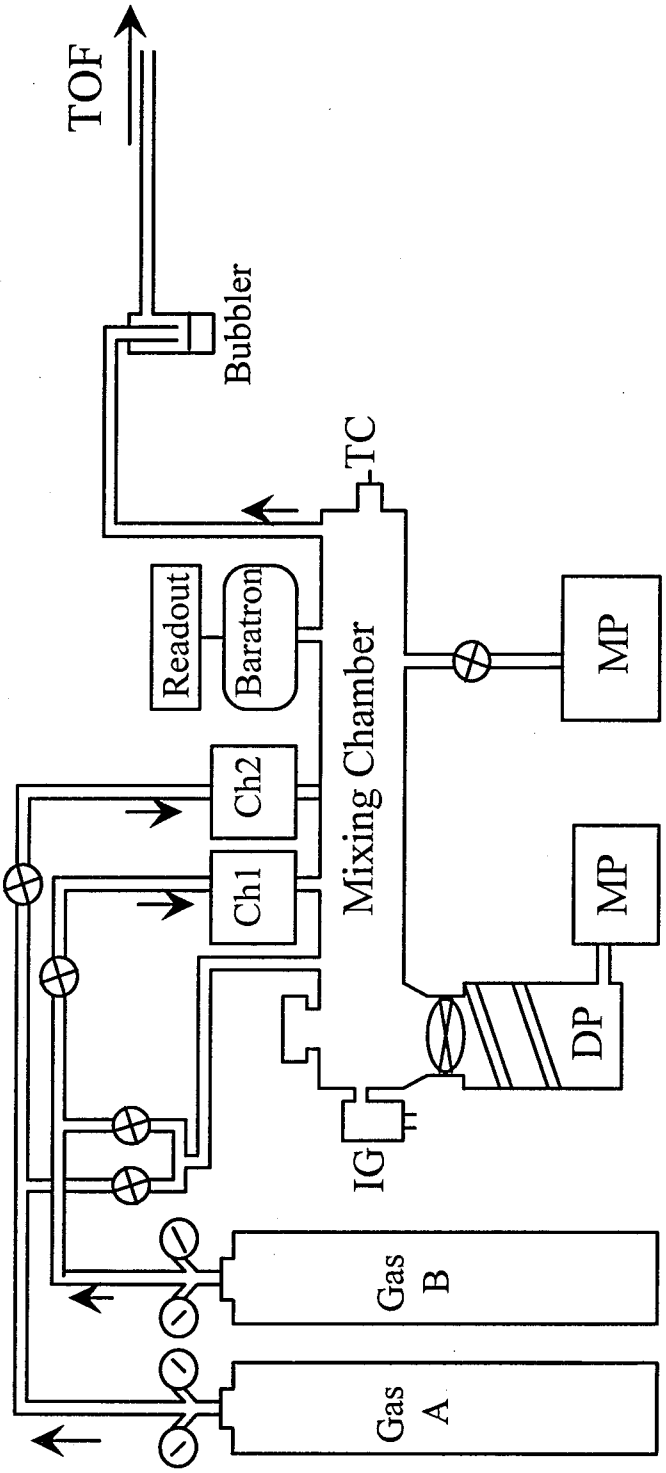
TOF
Bubbler
TC
Readout
Baratron
Mixing Chamber
MP
Ch2
Ch1
MP
DP
IG
Gas B
Gas A

Figure 2.

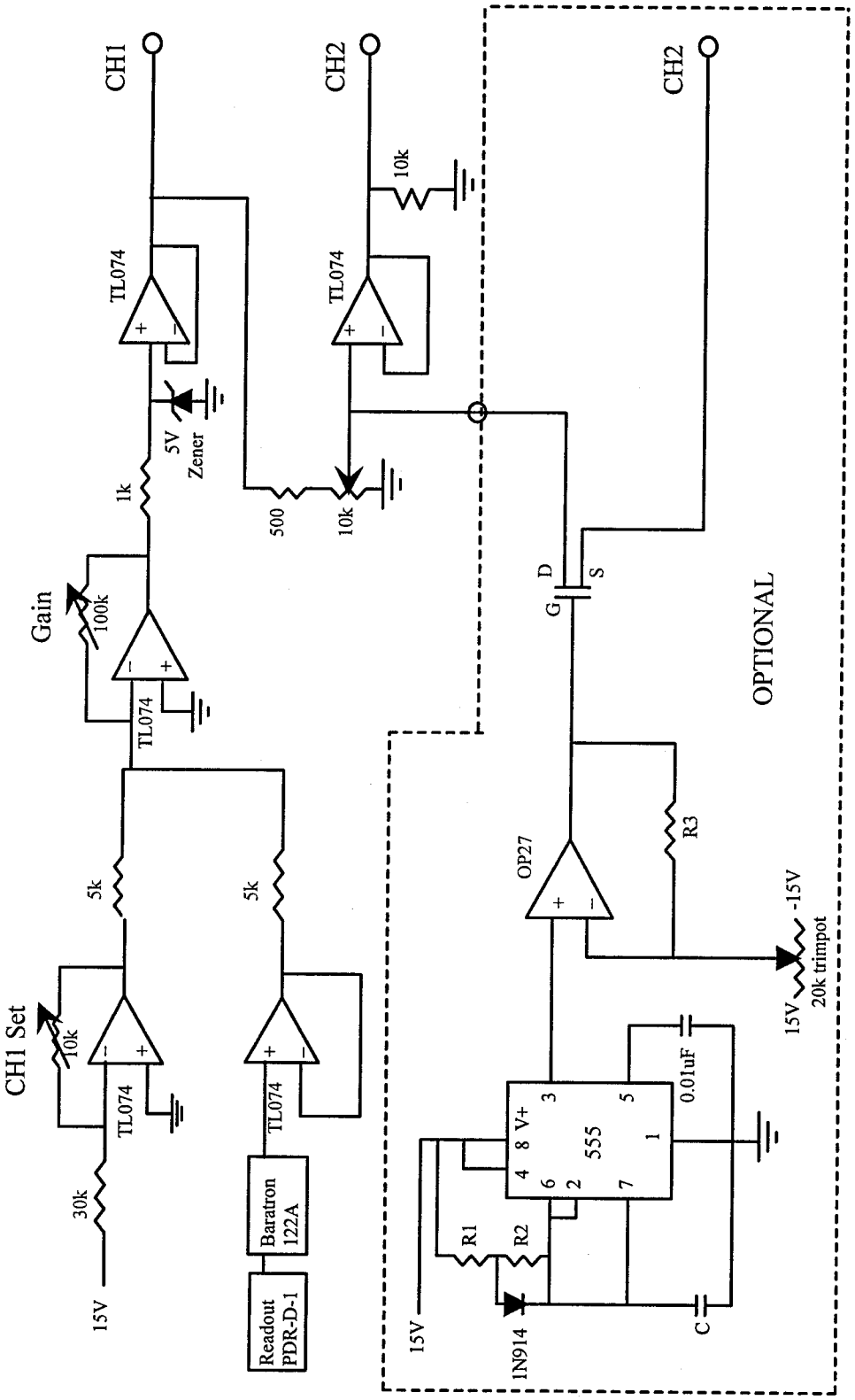
CH1
CH2
CH2
TL074
TL074
TL074
TL074
TL074
TL074
10k
10k
5V
Zener
1k
500
10k
Gain
100k
5k
5k
CH1 Set
10k
30k
15V
Baratron
122A
Readout
PDR-D-1
OPTIONAL
G
D
S
OP27
R3
-15V
15V
20k trimpot
15V
R1
R2
1N914
555
V+
0.01uF
C

Figure 3.

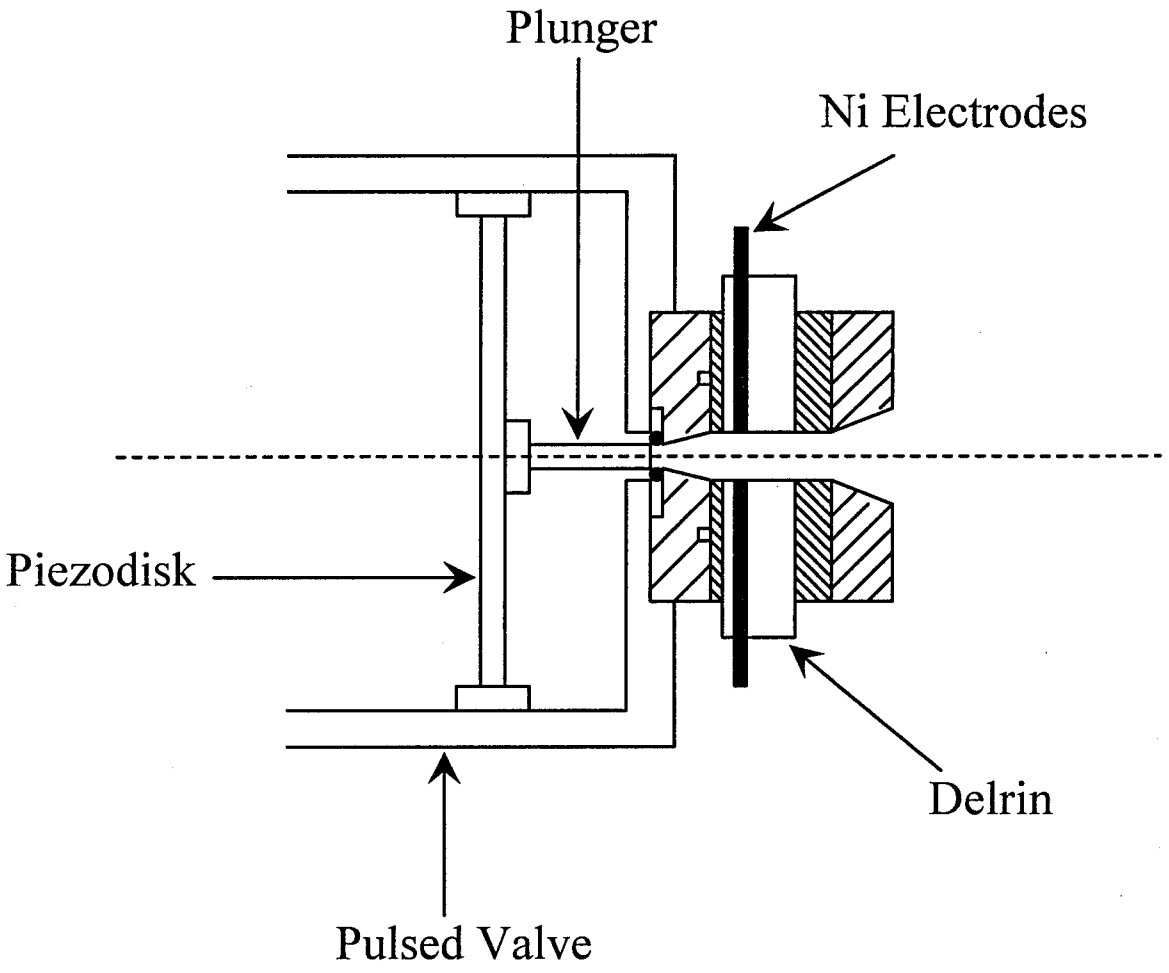

Figure 4.

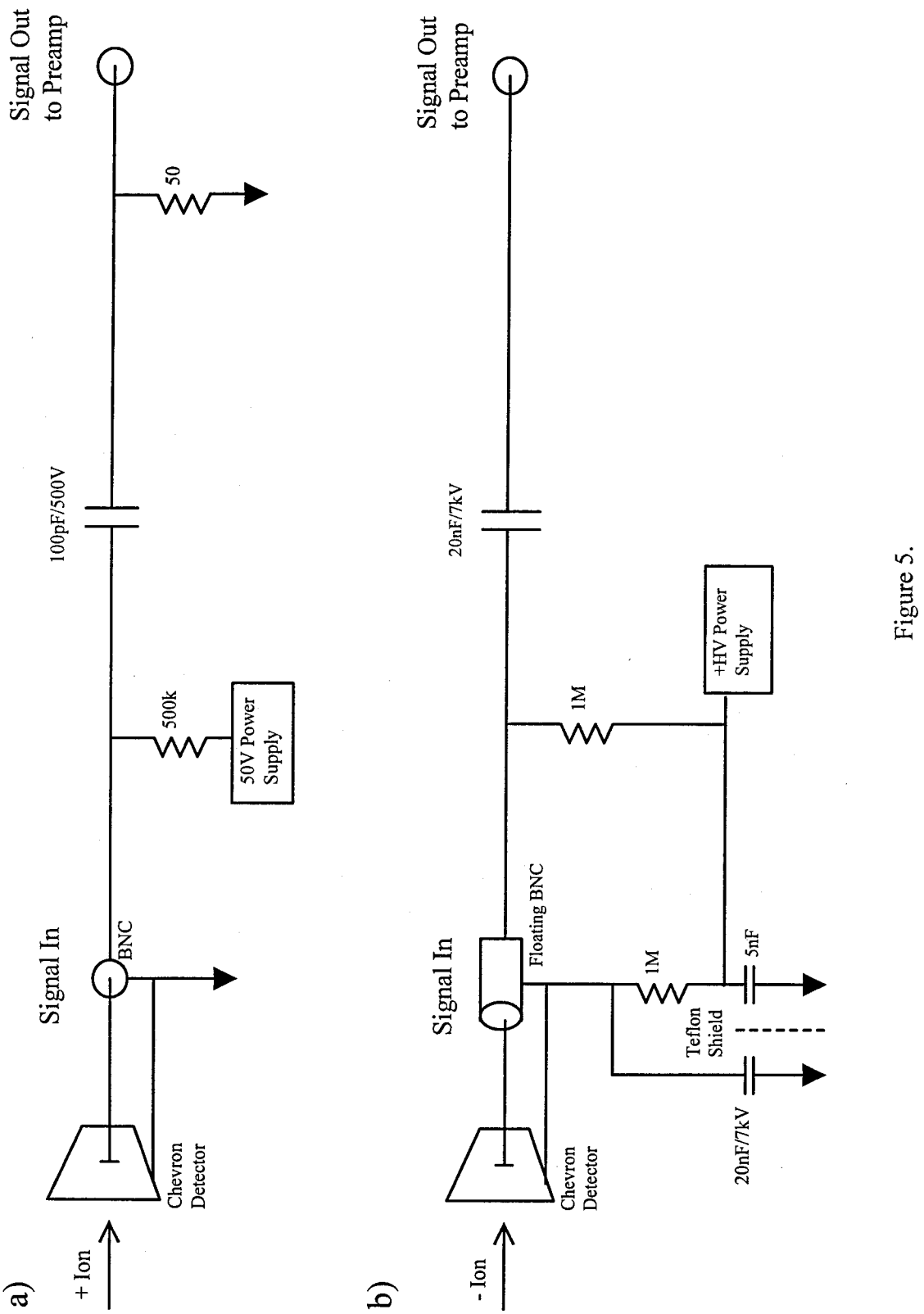
a)
+ Ion
Chevron Detector
Signal In
BNC
100pF/500V
500k
50V Power Supply
50
Signal Out to Preamp
b)
- Ion
Chevron Detector
Signal In
Floating BNC
20nF/7kV
1M
+HV Power Supply
1M
5nF
Teflon Shield
20nF/7kV
Signal Out to Preamp

Figure 5.

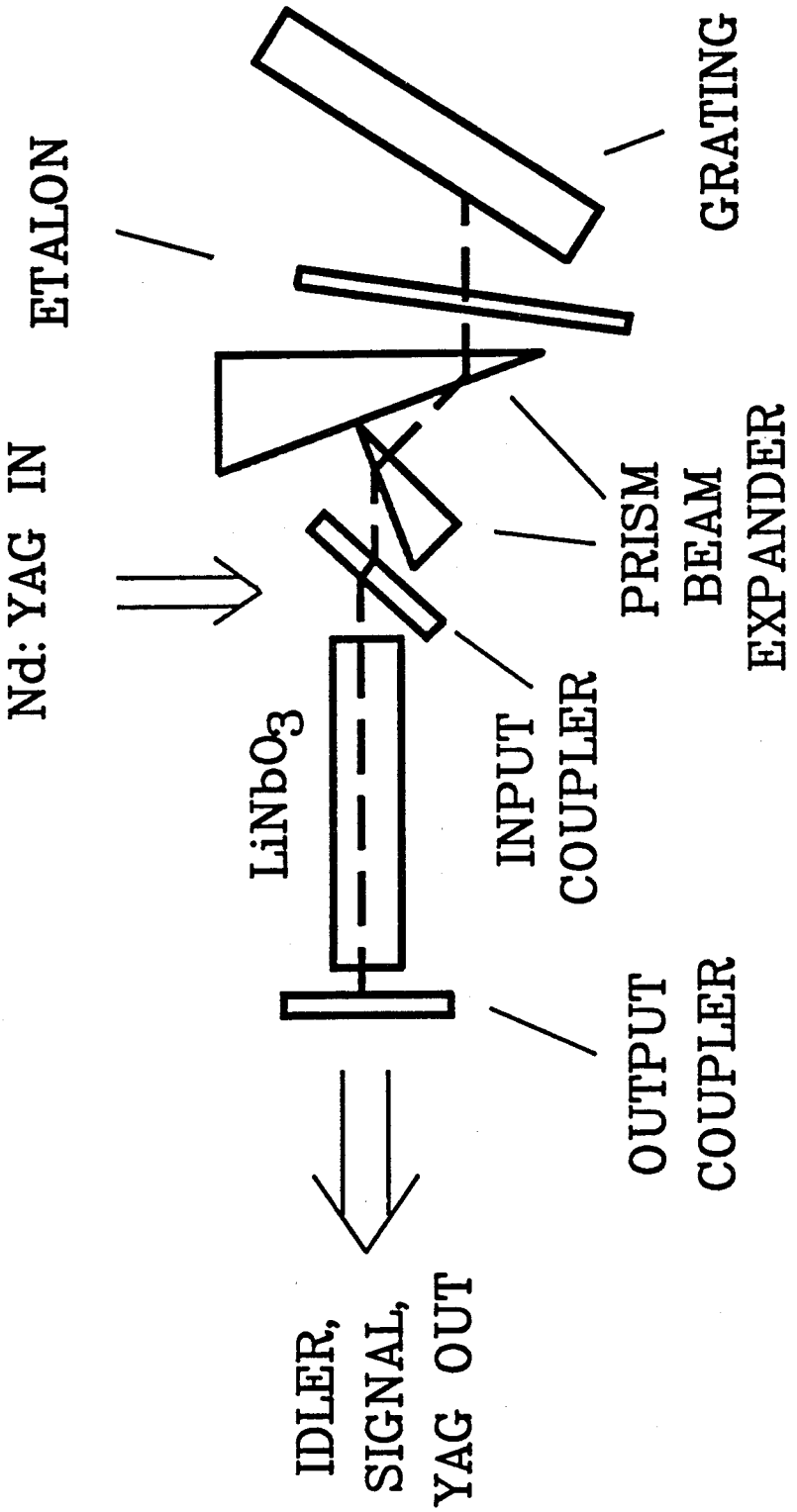
Nd: YAG IN
ETALON
GRATING
PRISM
BEAM
EXPANDER
INPUT
COUPLER
LiNbO3
OUTPUT
COUPLER
IDLER,
SIGNAL,
YAG OUT

Figure 6.

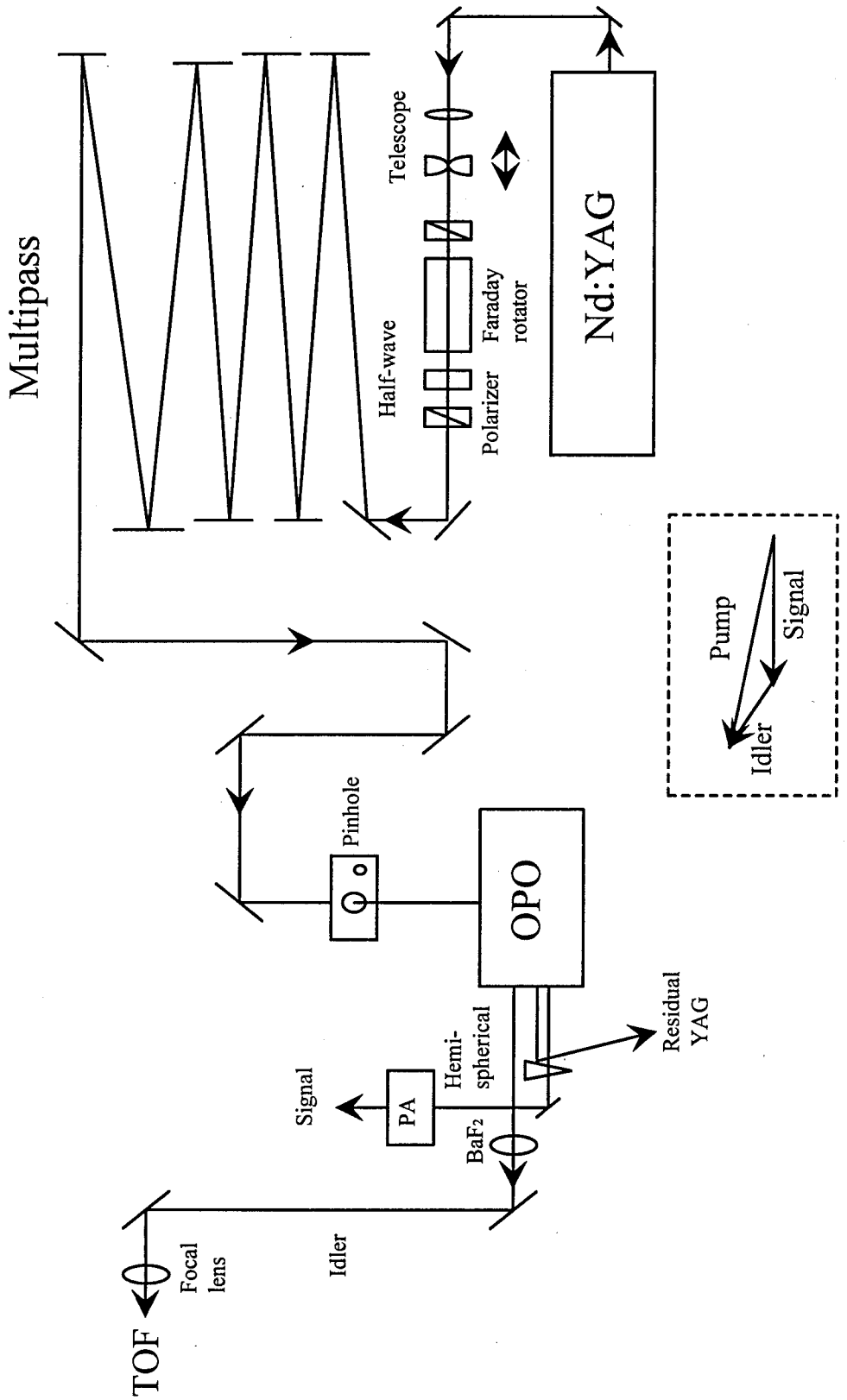
Multipass
Telescope
Half-wave
Faraday rotator
Polarizer
Nd:YAG
Pump
Signal
Idler
Pinhole
OPO
Residual YAG
Signal
PA
Hemi-spherical
BaF_2
Idler
Focal lens
TOF

Figure 7.

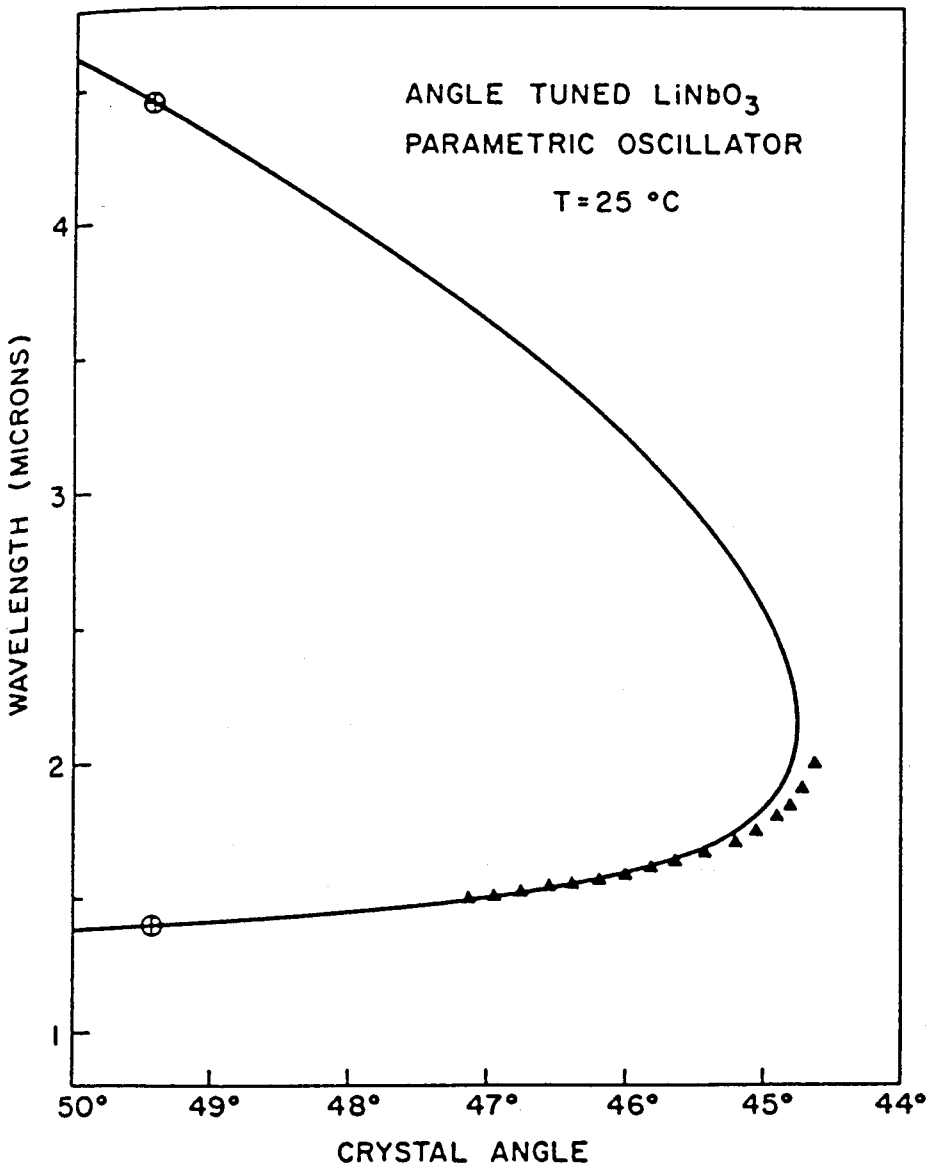
ANGLE TUNED LiNbO3
PARAMETRIC OSCILLATOR
T=25 °C
WAVELENGTH (MICRONS)
4
3
2
1
50°
49°
48°
47°
46°
45°
44°
CRYSTAL ANGLE

Figure 8.

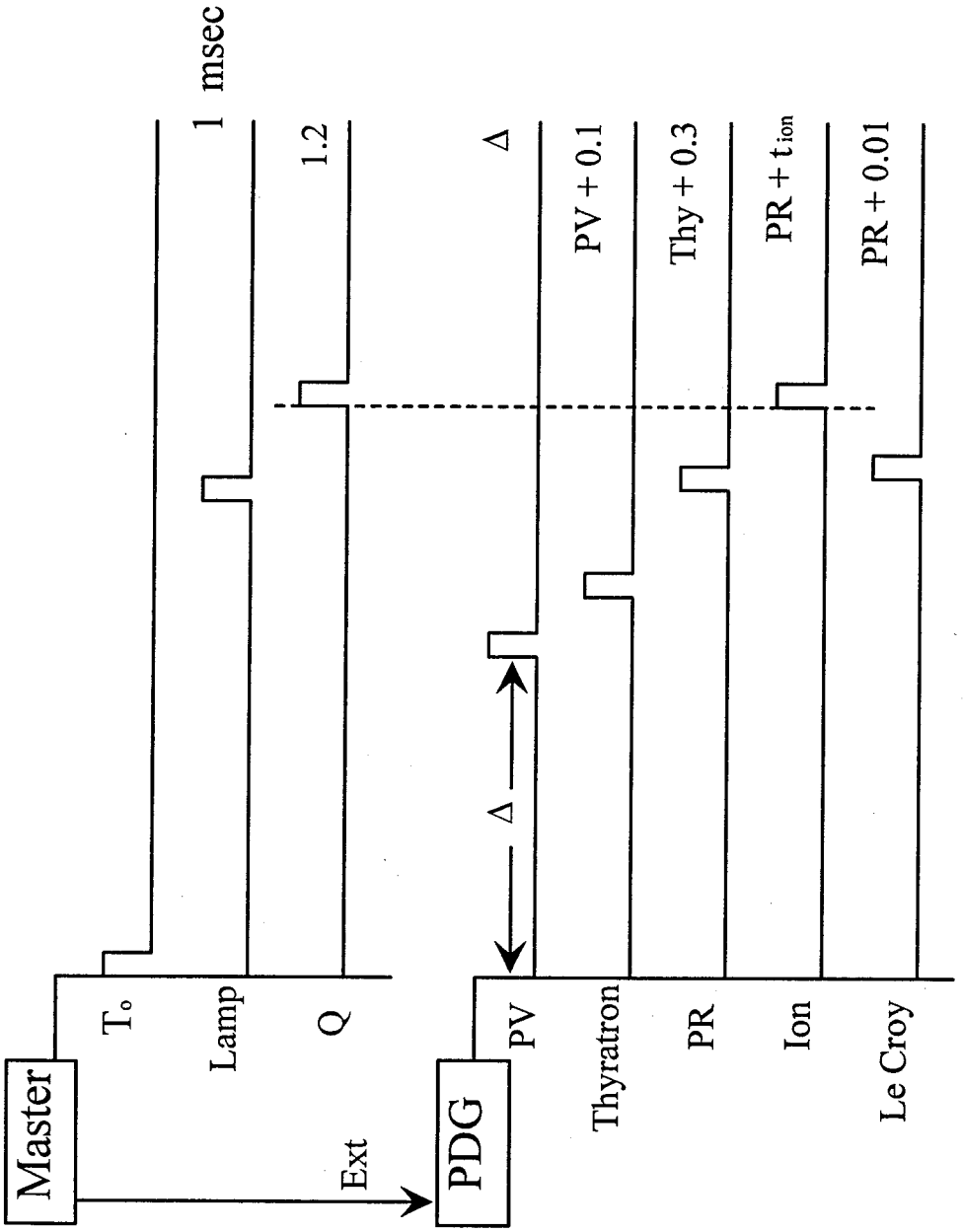
Master
Ext
T₀
Lamp
Q
1 msec
1.2
PDG
PV
Thyratron
PR
Ion
Le Croy
Δ
Δ
PV + 0.1
Thy + 0.3
PR + t ion
PR + 0.01

Figure 9.

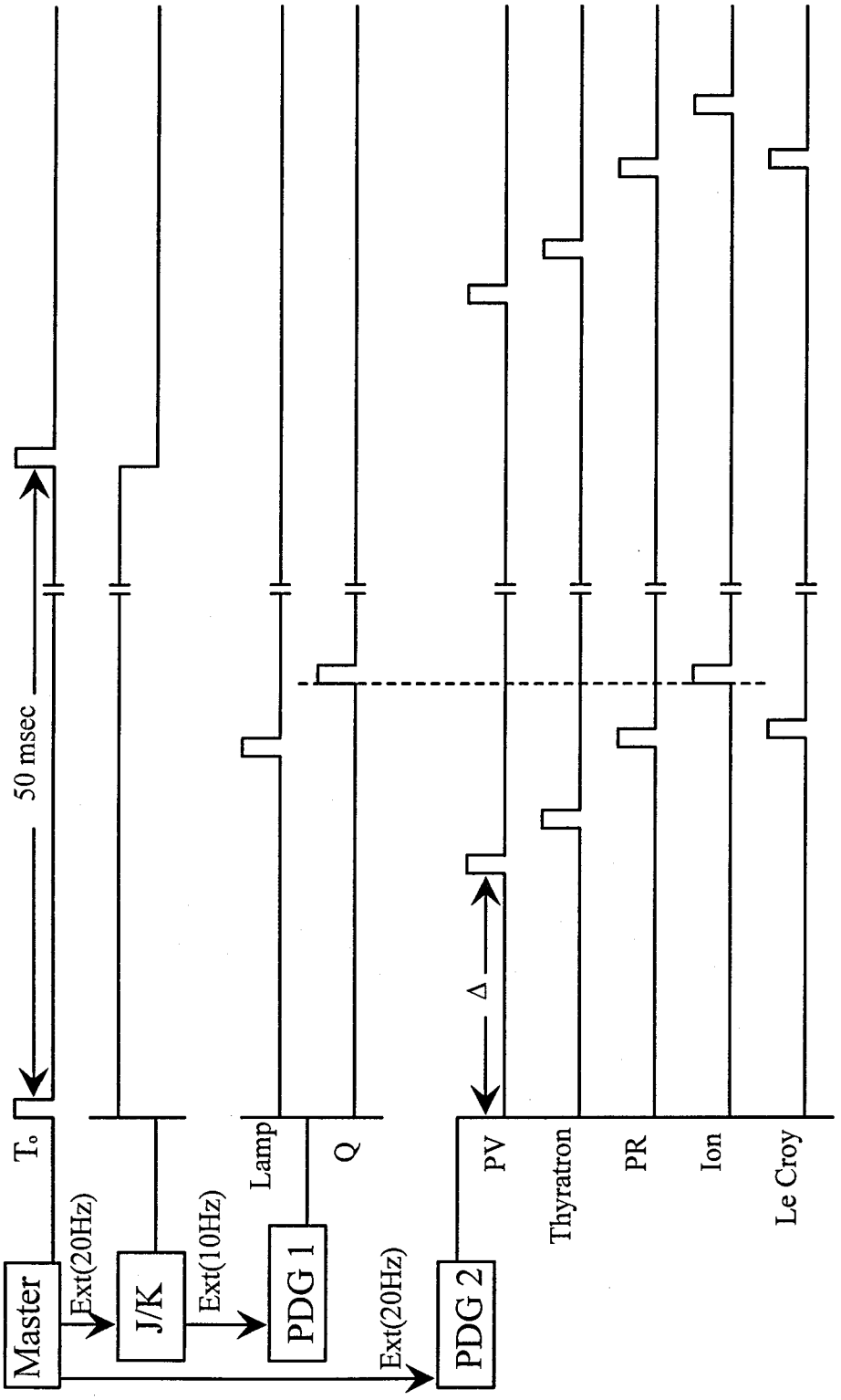
Master
Ext(20Hz)
J/K
Ext(10Hz)
PDG 1
Ext(20Hz)
PDG 2
T₀
50 msec
Lamp
Q
Δ
PV
Thyratron
PR
Ion
Le Croy

Figure 10.

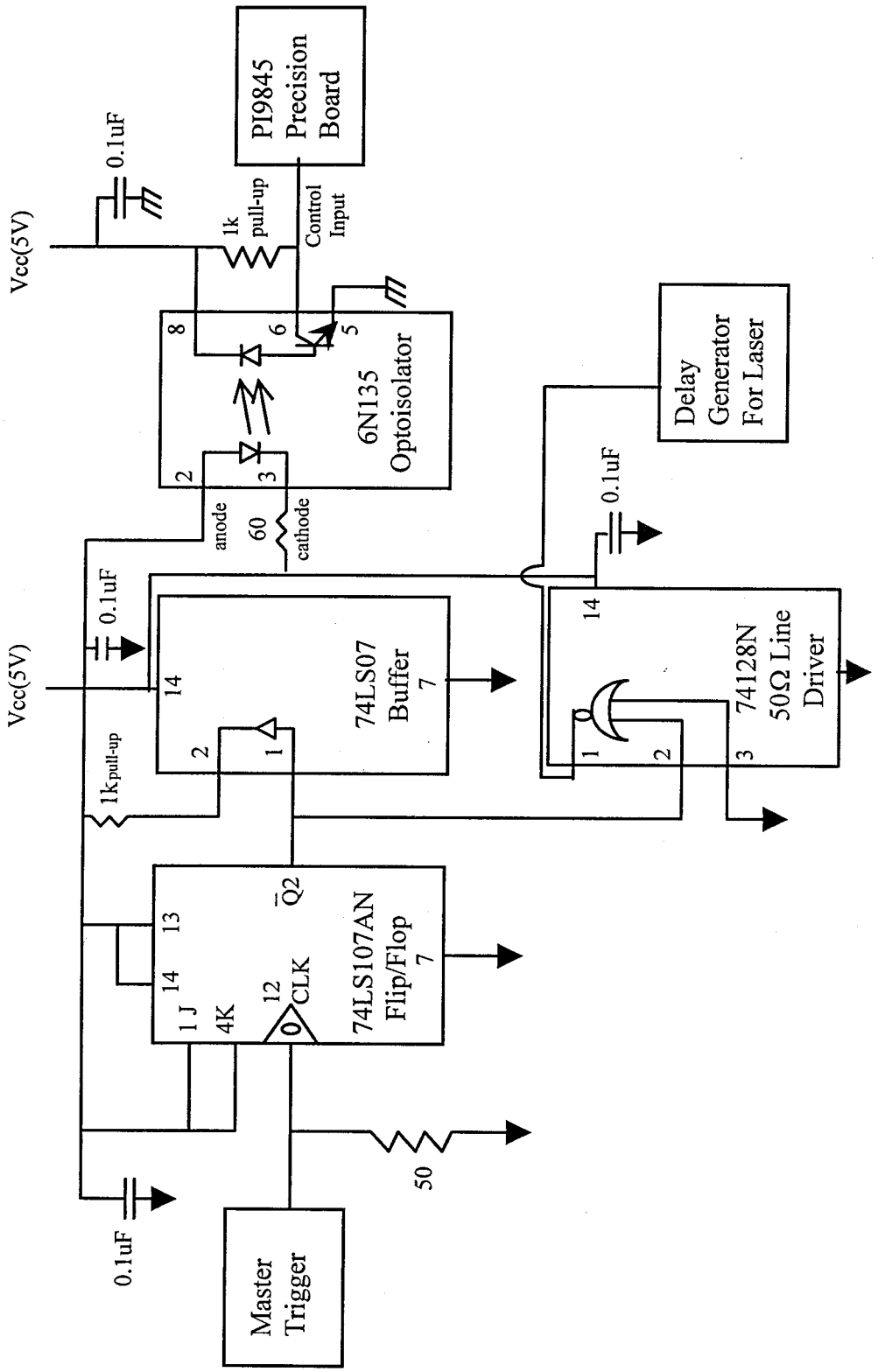
PI9845
Precision
Board
Control
Input
1k
pull-up
0.1uF
Vcc(5V)
6N135
Optoisolator
anode
cathode
60
Delay
Generator
For Laser
74LS07
Buffer
74128N
50Ω Line
Driver
74LS107AN
Flip/Flop
1J
4K
CLK
Q2
1kpull-up
50
Master
Trigger

Figure 11.

CHAPTER 3

Infrared Spectroscopy of $NO^+(H_2O)_n$: Evidence for the Intracluster Reaction $NO^+(H_2O)_n \rightarrow H_3O^+(H_2O)_{n-2}(HONO)$ at $n \geq 4$

3.1 INTRODUCTION

The nitrosonium ion NO^+ and its hydrates play an important role in the ion chemistry of Earth's upper atmosphere.[1] The NO radical possesses a low ionization potential (9.25 eV) and is thus readily ionized by either photoionization or charge transfer. NO^+ is the major primary ion in the D-region of the ionosphere, where it is formed by solar Lyman-α radiation. However, measurements of the positive ion composition in the ionosphere, beginning with rocket-borne mass-spectrometric observations by Narcisi and Bailey, have revealed that the predominant ionic species in the D-region are the hydronium ion hydrates, $H_3O^+(H_2O)_n$, with the distribution peaked at $n = 1$.[2] The conversion of NO^+ to $H_3O^+(H_2O)_n$ is now known to occur by a hydration mechanism.[3,4] NO^+ first undergoes a sequence of solvation steps to form a hydrated cluster ion, $NO^+(H_2O)_3$. This cluster subsequently reacts with another water molecule

$$NO^+(H_2O)_3 + H_2O \rightarrow H_3O^+(H_2O)_2 + HONO \qquad (1)$$

to form the hydrated hydronium ions.

Gas phase experiments on hydrated NO^+ clusters have examined the association kinetics and thermochemistry in order to understand the processes occurring in the ionosphere. Several groups used stationary[4,5] and flowing afterglow techniques[6,7] to measure the rate constants of the successive hydration steps and the final reaction (1). Puckett and Lineberger[8] identified the neutral product HONO in their stationary afterglow apparatus from their negative ion mass spectrum. French, Hills, and Kebarle[9] studied the kinetics and equilibria of NO^+ hydration by pulsed high-pressure mass spectrometry. They obtained hydration enthalpies of $\Delta H^\circ_{0,1} = -18.5 \pm 1.5$ kcal/mol for

NO^+ and $\Delta H°_{1,2} = -16.1 \pm 1.0$ kcal/mol for $NO^+(H_2O)$. They extrapolated these values to estimate $\Delta H°_{2,3} = -13.5 \pm 1.0$ kcal/mol. Burdett and Hayhurst[10] found a similar value for the hydration of NO^+ of $\Delta H°_{0,1} = -19.3 \pm 2.4$ kcal/mol in their studies of boundary layer cooling of ions sampled from flames.

In aqueous solution, NO^+ is a key intermediate in the nitrosation reactions of organic compounds.[11] Studies of nitrosation reactions have established that the mechanism depends on acidity. Both NO^+ and protonated nitrous acid are thought to participate in the rate-determining step at high acidity (pH ≤ 1). Protonated nitrous acid, $H_2NO_2^+$ (nitrosohydronium or nitrous acidium ion), is believed to exist as a weakly bound complex of NO^+ and H_2O, depicted in Fig. 1a, in equilibrium with NO^+:

$$H^+ + HONO \leftrightarrow NO^+(H_2O) \leftrightarrow NO^+ + H_2O \qquad (2)$$

The equilibrium constants are not accurately known and there has been no direct detection of $NO^+(H_2O)$ in the condensed phase.

Several theoretical calculations[12-17] have examined the optimized geometries of protonated nitrous acid, although no theoretical studies of the higher hydrates of NO^+ have been performed. The consensus is that the most stable form is an ion-molecule complex between NO^+ and H_2O, rather than a purely covalently bound cation. De Petris *et al.*[17] performed *ab initio* calculations that include electron correlation and predicted that protonated nitrous acid has six different isomers which are true minima on the potential energy hypersurface. For the lowest energy form, $NO^+(H_2O)$, they obtained an enthalpy of formation $\Delta H°_f = 160 \pm 2$ kcal/mol, in good agreement with the experimental value of 159.0 ± 1.5 kcal/mol based on the binding energy of $NO^+(H_2O)$.[9] They found

that the next lowest energy isomers are formed by protonating either the terminal oxygen to form $N(OH)_2^+$, or the nitrogen atom to form $HON(H)O^+$, isomers shown in Fig. 1. Both structures were calculated to have ΔH°_f over 41 kcal/mol higher than that of the $NO^+(H_2O)$ complex. Such energetic metastable isomers have not been observed experimentally.

If the complex $NO^+(H_2O)$ is the lowest energy isomer of protonated nitrous acid, the proton affinity of HONO is PA = 187.7 kcal/mol,[9] 21 kcal/mol higher than that of H_2O. Direct protonation of nitrous acid has not been observed in the gas phase because of the difficulty in generating pure HONO. Using collisionally-activated dissociation (CAD) mass spectrometry, De Petris *et al.*[17] found that only one isomer of protonated nitrous acid is produced in proton transfer reactions such as $H_3^+ + CH_3ONO$. They presented circumstantial evidence that this isomer is the complex $NO^+(H_2O)$. However, they observed no metastable signal and thus were unable to glean further structural information on protonated nitrous acid from kinetic energy release measurements.

Basic thermodynamic and kinetic data have been measured for reaction (1), but little is known about the mechanism and the role of the solvent H_2O in assisting the reaction. The reaction is estimated to be slightly endothermic (about +2 kcal/mol).[9,18] The rate constant[4-7] was found to be $k \approx 7 \times 10^{-11}$ cm^3/s based on disappearance of the $NO^+(H_2O)_3$ cluster. The production of $H_3O^+(H_2O)_2$ was inferred rather than directly measured because the hydronium ion hydrates equilibrated too rapidly. In speculating about the molecular mechanism of reaction (1), Fehsenfeld *et al.*[6] postulated intermediate cluster configurations in which not all H_2O moieties solvated the NO^+, but conventional

mass spectrometric and kinetics experiments have shed no further light on their key idea that the reaction requires solvent reorganization within an activated cluster.

IR photodissociation spectroscopy coupled with tandem mass spectrometry has proven to be a powerful method for investigating cluster ions.[19-22] We have recently investigated similar intracluster reactions in hydrated nitronium ion clusters $NO_2^+(H_2O)_n$ using the technique of vibrational predissociation spectroscopy.[23,24] In these experiments, the infrared spectra of mass-selected ions are obtained by detecting photofragment ions as a function of laser frequency. We observed a dramatic change in the vibrational spectrum and dissociation branching ratio of the NO_2^+ hydrate clusters at a critical cluster size, indicative of an intracluster reaction.

In this chapter we describe our investigations of the vibrational predissociation spectroscopy of the hydrated clusters of the nitrosonium ion, $NO^+(H_2O)_n$. We report infrared spectra and photofragment yields for $n = 1–5$. We have also performed *ab initio* calculations of the vibrational frequencies and intensities of the clusters $n = 1$ and 2 to confirm our vibrational assignments. Our calculations were undertaken because there were no published theoretical estimates of the vibrational frequencies for $n = 1$, nor of the structure, energetics, and vibrational frequencies for $n = 2$.

3.2 EXPERIMENT

The apparatus employed in these experiments was described in Chapter 2 and other reference,[24] and only a brief account will be presented here. $NO^+(H_2O)_n$ ($n = 1$ to 5) clusters were generated by a high pressure, pulsed discharge source. An MKS mass-flow

controller was used to produce a mixture of 12% NO (Matheson Gas Co. purity 99%) seeded in ultrahigh purity (99.999%) H_2 or He. Hydrate clusters could be readily formed using only the trace water vapor already present in the stainless steel inlet line. The pressure was 1000 Torr at room temperature in the stagnation volume of a piezo-driven pulsed valve. Gas was pulsed (200 μs wide) at a repetition rate of 10 Hz into a 1 mm diameter, 1.5 cm long channel and expanded into the first differential vacuum chamber maintained at 2 to 5 $\times 10^{-5}$ Torr by a 10 in. diffusion pump. A discharge was struck as the gas flowed through the channel by applying a high voltage pulse (-1.0 to -3 kV, 100 μs wide) between two electrodes near the entrance. The ions formed in the plasma were thermalized as the gas flowed through the channel and further cooled in the supersonic expansion. The expanding plasma was skimmed and entered a second region (6 in. diffusion pump, 1×10^{-6} Torr) containing the time-of-flight ion optics. The ions were extracted by a pulsed electric field 15 μs in duration and accelerated to 1.3 kV, focused by a pair of einzel lenses. The ions passed through an additional stage of differential pumping (4 in. diffusion pump, 1×10^{-6} Torr) and entered the photolysis chamber (500 *l*/s turbomolecular pump, 3×10^{-7} Torr).

Parent ions of a specific mass were selected by a 1-cm-long mass gate which rejected all ions of other *m/e*. The ions were vibrationally excited by a collimated infrared beam, which was generated by a pulsed $LiNbO_3$ optical parametric oscillator[25] (OPO) and timed to intersect the selected ions at the spatial focus of the time-of-flight mass spectrometer. The OPO was pumped by a Quanta Ray GCR 12S Nd:YAG laser whose 1.06 μm output was propagated 3 m to achieve a nominally Gaussian transverse

mode at the input of the OPO. The OPO was tunable from 2700 to 6700 cm^{-1} by simultaneously adjusting the crystal and grating angles. Typical OPO pulse energies were about 3 to 5 mJ with a line width of 1.5 cm^{-1}. The laser beam path from the OPO to the vacuum chamber was purged with dry air to eliminate absorption by water vapor.

The fragment ions resulting from IR excitation were separated from the parent ions using a reflectron energy-analyzer, and then detected by a microchannel plate detector. The signal was preamplified and then collected by a transient digitizer. Predissociation spectra were obtained by stepping the OPO wavelength and averaging the photofragment ion signal for 200 shots at each wavelength. Fragment ion background arising from dissociation of metastable parents was subtracted to obtain the fragment signal due solely to photodissociation. The data were then normalized with respect to the OPO pulse energy. Between 2 and 14 such scans were averaged, depending on the photofragment signal intensity. The OPO laser wavelength was calibrated during the scan by simultaneously recording the rovibrational spectra of either methane or hydrogen chloride in a photoacoustic cell.

3.3 EXPERIMENTAL RESULTS

A typical time-of-flight mass spectrum of nitrosonium ion hydrate clusters is shown in Fig. 2. While this distribution peaked at $NO^+(H_2O)_2$, it could be shifted by varying the stagnation pressure, temperature, source voltage, and pulsed valve settings. Two additional series of hydrates can be seen in Fig. 2, $H_3O^+(H_2O)_n$ and, very weakly,

$(NO)_2^+(H_2O)_n$. The relative intensities of these species also varied, but did not interfere with the measurements reported here.

We recorded infrared spectra of mass-selected clusters $NO^+(H_2O)_n$ for n = 1–5 in the 2700–3800 cm^{-1} region. Fig. 3 presents the infrared spectra for n = 1–5 over the entire frequency range and Table I lists the observed band maxima.

A. Photodissociation behavior

The only photofragment ions detected upon infrared excitation of the clusters $NO^+(H_2O)_n$ (n = 1 to 3) were $NO^+(H_2O)_{n-1}$, indicating that a single water molecule evaporated upon vibrational excitation:

$$NO^+(H_2O)_n \rightarrow NO^+(H_2O)_{n-1} + H_2O, \qquad n = 1-3 \qquad (3)$$

Fig. 4 shows the dependence of the photodissociation signal on laser pulse energy for these three clusters when exciting the band observed at ~3620 cm^{-1}. The dissociation signal for n = 1 exhibited a quadratic dependence, as seen from the linear dependence of the square root of the signal plotted against laser pulse energy in Fig. 4a. The dissociation of n = 1 clusters thus involved two-photon excitation. The rollover at high fluence probably resulted from saturation. In the case of n = 2, the fragment ion signal showed both linear and nonlinear behavior depending on source conditions. In Fig. 4b, the signal was a sum of linear and quadratic terms, since the plot of the square root of signal vs. pulse energy approached a straight line only at higher energies. Under alternate source conditions, shown in Fig. 4c, the signal depended linearly on the pulse energy. The detected signal for n = 3 depended linearly on laser power as shown in Fig. 4d, indicating that the predissociation of this cluster was a single photon process.

Infrared excitation of the $n = 4$ cluster produced photofragments at three masses, corresponding to $NO^+(H_2O)_3$, $NO^+(H_2O)_2$, and $H^+(H_2O)_3$. Thus, the following photodissociation processes were competing:

$$NO^+(H_2O)_4 \rightarrow NO^+(H_2O)_3 + H_2O \quad (4a)$$

$$\rightarrow NO^+(H_2O)_2 + 2H_2O \quad (4b)$$

$$\rightarrow H_3O^+(H_2O)_2 + HONO \quad (4c)$$

The major dissociation channel was loss of one water, channel (4a). The minor $NO^+(H_2O)_2$ product in (4b) is likely due to evaporation of a neutral water dimer $(H_2O)_2$, although an alternative is the secondary spontaneous dissociation of the primary product ion in channel (4a), a process which requires more energy. The observation of channel (4c) signaled the onset of a new dissociation channel, loss of a nitrous acid molecule. The relative yields were wavelength dependent. When exciting absorption bands observed in the 3600-3800 cm^{-1} region, the branching ratio of channels, (4a), (4b), and (4c) was 8 : 1.5 : 1. Contributions from (4b) and (4c) were negligible when exciting bands in the 3400 cm^{-1} region.

There was a significant change in the photofragmentation pattern of the $n = 5$ cluster, $NO^+(H_2O)_5$. We detected photofragments at three masses: $H^+(H_2O)_4$, $H^+(H_2O)_3$, and $NO^+(H_2O)_4$. The dominant channel throughout the observed spectral region was

$$NO^+(H_2O)_5 \rightarrow H_3O^+(H_2O)_3 + HONO \quad (5)$$

Thus, unlike the smaller clusters, infrared excitation of $n = 5$ led almost exclusively to loss of neutral nitrous acid.

B. Vibrational predissociation spectra

The infrared spectrum of protonated nitrous acid (n = 1) exhibited a single vibrational band in the 2700-3800 cm^{-1} range (Fig. 3a). This band was only 50 cm^{-1} lower in frequency than the symmetric stretch of the water monomer (Table I). Closer examination revealed that the band was a doublet with maxima at 3599 cm^{-1} and 3611 cm^{-1}, as seen in Fig. 5a.

The clusters $NO^+(H_2O)_n$, (n = 2 and 3) had two absorption bands in the 2700–3800 cm^{-1} region (Figs. 3b and c, Table I). The lower frequency bands at ca. 3625 cm^{-1} were sharp and resembled in shape and position the band observed for $NO^+(H_2O)$. The higher frequency bands at ca. 3700 cm^{-1} were broad. Based on the proximity of these bands to the H_2O monomer stretch frequencies,[26] we assigned these bands to the symmetric and antisymmetric stretch modes of water ligands respectively.

The spectrum of n = 4, shown in Fig. 3d, consisted of four bands. Two bands at 3635 cm^{-1} and 3713 cm^{-1} were similar to the bands observed in $n \leq 3$, while two new bands at 3230 cm^{-1} and 3375 cm^{-1} were substantially broader. The two high frequency bands were assigned to H_2O symmetric and antisymmetric stretches, respectively. The two lower frequency bands were broad and significantly red-shifted relative to the other OH bands, indicative of an OH bond involved as a donor in hydrogen bonding.

The spectrum of the n = 5 cluster was qualitatively different from those of the smaller clusters. The infrared absorption spectrum of the $NO^+(H_2O)_5$ cluster shown in Fig. 3e possessed seven distinct bands, two in the 2700-3200 cm^{-1} region, and five others in the 3500-3800 cm^{-1} region.

The strongest band, at 2800 cm^{-1}, was broad and had the appearance of the stretching band of an ionic OH group participating as a donor in hydrogen bonding. Such bands were first observed in $H_3O^+(H_2O)_n$ clusters by Schwarz.[27] Lee and co-workers[19] in their studies of $H_3O^+(H_2O)_n$ clusters and Cao *et al.*[23] in their studies of $NO_2^+(H_2O)$ observed similar bands and assigned them to the hydrogen-bonded OH antisymmetric stretch of the H_3O^+ ion. In general, these vibrations occurred below 2700 cm^{-1} unless the hydronium ion was fully solvated. We therefore concluded that the n = 5 clusters possessed a hydronium ion core, with ligands bonded to all three OH bonds.

The strong H_3O^+ band is often accompanied by a broad but weaker band at higher frequency. We assigned the weaker 3190 cm^{-1} band as this companion mode. The exact assignment of such bands (symmetric stretch of H_3O^+, bending overtone, combination band) is still a matter of uncertainty.[19,27]

The five higher frequency bands of the n = 5 spectrum can be assigned as OH stretches of the ligands bound to the H_3O^+ core. One of the two bands near the OH stretching frequency of the *trans* nitrous acid monomer[28,29] (3591 cm^{-1}) could be assigned to the free OH stretch of HONO; the remaining bands we assigned to H_2O. Detailed assignments based on a proposed structure will be discussed below.

3.4 *AB INITIO* CALCULATIONS

To help the analysis of the predissociation spectra of the n = 1 and n = 2 clusters, Keith Kuwata in our group performed *ab initio* calculations using the Gaussian 92 system

of programs[30] on a Cray Y-MP supercomputer. Detailed description is given in the reference and only a salient account is given here.*

Geometries and vibrational frequencies were calculated at the Hartree-Fock (HF) and the second-order Møller-Plesset (MP2) level using the 6-31G** basis.[31,32] In order to relate the *ab initio* frequencies to experimental values, the two stretch frequencies of free H_2O at the MP2/6-31G** level were also calculated: 3894 cm^{-1} (ν_1) and 4032 cm^{-1} (ν_3). Single point energies were computed at the coupled cluster with single and double excitations (CCSD) level of theory using the 6-31G** basis set for n = 2, and the 6-311G(2*df*,2*pd*) basis set for the n = 1 isomers (see Table II). All electrons were correlated at the MP2 level, but core electrons were frozen at the CCSD level. CCSD-level binding energies and enthalpies were calculated at their MP2-optimized geometries. Corrections for zero-point vibrational energy were made to both the MP2 and CCSD energies using the MP2-level vibrational frequencies. Binding enthalpies at 298 K were estimated using the MP2 frequencies.

For n = 1, the three geometries obtained by De Petris *et al.*,[17] $NO^+(H_2O)$, $N(OH)_2^+$, and $HON(H)O^+$, were used as the initial guesses and optimized at the MP2/6-31G** level. Substantially the same results were obtained for all three isomers. Harmonic vibrational frequencies and infrared intensities (Tables III, IV, and V) were then determined using analytical second derivatives. All frequencies found were real, which confirmed that the optimized structures obtained were true minima of the potential energy hypersurface. The optimized wave function of $NO^+(H_2O)$ (Fig. 1a) showed that the oxygen atom of the water binding to the nitrogen end of the cation carries ~70% of

the charge. The N···O separation is 2.202 Å, and the O=N···O bond angle is 100.2°. The geometries of the NO^+ and H_2O moieties do not differ significantly from those of free NO^+ and H_2O.

The binding enthalpy of the ground state isomer is $\Delta H°_{298}$ = 20.9 kcal/mol (see Table VII), slightly higher than the experimental enthalpy of 18.5 kcal/mol.[9] The 'W' shaped isomer, $HONOH^+$, had an enthalpy $\Delta H°_{298}$ = 31.5 kcal/mol above that of the $NO^+(H_2O)$ isomer. The enthalpy of the $HON(H)O^+$ isomer, formed by protonating the nitrogen atom of *cis* HONO, was $\Delta H°_{298}$ = 34.6 kcal/mol above the cluster isomer. Both higher lying isomers possessed strong X–H (X = N, O) absorption bands, but the scaled vibrational frequencies all were below 3500 cm^{-1} (see Tables IV and V).

There has apparently been no previous theoretical work on the n = 2 clusters. It was assumed that the isomer of interest would be of the form $NO^+(H_2O)_2$, with at least C_s and perhaps C_{2v} symmetry. The structure was fully optimized under these symmetry constraints at both the HF and the MP2 levels. Fig. 6 shows the optimized C_s geometry obtained for the minimum energy structure of $NO^+(H_2O)_2$ at the MP2/6-31G** level. The H_2O molecules both bind to the nitrogen atom. The ion-solvent bond lengths are 2.318 Å and the O···N···O angle is 109.9°. The N-O bond is predicted to be only 5.9° from perpendicular with respect to the O···N···O plane. The CCSD binding enthalpy (Table VII) is 17.5 kcal/mol, in good agreement with the value of 16.1 ± 1.0 kcal/mol measured by French *et al.*[9]

3.5 DISCUSSION

A. Protonated nitrous acid, $NO^+(H_2O)$

The experimental results on the $n = 1$ cluster are most consistent with the structure of a weakly bound ion-molecule complex, $NO^+(H_2O)$. We find that photodissociation of protonated nitrous acid leads to $NO^+ + H_2O$ products. The frequency of the observed vibrational band, 3605 cm^{-1}, agrees within 5% of the scaled MP2 frequency of the H_2O symmetric stretch, 3587 cm^{-1}. We do not observe an antisymmetric stretch band, which our calculations predict would occur at 3671 cm^{-1} (scaled) with an intensity 80% of that of the symmetric stretch.

From the quadratic fluence dependence, we find that dissociation requires at least two photons, placing a lower limit of 10.3 kcal/mol on the $NO^+\cdots(H_2O)$ binding energy. This lower bound is consistent with the dissociation enthalpy measured by French *et al.*[9] of 18.5 ± 1.5 kcal/mol, and with our CCSD estimate of the dissociation enthalpy, $\Delta H°_{298}$ = 20.9 kcal/mol. Our result places a lower bound on the proton affinity of nitrous acid of PA ≥ 179.5 kcal/mol, consistent with the theoretical value of PA = 187 kcal/mol calculated by De Petris *et al.*[17]

The O=N···O angle predicted by the MP2/6-31G** calculation is sharply bent, and the water molecule is oriented with a lone pair pointed towards the N atom. This geometry can be understood as the lone pair electrons of the O atom of H_2O donating density into the empty π^* orbitals of NO^+, which have significant p character on the N atom.

The *ab initio* structure for $NO^+(H_2O)$ is a near prolate top with rotational constants of $A = 1.96$ cm^{-1}, $B = 0.239$ cm^{-1}, and $C = 0.219$ cm^{-1}, yielding an asymmetry parameter of $\kappa = -0.977$. Using this calculated geometry, we can simulate the rotational envelope of the H_2O symmetric stretch band. The symmetry axis of the H_2O moiety is approximately collinear with the *a* axis of the cluster; therefore, excitation of the symmetric H_2O stretch will result in approximate *a*-type selection rules. We have modeled the rotational contour by deriving a predicted rovibrational spectrum for a semi-rigid rotor and then convoluting it with a Gaussian linewidth function. We used centrifugal distortion constants and differences between upper and lower state constants similar to those in HONO,[28] although the $NO^+(H_2O)$ complex will be floppier. Fig. 5 compares the observed band contour with a simulation of the rovibrational spectrum at a rotational temperature 120 K, convoluted with our laser linewidth of 1.5 cm^{-1}. This temperature is realistic, given that we have successfully fit a spectrum of SiH_7^+ clusters formed in the same source using 90 K.[20] Both the width of the band and the doublet shape and splitting are well simulated. The relatively narrow width of the band can only be simulated by an *a*-type transition. The doublet structure stems from the *P* and *R* branches, with the relatively weak *Q* branch blending into the *P* branch. The band intensity is weighted towards the *P* branch, indicating that the rotational constant ½ $(B'+C')$ increases slightly in the upper state. Such a change can occur if the O=N···O angle decreases slightly upon excitation. In summary, the rotational contour is consistent with both the predicted rotational constants and selection rules, and provides further confirmation in support of the proposed structure.

The only discrepancy between the experimental results and the proposed structure is the absence of the antisymmetric stretch in the experimental spectrum. Our *ab initio* calculations predict that in $NO^+(H_2O)$, both OH stretch bands have intensities considerably enhanced over those in neutral H_2O. However, the antisymmetric band intensity, normally significantly stronger than that of the symmetric stretch, is calculated to be slightly weaker.

An explanation for the observation of only one OH stretch band is that the structure is the covalently bound $N(OH)_2^+$ (Fig. 1b), for which the two OH vibrations are nearly degenerate. We discount this possibility for several reasons. First, it is unlikely that this isomer is formed. $N(OH)_2^+$ is calculated to be a highly energetic metastable lying ΔE_0 = 31.5 kcal/mol above the ion-molecule complex. Previous experiments find no evidence for this isomer in flow tubes, stationary afterglows, and high pressure discharges. Our source is also a high pressure discharge with the plasma occurring in a narrow channel followed by supersonic expansion, and the chemistry is similar. Second, in order for two photon excitation to dissociate $N(OH)_2^+$, an intramolecular hydrogen atom transfer over two atoms, from one O atom to the other, must occur followed by cleavage of the $NO^+\cdots(OH_2)$ bond. The barrier for what is essentially a 1,3 hydrogen shift must be less than 21 kcal/mol. Third, our MP2 calculations predict that the OH stretches for this isomer are not actually degenerate, but are rather split by 50 cm^{-1}. Furthermore, the scaled OH symmetric and antisymmetric stretching frequencies of $N(OH)_2^+$ are predicted at 3390 and 3338 cm^{-1} respectively, *i.e.*, more than 200 cm^{-1} below the observed transition, and thus disagree with experiment.

Similar reservations apply to the covalent structure formed by protonating the nitrogen atom, $HON(H)O^+$. This isomer is predicted to be ΔE_0 = 36 kcal/mol above the $NO^+(H_2O)$ energy, and it can only dissociate to $NO^+ + H_2O$ following isomerization by a hydrogen shift. The barrier for this shift, with the proton bridging an N—O sigma bond, is also likely to be high. Furthermore, our calculations predict that there will be two bands in the region scanned, the OH and NH stretches, both having scaled frequencies 280 cm^{-1} or more to the red of the observed band.

The reason for the absence of an antisymmetric H_2O stretch absorption may lie in the fact that the spectra are not absorption spectra, but rather two-photon dissociation spectra. A discrepancy can come about if (a) the multiphoton absorption process is highly inefficient for ν_3 relative to ν_1 absorption, or (b) clusters excited in this mode do not efficiently dissociate.

There is a physical basis for a larger two photon absorption cross section for the v_1 absorption. Multiphoton absorption occurs either by sequential absorption, *e.g.*, $0 \rightarrow v_3 \rightarrow 2v_3$ or nonresonantly via an intermediate virtual state. In the free H_2O monomer, the anharmonicity constants[33] are x_{11} = –43 cm^{-1}, x_{13} = –155 cm^{-1}, and x_{33} = –46 cm^{-1}. Thus, the $v_1 \rightarrow 2v_1$ and $v_3 \rightarrow 2v_3$ transitions are off resonance from the fundamentals by over ~170 cm^{-1}. However, the $v_1 \rightarrow v_1 + v_3$ transition is at 3600 cm^{-1}, close to the v_1 frequency of 3657 cm^{-1}. Thus, two photon excitation of the symmetric stretch will be far more efficient because the second photon can excite the red-shifted antisymmetric stretch hot band transition. The $0 \rightarrow v_1 \rightarrow v_1 + v_3$ process is therefore a near-resonant two photon process. While the frequencies differ in the n = 1 cluster, this effect should still

be qualitatively correct. Thus, two-photon dissociation was observed for ν_1 while the ν_3 band was too weak to be detected experimentally. We plan to test this hypothesis in a two color photodissociation experiment.

The weakness of two photon ν_3 absorption is also consistent with the appearance of the antisymmetric stretch band in all larger hydrates of NO^+ and its increases in intensity with cluster size relative to the ν_1 band. As discussed in the next section, this result can be explained if the ν_3 signal in the larger clusters arises from one photon dissociation.

The absence of a band due to the ν_3 vibration could also arise because this mode relaxes more slowly than ν_1. The ν_3 mode has A'' symmetry and will be not be as strongly coupled to the intermolecular stretch as the ν_1 mode, which possesses A' symmetry. The differences in coupling could then lead to variations in predissociation rates. If clusters prepared by exciting the ν_3 band predissociate with lifetimes greater than ca. 10 μs, they would be undetected. Alternatively, relaxation rates could affect the observed action spectra if two-photon absorption takes place by the following three-step process: excitation of a 0 to 1 transition, intramolecular vibrational relaxation (IVR) of the O-H stretch, and subsequent reexcitation of the 0 to 1 transition of the hot cluster. If IVR from the ν_3 levels occurs on time scales longer than the laser pulsewidth (10^{-8} s), the second photon would not be absorbed, and no dissociation would occur. IVR from ν_1 mode must then occur at rates faster than 10 *n*s to account for the observed band. This possibility could be tested by exciting clusters at ν_3 with two pulses separated by about 100 *n*s.

B. $NO^+(H_2O)_n$, $n = 2$ and 3

The predissociation spectra and the photoproducts of $NO^+(H_2O)_n$ (n = 2 and 3) suggest that these clusters also have water ligands bound to an NO^+ ion core. Unlike the n = 1 cluster, both symmetric and antisymmetric stretch bands are observed. These vibrations gradually shift to higher frequencies with cluster size going from n = 1 to 3 (Fig. 3), as expected for the increasing hydration of the NO^+ ion core.

The reduction in binding energy with n is also evident in the fluence dependence of the photodissociation yield when exciting the ν_1 band. This dependence can be either linear or nonlinear for n = 2, and becomes linear for n = 3. In the n = 2 case, the photon energy is less than the cluster dissociation energy and the linear dependence arises from dissociation of vibrationally hot ions. When the distribution is cold, then signal from two photon dissociation is comparable to one photon dissociation of a smaller population of vibrationally hot complexes, resulting in both linear and quadratic contributions to the fluence dependence. When the distribution is hotter, one photon dissociation dominates.

In the *ab initio* structure of the n = 2 complex, the water ligands both bind to the nitrogen atom of the NO^+, as in n = 1. The N=O bond is directed almost perpendicular to the ONO plane, indicating that the water molecules again interact with the p orbitals of the N atom, one H_2O donating lone pair density into the π_x^* orbital, the other into the π_y^* orbital.

The n = 3 spectrum indicates that all three H_2O are equivalent, and a postulated structure for $NO^+(H_2O)_3$ is shown in Fig. 7a. The third H_2O also binds to the N atom of NO^+, with a lone electron pair of each of the H_2O molecules again donating into the π^*

orbital. We expect that the three water ligands will be symmetrically positioned about the ion.

The H_2O antisymmetric stretch transitions appear as broad features that grow in intensity with cluster size relative to the narrower symmetric stretch band. Indeed, there appears to be a progression from a complete absence in $n = 1$, to a relatively weak shoulder in $n = 2$, to a strong band in $n = 3$. This result can be understood if the ν_3 signal primarily arises from one photon dissociation of vibrationally excited clusters. For the $n = 1$ cluster, few of the ions are hot enough to dissociate after absorption of a single photon and no ν_3 band is observed. For the $n = 2$ cluster, the H_2O binding energy is 3.5 kcal/mol lower and a detectable fraction of the clusters is able to dissociate upon absorption of a photon. ν_3 dissociation signal becomes even larger for $n = 3$, since the binding energy decreases and the total internal energy increases with the increase in cluster size.

C. $NO^+(H_2O)_4$ and Opening of the Reactive Channel

The observed spectrum (Fig. 3) of the $n = 4$ cluster suggests that this complex is also comprised of water ligands bound to an NO^+ core; however, the fourth water ligand does not apparently bind directly to the NO^+ cation. The appearance of bands at 3375 and 3230 cm^{-1} indicate that hydrogen bonds have formed and that the fourth H_2O binds to the other water ligands, beginning a second solvation shell. Below, we discuss several plausible solvent configurations.

The simplest configuration involves the fourth water forming a hydrogen bond with one of the first shell H_2O molecules, as depicted in Fig. 7b. The binding energy for

a second shell H_2O should be on the order of 6–10 kcal/mol, and thus will be comparable to the estimated energy for binding a fourth water ligand directly to the NO^+ core. The dissociation channel leading to loss of two H_2O molecules can then be understood as evaporation of $(H_2O)_2$, with a first solvation shell water carrying along its second shell partner. However, this configuration will give rise to only one hydrogen-bonded OH absorption band.

Small water clusters are well known for forming cyclic structures in order to maximize stabilization by hydrogen bonding.[34] The second shell energy would be more favorable if the fourth H_2O could form hydrogen bonds with two H_2O ligands, as depicted in Fig. 7c. In this structure, the water bridges two adjacent ligands to form a ring of four heavy atoms (three water O atoms and the N^+). If we assume that the $H_2O\cdots N\cdots OH_2$ angle is 120° and the N···O bond length is 2.4 Å (slightly longer than calculated for $n = 2$), the separation between O atoms on the H_2O ligands is 4.2 Å, comparable to the 4.48 Å distance in ice. The hydrogen-bonded rings in ice I are six-membered, but tetrahedral structures similar to those proposed here exist in ice VI. The strain will be lower in the unconstrained cluster, because the soft N···O stretches and O···N···O bend allow the cluster to readily deform. By forming two hydrogen bonds, the second shell H_2O should bind by at least 6–10 kcal/mol. This structure should be at least comparable in stability to having four waters in the first shell. The bands observed at 3230 and 3375 cm^{-1} could then be assigned as symmetric and antisymmetric stretch modes of the two hydrogen-bonded OH bonds.

An alternative structure, shown in Fig. 7d, consists of the adducts of the reaction products, with a HONO molecule and two H_2O bound to a central hydronium ion core. This structure is not in accord with the observed spectrum. The hydronium ion OH bonds would all be red-shifted below 2700 cm^{-1}, and thus unobserved. The two bands above 3600 cm^{-1} can be assigned to the H_2O molecules, but the 3375 and 3230 cm^{-1} bands cannot be accounted for. Furthermore, an OH stretch band of the HONO ligand is not observed.

The structure we propose in Fig. 7d is topologically equivalent to the structure proposed by Fehsenfeld *et al.*[6] (shown in Fig. 7e). This structure was suggested as an intermediate in reaction (1) from $NO^+(H_2O)_3 + H_2O$ to $H_3O^+(H_2O)_2 + HONO$. They proposed that one (first shell) H_2O was bound to NO^+, with a single H_2O in turn bound to that. The remaining two H_2O molecules were in the third shell, hydrogen-bonded to the second shell H_2O. This structure is more consistent with our observed spectrum, since there are three hydrogen-bonded OH groups, as well as two H_2O ligands with free OH groups. If the charge remains localized on the N atom, however, this configuration will be highly energetic, and unlikely to be formed.

Fehsenfeld *et al.* also proposed a "linear" structure, in which the four H_2O molecules form a single hydrogen-bonded chain with the O atom on a terminal water binding to the NO^+:

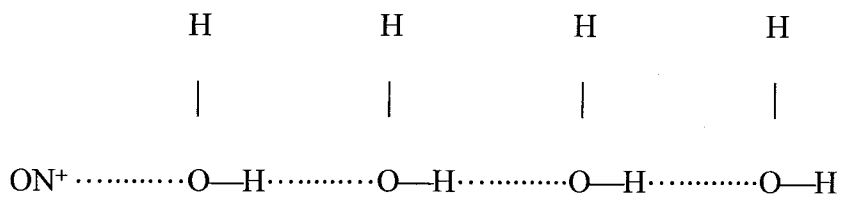

This structure is not consistent with the observed spectrum. We would expect to observe a progression of three hydrogen-bonded OH stretches of increasing red-shift and intensity, and the ν_1 band of H_2O should be significantly weaker, since only one water molecule is not a donor. Such a structure, while possibly a local energy minimum, is also energetically unfavored. Two of the water molecules are over 7 Å from the charge, and will contribute little to the solvation energy. Furthermore, if we postulate a structure in which HONO is formed and a proton is transferred to the second H_2O to form H_3O^+, ~5–10 kcal/mol are lost in having the last water in a second shell position, making the reaction significantly endothermic.

From the observation of HONO products in the absence of a HONO absorption band, we conclude that one IR photon can induce the reaction

$$NO^+(H_2O)_4 \rightarrow H_3O^+(H_2O)_2 + HONO \qquad (4c)$$

French *et al.*[9] estimate that the two channels, loss of H_2O (4a) and loss of HONO (4c), are almost identical in energy, but we find that the yield of HONO is significantly lower (10%). There are several plausible reasons why unimolecular decay of excited $NO^+(H_2O)_4$ favors H_2O loss. First, the estimated dissociation energies are comparable to the photon energy; if the molecule is excited close to threshold, differences of even a few kcal/mol can greatly influence the branching ratio. Second, the reaction (4c) may have an activation energy significantly larger than the H_2O binding energy, $E_{act} > 10$ kcal/mol. A barrier between $NO^+(H_2O)_4$ and $H_3O^+(H_2O)_2(HONO)$ is plausible, especially if the solvent H_2O must rearrange as the charge is transferred. Finally, unimolecular decay via the reactive channel may also be limited by the entropy of activation. Evaporation of

H_2O from $NO^+(H_2O)_4$ proceeds by simple bond fission, but formation of HONO may occur by a concerted reaction. In particular, substantial solvent rearrangement within the cluster may inhibit the reaction even if the HONO channel is energetically accessible.

D. The $n = 5$ Cluster: $H_3O^+(H_2O)_3(HONO)$

The large differences in the spectrum of $n = 5$ compared to the spectra of the smaller clusters signal a qualitative change in the nature of the clusters. The broad, strong absorption band near 2800 cm^{-1} and the weaker band at 3190 cm^{-1}, which we assigned as the OH stretches of H_3O^+, provide clear evidence that the $n = 5$ complex has an H_3O^+ ion core hydrogen-bonded to three solvating ligands. The appearance of the higher frequency bands of the $n = 5$ cluster is also distinct, with several sharp bands instead of the pattern of a sharp ν_1 and broad ν_3 bands observed in the smaller clusters. Because HONO is the dominant dissociation product, we infer that HONO forms weaker hydrogen bonds than H_2O. We thus propose that the $n = 5$ clusters have the structure shown in Fig. 7f, with the H_3O^+ bound to three water molecules in the first solvation shell and a HONO molecule in the second shell hydrogen-bonded to one of the first shell waters.

Given this structure, we can assign the five bands observed in the 3500 to 3800 cm^{-1} region (shown in more detail in Fig. 8). We distinguish between the two H_2O ligands which do not act as donors in a hydrogen bond, and the third H_2O ligand, which forms a hydrogen bond with the HONO in the second solvation. The bands at 3644 cm^{-1} and 3734 cm^{-1} are close to the free H_2O monomer bands, and are assigned as the symmetric and antisymmetric OH stretches of the two water ligands (not bound to

HONO). The third H_2O will have one OH stretch significantly red-shifted, while the other will remain essentially unperturbed. We assign the 3710 cm^{-1} band to the free OH of this perturbed molecule, and the broader band at 3530 cm^{-1} (shifted 125 cm^{-1} from ν_1 band of H_2O monomer) to the HO—H···O bond. The remaining band is the sharp, strong feature at 3576 cm^{-1}, 15 cm^{-1} to the red of the *t*-HONO monomer band. We assign this feature as the OH stretch of the nitrous acid ligand.

The frequency of the OH stretch of the nitrous acid ligand suggests that it is the *trans* conformer, since the *t*-HONO monomer stretch has a frequency of 3591 cm^{-1}, while *c*-HONO absorbs at 3426 cm^{-1}.[28] The effect of hydrogen bonding on the OH stretch of HONO is unknown. Thus, the issue of how the HONO is hydrogen bonded to the cluster (terminal oxygen, N atom, hydroxy group O atom, or bridging) remains uncertain.

E. The Intracluster Reaction of NO^+

The cluster we observed are intermediate complexes along the pathways for the reaction

$$NO^+(H_2O)_{n-1} + H_2O \rightarrow H_3O^+(H_2O)_{n-2} + HONO \qquad (6)$$

The energetics along the reaction coordinates for $n = 2 - 5$ are illustrated in Fig. 9. From their hydration enthalpy measurements, French *et al.*[9] show that the reaction is endothermic for $n = 2$ and 3 by 23.6 and 8.1 kcal/mol, respectively. Using their estimated value of $\Delta H_{2,3}$, the reaction for $n = 4$, *i.e.*, reaction (1), is slightly endothermic (~2 kcal/mol). If we continue their extrapolation, then $\Delta H_{3,4}$ is ~10 kcal/mol, and we estimate that the reaction enthalpy for $n = 5$ is –6 kcal/mol.

Our results are consistent with the thermodynamics. For reactions which are endothermic ($n \leq 4$), the complexes we observed are adducts of the reactants, NO^+ and H_2O. The structure of $n = 5$ cluster, $H_3O^+(H_2O)_3(HONO)$, reflects the fact that the reaction for $n = 5$ is exothermic. Although the cluster $NO^+(H_2O)_5$ may be stable, it is probably higher in energy than the observed cluster (see Fig. 9).

While the reaction goes to completion for five water molecules, we find evidence for the onset of reaction in the $n = 4$ cluster, even though the reaction is probably endothermic. Absorption of one IR photon (~10.5 kcal/mol) leads to ~12% yield of HONO formation. The photon energy is approximately equal to the internal energy of the activated complex formed in the thermal collision $NO^+(H_2O)_3 + H_2O$. Thus, we would expect that such collisions would lead to reaction approximately 10% of the time. This reaction efficiency is consistent with the observed rate constant, 7×10^{-11} cm^3/s, which is about one order of magnitude lower than the rate constant for ion-dipole collisions.

In the earlier static and flow tube experiments, $NO^+(H_2O)_4$ was not observed. This can be understood since the reaction rate is greater than three-body stabilization of the adduct. Furthermore, once $H_3O^+(H_2O)_2$ is formed, it quickly equilibrates to form larger hydrates. The back reaction is inhibited by the reduced concentration of $H_3O^+(H_2O)_2$ and the negligible concentration of HONO.

Reorganization of the H_2O molecules is almost certainly required for the reaction to proceed, because the charge is transferred from the nitrogen atom to a H_3O^+ moiety. The barrier for this process is still relatively high in $n = 4$, but is readily overcome in $n =$

5. Additional experiments on the $n = 4$ cluster, aided by computational studies, may provide further insights into the activation steps of this reaction.

3.6 SUMMARY

Our results provide clear evidence for a rearrangement of $NO^+(H_2O)_n$ at larger cluster sizes. The experimental results indicate that the smaller clusters are nitrosonium ions bound by water ligands and are in accord with the theoretical calculations for $n = 1$ and 2. The cluster $n = 4$, however, begins to deviate from this picture with the appearance of new hydrogen-bonded OH stretch absorptions and the opening of a minor photodissociation channel giving rise to loss of HONO. This behavior presages the large changes in the vibrational spectrum and photodissociation behavior observed after adding a fifth water molecule. The $n = 5$ cluster forms an adduct of the reaction products, $H_3O^+(H_2O)_3(HONO)$.

3.7 REFERENCES

* The chapter is modified from the paper published: J.-H. Choi, K.T. Kuwata, B.-M. Hass, Y. Cao, M.S. Johnson, and M. Okumura, J. Chem. Phys. **100**, 7153 (1994).

1. E.E. Ferguson, F. Fehsenfeld, and D.L. Albritton, in *Gas Phase Ion Chemistry*, edited by M.T. Bowers, Academic Press, New York (1979); G. Brasseur and S. Solomon, *Aeronomy of the Middle Atmosphere*, D. Reidel, Dordrecht, Holland (1986).

2. R.S. Narcisi and A.D. Bailey, J. Geophys. Res. **70**, 3687 (1965).

3. F.C. Fehsenfeld and E.E. Ferguson, J. Geophys. Res. **74**, 2217 (1969).

4. W.C. Lineberger and L.J. Puckett, Phys. Rev, **187**, 286 (1969).

5. L. J. Puckett and M. W. Teague, J. Chem. Phys. **54**, 2564 (1971).

6. F.C. Fehsenfeld, M. Mosesman, and E.E. Ferguson, J. Chem. Phys. **55**, 2120 (1971).

7. C.J. Howard, H.W. Rundle, and F. Kaufman, J. Chem. Phys. **55**, 4772 (1971).

8. L.J. Puckett and W.C. Lineberger, Phys. Rev. A **1**, 1635 (1970).

9. M.A. French, L.P. Hills, and P. Kebarle, Can. J. Chem. **51**, 456 (1973).

10. N.A. Burdett and A.N. Hayhurst, J. Chem. Soc., Faraday Trans. I, **78**, 2997 (1982).

11. S. Patai, *The Chemistry of Amino, Nitroso and Nitro Compounds and Their Derivatives* (Wiley, N.Y., 1970) and references therein.

12. M.J. S. Dewar, M. Shanshal, and S.D. Worley, J. Am. Chem. Soc. **91**, 3590 (1969).

13. K.A. Jorgensen and S.O. Lawessen, J. Chem. Soc., Perkin Trans. 2, 231 (1985).

14. A. Dargelos, S.El Ouadi, D. Liotard, M. Chaillet, and J. Elguero, Chem. Phys. Lett. **51**, 545 (1977).

15. W D. Edwards and H. Weinstein, Chem. Phys. Lett **56**. 582 (1978).

16. M.T. Nguyen and A.F. Hegarty, J. Chem. Soc., Perkin Trans. 2, 2037 (1984).

17. G. De Petris, A.D. Marzio, and F. Grandinetti. J. Phys. Chem. **95**, 9782 (1991).

18. H.M. Rosenstock, K. Draxl, B.W. Steiner, and J.T. Herron, J. Phys. Chem. Ref. Data **6**, Supp.1 (1977).

19. M. Okumura, L.I. Yeh, J.D. Myers, and Y.T. Lee, J. Phys. Chem. **94**, 3416 (1989); L.I. Yeh, M. Okumura, J.D. Myers, J.M. Price, and Y.T. Lee, J. Chem. Phys. **91**, 7139 (1989); J.M. Price, Ph.D. Thesis, University of California at Berkeley (1990); J.M. Price, M.W. Crofton, G. Neidenauer, and Y.T. Lee, J. Phys. Chem. **95**, 2182 (1991).

20. Y. Cao, J.-H. Choi, B.-M. Haas, M.S. Johnson, and M. Okumura, J. Phys. Chem. **97**, 5215 (1993).

21. W. L. Liu and J. M. Lisy. J. Chem. Phys., **89**, 605 (1988).

22. *Ion and Cluster Ion Spectroscopy and Structure*, edited by J.P. Maier (Elsevier, Amsterdam,1989).

23. Y. Cao, J. -H. Choi, B. -M. Haas, M. S. Johnson, and M. Okumura, J. Chem. Phys. **99**, 9307 (1993).

24. Y. Cao, J.-H. Choi, B.-M. Haas, and M. Okumura, J. Phys. Chem. **98**, 12176 (1994).

25. S.J. Bronsnan and R.L. Byer, IEEE J. Quantum Electron. **QE-15**, 415 (1979).

26. G. Herzberg. *Molecular Spectra and Molecular Structure III, Electronic Spectra of Polyatomic Molecules* (van Nostrand Reinhold, New York, 1966).

27. H.S. Schwarz, J. Chem. Phys. **67**, 5525 (1977).

28. C.M. Deeley and I.M. Mills. J. Mol. Struct., **100**, 199 (1983); S.M. Holland, R.J. Stickland, M.N.R. Ashfold, D.Z. Newnham, and I.M. Mills. J. Chem. Soc., Faraday Trans. **87**, 3461 (1991).

29. M.E. Jacox, J. Phys. Chem. Ref. Data **19**, 1387 (1990).

30. Gaussian 92, Revision D.2., M.J. Frisch, G.W. Trucks, M. Head-Gordon, P.M.W. Gill, M.W. Wong, J.B. Foresman, B.G. Johnson, H.B. Schlegel, M.A. Robb, E.S. Replogle, R. Gomperts, J.L. Andres, K. Raghavachari, J.S. Binkley, C. Gonzalez, R.L. Martin, D.J. Fox, D.J. Defrees, J. Baker, J.J.P. Stewart, and J.A. Pople, Gaussian, Inc., Pittsburgh, PA, 1992.

31. C. Mϕller and M.S. Plesset, Phys. Rev. **46**, 618 (1931).

32. W.J. Hehre, R. Ditchfield, and J.A. Pople, J. Chem. Phys. **56**, 2257 (1972); P.C. Hariharan and J.A. Pople, Theor. Chim. Acta. **28**, 213 (1973).

33. G. Herzberg, *Molecular Spectra and Molecular Structure II, Infrared and Raman Spectra of Polyatomic Molecules* (van Nostrand Reinhold, New York, 1945).

34. See for example S.S. Xantheas and T.H. Dunning, J. Chem. Phys. **99**, 8744 (1994).

TABLE I. Observed vibrational frequencies of $NO^+(H_2O)_n$ ion clusters.

cluster	frequency/cm^{-1}	assignment
$NO^+(H_2O)$	3599	H_2O sym. stretch
	3611	H_2O sym. stretch
$NO^+(H_2O)_2$	3622	H_2O sym. stretch
	3695	H_2O antisym. stretch
$NO^+(H_2O)_3$	3630	H_2O sym. stretch
	3712	H_2O antisym. stretch
$NO^+(H_2O)_4$[a)]	3230	H-bonded OH stretch
	3375	H-bonded OH stretch
	3635	H_2O sym. stretch
	3713	H_2O antisym. stretch
$NO^+(H_2O)_5$	2800	H-bonded H_3O^+ stretch
	3190	H-bonded H_3O^+ stretch
	3530	H-bonded H_2O donor OH stretch
	3576	HONO OH stretch
	3644	H_2O sym. stretch
	3710	H-bonded H_2O free OH stretch
	3734	H_2O antisym. stretch
H_2O monomer[b)]	3657	sym. stretch, ν_1
	3756	antisym. stretch, ν_3
HONO (*trans*) monomer[c)]	3591	OH stretch
HONO (cis) monomer[c)]	3426	OH stretch

a) Band assignments are based on the structure of Fig. 7.
b) Ref. 26.
c) Ref. 28.

TABLE II. *Ab initio* relative stabilities for $H_2NO_2^+$ isomers. MP2 calculations use 6-31G** basis set. CCSD calculations use 6-311G(2*df*,2*pd*) basis set.

	ΔE/kcal mol^{-1}				ΔH_{298}/kcal mol^{-1}	
Cluster	MP2	MP2+ZPE	CCSD	CCSD +ZPE[a)]	MP2	CCSD[a)]
$NO^+(H_2O)$	0	0	0	0	0	0
$HON(H)O^+$	37.8	40.8	35.1	38.1	39.6	36.9
$N(OH)_2^+$	38.3	41.2	31.4	34.3	40.1	33.2

a) Using the MP2 harmonic vibrational frequencies.

TABLE III. *Ab initio* harmonic frequencies (MP2/6-31G**) for $NO^+(H_2O)$.

Mode	Approx. Description	Frequencies/cm^{-1} (Intensities/km mol^{-1})
$\omega_1(a')$	O-H sym stretch	3820(196)
$\omega_2(a')$	N-O stretch	2099 (92)
$\omega_3(a')$	H_2O bend	1682 (65)
$\omega_4(a')$	H_2O wag	472 (272)
$\omega_5(a')$	N···O stretch	281 (101)
$\omega_6(a')$	O-N···O bend	248 (10)
$\omega_7(a'')$	O-H antisym stretch	3942 (159)
$\omega_8(a'')$	H_2O rock	470 (56)
$\omega_9(a'')$	H_2O twist	116 (36)

TABLE IV. *Ab initio* harmonic frequencies (MP2/6-31G**) for $N(OH)_2^+$.

Mode	Approx. Description[a)]	Frequencies/cm^{-1} (Intensities/km mol^{-1})
$\omega_1(a_1)$	O-H sym stretch	3610 (105)
$\omega_2(a_1)$	N-O sym stretch + NOH bend	1539 (77)
$\omega_3(a_1)$	N-O sym stretch	1280 (22)
$\omega_4(a_1)$	ONO bend	713 (20)
$\omega_5(a_2)$	ONO shear	760 (0)
$\omega_6(b_1)$	NOH shear	875 (291)
$\omega_7(b_2)$	O-H antisym stretch	3583 (848)
$\omega_8(b_2)$	N-O antisym str + NOH bend	1560 (115)
$\omega_9(b_2)$	N-O antisym str + ONO shear	1293 (439)

Table V. *Ab initio* harmonic frequencies (MP2/6-31G**) for $HON(H)O^+$.

Mode	Approx. Description	Frequencies/cm^{-1} (Intensities/km mol^{-1})
$\omega_1(a')$	O-H_1 stretch	3550 (320)
$\omega_2(a')$	N-H_2 stretch	3355 (135)
$\omega_3(a')$	N-O_2 stretch	1656 (159)
$\omega_4(a')$	O_1NH_2 bend + N-O_2 stretch	1509 (83)
$\omega_5(a')$	H_1O_1N bend + N-O_1 stretch	1430 (9)
$\omega_6(a')$	O_1NH_2 bend + N-O_1 stretch	1239 (215)
$\omega_7(a')$	O_1NO_2 ip bend	668 (53)
$\omega_8(a'')$	$O_1N(H_2)O_2$ umbrella	1065 (110)
$\omega_9(a'')$	O_1NO_2 op bend	752 (181)

TABLE VI. *Ab initio* harmonic frequencies for $NO^+(H_2O)_2$.

Mode	Approx. Description[a)]	Frequencies/cm^{-1}(Intensities/km mol^{-1})	
		RHF/6-31G**	MP2/6-31G**
$\omega_1(a')$	O-H antisym stretch	4213 (292)	3978 (180)
$\omega_2(a')$	O-H sym stretch	4114 (14)	3859 (75)
$\omega_3(a')$	N-O stretch	2800 (101)	2097 (36)
$\omega_4(a')$	H_2O bend	1794 (20)	1698 (82)
$\omega_5(a')$	H_2O rock	425 (165)	423 (126)
$\omega_6(a')$	H_2O wag	378 (764)	397 (482)
$\omega_7(a')$	N···O sym stretch	202 (2)	254 (52)
$\omega_8(a')$	N···OH bend	27 (0)	201 (14)
$\omega_9(a')$	H_2O twist	65 (6)	105 (22)
$\omega_{10}(a')$	O···N···O bend	85 (0)	33 (0)
$\omega_{11}(a'')$	O-H antisym stretch	4213 (32)	3977 (66)
$\omega_{12}(a'')$	O-H sym stretch	4112 (179)	3857 (132)
$\omega_{13}(a'')$	H_2O bend	1793 (194)	1693 (69)
$\omega_{14}(a'')$	H_2O wag	360 (0)	379 (118)
$\omega_{15}(a'')$	H_2O rock	414 (56)	375 (84)
$\omega_{16}(a'')$	N···O antisym stretch	238 (23)	224 (4)
$\omega_{17}(a'')$	N···OH bend	318 (41)	207 (1)
$\omega_{18}(a'')$	H_2O o.p. twist	28 (0)	26 (7)

TABLE VII. *Ab initio* thermochemical data for $NO^+(H_2O)_n \rightarrow NO^+(H_2O)_{n-1} + H_2O$

	ΔE_n/kcal mol^{-1}						ΔH^0_{298}/kcal mol^{-1}			
Cluster	MP2 6-31G**	MP2+ZPE 6-31G**	CCSD 6-31G**	CCSD +ZPE[a] 6-31G**	CCSD EXT[b]	CCSD+ZPE[a] EXT[b]	MP2 6-31G**	CCSD[a] 6-31G**	CCSD[a] EXT[b]	Expt.
n=1	25.1	23.1	23.9	21.9	22.2	20.2	23.8	22.6	20.9	18.5[c], 19.3[d]
n=2	19.5	18.0	18.9	17.4			18.0	17.5		16.1[c]

[a]Using the MP2/6-311G** harmonic vibrational frequencies.

[b]EXT refers to the 6-311G(2*df*,2*pd*) basis set.

[c]Reference 9.

[d]Reference 10.

3.8 Figure Captions

FIG. 1. Isomers of protonated nitrous acid. The geometry of the most stable structure predicted at the MP2/6-31G** level is a) $NO^+(H_2O)$, while b) $HONOH^+$ and c) $HON(H)O^+$ are potential energy minima lying at higher energies.

FIG. 2. Time-of-flight mass spectrum of hydrated nitrosonium clusters (n = 0–4). The ions were formed in a glow discharge of 12% NO seeded in ultrahigh purity H_2 at 1000 Torr. The formation of hydrates is due to the presence of a trace of H_2O vapor.

FIG. 3. Vibrational predissociation spectra of $NO^+(H_2O)_n$ (n = 1–5). The photofragment ions detected were $NO^+(H_2O)_{n-1}$ (n = 1–4) and $H_3O^+(H_2O)_3$ (n = 5), respectively.

FIG. 4. The dependence on laser pulse energy of the fragment signal from photodissociation of the parent ions $NO^+(H_2O)_n$, (n = 1–3) excited in the H_2O symmetric stretch. In the upper two panels, the square root of the photodissociation signal is plotted for a) n = 1 and b) n = 2. In the lower two panels, the photodissociation signal is plotted directly for c) n = 2 and d) n = 3.

FIG. 5. a) Detail of the 3605 cm^{-1} band from the vibrational predissociation of $NO^+(H_2O)$. The ordinate is the yield of photofragment ions NO^+. b) Simulation of the rotational band contour using rotational constants calculated from the *ab initio* structure of $NO^+(H_2O)$. Upper and lower state differences and centrifugal distortion constants

were estimated from those of *t*-HONO. The predicted asymmetric rotor spectrum used a rotational temperature of 120 K and was convoluted with a resolution linewidth of 1.5 cm^{-1}.

FIG. 6. The optimized geometry of $NO^+(H_2O)_2$ predicted at the MP2/6-31G** level. In the calculation, the geometry of the cluster was constrained to C_s symmetry.

FIG. 7. Proposed structures of the nitrosonium ion hydrates $NO^+(H_2O)_n$, for $n = 3$ to 5.

FIG. 8. Details of the vibrational predissociation spectrum of $NO^+(H_2O)_5$ in the 3500-3800 cm^{-1} region. The ordinate is the yield of photofragment ions $H_3O^+(H_2O)_3$.

FIG. 9. Energy level diagram for the reactions $NO^+(H_2O)_{n-1} + H_2O \rightarrow NO^+(H_2O)_n \rightarrow H_3O^+(H_2O)_{n-2} + HONO$. Dashed lines indicate hypothesized reaction paths and transition states. Each reaction pathway for a cluster n is lowered relative to the n-1 pathway by the hydration enthalpies. Numbers are hydration enthalpies in kcal/mol, those in parentheses are estimates only.

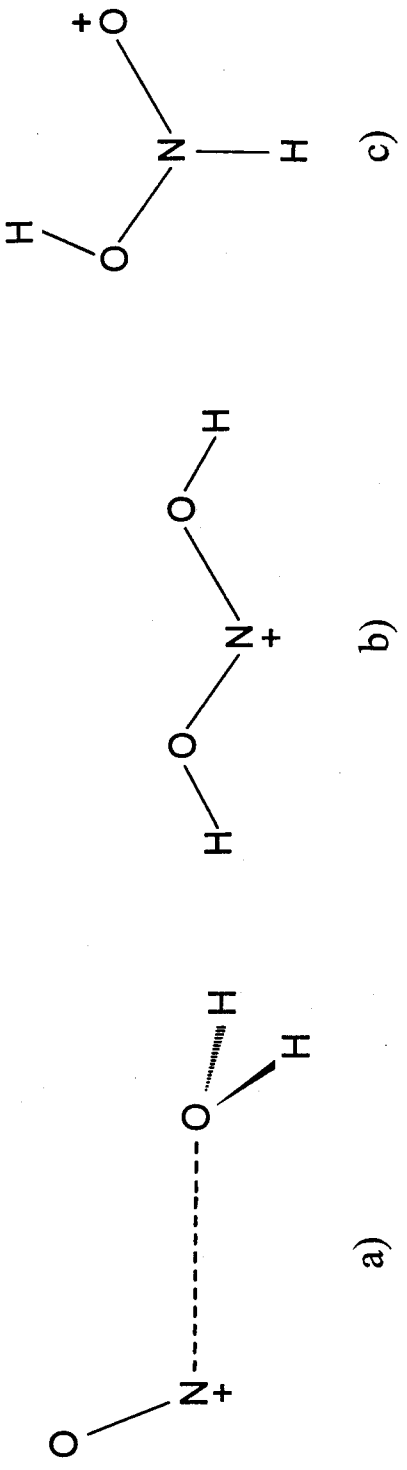

Figure 1.

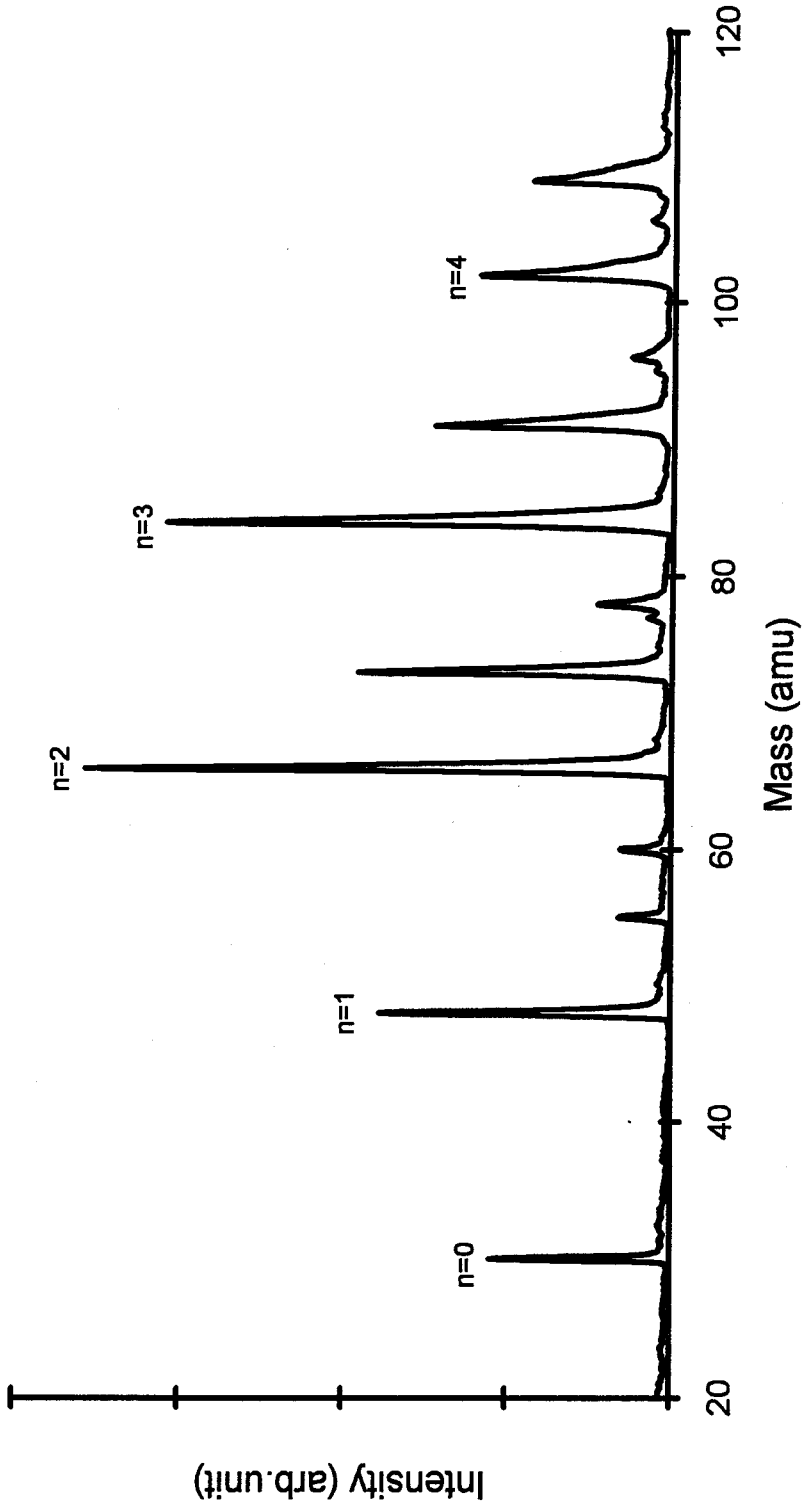

Figure 2.

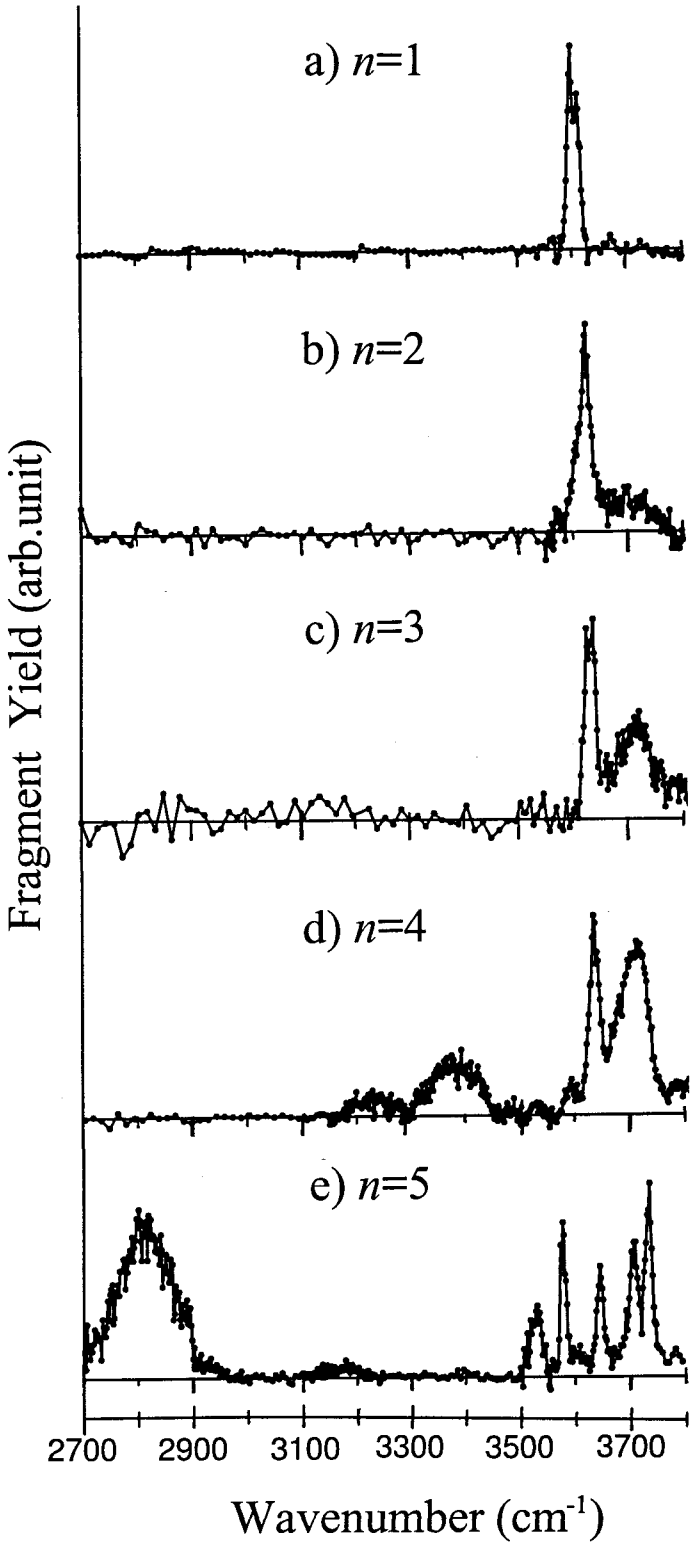
a) n=1
b) n=2
c) n=3
d) n=4
e) n=5
Fragment Yield (arb.unit)
2700
2900
3100
3300
3500
3700
Wavenumber (cm-1)

Figure 3.

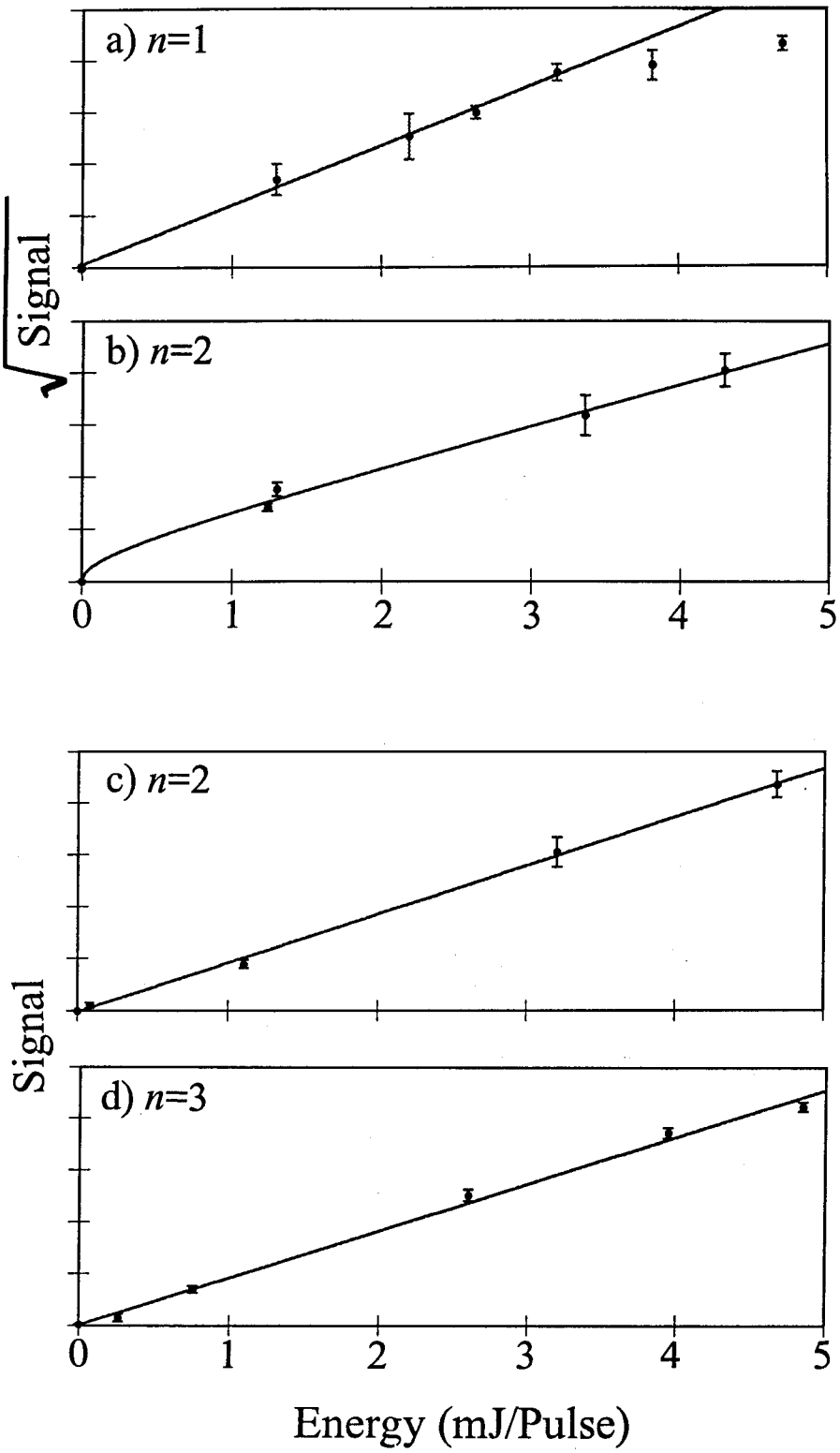

Figure 4.

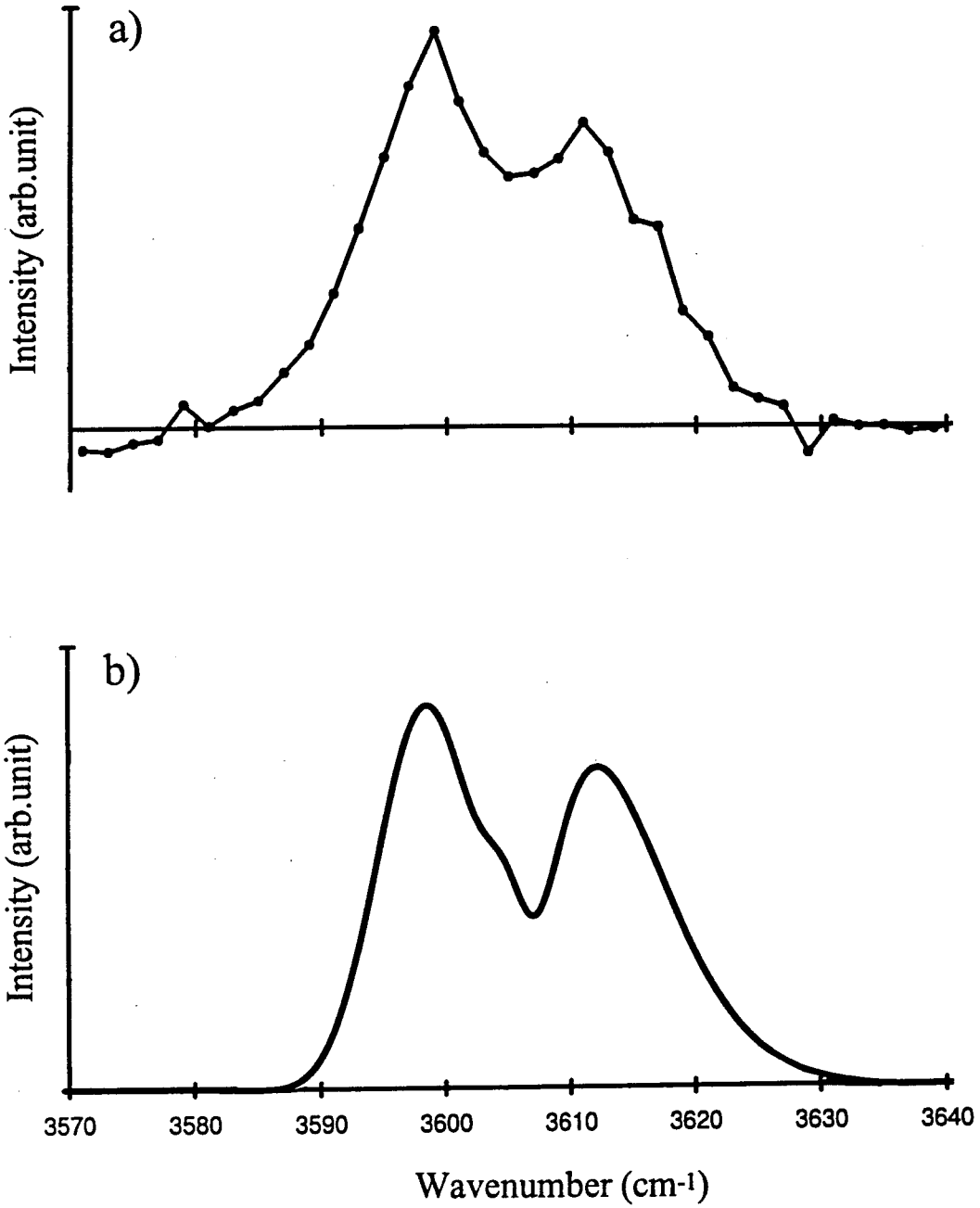
a)
Intensity (arb.unit)
b)
Intensity (arb.unit)
3570
3580
3590
3600
3610
3620
3630
3640
Wavenumber (cm-1)

Figure 5.

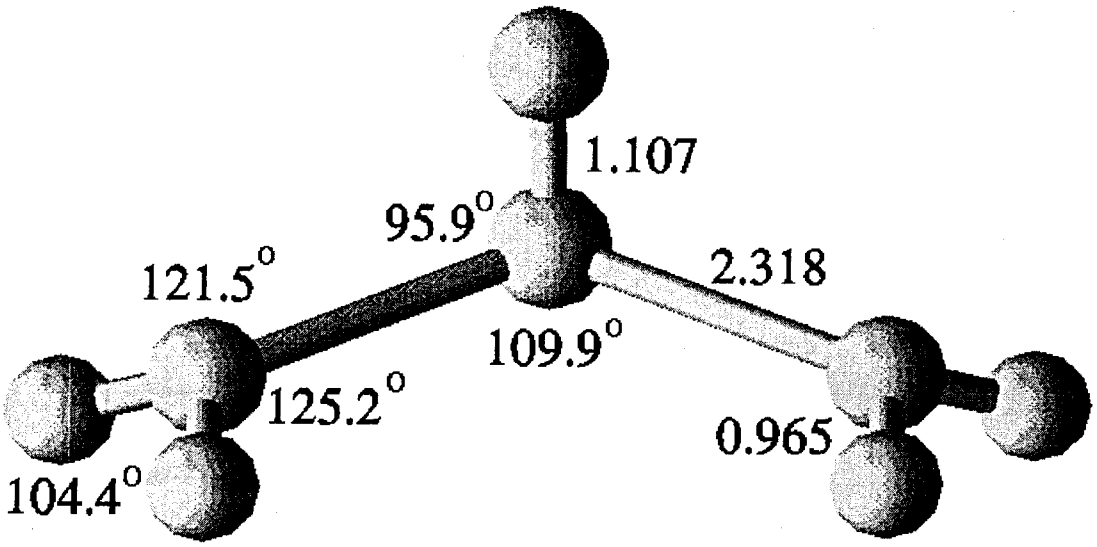

Figure 6.

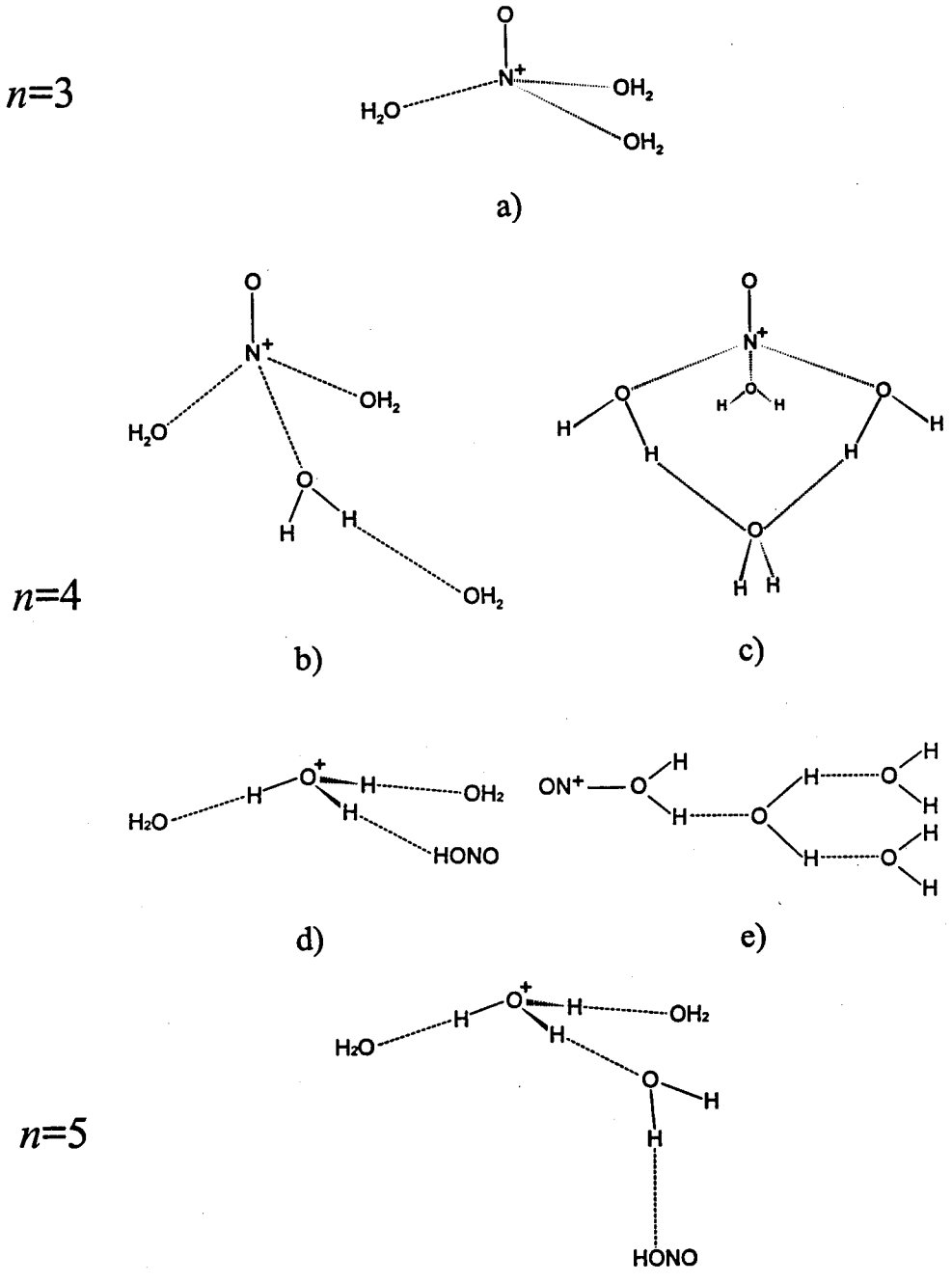

Figure 7.

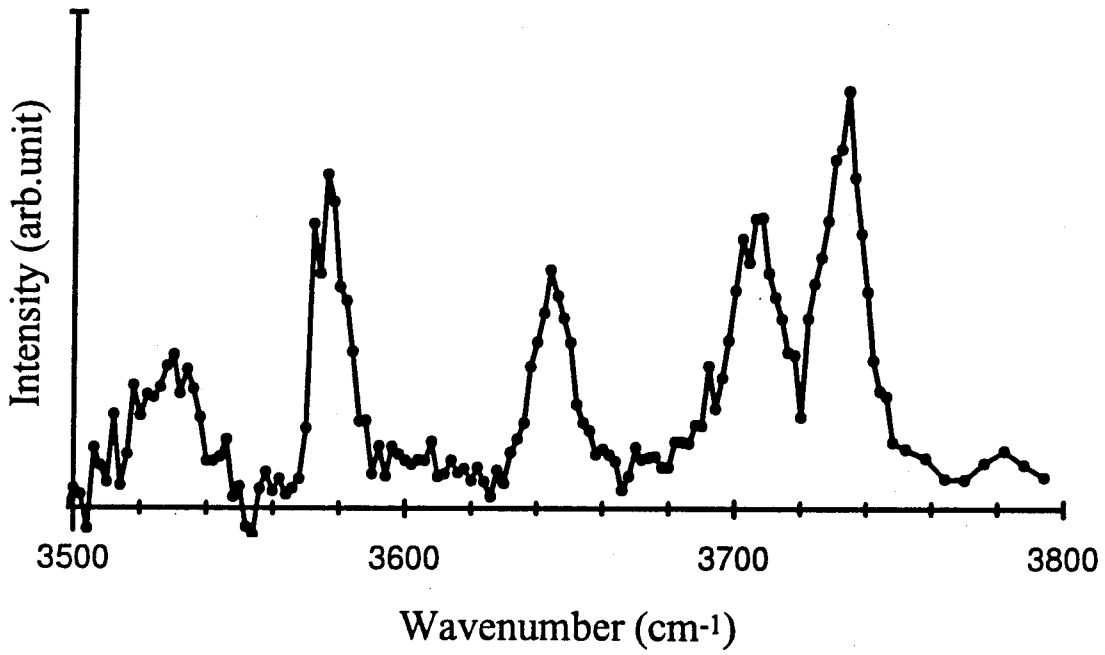

Figure 8.

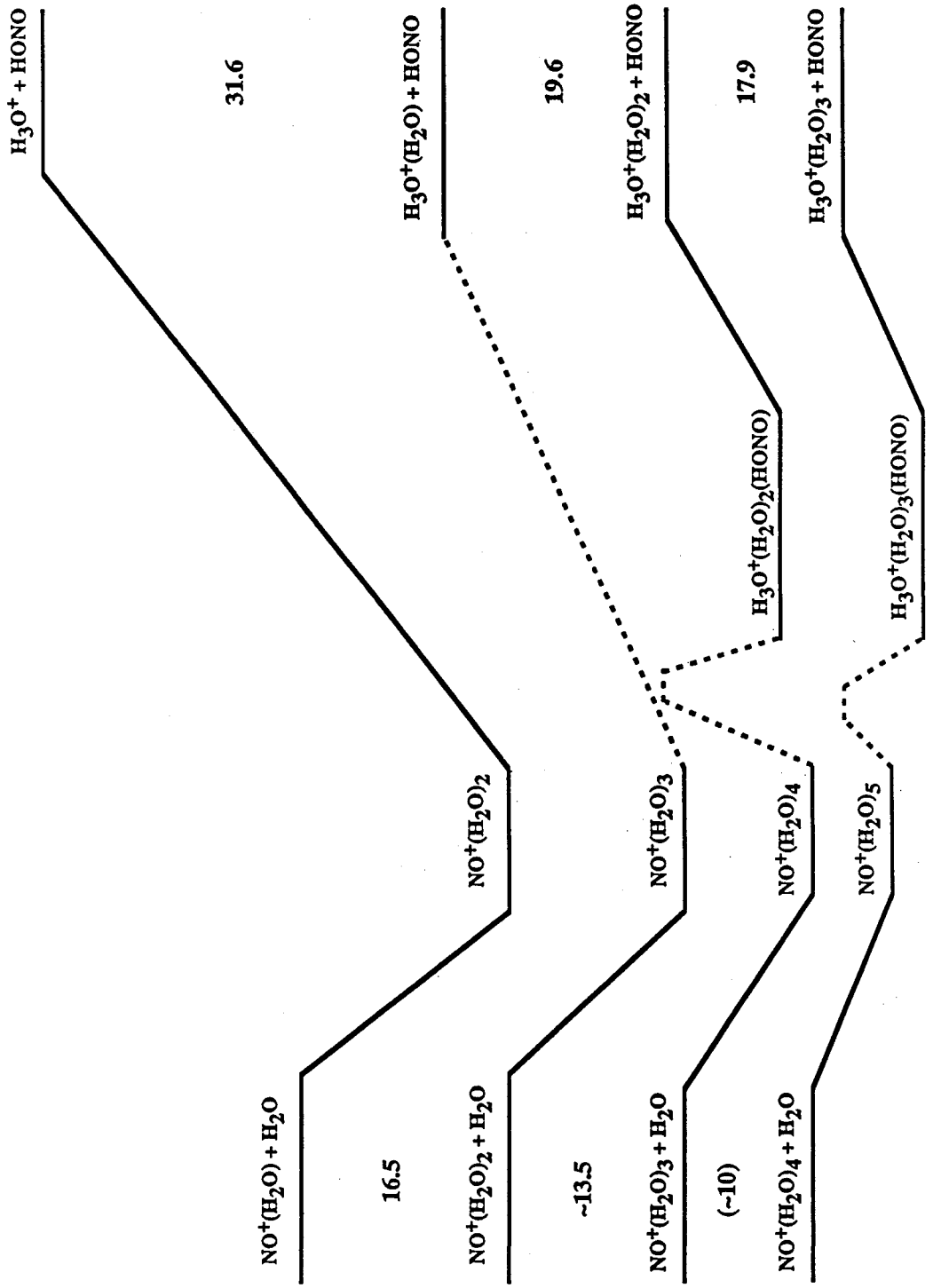
$H_3O^+ + HONO$
31.6
$H_3O^+(H_2O) + HONO$
19.6
$H_3O^+(H_2O)_2 + HONO$
17.9
$H_3O^+(H_2O)_3 + HONO$
$NO^+(H_2O) + H_2O$
16.5
$NO^+(H_2O)_2 + H_2O$
-13.5
$NO^+(H_2O)_3 + H_2O$
(-10)
$NO^+(H_2O)_4 + H_2O$
$NO^+(H_2O)_2$
$NO^+(H_2O)_3$
$NO^+(H_2O)_4$
$NO^+(H_2O)_5$
$H_3O^+(H_2O)_2(HONO)$
$H_3O^+(H_2O)_3(HONO)$

Figure 9.

CHAPTER 4

Infrared Spectroscopic Studies on Protonated XNO_3 (X = H, D, ^{35}Cl, ^{37}Cl)

4.1 INTRODUCTION

In 1985, Farman and co-workers published a paper on the observation of a decrease in stratospheric ozone concentrations over Antarctica during the austral spring.[1] Their ozone column measurements showed that at Halley Bay there was a remarkable decrease of the daily value for mean total ozone in October from ca. 300 DU in the mid-1970s to values lower than 200 DU.* In addition, Hofmann *et al.* presented ozone vertical profiles from balloon measurements indicating that the ozone depletion was occurring at altitudes from about 10 to 20 km.[2] Based on the steady increase of tropospheric and stratospheric halocarbons, Farman and co-workers suggested that reactions involving active chlorine in a catalytic cycle might have a close relationship with the observed ozone losses.

The idea of chlorine-initiated ozone depletion was initially proposed by Molina and Rowland who studied the mechanisms for removal of chlorofluorocarbons (CFCs) such as Freon 11($CFCl_3$) and Freon 12 (CF_2Cl_2) from the atmosphere.[3,4] They maintained that due to the chemical inertness of the CFCs and their insolubility in water, the major removal mechanism proceeded by diffusion into the stratosphere where the CFCs are photolyzed by

---

* The Dobson Unit (DU) is named after G.M.B. Dobson, who pioneered measurements of the stratospheric ozone in the 1920s and 1930s, and is now used to describe the total column density of ozone. One DU equals the thickness, in hundredths of a millimeter, of the ozone column at O °C and 1 atmosphere. Multiplying a measured DU number by the number density of air molecules in cubic centimeters gives the total number of ozone molecules per square centimeter.

solar ultraviolet radiation. They predicted that these photolysis reactions generate significant amounts of chlorine atoms which could attack the ozone and oxygen atoms:

$$Cl + O_3 \rightarrow ClO + O_2$$

$$ClO + O \rightarrow Cl + O_2$$

Anderson and co-workers performed concentration measurements of ozone and ClO in the polar stratospheric region using an ER-2 reconnaissance aircraft.[5] They confirmed that the ozone loss is correlated to increased chlorine concentrations and that the chlorine species in the stratosphere mostly come from CFCs.

Although the participation of chlorine was correctly hypothesized, the original mechanism could not explain the observed ozone losses over Antarctica. The model predicted that the reactive chlorine atom would be sequestered in relatively inert chemical species, such as $ClONO_2$ and HCl, which would act as stable chlorine reservoirs, but did not take into account the possibility of heterogeneous reactions. The cold temperature, down to below 200K during the austral winter, induces formation of polar stratospheric cloud (PSC) aerosols, which are believed to be composed of nitric acid hydrates (type I) or water ice (type II). On the surface of these PSC aerosols, the following heterogeneous reactions[6-12] occur:

$$ClONO_2 + H_2O(s) \rightarrow HOCl(g) + HNO_3(ad) \quad (1)$$

$$ClONO_2 + HCl(ad) \rightarrow Cl_2(g) + HNO_3(ad) \quad (2)$$

$$HOCl + HCl(ad) \rightarrow Cl_2(g) + H_2O(s) \quad (3)$$

These reactions convert the stable chlorine reservoir species into more photosensitive forms, HOCl and Cl_2, which are photolyzed in the austral spring, leading to the generation of ClO

radicals. The following catalytic cycles involving the formation of a ClO dimer destroy ozone:

$$2\ (Cl + O_3 \rightarrow ClO + O_2)$$

$$ClO + ClO + M \rightarrow (ClO)_2 + M$$

$$(ClO)_2 + h\nu \rightarrow Cl + ClOO$$

$$ClOO + M \rightarrow Cl + O_2 + M$$

Net reaction: $2\ O_3 \rightarrow 3\ O_2$

This mechanism proposed by Molina *et al.* can account for ca. 70% of the ozone depletion in the polar stratosphere.[13] Much of the remaining depletion is thought to occur through a bromine mechanism.[14]

The current status of ozone-depletion chemistry is that the principal gas-phase processes that control stratospheric ozone have been identified and mostly well-understood. Present attention is focused on chemistry of the heterogeneous reactions occurring on PSC aerosols, such as reactions (1) to (3), to have a more comprehensive understanding of the chemistry linking gas-phase species and stratospheric particles.

Some detailed information on the heterogeneous reactions of the chlorine reservoir species $ClONO_2$ has been obtained in recent years.[8-12] Laboratory measurements taken using flow tubes and Knudsen cells showed that the reactions of $ClONO_2$ with water and HCl (reactions 1 and 2) are catalyzed by the surface of PSC aerosol particles. To explain the catalyst action of an ice surface, Molina *et al.* postulated that the dissociation of $ClONO_2$ on the surface of PSCs is acid-catalyzed via the following ionic mechanism:

$$ClONO_2 + H^+ \rightarrow HNO_3\text{-}Cl^+ \quad (4)$$

where the reaction leads to a Cl^+ leaving group.[15] The idea of an electronegative chlorine as a positive leaving group is, however, inconsistent with the high ionization potential of Cl (12.97 eV) and general chemical concepts. Another proposed mechanism is through the solvation of chlorine nitrate by water molecules, leading to the lower activation barrier of the bond cleavage step.

We have performed several experiments to elucidate the mechanism of heterogeneous chlorine nitrate reactions at the molecular level. Nelson and Okumura investigated the reactions of small protonated water clusters, $H_3O^+(H_2O)_m$ with chlorine nitrate using time-of-flight mass spectrometry.[16] A supersonic ion cluster beam was introduced into a reaction cell containing chlorine nitrate, and various forms of protonated nitric acid clusters, $NO_2^+(H_2O)_n$ (n = 0, 1, 2), were detected as the reaction products. Their observations confirmed the hypothesis that heterogeneous reactions on PSCs are acid-catalyzed. In contrast to the intermediate shown in reaction (4), they proposed a weakly bound ion-molecule complex of NO_2^+ and HOCl:

$$H^+ + ClONO_2 \rightarrow HOClNO_2^+ \rightarrow NO_2^+ + HOCl \quad (5)$$

where the protonation occurs at the center oxygen to form HOCl, which is followed by charge transfer to NO_2^+.

This protonated species has been confirmed both theoretically and experimentally. Lee and Rice carried out *ab initio* calculations on the protonation reactions of chlorine nitrate. Energetics, equilibrium structures, and vibrational frequencies were obtained using MP2 (second-order Møller-Plesset) perturbation theory and CCSD (singles and doubles

coupled-cluster) method.[17] They show that the lowest energy form of protonated chlorine nitrate corresponds to a complex between NO_2^+ and HOCl bound by 12.9 ± 2 kcal/mol (Figure 1). This predicted *ab initio* structure is in a good agreement with the complex intermediate shown in reaction (5). Van Doren *et al.* recently performed a selected-ion flow tube (SIFT) experiment under thermal conditions at 223 K.[18] They observed the proton transfer reaction of H_3O^+ to $ClONO_2$, and postulated as an intermediate the same weakly bound complex of $NO_2^+(HOCl)$ observed in the mass spectrometric studies.

Another study of the heterogeneous reactions was performed by Haas *et al.* using Fourier-transform ion-cyclotron-resonance (FT-ICR) spectrometry.[19] They determined the reaction rate constant at 298 K for the gas-phase reaction of Cl^- with $ClONO_2$ to form Cl_2 and NO_3^-. Correlated *ab initio* calculations found that the reaction surface shows no barrier for the approach of Cl^- toward the Cl atom on chlorine nitrate and that a minimum along the reaction coordinate corresponding to an ion-molecule complex, $NO_3^-(Cl_2)$, exists. These studies suggest that chloride ions may undergo a direct reaction with $ClONO_2$ on water ice films and type II PSC particles.

In this chapter, infrared predissociation spectroscopy has been applied to the protonation reactions of $^{35,37}ClONO_3$ to examine the ionic mechanism of chlorine nitrate activation proposed by our group. We also studied the protonated HNO_3 and DNO_3 systems as prototypes of chlorine nitrate. Both pulsed glow-discharge and continuous electron-impact schemes were employed to generate molecular ion beams. The analysis of the observed infrared predissociation spectra presents direct information on the various

isomer structures of the protonated species and provides insights into the heterogeneous mechanism at the molecular level.

4.2 EXPERIMENT

The time-of-flight mass spectrometry in combination with the infrared predissociation technique employed in these experiments has been described in Chapter 2 and other refercences.[20,21] In this section, only a brief description relevant to the experiment is presented.

The concentrated nitric acid (ca. 70% wt.), deuterated nitric acid (68% in D_2O) and D_2O were purchased from J.T. Baker Inc., Sigma Chemical Co., and Cambridge Isotope Lab. Inc., respectively. Carrier gases of ultra high purity (99.999%) He and H_2 were obtained from Matheson Gas Products Inc. The chlorine nitrate was synthesized from the reactions of Cl_2O and N_2O_5, using the Schmeisser's procedure described in the literature.[22] The sample was purified using trap-to-trap distillation at 195 and 175 K to remove Cl_2 and Cl_2O impurities. The nitric acid impurities were excluded by transferring the $ClONO_2$ through cannula out of the solid HNO_3 at 195 K. Pure chlorine nitrate is a pale yellow solid at 77 K.

For the protonation reaction experiments of $H(D)NO_3$, UHP H_2 or He was seeded with $H(D)NO_3/H(D)_2O$ vapor by passage over a bubbler containing concentrated $H(D)NO_3$ at O °C (partial pressure; $p(HNO_3)$ =1.7 Torr, and $p(H_2O)$ = 0.53 Torr).[23] The mixture of HNO_3, H_2O and H_2 (or He) at a total stagnation pressure of 1000 Torr was introduced into the vacuum through a nozzle of 0.5 mm opened by a piezo-driven pulsed valve at a

repetition rate of 10 Hz (ca. 200 μs wide). The piezoelectric disc element was coated with halocarbon grease to prevent reactions with nitric acid occurring on the disc surface. Ion beams of protonated nitric acid were produced by both electron impact and glow discharge sources. In the case of the electron impact source, the mixture was intersected by a continuous 750 eV electron beam at the throat of the supersonic expansion. Typical emission and Faraday-cup currents were about 2 mA, and 50 to 200 μA, respectively. For the glow discharge source, the gas mixture was pulsed into a 1-mm-diameter and 1.5-cm-long channel where a high voltage pulse (-1.5 to -3 kV, 100 μs wide) was applied between two electrodes near the entrance to initiate a glow discharge. The ions formed in the discharge source were thermalized as the gas flowed through the channel and further cooled in the supersonic expansion.

The resulting ion beam was skimmed and entered a time-of-flight chamber where the ions were extracted by a pulsed electric field (15 μs wide), accelerated to 2.6 kV and mass-selected. A pulsed tunable infrared laser, a $LiNbO_3$ optical parametric oscillator with 1.5 cm^{-1} resolution, was timed to excite only the protonated nitric acid ion selected by a mass gate which rejected all ions of other *m/e*. Upon infrared photon absorption, vibrationally predissociated ions were separated from the parent ions using a reflectron energy analyzer, then detected by a microchannel plate detector. Action spectra were obtained by measuring the photofragment ion intensity as a function of the laser wavelength. Photofragment spectra were corrected by subtracting the background ion signal, primarily caused by collision-induced dissociation of metastable parents in the ion optics chamber, and by normalizing to the laser fluence.

For $ClONO_2$, the experimental procedure was the same as above. Due to the high vapor pressure and the possible decomposition of chlorine nitrate, however, extra heed was paid to the sample preparation step. The chlorine nitrate was kept in a Pyrex cylinder with a halocarbon-greased valve at 77 K. The gas line was first evacuated and then passivated with chlorine nitrate by warming the opened cylinder in a dry ice bath (200 K) until the line pressure reached ca. 10 Torr, as measured by an MKS capacitance manometer. After closing the cylinder, the $ClONO_2$ was allowed to passivate the gas line for two or three hours. This was repeated several times. During the experiment, the $ClONO_2$ sample was kept at -78 °C ($p(ClONO_2) \approx 1$ Torr).

During the experiments on protonated DNO_3 and chlorine nitrate, the resolution of the time-of-flight mass spectra was carefully examined to separate the isotopes of hydrogen and chlorine. In the case of the $HDNO_3^+$ ion (m/e = 65), for example, we could also see $H_2NO_3^+$ and $D_2NO_3^+$ ions (m/e = 64 and 66, respectively). Under typical experimental conditions of E_{ION} = 2.6 keV, V_{REFL} = 2.65 keV and V_{DET} = 1200 V, each peak had a full-width-at-half-maximum (FWHM) of ca. 100 *n*sec, and the peak-to-peak separation between two neighboring peaks (i.e., either m/e = 64 and 65, or 65 and 66) was ca. 270 *n*sec. Although this separation was sufficient to allow the mass gate to work properly, higher detector voltages were required to observe a weak photofragment signal in the experiment. Such conditions usually induce a small fraction of partially mass-gated metastable ions to appear in the photofragment spectrum. In some poorly resolved cases, the arrival times of these unwanted metastable ions might be shifted with the reflectron set to $(m_f / m_p)\ V_{REFL.P}$, leading to partial overlapping with the photofragment ions of interest. To check this

possibility, the time profiles of photoproducts together with those of neighboring metastable ions were carefully monitored at a higher detector voltage, V_{DET} = 1700 V. In the case of $HDNO_3^+$, the FWHM of each metastable peak was about 60 *n*s. The shift in flight time of neighboring metastables toward that of photofragments of *m/e* = 65 by changing the reflectron voltage $V_{REFL.P}$ = 2650 V to 1875 V (= 46 x 2650/65) was about 100 *n*s. Since our integration-range setting and the peak-to-peak separation between parents were about 80 and 270 *n*sec, respectively, the contamination of photofragment signals with unwanted neighboring metastable ions was insignificant.

4.3 EXPERIMENTAL RESULTS

Typical time-of-flight mass spectra of the protonated species are shown in Figures 2 to 4. Figure 2 corresponds to protonated HNO_3 hydrate clusters, $NO_2^+(H_2O)_n$ (n = 0 to 5), formed in a pulsed discharge source. The other major peaks are of the hydrated hydronium clusters, $H_3O^+(H_2O)_n$, due to the presence of a trace of water vapor in the gas line. Figure 3 exhibits protonated DNO_3 hydrate clusters obtained by electron impact ionization. Ions of $NO_2^+(H_2O)$, $NO_2^+(HOD)$ and $NO_2^+(D_2O)$ (*m/e* = 64, 65, and 66, respectively) appear together. In the case of chlorine nitrate (Figs. 4a and 4b), the protonated species could be observed only using the electron-impact ionization method. The mass spectrum shows two ionic species of $HClONO_2^+$ at mass 98 and 100 due to the isotopes of chlorine (with a 3:1 intensity ratio). The distributions could be shifted by changing the stagnation pressure, temperature, discharge voltage, electron beam energy, and pulsed valve settings.

We recorded infrared spectra of protonated HNO_3, DNO_3, and $ClONO_2$ in the 3300-3750 cm^{-1} region. Figures 5 to 7 present the infrared spectra for the protonated ion species over the entire frequency range and Table I lists the observed maxima.

A. Photodissociation behavior

NO_2^+ was the only photofragment ion detected upon infrared excitation of the protonated species, indicating that a single water molecule evaporated upon vibrational excitation:

$$NO_2^+(HOX) \rightarrow NO_2^+ + HOX, \qquad X = H, D, {}^{35}Cl, {}^{37}Cl \quad (6)$$

Figure 8 shows the dependence of the photodissociation signal on laser pulse energy for protonated nitric acid and chlorine nitrate. In both cases, a sum of linear and quadratic terms gave a better fitting result than either term alone. For the $NO_2^+(H_2O)$ in the glow discharge source, the 3626 cm^{-1} band showed a nearly quadratic dependence. For the $NO_2^+(HOCl^{35})$ by electron impact ionization, the 3574 cm^{-1} band possessed a nearly linear dependence. These observations suggested that both photodissociations were a result of a combination of two-photon absorption by vibrationally cold clusters and one-photon absorption by vibrationally hot clusters. Similar behavior was observed in the photodissociation of $NO^+(H_2O)_2$ cluster as discussed in Chapter 3.

B. Vibrational predissociation spectra

The infrared spectra of protonated nitric acid shown in Figure 5 exhibited a dramatic dependence on the method of ion generation. Under discharge conditions, the spectrum consisted of two absorption bands in the 3300 - 3750 cm^{-1} region. The band centered at 3626 cm^{-1} possessed *P*, *Q*, and *R* subbands and was only ca. 30 cm^{-1} lower in frequency

than the symmetric stretch of the water monomer. The 3704 cm^{-1} band was a doublet with maxima at 3700 and 3708 cm^{-1}, and was ca. 50 cm^{-1} lower than the water antisymmetric stretch. In the case of the electron-impact ionization scheme, one additional band near 3375 cm^{-1} was observed. Furthermore, the two bands in the 3500 - 3750 cm^{-1} region were broader compared to the bands observed in the discharge. This behavior was solely due to the ion generation scheme employed in the experiments and a detailed explanation will be discussed below.

For the protonated DNO_3 ion, a similar dependence was observed in the infrared spectra shown in Figure 6. The ions generated in the discharge showed two bands centered at 3666 and 3724 cm^{-1}. Under electron-impact conditions, an additional band appeared at 3380 cm^{-1}. The ratio of intensity between 3380 and 3666 cm^{-1} bands was about 4.5 : 1.

For the protonated chlorine nitrate observed only in the electron-impact scheme, the infrared spectrum of $H^{35}ClONO_2^+$ (*m/e* = 98) in Figure 7 consisted of three bands: one strong band centered at 3382 cm^{-1}, a medium band at 3574 cm^{-1}, and a weak band at 3706 cm^{-1}. For the *m/e* = 100 species, we could see the same features in the spectrum although the weak band was not observed due to the poor signal-to-noise ratio.

4.4 DISCUSSION

A. Protonated HNO_3 and DNO_3

The experimental results on the protonated HNO_3 and DNO_3 formed in a glow discharge are most consistent with a weakly bound ion-molecule complex structure of NO_2^+ and water. We find that photodissociation of both species leads only to NO_2^+ and water

products. The observed infrared spectrum of $NO_2^+(H_2O)$ is analogous to that of a water molecule. The two bands at 3626 and 3704 cm^{-1} are red-shifted by 31 and 52 cm^{-1} from the symmetric and antisymmetric stretches of water, respectively, due to the perturbation of the NO_2^+ ion core.

For $HDNO_3^+$ ion, the band at 3666 cm^{-1} is red-shifted by 35cm^{-1} from the OH stretch of free HOD. The observation of the band at 3724 cm^{-1} was surprising. Since NO_2^+ (HOD) has only one OH stretch in this region, only one band is expected. This band might be the combination of the symmetric and antisymmetric stretch modes ($\nu_1 + \nu_3$) of the NO_2^+ ion core. A similar combination band was recently observed in matrix-isolation studies on NO_2^+ carried out by Forney *et al.*[24] They showed that the NO_2^+ combination band in the presence of small matrix perturbation appears at 3711 cm^{-1}, which is very close to our observed band. In the case of $NO_2^+(H_2O)$ the combination band is probably embedded in the strong antisymmetric stretch band of the H_2O group, which appears at 3704 cm^{-1}. However, for NO_2^+(HOD), the OH stretch is shifted away from the combination band. The strength of the combination band may arise form a Fermi resonance with the allowed OH antisymmetric stretch.[25]

We carried out an experiment on the $NO_2^+(D_2O)$ system, but observed no such bands in the 3700 cm^{-1} region. This suggests that since this deuterated species does not possess any OH stretches in the region of interest, no enhancement of intensity through the resonance is expected. As a further confirmation, we are planning to study NO_2^+X (X= inert gas such as Ar, Ne) clusters which have no bands close to the combination band.

Our results on $NO_2^+(H_2O)$ support recent *ab initio* calculations on protonated nitric acid performed by Lee and Rice.[26] They have shown that protonated nitric acid has two low energy isomers (Figure 9). The two isomers are ion-molecule complexes of NO_2^+ and water, differ by rotation of water with respect to the NO_2^+ ion core, and are very close in energy (ΔE < 0.5 kcal/mol). The (scaled) *ab initio* OH frequencies (3617 and 3710 cm^{-1}, respectively) of the ion-molecule complex at the CCSD(T) level of theory agree quite well (within 2%) with the observed frequencies of bands for protonated nitric acid.

From the nearly quadratic fluence dependence of photofragment signals in Figure 8, we find that two photons are required to dissociate the ion-molecule complex and that the range of binding energy is between 10.5 and 21 kcal/mol. This range is quite consistent with a recent experimental value of 14.8 ± 2.0 kcal/mol and *ab initio* value of 17.3 ± 2.0 kcal/mol.

The *ab initio* structure for $NO_2^+(H_2O)$ can be used to simulate the rotational envelopes of the partially resolved vibrational bands. The theoretical geometry has a planar structure with a nearly linear NO_2^+ bound to an H_2O ligand 2.45 Å away and is a highly asymmetric rotor, with rotational constants of A = 0.398 cm^{-1}, B = 0.202 cm^{-1}, and C = 0.134 cm^{-1}. The symmetry axis of the H_2O ligand is collinear with the a axis of the complex; therefore, excitation of the symmetric stretch will lead to an a-type transition and the antisymmetric stretch an b-type transition. The rotational contours have been obtained by deriving a predicted rovibrational spectrum at a rotational temperature of 80K with a rigid rotor approximation and then convoluting it with a Gaussian linewidth function. The temperature is reasonable, since we have successfully fit spectra of SiH_7^+ and $NO^+(H_2O)$

clusters generated in the same source using 90 K and 120 K, respectively. The predicted contour is shown in Figure 10 and shows a good agreement with the observed bands. In particular, the observed 8 cm^{-1} separation between the two maxima of the antisymmetric stretches agrees well with the simulation. This good agreement provides further confirmation in support of an ion-molecule complex structure.

Our results performed using a glow discharge do not show any indication of forming two other high energy isomers $(OH)_2NO^+$ predicted by *ab initio* calculations (Figure 9).[26] The isomers are formed by protonation of a terminal oxygen. They are also energetically very close, and about 20 kcal/mol less stable than the ion-molecule complex. The two (scaled) OH stretching frequencies are nearly degenerate and are predicted to appear at ca. 3435 cm^{-1} with a 13 cm^{-1} splitting. Such bands were not observed in the infrared spectra. Therefore, we conclude that the higher energy isomers were not formed in our discharge source.

For the protonated HNO_3 and DNO_3 generated by the electron-impact source, however, we found evidence for the high energy isomers, $(OH)_2NO^+$. In both spectra of Figures 5 and 6, a new band was observed in the 3380 cm^{-1} region. This band agrees within 3% of the scaled *ab initio* OH frequency, 3435 cm^{-1}.[26] In order to predissociate $(OH)_2NO^+$, proton transfer mechanism must occur. After absorption, an intramolecular hydrogen atom transfer occurs over two atoms from one O atom to the hydroxyl group, followed by cleavage of the $NO_2^+\cdots H_2O$ bond. This mechanism, initiated with a 1,3 hydrogen shift, is commonly observed in chemical reactions.

The different results from the two types of ion sources can be rationalized in terms of the extent of relaxation and isomerization upon expansion. Our discharge source involves a high-pressure discharge with the plasma occurring in a narrow channel just after the valve orifice. Thermalizing collisions cool ions in the plasma as the gas flows through the channel. The plasma is further cooled in the following supersonic expansion. Figure 11 shows an energy level diagram (based upon *ab initio* calculations) for the protonation process leading to two types of isomers. The higher energy isomer formed in the discharge may undergo enough collisions to rearrange and form the most stable isomer. Therefore, the ion beam would contain only the lowest energy ion-molecule complex. In the case of the electron-impact source, however, the plasma is generated at the throat of the expansion. Compared to the discharge source, this source results in far fewer collisions and some metastable isomers may relax into the metastable conformation without rearranging, leading to the observed mixture of isomers. The high energy isomer could only be observed in the infrared spectra by a 1,3 hydrogen shift that overcame the activation barrier shown in Figure 11. The barrier for the H atom transfer and simultaneous charge transfer must be on the order of one photon in energy, i.e., approximately 10 kcal/mol.

B. Protonated $^{35,37}ClONO_2$

The protonated chlorine nitrate generated by the electron-impact source shows behavior similar to that of the protonated DNO_3 formed in the same source. We observed NO_2^+ + HOCl photoproducts, and three bands in the 3300-3750 cm^{-1} region. The two bands in the 3500-3750 cm^{-1} region in Figure 7 are thought to arise from the weakly bound ion-molecule complex, NO_2^+(HOCl). The strongest band at 3574 cm^{-1} is assigned to the

OH stretch, and the weakest band at 3706 cm^{-1}, to the combination band of symmetric and antisymmetric stretches of the NO_2^+ ion core, as observed in the NO_2^+(HOD). This combination band was not observed in the $H^{37}ClONO_2^+$ due to the poor signal-to-noise. The medium intensity band at 3382 cm^{-1} was observed in both protonated HNO_3 and DNO_3 and assigned to the OH stretch of $(OH)(OCl)NO^+$. This band suggests that the electron-beam generated ion beam contains a mixture of two isomers, just as that in case of the protonated nitric acid.

The observed bands in the infrared spectrum agree quite well with vibrational *ab initio* frequencies.[17] The calculations predict that the lowest energy form of protonated $ClONO_2$ corresponds to a complex between HOCl and NO_2^+, similar to the case for nitric acid and CH_3ONO_2 (Figure 1). The (scaled) CCSD(T) OH frequency of $NO_2^+(HO^{35}Cl)$, 3513 cm^{-1}, agrees well with the band at 3574 cm^{-1}. The second most stable isomer is a covalently bound species of $(OH)(OCl)NO^+$, formed by protonation on the terminal oxygen and calculated to be 20 kcal/mol higher than the ion-molecule complex. The (scaled) OH stretch, 3410 cm^{-1}, differs by only 24 cm^{-1} from the observed band at 3382 cm^{-1}.

The measurements of photofragment signals at 3574 cm^{-1} as a function of laser fluence in Figure 8 show that the dependence is nearly linear, indicating that one photon is required to dissociate the protonated species. This observation suggests that the binding energy of protonated chlorine nitrate is smaller than that of protonated nitric acid and closer to the photon energy of ca. 10.5 kcal/mol. This limit is consistent with the *ab initio* value of 12.9 ± 2.0 kcal/mol at the CCSD(T) level of theory.[17]

In contrast to the results from the electron-impact ionization method described above, no protonated species were found in the glow discharge. This fact can be ascribed to the likelihood of switching reactions, given by the large number of collisions occurring in our discharge source. After the plasma is generated, many thermalizing collisions occur as the gas flows through the channel. Although the metastable isomer of protonated chlorine nitrate may be initially formed, the presence of trace water entrained in the beam can induce the replacement of the HOCl ligand. The driving force for this substitution can be found in the thermodynamic stability. According to the *ab initio* theory at the CCSD(T) level, the binding energy of $NO_2^+(H_2O)$ is 4.4 kcal/mol larger than that of $NO_2^+(HOCl)$. Therefore, the dominant ions are the series of $NO_2^+(H_2O)_n$ clusters in the absence of protonated chlorine nitrate species (Figure 4).

C. Reactions of $ClONO_2$ on PSCs

One of the heterogeneous reactions occurring on the surface of the PSCs is the hydrolysis reaction converting chlorine nitrate into HOCl and nitric acid:

$$ClONO_2 + H_2O(s) \rightarrow HOCl(g) + HNO_3(ad) \qquad (1)$$

This reaction is too slow to have been measured in the gas phase.[27-29] Since the surface is acidic due to the presence of HCl and HNO_3 in the stratosphere, however, Molina proposed that the reaction would proceed by proton catalysis.[16] Due to the higher gas-phase proton affinity of $ClONO_2$ (176.8 ± 3 kcal/mol) compared to that of water (166.5 kcal/mol), the first step might be the proton transfer from H_3O^+ to chlorine nitrate:

$$H_3O^+(s) + ClONO_2 \rightarrow H_2O(s) + HClONO_2^+ \qquad (2)$$

As we have observed, the protonated chlorine nitrate is a weakly bound ion-molecule complex of $NO_2^+(HOCl)$. This reaction intermediate is surrounded by water molecules and therefore undergoes the ligand replacement of HOCl by water, resulting in thermodynamically more stable $NO_2^+(H_2O)$. Recent infrared spectroscopic results on the $NO_2^+(H_2O)_n$ (n = 1 to 5) obtained in our group[20,30] show that when the NO_2^+ is sufficiently hydrated, the intracluster rearrangement reaction $NO_2^+(H_2O)_n \rightarrow H_3O^+(H_2O)_{n-2} + HNO_3$ occurs within the cluster due to the more favorable solvent stabilization of the H_3O^+ ion core. The net reaction of this hydration step is

$$NO_2^+ + 2H_2O(s) \rightarrow H_3O^+ + HNO_3\,(ad) \qquad (6)$$

The overall steps can be summarized in the following catalytic cycle:

$$H^+ + H_2O(s) \rightarrow H_3O^+(s)$$

$$H_3O^+(s) + ClONO_2 \rightarrow H_2O(s) + HClONO_2^+$$

$$HClONO_2^+ \rightarrow HOCl(g) + NO_2^+$$

$$NO_2^+ + 2H_2O(s) \rightarrow H_3O^+(s) + HNO_3\,(ad)$$

$$H_3O^+(s) \rightarrow H^+ + H_2O(s)$$

Net reaction: $ClONO_2 + H_2O(s) \rightarrow HOCl(g) + HNO_3(ad)$

Our infrared studies suggest that if the heterogeneous reaction is acid-catalyzed, then the intermediate may be a complex of NO_2^+ and H_2O.

A similar reaction mechanism was recently found on the N_2O_5-doped ice surface. Horn *et al.* studied the reaction of N_2O_5 on PSCs using reflectance absorption infrared

spectroscopy (RAIRS).[31] Through the observation of infrared bands of NO_2^+ and NO_3^-, they proposed the following acid-catalyzed reaction mechanism:

$$H_3O^+(s) + N_2O_5 \rightarrow H_2O(s) + NO_2^+(HNO_3) \quad (7)$$

The species $NO_2^+(HNO_3)$ undergoes the same type of dissociation into $NO_2^+ + HNO_3$, followed by dissociative ionization of HNO_3 into $H^+ + NO_3^-$.

4.5 SUMMARY

Our experimental results show that there is a remarkable similarity in the chemistry of protonated nitric acid and chlorine nitrate. Both species have the same pattern of photodissociation into $NO_2^+ + HOX$ (X = H, D, ^{35}Cl, ^{37}Cl). Infrared spectra show that the protonated species generated by our discharge and electron-impact sources has two types of isomers. The structure of the ground-state isomer is an ion-molecule complex, $NO_2^+(HOX)$, and the second most stable isomer is a covalently bound species, $(OH)(OX)NO^+$, formed by protonation of the terminal oxygen. We found evidence for an IR photon-induced isomerization reaction. These spectroscopic results are quite consistent with the predictions of *ab initio* theory.

The structural information obtained from our infrared spectroscopy may provide an important clue to the mechanism of the heterogeneous reactions on PSCs. The studies suggest that if the heterogeneous reaction is acid-catalyzed, then the intermediate may be an ion-molecule complex of NO_2^+ and HOX.

4.6 REFERENCES

1. J.C. Farman, B.G. Gardiner, and J.D. Shankin, Nature, **315**, 207 (1985).

2. D.J. Hofmann, J.W. Harder, S.R. Rolf, and J.M. Rosen, Nature, **326**, 59 (1986).

3. M.J. Molina and F.S. Rowland, Nature, **249**, 810 (1974).

4. J.P.D. Abbatt and M.J. Molina, Annu. Rev. Energy Environ. **18**, 1 (1993) and references therein.

5. J.G. Anderson, D.W. Toohey, and W.H. Brune, Science, **251**, 39 (1991).

6. S. Solomon, R.R. Garcia, F.S. Rowland, and D.J. Wuebbles, Nature, **321**, 755 (1986).

7. D.W. Toohey, L.M. Avallone, L.R. Lait, P.A. Newman, and M.R. Schoeberl, Science, **261**, 1134 (1993).

8. M.T. Leu, Geophys. Res. Lett. **15**, 17 (1988).

9. M.A. Tolbert, M.J. Rossi, and D.M. Golden, Geophys. Res. Lett. **15**, 847 (1988).

10. M.A. Tolbert, M.J. Rossi, P.Malhotra, and D.M. Golden, Science, **238**, 1258 (1987).

11. M.J. Rossi, R.Malhotra, and D.M. Golden, Geophys. Res. Lett. **14**, 127 (1987).

12. M.T. Leu, S.B. Moore, and L.F. Keyser, J. Phys. Chem. **95**, 7763 (1991).

13. L.T. Molina and M.J. Molina, J. Phys. Chem. **91**, 433 (1987).

14. M.B. McElroy, R.J. Salawitch, S.C. Wofsy, and J.A. Logan, Nature, **321**, 755 (1986).

15. S.C. Wofsy, M.J. Molina, R.J. Salawitch, L.E. Fox, and M.B. McElroy, J. Geophys. Res. **93**, 2442 (1988).

16. C.M. Nelson and M. Okumura, J. Phys. Chem. **96**, 6112 (1992).

17. T.J. Lee and J.E. Rice, J. Phys. Chem. **97**, 6637 (1993).

18. J.M. van Doren, A.A. Viggiano, and R.A. Morris, J. Amer. Chem. Soc. **116**, 6957 (1994).

19. B.-M. Haas, K.C. Crellin, K.T. Kuwata, and M. Okumura, J. Phys. Chem. **98**, 6740 (1994).

20. Y. Cao, J.-H. Choi, B.-M. Haas, and M. Okumura, J. Phys. Chem. **98**, 12176 (1994).

21. J.-H. Choi, K.T. Kuwata, B.-M. Hass, Y. Cao, M.S. Johnson, and M. Okumura, J. Chem. Phys. **100**, 7153 (1994).

22. M. Schmeisser, Inorg. Synth. **9**, 127 (1967).

23. Landolt-Bornstein, *Zahlenwerte und funktionen aus physik, chemie, astronomie, geophysik technik*, Springer-Verlag (1960).

24. D. Forney, W.E. Thompson, and M.E. Jacox, J. Chem. Phys. **99**, 7393 (1993).

25. G. Herzberg. *Molecular Spectra and Molecular Structure II, Infrared and Raman Spectra of Polyatomic Molecules* (van Nostrand Reinhold, New York, 1945).

26. T.J. Lee and J.E. Rice, J. Phys. Chem. **96**, 650 (1992).

27. R. Atkinson, E.C. Tuazon, H. MacLeod, S.M. Aschmann, and A.M. Winer, Geophys. Res. Lett. **13**, 117 (1986).

28. R. Atkinson, S.M. Aschmann, E.C. Tuazon, M.A. Goodman, and A.M. Winer, J. Atmos. Chem. **5,** 83 (1987).

29. L.T. Molina, M.J. Molina, R.A. Stachnik, and R.D. Tom, R. D. J. Phys. Chem. **89**, 3779 (1985).

30. Y. Cao, J.-H. Choi, B.-M. Haas, M.S. Johnson, and M. Okumura, J. Chem. Phys. **99**, 9307 (1993).

31. A.B. Horn, T. Koch, M.A. Chesters, M.R.S. McCoustra, and J.R. Sodeau, J. Phys. Chem. **98**, 946 (1994).

TABLE I. Observed vibrational frequencies of protonated HNO_3.

Protonated species	Discharge	Electron-impact	assignment
	frequency/cm^{-1}		
$NO_2^+(H_2O)$	3626	3625	H_2O sym. stretch
	3700, 3708	3698	H_2O antisym. stretch
		3375	OH stretch of $(OH)_2NO^+$
$NO_2^+(HOD)$	3666	3666	OH stretch
	3724	3726	NO_2^+ combination band
		3380	OH stretch of $(OH)(OD)NO^+$
$NO_2^+(HOCl)$*		3574 (3580)	OH stretch
		3706	NO_2^+ combination band
		3382 (3386)	OH stretch of $(OH)(OCl)NO^+$

* The number in parentheses belongs to ^{37}Cl isotope.

4.7 FIGURE CAPTIONS

FIG. 1. Graphical representation of four isomers of protonated chlorine nitrate obtained using the CCSD(T) method. Structure a) is found to be minimum and corresponds to a complex between NO_2^+ and HOCl. The other four isomers, b), c), d) and e), corresponding to local minima are also very close in energy and about 20 kcal/mol less stable than the ground state isomer.

FIG. 2. Time-of-flight mass spectrum of the protonated nitric acid hydrate clusters, $NO_2^+(H_2O)_n$ (n = 0 to 5). The ions were formed in a glow discharge of nitric acid and water vapor seeded in UHP helium at 0 °C and 1000 Torr. The other major peaks are the hydrated hydronium clusters, $H_3O^+(H_2O)_n$, due to the presence of a trace of water vapor in the gas line.

FIG. 3. Time-of-flight mass spectrum of the protonated DNO_3 hydrate ion, $NO_2^+(HOD)$ (m/e = 65). The ions were formed by electron impact ionization. Ions of $NO_2^+(H_2O)$ and $NO_2^+(D_2O)$ appear together.

FIG. 4. Time-of-flight mass spectrum of protonated chlorine nitrate generated a) by electron beam ionization and b) in a glow discharge. Two ionic species of $HClONO_2^+$ at mass 98 and 100 due to the two isotopes of chlorine are seen only in a).

FIG. 5. Vibrational predissociation spectra of protonated nitric acid formed a) in a glow discharge and b) by electron impact ionization. The band at 3375 cm^{-1} is due to the OH stretches of the high energy isomer, $(OH)_2NO^+$.

FIG. 6. Vibrational predissociation spectra of the protonated DNO_3 ion formed a) in a glow discharge and b) by electron impact ionization.

FIG. 7. Vibrational predissociation spectra of the protonated $ClONO_2$ ion formed by electron impact ionization. a) $m/e = 98$ and b) $m/e = 100$.

FIG. 8. The dependence on laser pulse energy of the fragment signal from photodissociation of the parent ions $NO_2^+(H_2O)$ and $NO_2^+(HOCl^{35})$. The lines are fits to a sum of linear and quadratic terms. The fits show a) a nearly quadratic dependence for $NO_2^+(H_2O)$ and b) a nearly linear dependence for $NO_2^+(HOCl^{35})$.

FIG. 9. Graphical representation of four isomers of protonated nitric acid obtained using the CCSD(T) method. Structure a) is found to be minimum. Isomers a) and b) differ by rotation of H_2O and NO_2^+, and are very close energetically ($\Delta E < 0.5$ kcal/mol). The other two isomers, c) and d), corresponding to local minima are also very close in energy and about 20 kcal/mol less stable than the ground state isomer.

FIG. 10. a) Details of the OH stretching bands of the $NO_2^+(H_2O)$ cluster formed in a glow discharge. The ordinate is the yield of the photofragment ions NO_2^+. b) Simulation of the rotational band contour using rotational constants calculated from the *ab initio* structure. The predicted spectrum used a rotational temperature of 80 K and was convoluted with a resolution linewidth of 1.5 cm^{-1}.

FIG. 11. Energy diagram for the protonation reaction of HNO_3. This diagram is based on the *ab initio* values obtained by Lee *et al.*

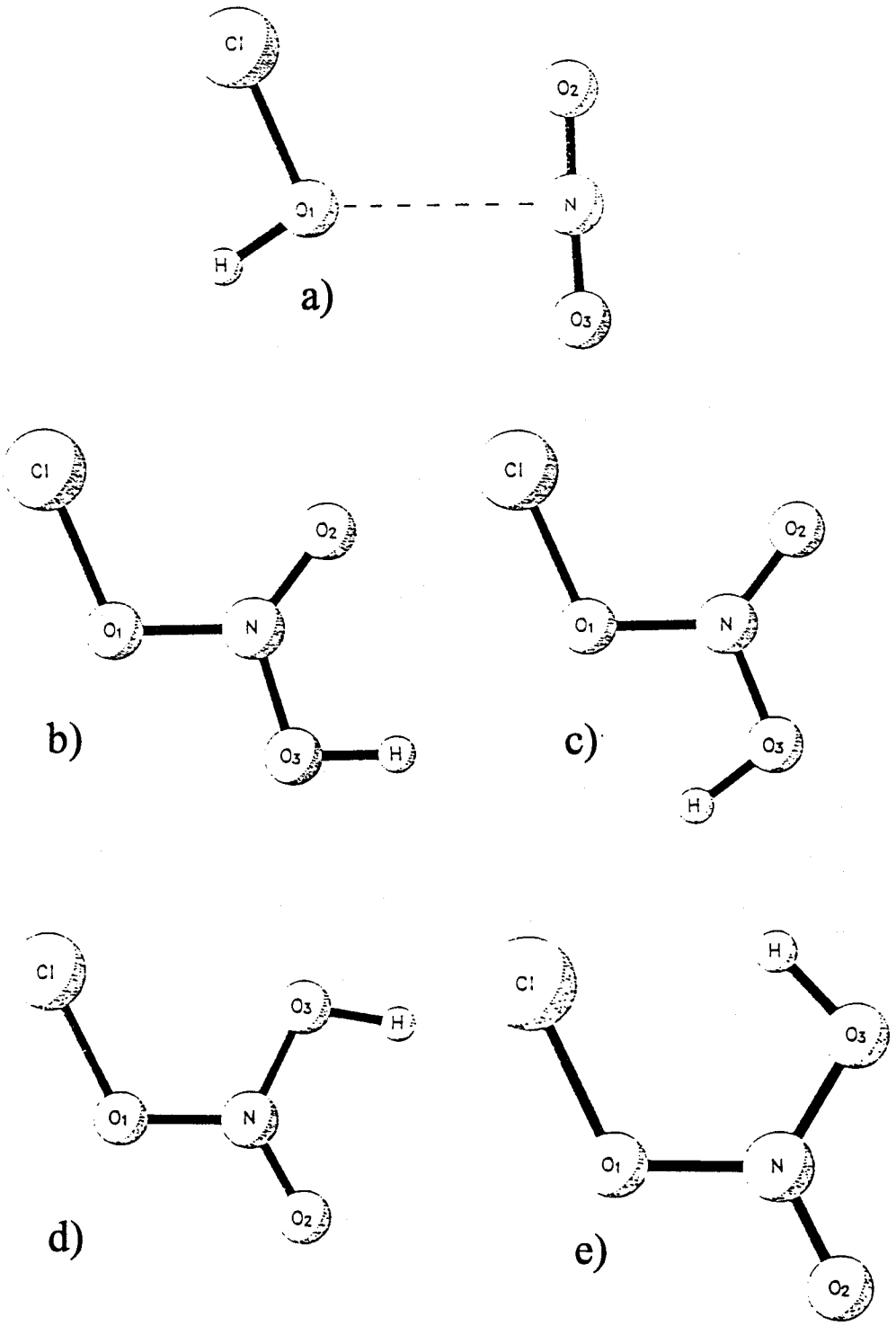
Cl
O2
O1
N
H
a)
O3
Cl
O2
O1
N
b)
O3
H
Cl
O2
O1
N
c)
O3
H
Cl
O3
H
O1
N
d)
O2
H
Cl
O3
O1
N
e)
O2

Figure 1.

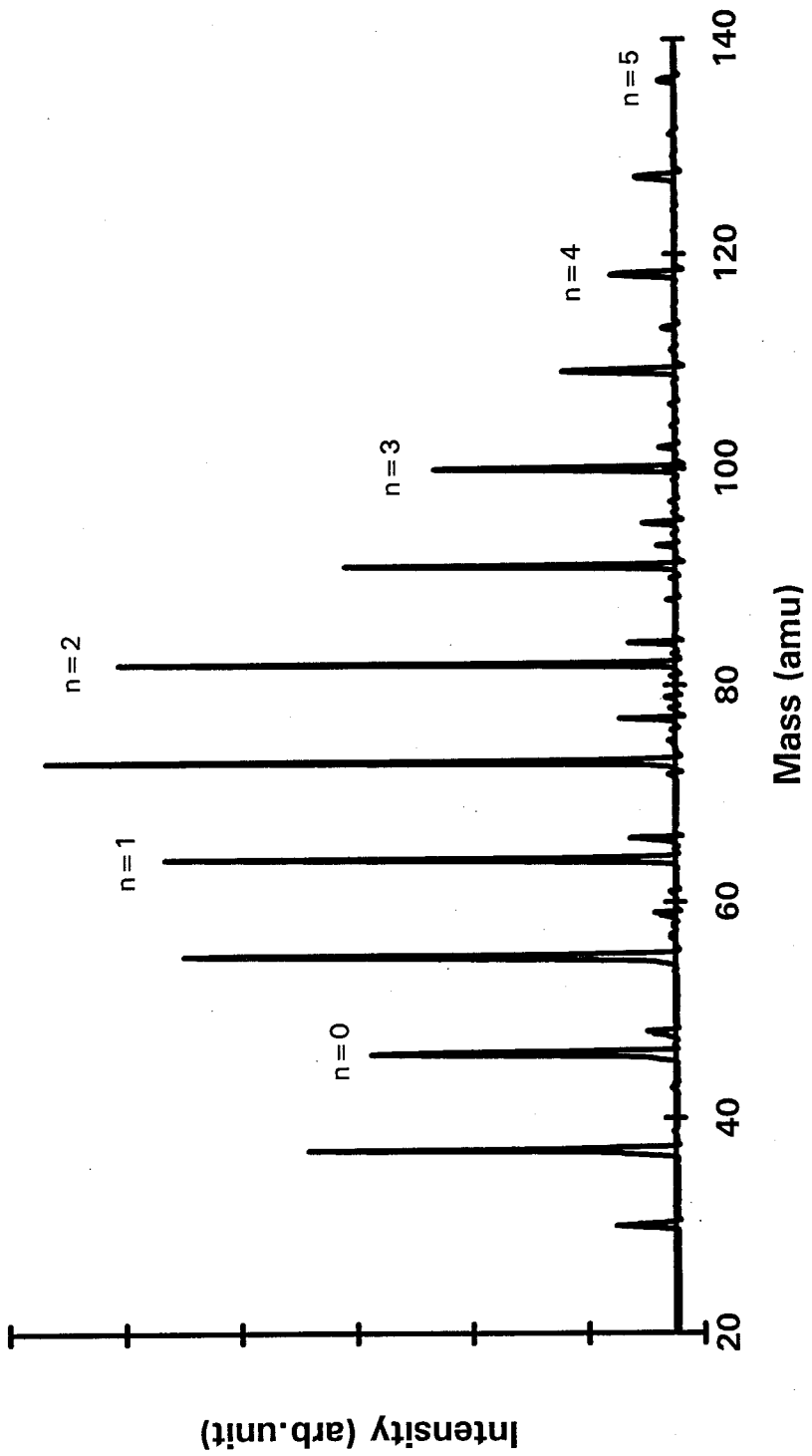
Intensity (arb.unit)
20
40
60
80
100
120
140
Mass (amu)
n=0
n=1
n=2
n=3
n=4
n=5

Figure 2.

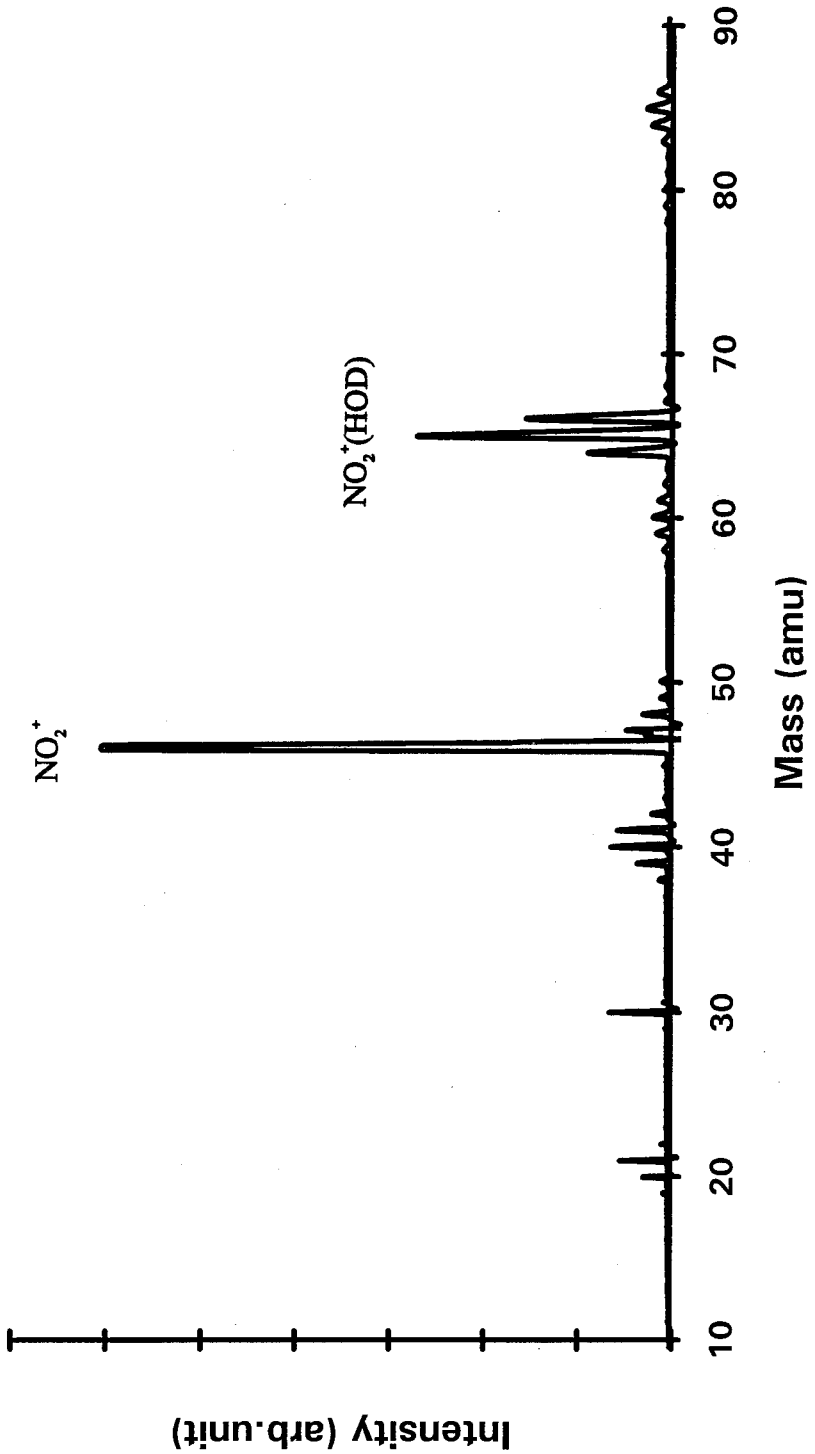
Intensity (arb.unit)
Mass (amu)
10
20
30
40
50
60
70
80
90
NO_2^+
NO_2^+(HOD)

Figure 3.

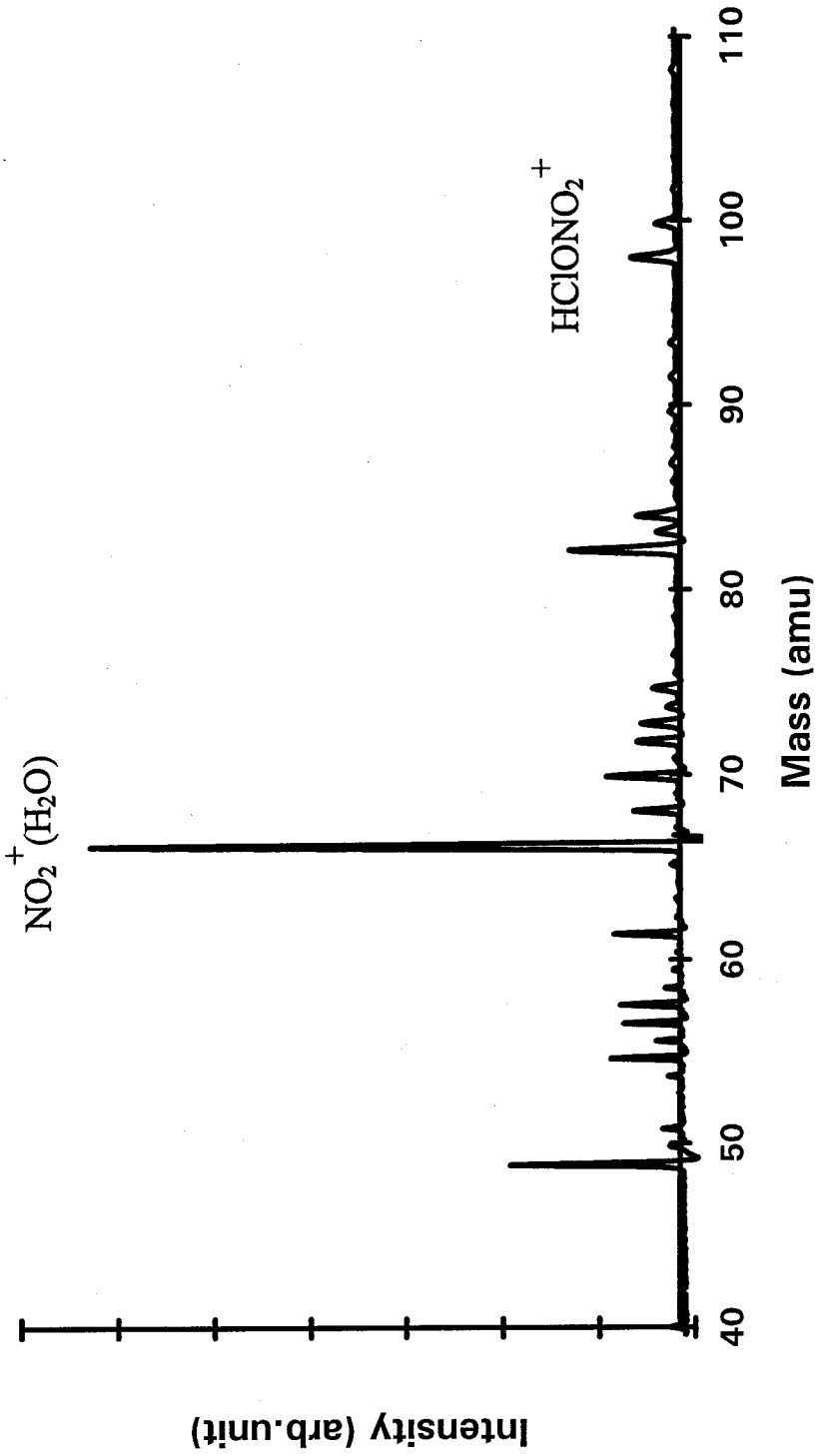
$NO_2^+(H_2O)$
$HClONO_2^+$
Intensity (arb.unit)
Mass (amu)
40
50
60
70
80
90
100
110

Figure 4a.

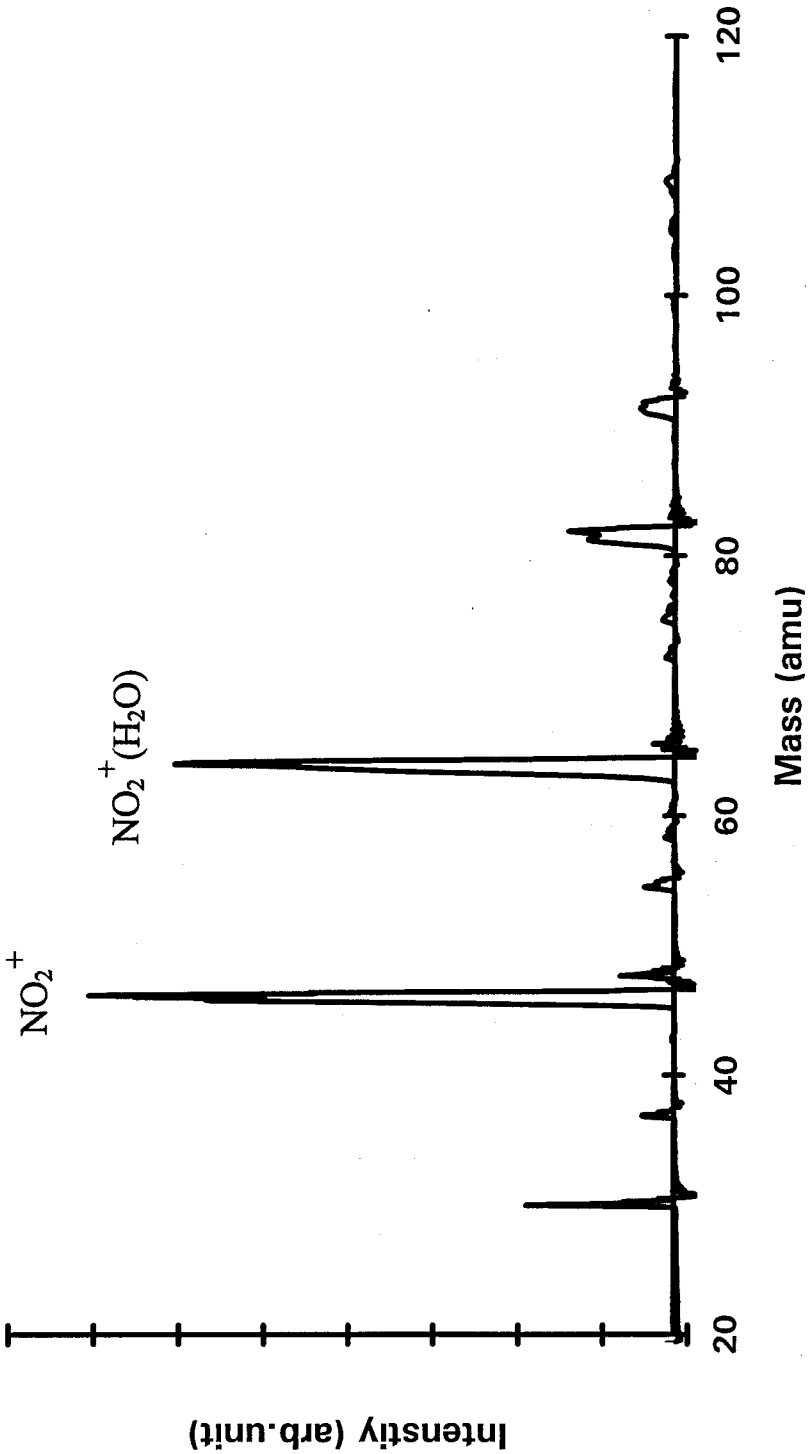

Figure 4b.

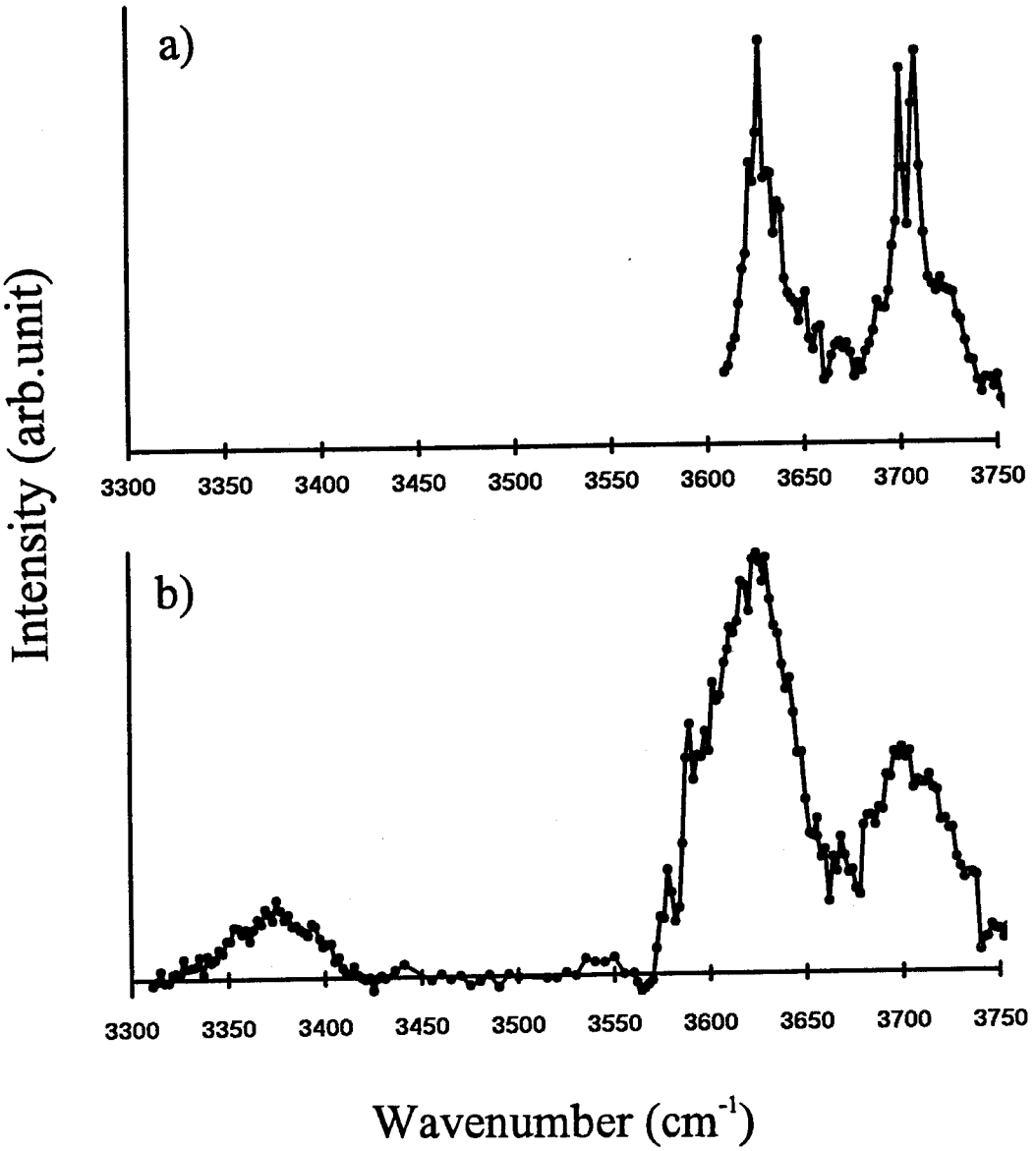
a)
b)
Intensity (arb.unit)
3300
3350
3400
3450
3500
3550
3600
3650
3700
3750
Wavenumber (cm-1)

Figure 5.

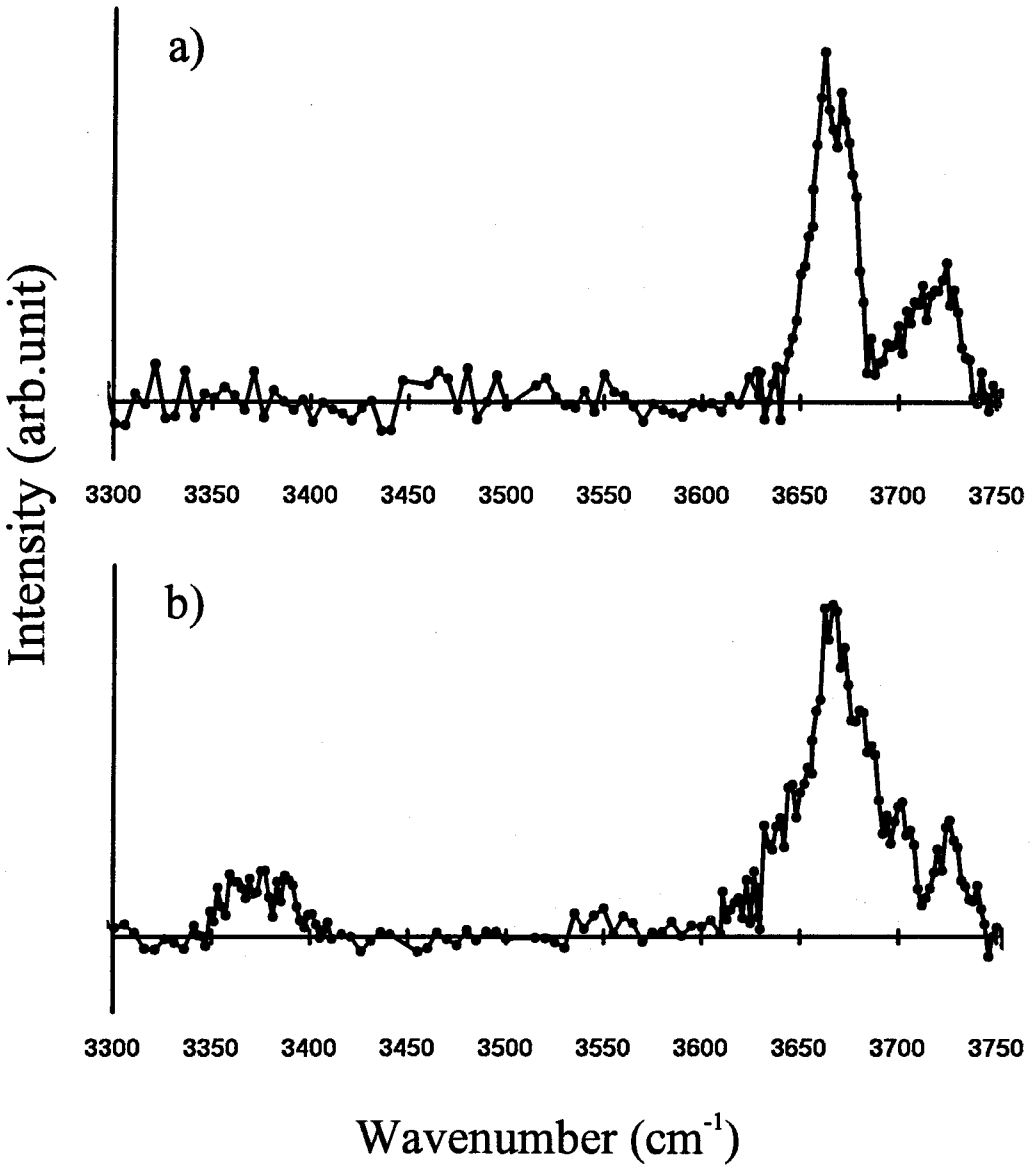
a)
b)
Intensity (arb.unit)
3300
3350
3400
3450
3500
3550
3600
3650
3700
3750
Wavenumber (cm-1)

Figure 6.

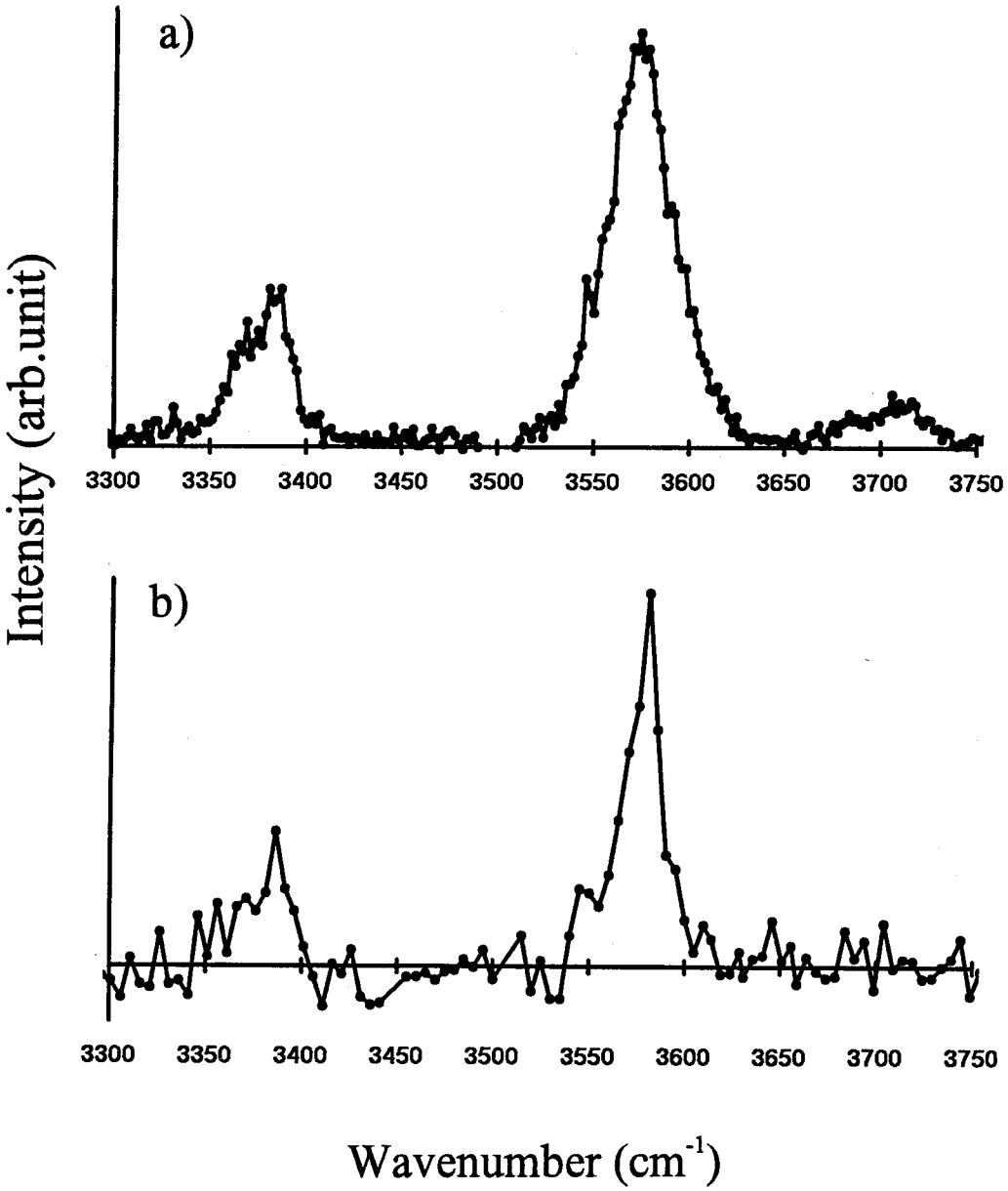
a)
b)
Intensity (arb.unit)
3300
3350
3400
3450
3500
3550
3600
3650
3700
3750
Wavenumber (cm-1)

Figure 7.

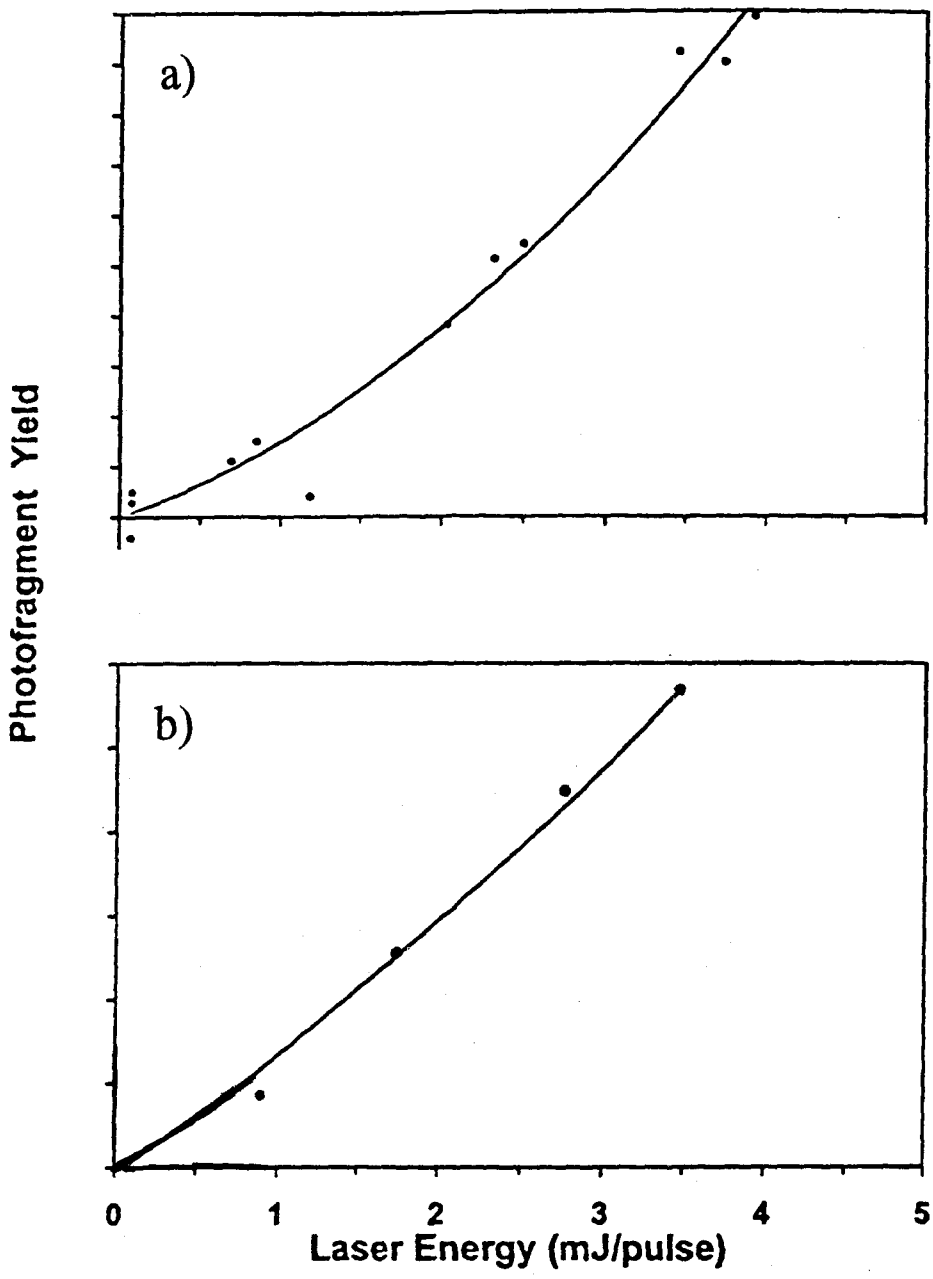

Figure 8.

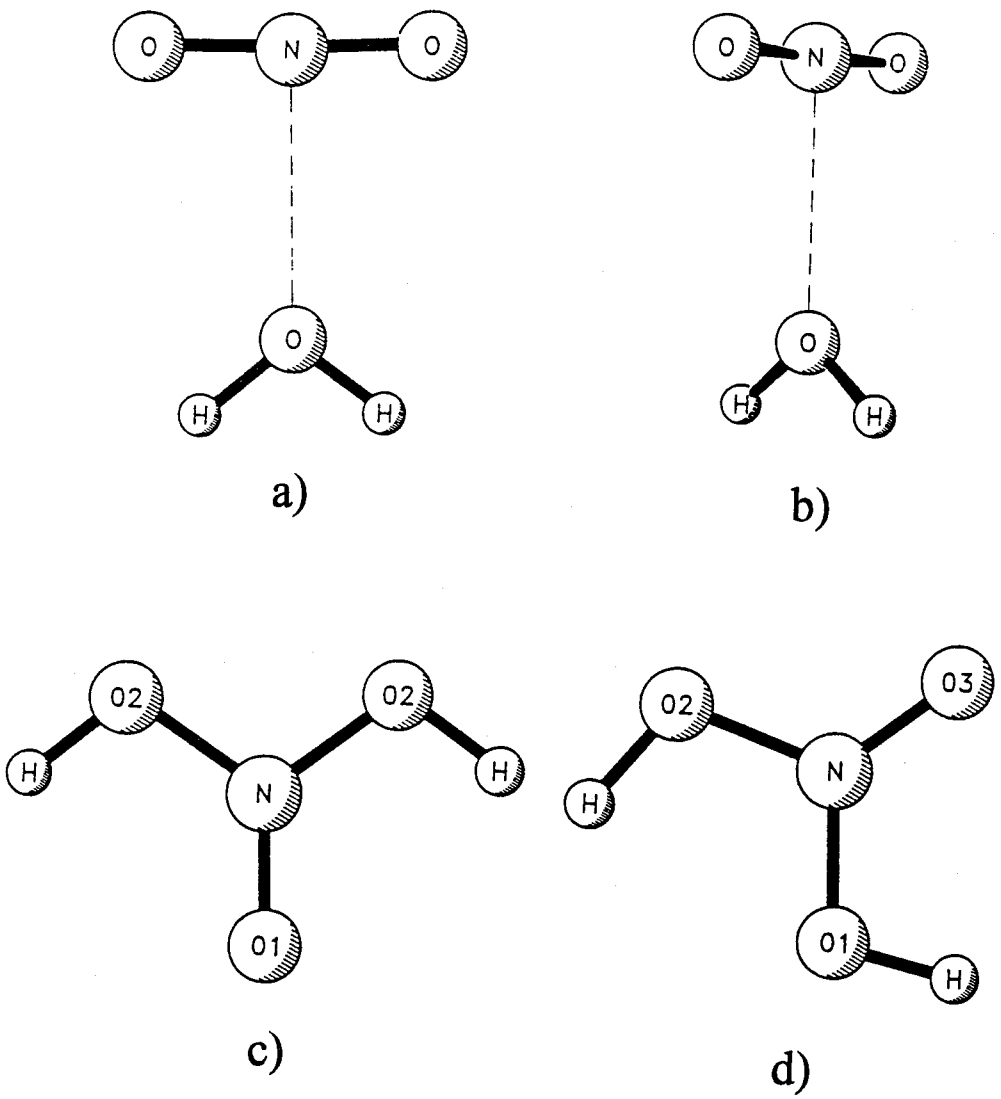

Figure 9.

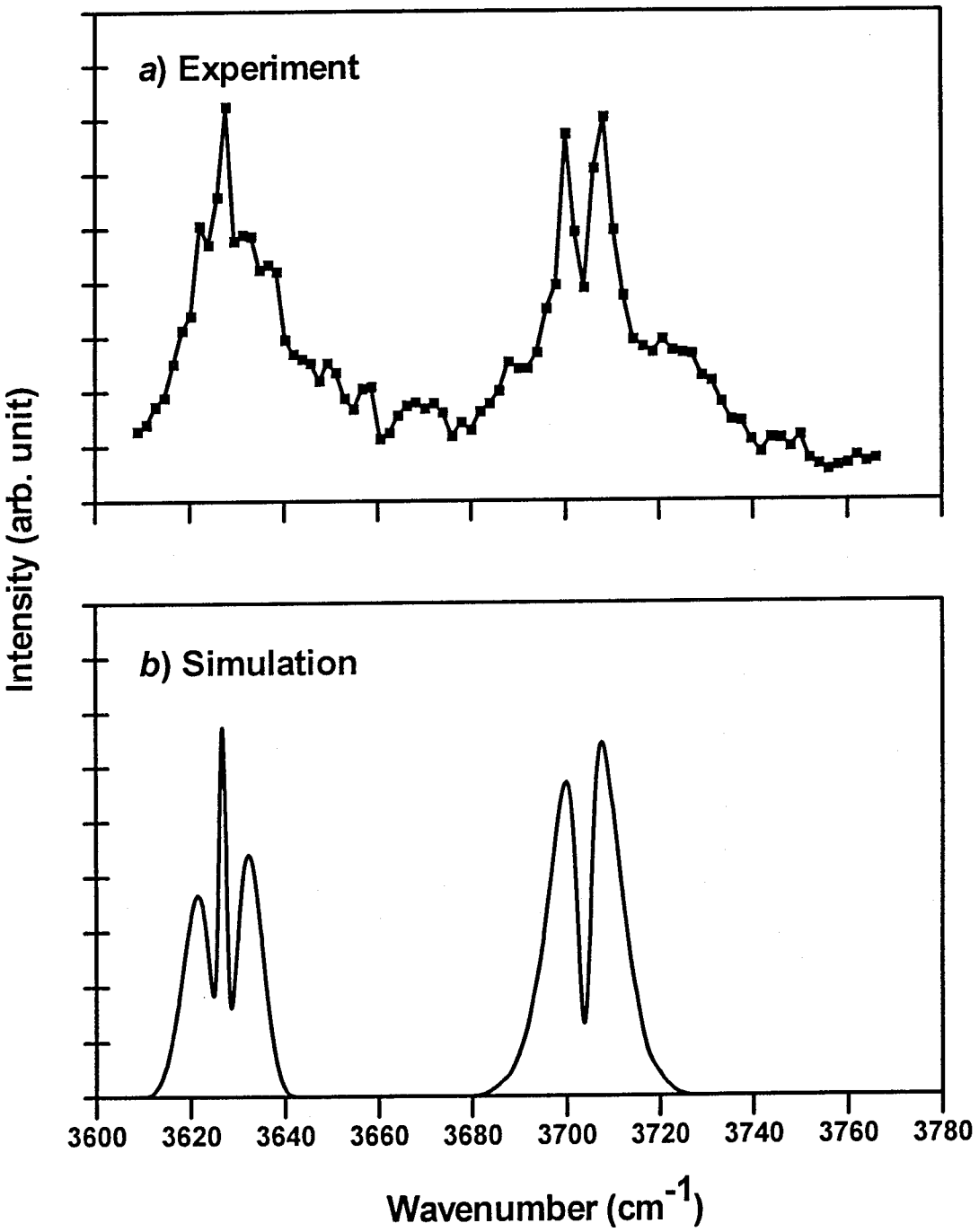
a) Experiment
b) Simulation
Intensity (arb. unit)
3600
3620
3640
3660
3680
3700
3720
3740
3760
3780
Wavenumber (cm-1)

Figure 10.

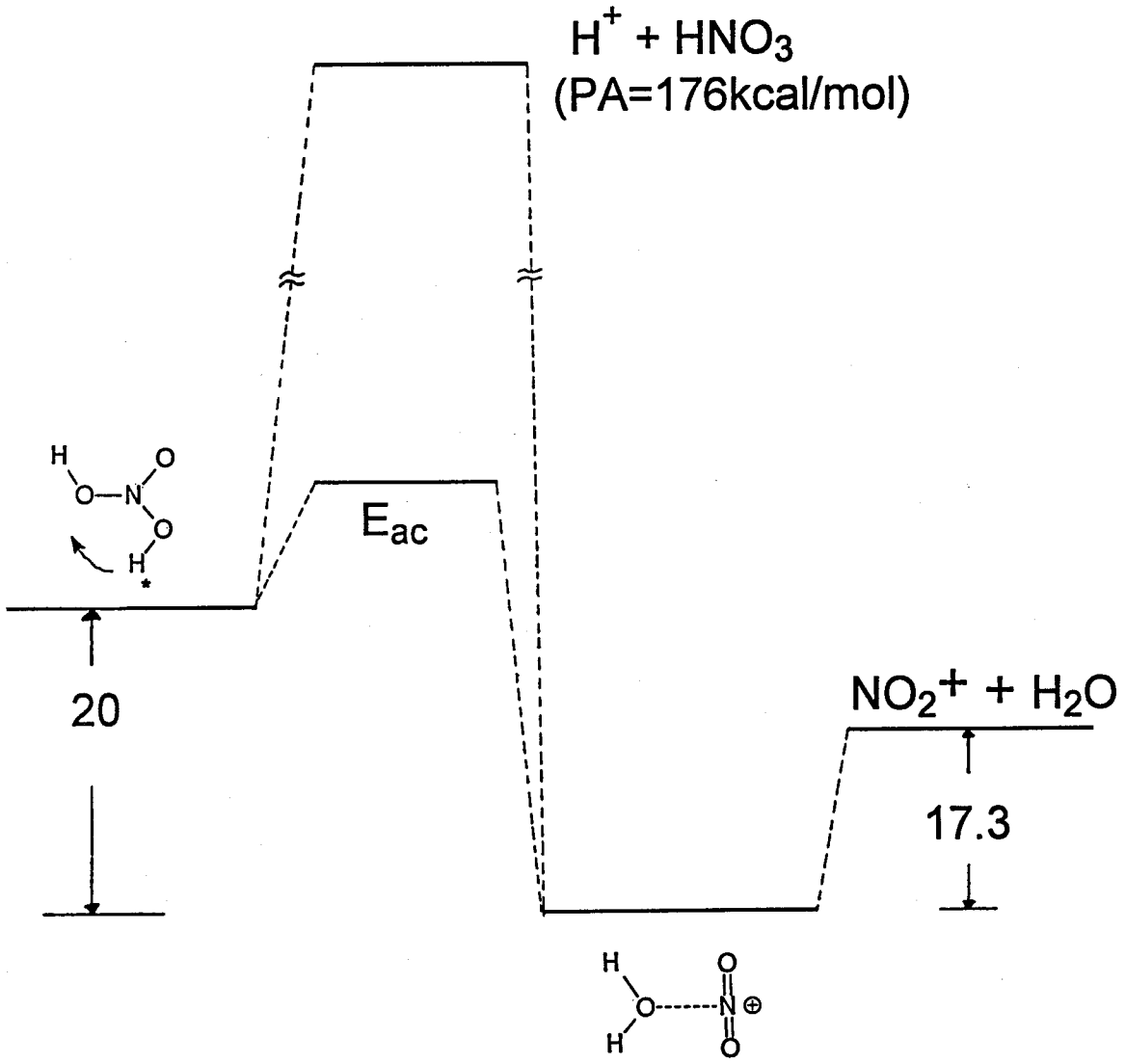

Figure 11.

CHAPTER 5

Infrared Predissociation Spectroscopy of

$Cl^-(H_2O)_n$ (n = 1 to 5)

Studies to elucidate details of ion-molecule interactions at the molecular level are of extreme importance for understanding the solvation process and ion-molecule reactions in clusters and in the condensed phase. In the quest of this purpose, in the previous chapters we presented infrared spectroscopic results on two positively charged ion systems. In Chapter 3 we examined the influence of stepwise ion hydration on the structure and reactivity of NO^+. In Chapter 4 we studied several protonated species, $NO_2^+(HOX)$, to investigate the mechanism of the heterogeneous reactions occurring on stratospheric aerosol particles. In line with these studies of positively charged cluster systems, we have started to investigate the stepwise hydration of negatively charged ion. In this chapter infrared spectroscopic studies on chloride-water clusters, $Cl^-(H_2O)_n$ (n = 1 to 5), the first hydrated anion system we probed, are presented.

5.1 INTRODUCTION

Characterizing gas-phase halide-water clusters is crucial for understanding ion-solvent interactions microscopically. Numerous experimental and theoretical studies have been undertaken to obtain information about energetics, structure, dynamics, and reaction kinetics.

The first experiments on hydrated halide clusters focused on the thermochemistry and association kinetics. Kebarle and co-workers and Hiraoka *et al.* separately obtained stepwise hydration enthalpies, entropies and free energies for halide ions (F^-, Cl^-, Br^-, and I^-) by high-pressure mass spectrometry.[1-6] Fehsenfeld and Ferguson employed the

flowing after-glow technique to examine the three-body association reactions of Cl^- with H_2O to understand processes occurring in the ionosphere.[7]

Structural information about halide-molecule complexes has mostly come from mass spectrometry, photoelectron spectroscopy and in particular, theoretical calculations. Brauman and co-workers[8-10] have employed an ICR mass-spectrometry technique to identify the structures of fluoride-molecule complexes of the form $(ROHF)^-$, where R stands for an organic group. These complexes are intermediates of proton transfer reactions between fluoride anions and alcohols, and have two possible geometries, F^-(ROH) or RO^-(HF). The structure, determined by the photodetachment threshold energies, turned out to be dependent on the organic group. Zook *et al.* generated halide-water clusters using a supersonic jet expansion and deduced some ambiguous structural information from the mass spectra.[11] Cheshnovsky and co-workers[12-15] have extensively applied photoelectron spectroscopy to the $Cl^-(H_2O)_n$, $Br^-(H_2O)_n$, and $I^-(H_2O)_n$ clusters (n = 1-7, 1-16, and 1-60, respectively) and measured the vertical binding energies. It has been shown that a surface isomer, in which an ion is located at the top of the hydrogen-bonded water cluster, and an isomer with the anion internally solvated may be differentiated by comparing experimental and theoretical values for their vertical ionization potentials and that the first solvation shell of the I^- is composed of six water molecules. However, Cheshnovsky and co-workers have recently noted that this approach may not yield a definitive signature of cluster structure.[15]

From the theoretical point of view, the halide water cluster system has been challenging. Structures and energetics have been modeled through either *ab initio* quantum calculations or statistical simulations via molecular dynamics (MD) or Monte Carlo (MC) methods. For $Cl^-(H_2O)$, *ab initio* calculations[16-19] show that the ground-state configuration corresponds to a linearly hydrogen-bonded isomer **Ia** where the Cl^- ion is asymmetrically bonded to water by one of its terminal hydrogens (Fig. 1). Another plausible geometry is a bridged structure **Ib** in which Cl^- is equally shared by both H atoms. However, *ab initio* calculations indicate that isomer **Ib** is a transition state, and that it is only ~1 kcal/mol higher in energy than the hydrogen-bonded minimum **Ia**.

For the large hydrated clusters, MD calculations performed by Perera and Berkowitz and Lybrand and Kollman[20-25] indicated that in halide-water clusters, $X^-(H_2O)_n$ ($n \leq 20$), the system takes one of two types of configuration. For Cl^-, Br^-, and I^-, the anion is not solvated inside a cage of water ligands, but instead attached to the surface of water clusters, $(H_2O)_n$. However, in the case of the F^-, due to size and entropy effects, the F^- ion is solvated within the clusters when $n \geq 4$. Recent MC simulations carried out by Nishimoto and co-workers,[26] however, pointed out that the major configuration at room temperature is the entropy-favored chloride-centered structure, which is inconsistent with the MD calculations.

Ab initio calculations by Combariza, Kestner, and Jortner, and Caldwell and Kollman [18,19,27,28] support the picture of a surface-bound structure for $X^-(H_2O)_n$ (X = F, Cl, Br, and I) for the smaller values of n (≤ 6) and predict that for the $F^-(H_2O)_n$ and I^-

$(H_2O)_n$, a transition from surface to interior structure occurs at n = 4 or 5, and n = 6, respectively. However, the small energy difference between two structures was found to preclude the definite assignment of the isomers as the energy minimum, and the inclusion of zero-point energies and entropy corrections reversed the predicted relative stability. Furthermore, their prediction for the hydrated I^- disagrees with the MD results by Perera *et al.*[20-24] Xantheas and Dunning recently obtained the optimal structures and harmonic vibrational frequencies of $F^-(H_2O)_n$ (n = 1-3) They suggested that for $n \geq 4$ one could not make a distinction between the structures due to the flatness of the potential energy surface.[29]

Infrared predissociation spectroscopy of mass-selected ions has proven to be a useful technique for probing the structure of gas-phase clusters. Our group has used vibrational predissociation spectroscopy, in conjunction with correlated *ab initio* calculations, to explore the structure of $SiH_5^+(H_2)$,[30] $NO_2^+(H_2O)_n$,[31,32] $NO^+(H_2O)_n$ (Chapter 3), and $NO_2^+(HOX)$ (X = H, D, ^{35}Cl, ^{37}Cl) (Chapter 4).

The main objective of this chapter is to investigate the structure of the hydrated chloride clusters, $Cl^-(H_2O)_n$ (n = 1 to 5), using infrared predissociation spectroscopy. To help our analysis of predissociation spectra and elucidate the interactions in the clusters, *ab initio* calculations of the vibrational frequencies, intensities and energies of the clusters n = 1 and 2 were also executed in our group. To our knowledge there have been no previously published theoretical estimates of the vibrational frequencies for n = 2.

5.2 EXPERIMENT

The details of cluster ion generation and spectroscopy have been given in Chapter 2 and other references,[32,33] and only a brief account is presented here. To generate chloride ion clusters, a mixture of H_2O/CCl_4 vapor (partial pressure; $p(CCl_4)$ = 124 Torr and $p(H_2O)$ = 3.6 Torr at 300 K) seeded with CH_4 buffer gas at a total stagnation pressure of ~1500 Torr was prepared. Due to the immiscibility of water and CCl_4, two separate bubblers were used in the middle of gas line. This mixture was introduced into the vacuum through a nozzle of 0.5 mm opened by a piezo-driven pulsed valve at a repetition rate of 10 Hz (ca. 200 μs wide) and intersected by a continuous 750-eV electron beam at the throat of the supersonic expansion. The piezoelectric disc element was coated with halocarbon grease to prevent possible reactions of carbon tetrachloride occurring on the disc surface. Typical emission and Faraday-cup currents were about 2.0 mA, and 100 to 400 μA, respectively.

The resulting $Cl^-(H_2O)_n$ cluster ion beam was skimmed and entered a time-of-flight chamber where the ions were extracted by a pulsed electric field (15 μs wide), accelerated to -0.9 kV and mass-selected. A pulsed tunable infrared laser, a $LiNbO_3$ optical parametric oscillator with 1.5 cm^{-1} resolution,[34,35] was timed to excite only the chloride-water cluster ion of interest as selected by a mass gate which rejected all ions of other *m/e*. The selected ions were excited by a 3 to 5 mJ/pulse of infrared photons, and those that absorbed could undergo vibrational predissociation. Fragment ions were separated from the parent ions using a reflectron energy analyzer, and then detected by a microchannel plate detector. Action spectra were obtained by stepping OPO wavelength and averaging the

photofragment ion signal for 200 shots at each wavelength. Depending on the photofragment signal intensity, scans of 800 to 15,000 shots per point were performed. Background ion signal, primarily caused by collision-induced dissociation (CID) of metastable parents in the ion optics chamber, was subtracted to obtain the fragment signal due only to infrared photodissociation; the spectra were also normalized to the laser fluence.

5.3 EXPERIMENTAL RESULTS

A typical time-of-flight mass spectrum of hydrated chloride clusters is shown in Figure 2. The spectrum clearly showed contributions from the two isotopes of chlorine (mass = 35 and 37) with an intensity ratio of 3 to 1. The distribution could be shifted by adjusting stagnation pressure, temperature, electron-beam energy and position with respect to the expansion nozzle, and pulsed valve settings.

We recorded infrared spectra of mass-selected $Cl^-(H_2O)_n$ for n = 1-5 in the 3100-3850 cm^{-1} region. Figure 3 presents the infrared spectra for n = 1-5 over the entire frequency range and Table I lists the observed band maxima.

A. Photodissociation behavior

The only photofragment ions observed upon vibrational excitation of the clusters $Cl^-(H_2O)_n$ (n = 1 to 5) were $Cl^-(H_2O)_{n-1}$, indicating evaporation of a single water molecule:

$$Cl^-(H_2O)_n \rightarrow Cl^-(H_2O)_{n-1} + H_2O, \qquad n = 1 \text{ to } 5 \qquad (1)$$

Figure 4 shows the dependence of the photodissociation signal on laser pulse energy for $Cl^-(H_2O)$ when exciting the band at 3285 cm^{-1}. The signal revealed a nearly linear dependence, suggesting that the photodissociation was a result of one-photon absorption. The rollover at high fluence is an indication of saturation.

B. Vibrational predissociation spectra

The infrared photodissociation spectrum of $Cl^-(H_2O)$ in Figure 3a consisted of three bands: a medium band at 3156 cm^{-1}, a large band at 3285 cm^{-1}, and a weak band in the blue tail at 3441cm^{-1} (Table I). The band at 3156 cm^{-1} was only 5 cm^{-1} apart from the first overtone of the free water bend (3151 cm^{-1}). The strongest band at 3285 cm^{-1} was significantly red-shifted relative to the H_2O monomer stretch frequencies (3657 and 3756 cm^{-1}), indicative of an OH bond involved as a donor in hydrogen bonding to the chloride ion.

The cluster $Cl^-(H_2O)_2$ exhibited three absorption bands in the 3100-3850 cm^{-1} region (Fig. 3b). The two lower-frequency bands at 3245 and 3317 cm^{-1} were strong and resembled the strongest band of the $n = 1$ spectrum in shape and position, suggesting the formation of two hydrogen-bonded OH stretches. The higher frequency band at 3698 cm^{-1} was very weak. Based upon the closeness of this band to the free OH stretches of a H_2O dimer, the weak band was assigned to the free OH stretch of the water ligands.

In the case of the $Cl^-(H_2O)_3$ cluster (Fig. 3c), we observed two strong bands in the 3200-3400 cm^{-1} region and a weak band at 3696 cm^{-1}. Both bands at 3257 and 3357 cm^{-1} are blue-shifted by 12 and 40 cm^{-1}, respectively, compared to the two bands observed for $n = 2$. The band at 3696 cm^{-1} is comparable to the free OH stretch of $n = 2$.

The predissociation spectrum of the $Cl^-(H_2O)_4$ cluster was qualitatively different from that of $n = 3$ (Fig. 3d). We observed six bands in the 3100-3850 cm^{-1} region. The lowest frequency band at 3249 cm^{-1} was red-shifted compared to both low frequency bands in the $n = 3$ cluster. The 3315 and 3405 cm^{-1} were blue-shifted from the analogous bands in the $n = 3$ spectrum and the band at 3490 cm^{-1} appeared as a shoulder in the blue tail of the 3490 cm^{-1} band. The band at 3600 cm^{-1} indicated that hydrogen bonding between water ligands was involved. We assigned the band at 3698 cm^{-1} to free OH stretches of water ligands.

For $n = 5$, the observed spectrum (Fig. 3e) was very broad in appearance although several bands were still evident. Overall, the spectrum resembled that observed in bulk water. Several possible structures will be discussed based on the spectral features.

5.4 *AB INITIO* CALCULATIONS

To help interpret the predissociation spectra of the $n = 1$ and $n = 2$ clusters, Keith Kuwata in our group performed *ab initio* calculations using the Gaussian 92 system of programs.[36] Only a brief account is given here. Optimized geometries, harmonic vibrational frequencies, and absolute infrared intensities of the clusters in question were calculated at the second-order Møller-Plesset (MP2) level[37] (Tables II to V). In addition, second-order coupled-cluster (CCSD) calculations[38] of the optimized geometries and harmonic vibrational frequencies were performed on $n = 1$ isomers. In all cases, the 6-311++G(*d*,*p*) basis set was used.[39-43] All MP2 and CCSD calculations neglected the correlation of core electrons.

To facilitate comparison of theory with experiment, the *ab initio* O-H stretch frequencies were scaled by comparing the frequencies for free H_2O predicted at the given level of theory with the experimental values in Table VI.

The *ab initio* calculations identified two $n = 1$ isomers shown in Fig. 1, a linear structure (**Ia**) and a bridged structure (**Ib**). The MP2 and CCSD vibrational frequencies indicate that the linear form is a minimum and that the bridged form is a transition state. The *ab initio* calculations also revealed three $n = 2$ isomers, as shown in Fig. 5, a non-hydrogen-bonded form (**IIa**), a hydrogen-bonded form (**IIb**) and a linear form (**IIc**). A linear arrangement of waters about Cl^-, predicted by Combariza, Kestner, and Jortner[19] to be a minimum at the self-consistent (SCF) level, is found to relax to the structure **IIa** at the MP2 level. The O-H stretch frequencies predicted for the two minima, **IIa** and **IIb**, are listed in Tables IV and V. In addition, **IIc** was optimized at the MP2 level under the constraint that the waters remain 180° apart. The O-H stretch frequencies of the resulting partially optimized structure are also listed in Table VII.

5.5 DISCUSSION

A. $Cl^-(H_2O)$

Structural information about $Cl^-(H_2O)$ can be derived from its photodissociation products and infrared spectrum in Figure 3a. The observation of a strong predissociation band at 3285 cm^{-1} leading to $Cl^- + H_2O$ suggests that the cluster is an ion-molecule complex with strong hydrogen bonding. The experimental results are most consistent

with the isomer **Ia** in Figure 1. The observed band at 3285 cm^{-1} agrees well with the (scaled) MP2 frequency of the hydrogen-bonded O-H stretch, 3266 cm^{-1} (Tables II and VI). The band at 3156 cm^{-1} is assigned to the first overtone of the bending mode of water. The H_2O bending fundamental is predicted to have significant oscillator strength (102 km/mol) at the MP2 level of theory, and may gain further intensity through a Fermi resonance interaction with the 3285 cm^{-1} mode. A similar type of Fermi resonance was observed in the NO_2^+(HOD) and NO_2^+(HOCl) clusters, where the intensity of the NO_2^+ combination band was enhanced due to the proximity of the OH fundamental stretch. The position of the observed band also agrees well with the first overtone of the free water bend, 3151 cm^{-1}.[44] The weak band centered at 3441 cm^{-1} is tentatively assigned to a combination of the bonded OH stretch and the Cl^---H intermolecular stretch (184 cm^{-1}, unscaled), which our calculations predict would appear at 3450 cm^{-1}.

Figure 4 shows the measurements of photofragment signals at 3285 cm^{-1} as a function of laser fluence. The dependence is nearly linear, indicating that one photon is required to dissociate the $Cl^-(H_2O)$. This observation suggests that the binding energy places the lower limit on the binding energy of ca. 10 kcal/mol. The observed value[6] is 14.7 ± 0.6 kcal/mol and the linear dependence indicated that the photodissociation was due to absorption of vibrationally hot ions. This limit is consistent with the *ab initio* value of 15.9 ± 2.0 kcal/mol at the CCSD(T) level of theory (Table VIII).

A discrepancy between the experimental spectrum and the *ab initio* calculations for the isomer **Ia** is the absence of a free OH stretch band, expected to occur in the 3700 cm^{-1} region. However, its absence is not surprising. Our calculations predict that the free

OH stretch of the proposed structure has an oscillator strength 35 times weaker than that of the bonded OH stretch. Furthermore, since the transition moment of the free stretch is almost perpendicular to the *a* axis of the complex, the intensity will be distributed over many wide-spaced sub-bands. Alternatively, it is possible that excitation of the free stretch may not couple well to the dissociative coordinate, such that the excited cluster may not predissociate.

The absence of a band at ca. 3700 cm^{-1}, on the other hand, might suggest that the cluster has the structure **Ib**. This structure is calculated to be energetically only ~1 kcal/mol higher in energy than the linear isomer **Ia**. However, we discount this possibility. Both predicted OH stretch bands of the bridged isomer have significant oscillator strength and would appear (scaled) at 3613 and 3644 cm^{-1}, respectively, frequencies which are more than 300 cm^{-1} above the single observed OH stretch band (Tables III and VI). Moreover, the bridged isomer is predicted to be a transition state even at the more sophisticated CCSD level of theory. We therefore conclude that the structure of $Cl^-(H_2O)$ is the ion-molecule structure **Ia** with one hydrogen-bonded OH stretch. We cannot exclude the possibility that we have probed some vibrational average of the linear and bridged structures, but if this is the case the averaged spectrum most resembles that predicted for the lowest energy isomer.

B. $Cl^-(H_2O)_2$

In the case of $n = 2$ (Fig. 3b), the two strong absorption bands in the 3200-3450 cm^{-1} region are evidence that two ionic hydrogen bonds have formed. Unlike for the $n = 1$ cluster, we have also observed a small band centered at 3698 cm^{-1}, corresponding to a

free OH stretch of a water ligand. Based on the infrared spectrum, we infer that the $n = 2$ cluster has a Cl^- core bound by two water ligands.

Our experimental results are most consistent with *ab initio* structure **IIa** shown in Figure 5a. The (scaled) symmetric and antisymmetric MP2 frequencies of the free OH stretches, 3687 and 3695 cm^{-1}, agree well with the observed band at 3698 cm^{-1}, and the observed splitting of the H-bonded OH stretches of ~70 cm^{-1} is comparable to the predicted harmonic splitting of ~45 cm^{-1} (Table VII).

The isomer we observed is probably not the hydrogen-bonded isomer **IIb**, even though it is predicted to be ~0.5 kcal/mol more stable than the non-hydrogen-bonded structure **IIa**. The key difference between the two isomers lies in the hydrogen bonding between the two water ligands. Our *ab initio* calculations predict that the hydrogen-bonded isomer have three bonded O-H stretches with significant oscillator strength, including two strong bands in the 3500-3650 cm^{-1} region (Table V). It would also be expected that at least one of the bonded OH stretches would be significantly blue-shifted relative to the $n = 1$ bonded stretch. However, in the spectrum two OH bands were observed below 3500 cm^{-1}, with no peaks in the 3500-3650 cm^{-1} region. Based on the inconsistencies, we therefore conclude that the water ligands are not hydrogen-bonded to each other.

Our experimental data rule out the possibility that the $n = 2$ isomer adopts the linear form, **IIc**. Although we did not find **IIc** to be a stationary point of the potential energy surface at the MP2 level of theory, it is possible that at a more extensive search of the MP2 surface, or a higher-level calculation, **IIc** is a stable isomer. The linear structure

is predicted to have nearly the same vibrational frequencies as the bent non-hydrogen-bonded structure, **IIa**. However, the *ab initio* absolute intensities of the bonded O-H stretches of **IIc** do not agree with the experimental intensities. The theory predicts that only one band will have appreciable intensity. Furthermore, the intensity of the weaker band is predicted to grow only gradually as the bond angle decreases and the H_2O's approach each other. It is therefore likely that the two water molecules adopt a bent configuration about the Cl^- ion, similar to that shown in **IIa**.

The only discrepancy between the experimental results and the *ab initio* calculations for isomer **IIa** is in the positions of the bonded OH stretch bands. Their positions with respect to the analogous $n = 1$ band is unlike what has been observed in other ionic cluster studies. For example, in the case of $H_3O^+(H_2O)_n$ clusters, the ionic hydrogen-bonded OH stretches of the water ligands shift to the blue as n increases because the hydrogen bond strength decreases as the ion core is more hydrated.[45]

In halide-water clusters, however, the operative mechanism appears to be polarization of the halide's electron density: the binding of one water to Cl^- enhances the binding of the other water to Cl^- on the same side of the anion. Following the procedure of Bauschlicher *et al.*,[46] we estimate that the polarizability of chloride ion favors the bent geometry by ~4 kcal/mol over the linear geometry. This effect should hold for the ligands about any closed-shell ion with a large polarizability. Bauschlicher *et al.* found that for $Sr^{2+}(H_2O)_2$, a polarization effect of 2.2 kcal/mol gives rise to an optimal O-Sr-O angle of 116°.

Given the discrepancy between experiment and theory as to the positions of the ionic hydrogen bonds, it is possible that we have not identified the true ground-state $n = 2$ isomer with our *ab initio* calculations. On the other hand, the hydrogen bonds are highly anharmonic, and *ab initio* calculations do not accurately estimate frequencies of OH bonds perturbed by hydrogen bonds. Also, at the temperature of our clusters, it is possible that we have generated a mixture of isomers. Computational studies indicate[19,26] that at room temperature, mixtures of small halide-water clusters may be dominated by internally solvated structures. We are currently studying the effects of source cooling on the observed predissociation spectra.

C. $Cl^-(H_2O)_3$

The observed predissociation spectrum and the photoproducts of the $n = 3$ cluster (Fig. 3c) suggests that this complex is also comprised of water ligands bound to a Cl^- core. We do not have *ab initio* frequencies to guide our assignments for $n = 3$ or larger clusters, and the published structures are all done optimized at low levels of *ab initio* theory or using classical Monte Carlo simulations. Below, six plausible ligand configurations are discussed.

The simplest geometry is the planar structure **IIIa** (Fig. 6) in which the chloride ion is located in the center of the cluster and the three water ligands are equivalent about the C_3 symmetric axis without forming hydrogen bondings between themselves. The structure is predicted to be the highest energy isomer in Monte Carlo simulations.[26] In the case of $F^-(H_2O)_3$, a structure with the same ligand configuration was found to be the transition state in *ab initio* calculations performed by Xantheas and Dunning.[29] The

spectroscopic feature in the 3200-3450 cm^{-1}, however, disagrees with the planar geometry. The geometry will give rise to one strong band arising from the antisymmetric stretch of the three Cl^--bonded OH bonds. The symmetric stretch might be expected to be very weak due to the small change of the dipole moment in the planar geometry.

The cluster we observed might not be the one shown as **IIIb** in Fig. 6. The geometry has C_3 symmetry with all three water ligands participating in cyclic hydrogen bonds between themselves both as proton donors (to Cl^- ion core and to another water) and proton acceptors. The structure is predicted to be the lowest energy isomer in the *ab initio* calculations and 5.9 kcal/mol more stable than the transition state **IIIa** in MC simulations.[19,26] However, the isomer does not possess free OH bonds and therefore could not account for the absorption band at 3696 cm^{-1}.

The most plausible geometry is a pyramidal isomer **IIIc** (Fig. 6). This structure does not possess any hydrogen bonding between the water ligands, which is consistent with the absence of bands between 3500 and 3650 cm^{-1}. Unlike the planar isomer **IIIa**, this pyramidal isomer is expected to have two strong bands in the 3200-3450 cm^{-1}, the A_1 symmetric and E antisymmetric hydrogen-bonded OH stretches. The bands observed at 3257 and 3357 cm^{-1} could then be assigned as antisymmetric and symmetric stretch modes of the three hydrogen-bonded OH stretches. The absence of hydrogen bonding between three water molecules might be ascribed to the entropy effect, which favors the non-hydrogen bonded geometry, as in the case of the $n = 2$.

The isomer **IIId** in Figure 6, which has hydrogen bonding between two adjacent water ligands, is inconsistent with the spectrum. This isomer is calculated to be ~2.2

kcal/mol more stable than the transition state isomer **IIIa** in MC simulations and expected to be more stable than the presumed structure **IIIc** due to the favorable hydrogen bonding between two water ligands.[26] However, the geometry will show four distinct OH stretch bands to the red of 3500 cm^{-1}: three from the water dimer moiety (as in the hydrogen-bonded n = 2 isomer) and a fourth from the other water ligand. There should also be two free OH absorption bands in our scanning region. This picture disagrees with the observed features.

The infrared spectrum is also not in accord with structure **IIIe** (Fig. 6), which involves a hydrogen-bonding bridge with two adjacent water ligands, leading to a ring of four heavy atoms (three O atoms and the Cl^-). For $F^-(H_2O)_3$, the same configuration is predicted to be the second most stable structure.[29] The bridge configuration was proposed in explaining the predissociation spectrum of the $NO^+(H_2O)_4$ cluster, based upon the structure of ice VI (Chapter 3). However, this isomer will, like **IIId**, give rise to four hydrogen-bonded OH stretches: two pairs of symmetric and antisymmetric bands from the two Cl^--bonded and the two bridging OH bonds, respectively. The two free OH stretches should be nearly degenerate, unlike for **IIId**.

Isomer **IIIf** (Fig. 6) is similar to the lowest energy structure **IIIb** except for the absence of a hydrogen bond between two water ligands, and is predicted to be 3.7 kcal/mol less stable than **IIIb** in the MC calculations.[26] The structure is expected to have three Cl^--bonded OH absorption bands, two hydrogen bonded OH stretches, and one free OH stretch, all of which is inconsistent with the observed bands.

The *ab initio* calculations predict that the potential energy surfaces in the clusters of $n \geq 3$ are extremely shallow, suggesting that at a low temperature the probed geometry of the clusters can be significantly displaced from the lowest energy configuration. Therefore, even though structure **IIIc** is not the absolute minimum of the potential energy surface, dynamical effects such as vibrational averaging and entropy may cause **IIIc** to be the configuration closest to what we probe in our experiment.

D. $Cl^-(H_2O)_4$

As discussed in the previous section, several local minimum geometries for the n = 4 cluster may exist, separated only by extremely flat regions of the potential-energy surface, and dynamical effects would probably be important in deducing the structural information. In fact, Xantheas and Dunning[29] pointed out that locating the optimal geometry would probably be very difficult for these large non-rigid clusters with $n \geq 4$. In this section, only qualitative arguments are presented based upon the comparison of the observed spectrum to several theoretically predicted structures.

The n = 4 cluster is the smallest cluster for which we observe a band which strongly suggests that a hydrogen bond between water ligands is formed within the cluster. In addition, we observe four bands in the 3100-3550 cm^{-1} region.

Figure 7 shows four geometries obtained from both low-level *ab initio* and electrostatic MC calculations.[19,26] The lowest energy isomer corresponds to the structure **IVa** in which the chloride ion is located outside the water tetramer cluster. A cyclic chain of hydrogen bonds between water ligands acting as both proton donors and acceptors is formed. This energy minimum structure is predicted to be more stable than the second

lowest energy isomer **IVb** by 2.8 kcal/mol in the *ab initio* calculations.[19] However, it gives rise to no free OH stretches, in disagreement with the observed spectrum.

Isomer **IVb**, predicted to be the second-most stable form in both *ab initio* and MC calculations, is also inconsistent with the spectrum.[19,26] The structure is expected to produce three Cl^--bonded OH stretches (one from a single water ligand and the other two from the water trimer as symmetric and antisymmetric bands), two hydrogen-bonded symmetric and antisymmetric OH stretches and one free OH band, which disagree with the observed absorption bands in the spectrum.

The isomer **IVc** (Fig. 7c) is predicted to be 1.7 kcal/mol less stable than the isomer **IVb** in MC simulations[26] and does not show an agreement with the observed features. The geometry will result in only two degenerate symmetric and antisymmetric Cl^--bonded OH absorption bands below 3500 cm^{-1}.

The observed spectrum is most consistent with the isomer **IVd**. In this configuration, which was found to be 7 kcal/mol less stable than the ground state isomer in MC simulations,[26] two of the water ligands interact with each other; while the other two do not. As discussed in the $n = 2$ cluster, the prominent features of such a structure are that the proton acceptor has a red-shifted Cl^--bonded OH stretch and a free OH stretch, and that the proton donor possesses a significantly blue-shifted Cl^--bonded OH stretch and a hydrogen-bonded OH stretch. We can assign the 3249 cm^{-1} band to the Cl^--bonded OH stretch of the proton acceptor and the 3490 cm^{-1} band (the shoulder in the blue tail of the 3400 cm^{-1} band) to the Cl^--bonded OH stretch of the proton donor. The band at 3600 cm^{-1} can be assigned to the hydrogen bonded OH stretch of the proton

donors. The two bands at 3315 and 3405 cm^{-1} arise from the symmetric and antisymmetric combinations of the OH stretches of the other two water ligands, respectively.

The above assignment assumes that only one isomer is present. However, if the clusters are all at the same temperature, then as *n* increases, more potential minima become accessible. We may therefore be observing spectra from a mixture of isomers. The signature of a mixture is the broad background. This ambiguity makes it difficult to assign features without the aid of predicted frequencies and intensities.

E. $Cl^-(H_2O)_5$

The observed infrared spectrum of the $n = 5$ cluster (Fig. 3e) is very broad and reminiscent of the water stretch bands of the liquid state, but several features are still evident. The band at 3233 cm^{-1} is red-shifted compared to the lowest frequency band in the $n = 4$ cluster, which is characteristic of forming a hydrogen bond between Cl^--bonded water ligands. The band in the 3500-3600 cm^{-1} region can be assigned to H_2O-H_2O hydrogen bond. The band at 3700 cm^{-1} is the free OH stretch. The other bands could be either H_2O-H_2O or ionic hydrogen-bonded OH stretches.

The broadness is most likely be due to the high vibrational temperature of the cluster, and to the flatness of the potential. Both *ab initio* and MC calculations[19,26] predict that the potential is extremely shallow and that locating energy minimum structures is not physically meaningful. For example, the energy difference between the two lowest energy isomers **Va** and **Vb** in Figure 8 is only 0.1 kcal/mol in the *ab initio* calculations and 0.3 kcal/mol in the MC simulations.

Based upon the observed bands, the lowest energy isomer **Va** would not contribute to the 3700 cm^{-1} region due to the absence of a free OH but could still be present as a component in a mixture. The four possible geometries **Vb**, **Vc**, **Vd**, and **Ve**, satisfy the observed band features and any of them or some combination might be the isomer probed in the spectrum.

5.6. SUMMARY

In our first application of vibrational predissociation spectroscopy to negatively charged ionic cluster systems, the infrared spectra of mass-selected hydrated chloride ion, $Cl^-(H_2O)_n$, (n = 1 to 5), were recorded from 3100 to 3850 cm^{-1}. All clusters showed the same photodissociation pattern, breaking into $Cl^-(H_2O)_{n-1} + H_2O$. In $Cl^-(H_2O)$, the water forms a nearly linear hydrogen bond with the chloride ion, and in $Cl^-(H_2O)_2$ and $Cl^-(H_2O)_3$, the water ligands hydrate the chloride ion asymmetrically, but do not form a hydrogen bond with each other. The observed band frequencies and intensities for n = 1 and 2 show a good agreement with the correlated *ab initio* calculations performed in our group. In the n = 4 clusters, the probed structure is the one in which at least one Cl^--bonded water ligand forms a hydrogen bond to an adjacent water ligand. In $Cl^-(H_2O)_5$, a liquid-phase-like broad spectrum was observed with several peaks still apparent.

5.7 REFERENCES

1. M. Arshadi, R. Yamdagni, and P. Kebarle, J. Phys. Chem. **74**, 1475 (1970).

2. M. Arshadi and P. Kebarle, J. Phys. Chem. **74**, 1483 (1970).

3. S. Yamabe, N. Ihira, and K. Hirao, Chem. Phys. Lett. **92**, 172 (1982).

4. S. Yamabe, Y. Furumiya, K. Hiraoka, and K. Morise, Chem. Phys. Lett. **131**, 261 (1986).

5. K. Hiraoka and S. Mizuse, Chem. Phys. **118**, 457 (1987).

6. K. Hiraoka, S. Mizuse, and S. Yamabe, J. Phys. Chem. **92**, 3943 (1988).

7. F.C. Rehsenfeld and E.E. Ferguson, J. Chem. Phys. **61**, 3181 (1974).

8. C.R. Moylan, J.A. Dodd, and J.I. Brauman, Chem. Phys. Lett. **118**, 38 (1985).

9. C.R. Moylan, J.A. Dodd, C.-C. Han, and J.I. Brauman, J. Chem. Phys. **86**, 5350 (1987).

10. D.M. Wetzel and J.I. Brauman, Chem. Rev. **87**, 607 (1987).

11. D.R. Zook and E.P. Grimsrud, Int. J. Mass Spectrom. Ion Processes. **107**, 293 (1991).

12. G. Markovich, R. Giniger, M. Levin, and O. Cheshnovsky, Z. Phys. D **20**, 69 (1991).

13. G. Markovich, R. Giniger, M. Levin, and O. Cheshnovsky, J. Chem. Phys. **95**, 9416 (1991).

14. G. Markovich, S. Pollack, R. Giniger, and O. Cheshnovsky, Z. Phys. D **26**, 98 (1993).

15. G. Markovich, S. Pollack, R. Giniger, and O. Cheshnovsky, J. Chem. Phys. **101**, 9344 (1994).

16. X.G. Zhao, A. Gonzalez-Lafont, D.G. Truhlar, and R. Steckler, J. Chem. Phys. **94**, 5544 (1991).

17. Z. Latajka, J. Molec. Struct. **253**, 225 (1992).

18. J.E. Combariza, N.R. Kestner, and J. Jortner, Chem. Phys. Lett. **203**, 423 (1993).

19. J.E. Combariza, N.R. Kestner, and J. Jortner, J. Chem. Phys. **100**, 2851 (1994).

20. L. Perera and M.L. Berkowitz, J. Chem. Phys. **95**, 1954 (1991).

21. L. Perera and M.L. Berkowitz, J. Chem. Phys. **96**, 8288 (1992).

22. L. Perera and M.L. Berkowitz, J. Chem. Phys. **99**, 4222 (1993).

23. L. Perera and M.L. Berkowitz, J. Chem. Phys. **99**, 4236 (1993).

24. L. Perera and M.L. Berkowitz, J. Chem. Phys. **100**, 3085 (1994).

25. T.P. Lybrand and P.A. Kollman, J. Chem. Phys. **83**, 2923 (1985).

26. T. Asada, K. Nishimoto, and K. Kitaura, J. Phys. Chem. **97**, 7724 (1993).

27. J.E. Combariza, N.R. Kestner, and J. Jortner, Chem. Phys. Lett. **221**, 156 (1994).

28. J.W. Caldwell and P.A. Kollman, J. Phys. Chem. **96**, 8249 (1992).

29. S.S. Xantheas and T.H. Dunning, Jr., J. Phys. Chem. **98**,13489 (1994).

30. Y. Cao, J.-H. Choi, B.-M. Haas, M.S. Johnson, and M. Okumura, J. Phys. Chem. **97**, 5215 (1993).

31. Y. Cao, J.-H. Choi, B.-M. Haas, M.S. Johnson, and M. Okumura, J. Chem. Phys. **99**, 9307 (1993).

32. Y. Cao, J.-H. Choi, B.-M. Haas, and M. Okumura, J. Phys. Chem. **98**, 12176 (1994).

33. Y. Cao, Ph.D. Thesis, California Institute of Technology (1994).

34. S.J. Brosnan and R. L. Byer, IEEE J. Quant. Elect. **QE-15**, 415 (1979).

35. T.K. Minton, S.A. Reid, H.L. Kim, and J.D. McDonald, Optics Commun. **69**, 289 (1989).

36. M.J. Frisch, G.W. Trucks, M. Head-Gordon, P.M.W. Gill, M.W. Wong, J.B. Foresman, B.G. Johnson, H.B. Schlegel, M.A. Robb, E.S. Replogle, R. Gomperts, J.L. Andres, K. Raghavachari, J.S. Binkley, C. Gonzalez, R.L. Martin, D.J. Fox, D.J. Defrees, J. Baker, J.J.P. Stewart, and J.A. Pople, Gaussian 92, Revision D.2., Gaussian Inc., Pittsburgh, PA, 1992.

37. C. Møller and M.S. Plesset, Phys. Rev. **46**, 618 (1934).

38. R.J. Bartlett, J. Phys. Chem. **93**, 697 (1989).

39. R. Krishnan, J.S. Binkley, R. Seeger, and J.A. Pople, J. Chem. Phys. **72**, 650 (1980).

40. A.D. McLean and G.S. Chandler, J. Chem. Phys. **72**, 5639 (1980).

41. T. Clark, J. Chandrasekhar, G.W. Spitznagel, and P.V.R. Schleyer, J. Comput. Chem. **4**, 294 (1983).

42. W.J. Hehre, R. Ditchfield, and J.A. Pople, J. Chem. Phys. **56**, 2257 (1972).

43. P.C. Hariharan and J.A. Pople, Theor. Chem. Acta **28**, 213 (1973).

44. G. Herzberg, *Molecular Spectra and Molecular Structure. II. Infrared and Raman Spectra of Polyatomic Molecules* (van Nostrand Reinhold, New York, 1945).

45. L.I. Yeh, M. Okumura, J.D. Myers, J.M. Price, and Y.T. Lee, J. Chem. Phys. 91, 7319 (1989).

46. C.W. Bauschlicher, M. Sodupe, and H. Partridge, J. Chem. Phys. **96**, 4453 (1992).

TABLE I. Observed vibrational frequencies of hydrated chloride ion.

cluster	frequency/cm^{-1}	assignment
$Cl^-(H_2O)$	3156	1st H_2O bending overtone
	3285	Cl^--bonded OH stretch
	3441	combination band of H-bonded OH and Cl^--H
$Cl^-(H_2O)_2$ [a)]	3245	Cl^--bonded antisym. OH stretch
	3317	Cl^--bonded sym. OH stretch
	3698	Free OH stretch
$Cl^-(H_2O)_3$ [b)]	3257	Cl^--bonded antisym. OH stretch
	3357	Cl^--bonded sym. OH stretch
	3696	Free OH stretch
$Cl^-(H_2O)_4$ [c)]	3249	Cl^--bonded OH stretch of proton acceptor
	3315	Cl^--bonded H_2O stretch
	3405	Cl^--bonded H_2O stretch
	3490	Cl^--bonded OH stretch of proton donor
	3600	H-bonded free OH stretch
	3698	Free OH stretch

a) Band assignments are based on the structure IIa of Fig. 5.
b) Band assignments are based on the structure IIIc of Fig. 6.
c) Band assignments are based on the structure IVd of Fig. 7.

TABLE II. *Ab initio* harmonic frequencies (MP2/6-311++G**) for the linear hydrogen-bonded $n = 1$ isomer.

Mode	Approx. Description	Frequencies/cm^{-1} (Intensities/km mol^{-1})
$\omega_1(a')$	O-H free stretch	3952 (30)
$\omega_2(a')$	Cl^--bonded O-H stretch	3475 (1026)
$\omega_3(a')$	H_2O bend	1708 (102)
$\omega_4(a'')$	H_2O wag	754 (120)
$\omega_5(a')$	H_2O rock	361 (73)
$\omega_6(a')$	Cl^--H intermol stretch	184 (24)

TABLE III. *Ab initio* harmonic frequencies (MP2/6-311++G**) for the bridged $n = 1$ isomer.

Mode	Approx. Description	Frequencies/cm^{-1} (Intensities/km mol^{-1})
$\omega_1(a')$	O-H free stretch	3877 (59)
$\omega_2(a')$	Cl^--bonded O-H stretch	3844 (111)
$\omega_3(a')$	H_2O bend	1698 (246)
$\omega_4(a'')$	H_2O wag	643 (198)
$\omega_5(a')$	H_2O rock	290*i*
$\omega_6(a')$	Cl^--H intermol stretch	156 (14)

TABLE IV. *Ab initio* harmonic frequencies (MP2/6-311++G**) for the non-hydrogen-bonded $n = 2$ isomer.

Mode	Approx. Description	Frequencies/cm^{-1} (Intensities/km mol^{-1})
ω_1	O-H free stretch	3930 (37)
ω_2	O-H free stretch	3923 (83)
ω_3	Cl^--bonded sym O-H stretch	3581 (1046)
ω_4	Cl^--bonded antisym O-H stretch	3534 (422)
ω_5	H_2O bend	1717 (112)
ω_6	H_2O bend	1711 (54)
ω_7		738 (157)
ω_8		712 (143)
ω_9		438 (95)
ω_{10}		425 (61)
ω_{11}		344 (18)
ω_{12}		194 (24)
ω_{13}		165 (57)
ω_{14}		117 (63)
ω_{15}		89 (8)

TABLE V. *Ab initio* harmonic frequencies (MP2/6-311++G**) for the hydrogen-bonded $n = 2$ isomer.

Mode	Approx. Description	Frequencies/cm^{-1} (Intensities/km mol^{-1})
ω_1	O-H free stretch	3949 (36)
ω_2	H-bonded O-H stretch	3867 (146)
ω_3	Cl^--bonded O-H stretch	3719 (401)
ω_4	Cl^--bonded O-H stretch	3408 (1008)
ω_5	H_2O bend	1730 (125)
ω_6	H_2O bend	1704 (80)
ω_7		813 (172)
ω_8		669 (191)
ω_9		474 (39)
ω_{10}		416 (62)
ω_{11}		364 (18)
ω_{12}		207 (32)
ω_{13}		181 (88)
ω_{14}		157 (2)
ω_{15}		88 (0)

TABLE VI. Observed and *ab initio* vibrational frequencies in cm^{-1} (intensities in km/mol) for $n = 1$ isomers.

Assignment	Expt.	Linear		Bridged	
		Unscaled	Scaled	Unscaled	Scaled
H_2O bend overtone	3156				
Cl^--bonded O-H stretch	3285	3475 (1026)	3266	3844 (111)	3613
Combination	3441				
O-H free stretch		3952 (30)	3715	3877 (59)	3644

TABLE VII. Observed and *ab initio* vibrational frequencies in cm^{-1} (intensities in km/mol^{-1}) for $n = 2$ isomers.

Assignment	Expt.	Non-H-Bonded		H-Bonded		Linear	
		Unscaled	Scaled	Unscaled	Scaled	Unscaled	Scaled
Cl^--bonded O-H stretch	3245	3534 (422)	3321	3408 (1008)	3204	3553 (1718)	3340
Cl^--bonded O-H stretch	3317	3581 (1046)	3366	3719 (401)	3496	3583 (29)	3368
H-bonded stretch				3867 (146)	3635		
O-H free stretch	3698	3923 (83)	3687	3949 (36)	3712	3928 (49)	3693
O-H free stretch		3930 (37)	3695			3929 (26)	3694

TABLE VIII. *Ab initio* thermochemical data[a] for $Cl^-(H_2O)_n \rightarrow Cl^-(H_2O)_{n-1} + H_2O$

	ΔE_0/kcal mol^{-1}				ΔH^0_{298}/kcal mol^{-1}		
Cluster	MP2	MP2+ZPE	CCSD	CCSD+ZPE	MP2	CCSD	Expt.[b]
$n = 1$ linear	15.5	14.2	17.3	15.9	14.2	15.9	14.7
$n = 1$ bridged	14.0	13.0	16.0		13.1		
$n = 2$ non-H-bonded	15.1	12.7			13.4		
$n = 2$ H-bonded	15.7	13.1			13.9		

[a] In all cases, the 6-311++G** basis set is used.
[b] Reference 6.

5.8 FIGURE CAPTIONS

FIG. 1. MP2-optimized geometries of $n = 1$ (**Ia** and **Ib**) isomers.

FIG. 2. Time-of-flight mass spectrum of chloride-water clusters generated by electron beam ionization. The spectrum shows the contributions from the two isotopes of chlorine (mass = 35 and 37).

FIG. 3. Vibrational predissociation spectrum of $Cl^-(H_2O)_n$ ($n = 1$ to 5). The ordinate is the photofragment signal of $Cl^-(H_2O)_{n-1}$.

FIG. 4. The dependence on laser pulse energy of the fragment signal from photodissociation of the parent ions $Cl^-(H_2O)$. The signal at low fluencies showed a nearly linear dependence and the rollover at high fluencies is an indication of saturation.

FIG. 5. MP2-optimized geometries of $n = 2$ (**IIa**, **IIb**, and **IIc**) isomers. For **IIa**, the H-Cl-H bond angle is 67.6°, and for **IIb**, the H-Cl-H bond angle is 66.3°. For **IIc**, the H-Cl-H bond angle was constrained to be 180°.

FIG. 6. Plausible structures of $n = 3$.

FIG. 7. Plausible structures of $n = 4$.

FIG. 8. Plausible structures of $n = 5$.

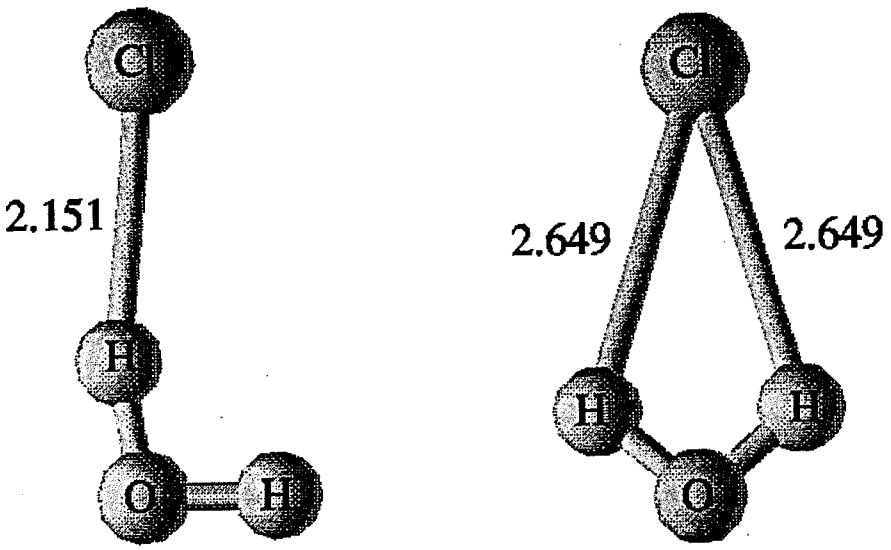

Ia) Ib)

Figure 1.

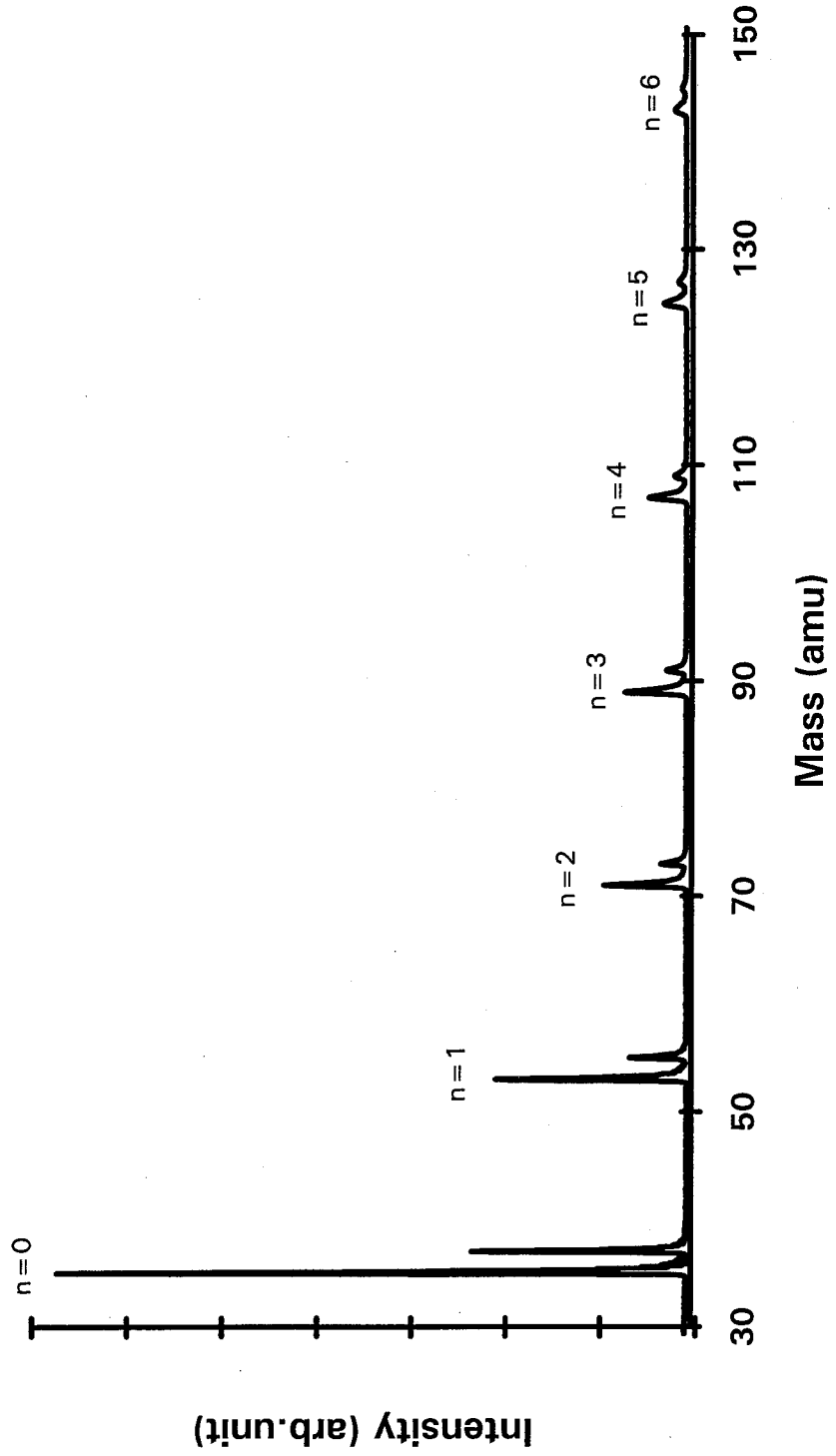
Intensity (arb.unit)
Mass (amu)
30
50
70
90
110
130
150
n = 0
n = 1
n = 2
n = 3
n = 4
n = 5
n = 6

Figure 2.

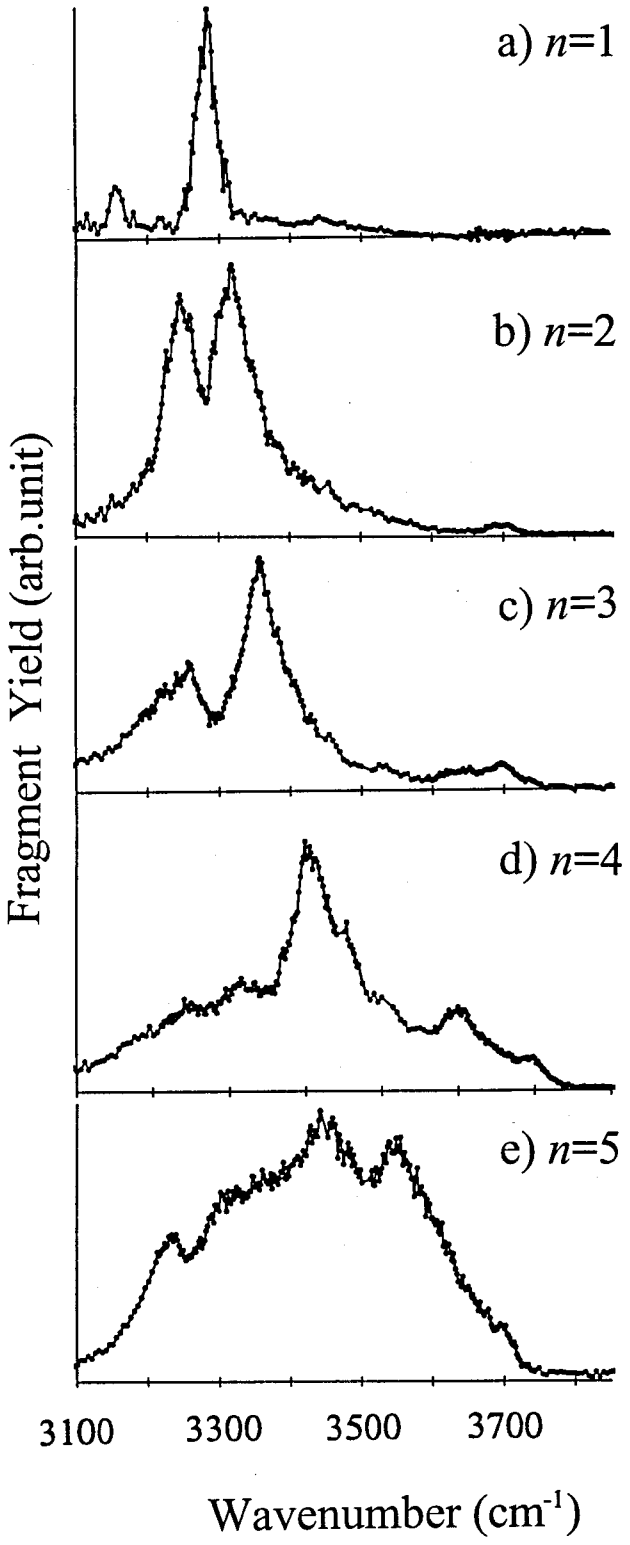
a) n=1
b) n=2
c) n=3
d) n=4
e) n=5
Fragment Yield (arb.unit)
3100
3300
3500
3700
Wavenumber (cm-1)

Figure 3.

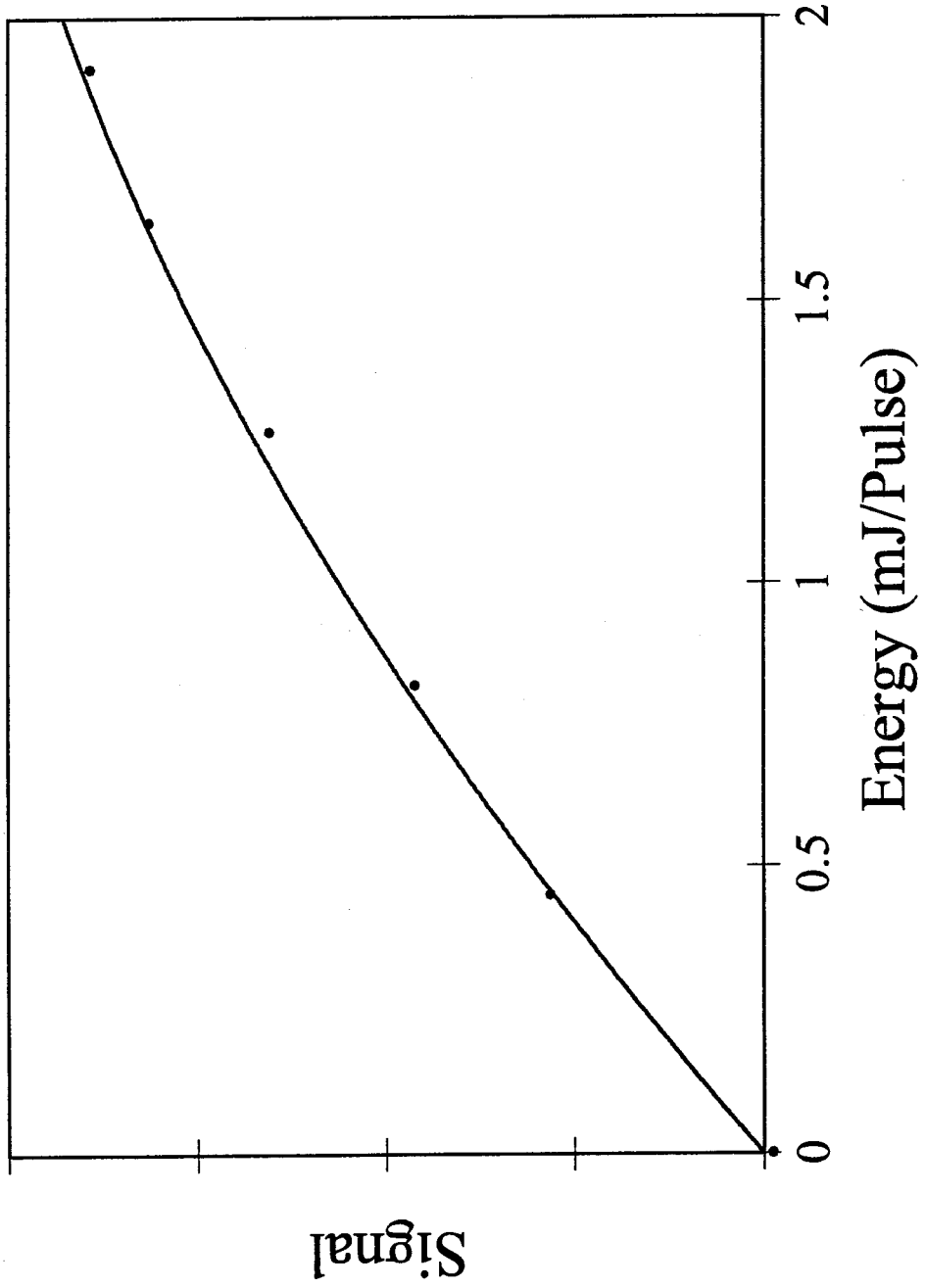

Figure 4.

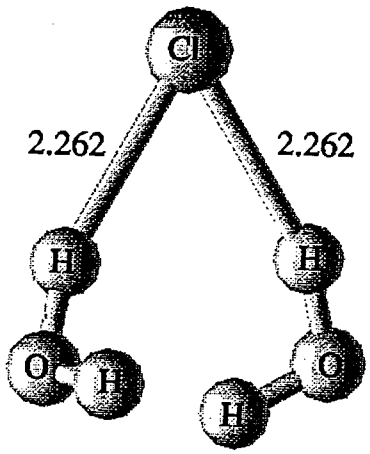

IIa)

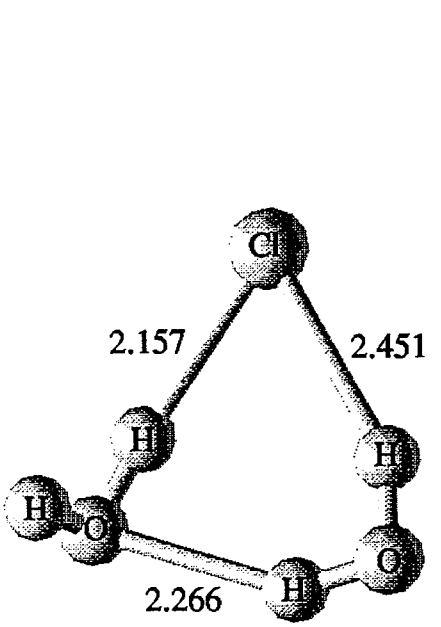

IIb)

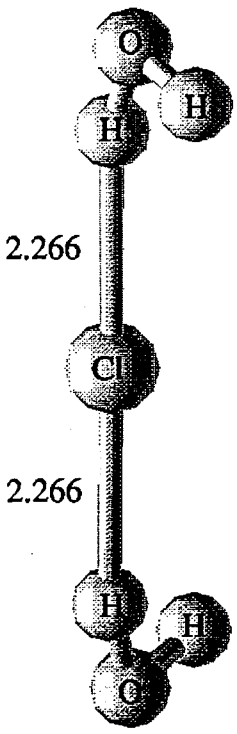

IIc)

Figure 5.

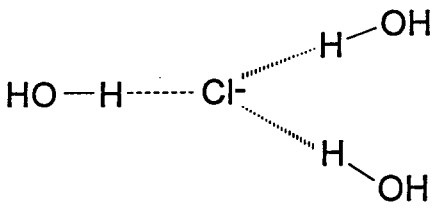

IIIa

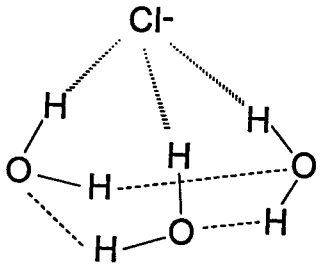

IIIb

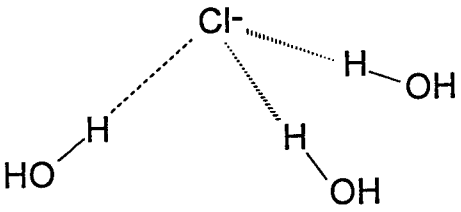

IIIc

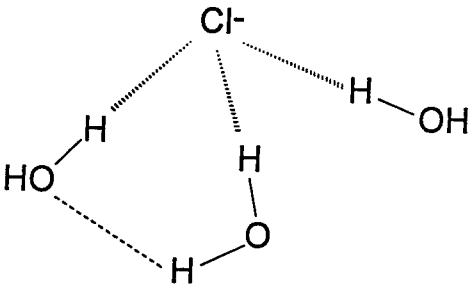

IIId

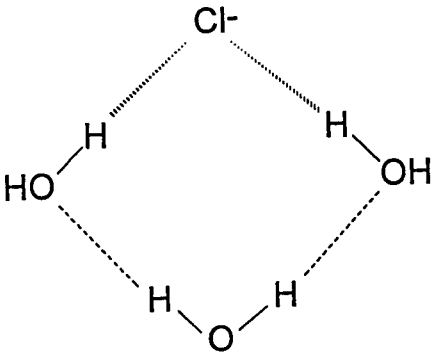

IIIe

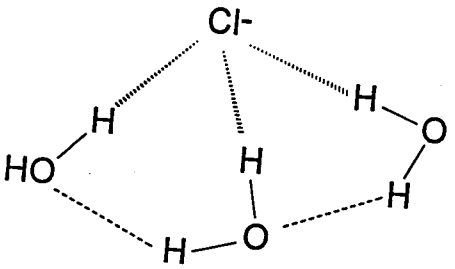

IIIf

Figure 6.

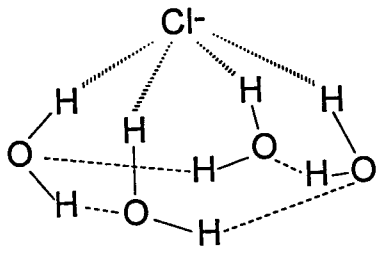

IVa

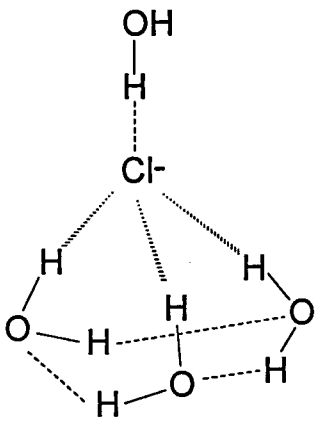

IVb

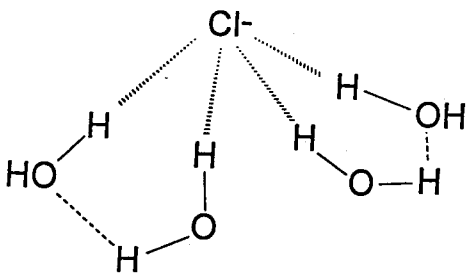

IVc

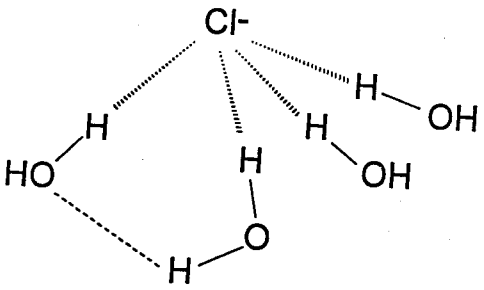

IVd

Figure 7.

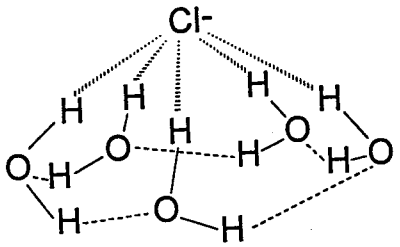

Va

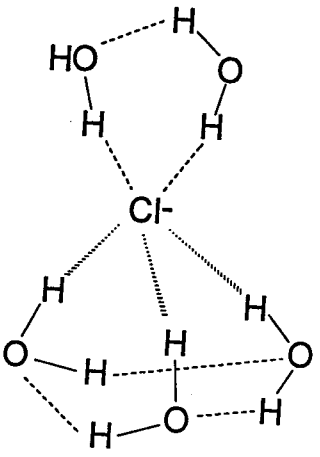

Vb

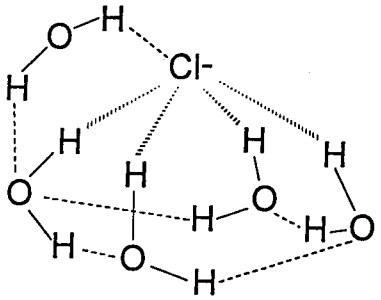

Vc

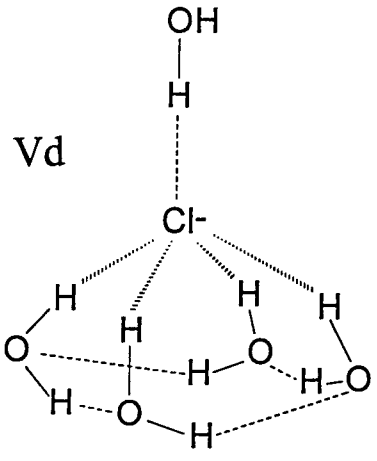

Vd

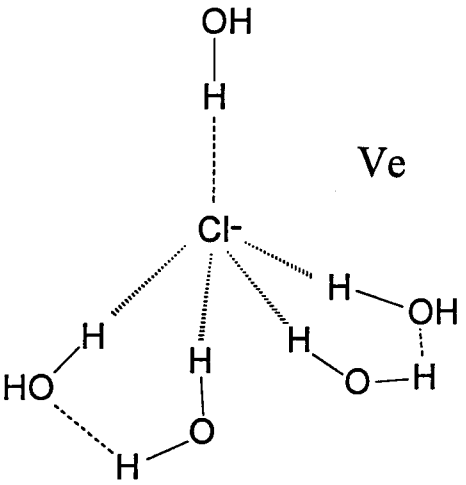

Ve

Figure 8.

APPENDIX

Reprinted from The Journal of Physical Chemistry, 1993, 97. 5215

Infrared Spectrum of the Silicon Hydride Cation SiH_7^+

Yibin Cao, Jong-Ho Choi, Bernd-Michael Haas, Matthew S. Johnson, and Mitchio Okumura*

Arthur Amos Noyes Laboratory of Chemical Physics,† California Institute of Technology, Pasadena, California 91125

Received: March 12, 1993; In Final Form: April 2, 1993

We report the infrared spectrum of the silicon hydride cluster ion SiH_7^+ obtained by vibrational predissociation spectroscopy. SiH_7^+ ions were excited by a tunable infrared laser, and the resulting SiH_5^+ photofragment intensity was measured as a function of the laser wavelength. We observed a vibrational band centered at 3866 cm^{-1}, which we assigned as a perturbed H_2 stretch. The absence of a second band between 3500 and 4200 cm^{-1} suggests that the ion forms a symmetric complex with the structure $H_2{\cdot}SiH_3^+{\cdot}H_2$, in contrast to the species CH_7^+, which has the structure $CH_5^+{\cdot}H_2$.

Introduction

Silanium ions are an important class of hypervalent molecules. Investigations of the chemistry of silicon hydride cations have been motivated by the possible role of ion–molecule reactions in the gas-phase silane chemistry occurring during chemical vapor deposition (CVD) of silicon films, especially plasma-enhanced CVD. Both experimental[1-9] and theoretical[10-13] studies have focused on reactions of Si^+ and SiH_3^+ with silane that produce hydrogenated silicon cluster ions $Si_nH_m^+$. Theoretical calculations[10-13] suggest that these cluster ions exhibit rather novel nonclassical bonding, analogous to but distinct from the nonclassical bonding observed in carbonium ions. Such bonding is believed to occur even in monosilane cluster ions such as SiH_5^+.[15]

Although the gas-phase chemistry of silicon hydride ions has been studied extensively, there have been few spectroscopic studies to date. Whitham *et al.* have obtained electronic predissociation spectra of SiH^+ and SiH_2^+ by using a fast ion beam apparatus.[16-18] Dyke *et al.*[19] have reported the frequency of the out-of-plane bending mode of SiH_3^+ from the photoelectron spectrum of the SiH_3 radical. Smith, Martineau, and Davies[20] have recently reported a high-resolution infrared absorption spectrum of the ν_3 band of the SiH_3^+ cation detected in a glow discharge. SiH_3^+ is the dominant ion in low-pressure silane discharges, and no other species have thus far been detected by this method.

Based on the analysis of the rotationally resolved ν_3 band, the SiH_3^+ cation has a classical trigonal planar structure like CH_3^+. In the case of SiH_5^+, *ab initio* calculations by Hu *et al.* suggest that an H_2 is bound to SiH_3^+ through a three-center, two-electron bond. This bonding is analogous to the case of CH_5^+, but the SiH_3^+–H_2 bond is weaker. The best theoretical estimate of the dissociation energy D_0 for SiH_5^+ is 10.3 kcal/mol, less than the experimental value of 17.8 kcal/mol.[4] Larger silicon hydride cations are expected to be more weakly bound. The SiH_7^+ ion has not been previously observed experimentally, and theoretical calculations on its structure have not yet been carried out.

Using an ion trapping tandem mass spectrometer apparatus, Lee and co-workers have obtained infrared vibrational predissociation and multiphoton photodissociation spectra for a number of ionic clusters.[21-24] This technique has proved to be a powerful method for obtaining spectra of mass-selected clusters. We have developed a simpler apparatus using pulsed techniques, based on the ion photodissociation spectrometer developed by Johnson and Lineberger.[25] We have begun to apply the vibrational predissociation method to silicon hydride cations, and in this paper we report our initial results on the infrared spectrum of the SiH_7^+ cation.

† Contribution No. 8760.

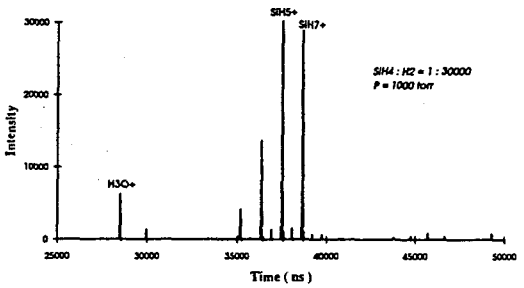

Figure 1. Time-of-flight mass spectrum of the silanium ions. The pulsed valve stagnation pressure was 1000 Torr. The gas mixing ratio SiH_4:H_2 was 1:30 000.

Experimental Section

Silanium ions were generated in a pulsed, high-pressure glow discharge source which we developed recently. A MKS gas flow control system was used to produce a mixture of 30 ppm SiH_4 in H_2 at 1000 Torr. This gas mixture expanded through a piezo-driven pulsed valve[26] (pulse width 200 μs) into a 0.5-mm-diameter channel. The gas then entered a small chamber with two tungsten electrodes (0.5-mm diameter) where a high-voltage pulse (typically ~1 kV, 100 μs wide) was applied to the cathode. Ions in the discharge were swept out by the gas pulse through a 1-mm-diameter, 1.5-cm-long channel and into the first differential vacuum chamber (pumped by a 10-in. baffled diffusion pump and maintained at a pressure of $(2–10) \times 10^{-5}$ Torr). This plasma was cooled as the gas flowed through the channel and underwent supersonic expansion. The effectiveness of the cooling was demonstrated by the formation of cluster ions with binding energies of 3 kcal/mol or less such as $H_3O^+{\cdot}H_2$. A typical time-of-flight mass spectrum is shown in Figure 1. The source, operated at a repetition rate of 30 Hz, produced intense and stable silanium ion beams.

The plasma expanded supersonically and was collimated by a skimmer to enter a second chamber (6-in. diffusion pump, 5×10^{-6} Torr) containing time-of-flight ion optics. A pulsed electric field between two plates 3 cm apart extracted the positive ions. The ions were further accelerated by additional electric fields and then entered a field-free region with a final kinetic energy of 1 keV. After passing through a third differential pumping region (4-in. diffusion pump, 1×10^{-6} Torr) and into a photolysis/detection chamber (500 L/s turbomolecular pump, 3×10^{-7} Torr), the ions entered a 1-cm-long mass gate where a pulsed transverse field was applied to deflect all incident ions except those of the mass of interest. The selected ions were focused into a packet

0022-3654/93/2097-5215$04.00/0

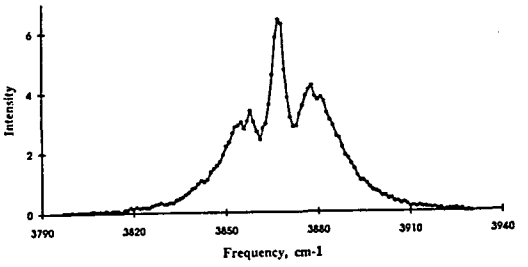

Figure 2. Vibrational predissociation spectrum of the SiH_7^+ ion in the 3800–3925-cm^{-1} region. No other predissociation bands were observed from 3500 to 4200 cm^{-1}.

9 mm long and 5 mm in diameter at 1.5 m downstream from the acceleration optics, where they were intersected by the infrared laser beam. The ions were then mass-analyzed by a 15-cm-long reflectron,[22] and the photofragments were detected by a microchannel plate detector. The signal was amplified and then collected by a LeCroy Model 8818 transient digitizer and Model 6010 signal averager.

The tunable, pulsed infrared radiation was produced by a $LiNbO_3$ optical parametric oscillator (OPO). The OPO, based on the design of Brosnan and Byer,[27] was pumped by a Continuum 661s Nd:YAG laser which generated 250-mJ pulses at 1.06 μm. To avoid damaging the $LiNbO_3$ crystal, the pump beam was multipassed 14 m to achieve a Gaussian intensity profile at the OPO entrance. The OPO was continuously tunable from 2700 to 4300 cm^{-1} by simultaneously adjusting the crystal and the grating angles. Typical OPO pulse energies were about 5 mJ with a line width of 1.5 cm^{-1}. The optical path from the laser to the vacuum chamber was purged with dry air to eliminate absorption caused by ambient water vapor.

Spectra were recorded by stepping the OPO wavelength and averaging the photofragment signal for 400 laser shots at each wavelength. To achieve a better signal-to-noise ratio, we averaged 10 such scans. Background signal, primarily caused by collision-induced dissociation in the ion optics chamber, was subtracted by firing the laser beam alternately at the parent ion arrival time and 10 μs before the ion arrival and taking the difference. The data were then normalized with respect to the OPO laser intensity, measured by a Molectron joulemeter. The OPO laser wavelength was calibrated during the scan by simultaneously recording the vibrational spectrum of acetylene in a photoacoustic cell.

Results and Discussion

An absorption band of SiH_7^+ was observed in the 3800–3925-cm^{-1} region, as shown in Figure 2. This band has clear P, Q, and R branches, with the Q branch centered at 3866 cm^{-1}. The only photofragment ion observed was SiH_5^+, indicating that the photodissociation process involved was $SiH_7^+ \rightarrow SiH_5^+ + H_2$. Due to the broad line width of the OPO laser (1.5 cm^{-1}), rotational structure of this band was not resolved. There were no other absorptions found from 3500 to 4200 cm^{-1}.

On the basis of the relatively high frequency and the strength of this absorption band, we assign it to an H–H stretching motion. This stretch is strongly perturbed, as evidenced by its 300-cm^{-1} frequency shift from the free H_2 fundamental of 4161 cm^{-1}. This assignment supports the notion that SiH_7^+ is an ionic cluster with at least one H_2 molecule bound to the charge center. The H–H stretch excitation in a free H_2 molecule is dipole forbidden; thus, the H–H stretch in the SiH_7^+ obtains its transition dipole moment through coupling with degrees of freedom that possess oscillator strength, e.g., motion of the charge center relative to the center of mass.

The observed frequency of 3866 cm^{-1} for SiH_7^+ is close to the harmonic frequency of 3991 cm^{-1} for SiH_5^+ predicted by Hu *et al.*, given that *ab initio* frequencies are generally 5–10% higher than experimental values. This agreement at first suggests that SiH_7^+ could be a complex with an H_2 molecule very weakly bound to the SiH_5^+ ion core, analogous to the structure proposed by Boo, Price, and Lee for the CH_7^+ ion (Figure 3B).[23] However, this H_2 moiety would be perturbed by the SiH_5^+ core and therefore exhibit an absorption band slightly below 4161 cm^{-1}, the vibrational frequency of a free H_2. In all previous cases involving an ion–molecule cluster with H_2 ligands, such an absorption band has been observed. In the case of CH_7^+, this absorption band occurs at 4077 cm^{-1}. We scanned the region from 3500 to 4200 cm^{-1}, but SiH_7^+ showed no evidence of a second absorption band. In addition, we observed that the SiH_7^+ ions could exist even under "hot" source conditions that made mostly SiH^+ ions, which suggests that the SiH_7^+ binding energy is quite large, much greater than the CH_7^+ binding energy of 1–2 kcal/mol.[23]

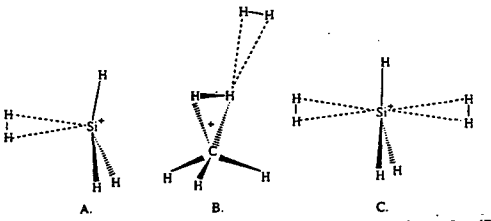

Figure 3. (A) SiH_5^+ structure predicted by Hu, Shen, and Schaefer. (B) CH_7^+ structure based on the experimental results of Boo, Price, and Lee. (C) The proposed structure of SiH_7^+.

We therefore propose that SiH_7^+ has the structure shown in Figure 3C: a planar SiH_3^+ with two H_2 ligands bound to opposite faces of the ion, equidistant from the Si atom. The H_2 most likely bind perpendicular to the SiH_3^+ symmetry axis, with the σ electrons donating into the empty p orbital of the silicon cation. Sideways binding generally occurs for molecular hydrogen in ion–molecule complexes, e.g., SiH_5^+ [15] and H_{2n+1}^+,[21] as well as in transition-metal dihydrogen complexes.[28] This structure is a near-prolate top. The two H_2 ligands rotate around the symmetry axis with a small energy barrier. This structure should result in two H–H stretching bands: the symmetric and antisymmetric combinations of the two H_2 stretches. The antisymmetric motion, with the two H_2 ligands vibrating 180° out of phase, will cause the Si^+ charge center to oscillate along the symmetry axis as it moves toward the extended H_2. This gives rise to the observed parallel band, which has apparent P, Q, and R branches. The symmetric combination, in which the two H_2 ligands expand and contract in phase, will induce little movement of the charge center and thus should have much weaker absorption intensity. Our current interpretation of the spectrum is that the symmetric combination is in fact weaker and obscured by the stronger antisymmetric mode.

In previous spectroscopic work on ion–molecule clusters with an H_2 ligand, a semiquantitative correlation between the frequency of the H–H stretching mode and the binding energy of that cluster was observed. The larger the frequency shift from the free H_2 fundamental, the more strongly the H_2 moiety is bound. With a frequency shift of 300 cm^{-1}, the SiH_7^+ binding energy is estimated as 7–9 kcal/mol. This crude binding energy estimate is about half of the experimental value of the SiH_5^+ binding energy, supporting the proposed structure of SiH_7^+, in which both of the H_2 ligands compete for the charge on the silicon atom.

Our proposed structure for SiH_7^+ is quite distinct from the structure proposed by Boo *et al.* for CH_7^+.[23] The differences can be rationalized by comparing the CH_5^+ and SiH_5^+ ions. The dissociation energy for $CH_5^+ \rightarrow CH_3^+ + H_2$ is 40 kcal/mol, and the strong three-center, two-electron bond in CH_5^+ results in charge delocalization among the three centers. In contrast, the dissociation energy for $SiH_5^+ \rightarrow SiH_3^+ + H_2$ is only 17.8 kcal/mol. The SiH_5^+ ion is thus closer to an SiH_3^+-H_2 complex, as

Hu *et al.* predict.[15] A second H_2 will bind to the Si atom, where most of the charge remains localized.

These results shed some light on the nonclassical structures of SiH_5^+ and SiH_7^+. A more definitive structure determination requires recording the rotationally resolved spectrum. If the H_2 ligands are about 2 Å from the planar SiH_3^+, then SiH_7^+ is a prolate top with a rotational constant B of 0.85 cm^{-1}. A fit to our unresolved infrared spectrum results in a rotational temperature of 90 K. Our newly upgraded OPO has a line width of 0.15 cm^{-1} and will easily resolve the spectra. The next step in silanium ion spectroscopy would be SiH_5^+. Since the dissociation energy for $SiH_5^+ \rightarrow SiH_3^+ + H_2$ is 17.8 kcal/mol, SiH_5^+ spectra can be obtained through two-photon photodissociation. Larger silicon hydride ions are also believed to possess unusual geometries. In $Si_2H_7^+$, for example, the two Si atoms are thought to bond through an H atom, with a structure of $H_3Si\text{-}H^+\text{-}SiH_3$. By using multiphoton dissociation techniques, we hope to probe the structure and novel bonding of these species as well.

Acknowledgment. We gratefully acknowledge the support of a NSF Presidential Young Investigator Award CHEM-8957243. Additional support was received from a Dreyfus Newly Appointed Faculty Award, the Irvine Foundation, the Chevron Fund, an AT&T Special Purpose Grant, and a Grace Fellowship (M.S.J.). We thank D. W. Boo and Prof. Y. T. Lee for their unpublished results.

References and Notes

(1) Yu, T. Y.; Cheng, T. M. H.; Kempten, V.; Lampe, F. W. *J. Phys. Chem.* **1972**, *76*, 3321.
(2) Henis, J. M. S.; Stewart, G. W.; Tripodi, M. K.; Gaspar, P. P. *J. Chem. Phys.* **1972**, *57*, 389.
(3) Cheng, T. M. H.; Yu, T. Y.; Lampe, F. W. *J. Phys. Chem.* **1974**, *78*, 1184.
(4) Boo, B. H.; Armentrout, P. B. *J. Am. Chem. Soc.* **1987**, *109*, 3549.
(5) Mandich, M. L.; Reents Jr., W. D.; Jarrold, M. F. *J. Chem. Phys.* **1988**, *88*, 1703.
(6) Reents Jr., W. D.; Mandich, M. L. *J. Phys. Chem.* **1988**, *92*, 2908.
(7) Mandich, M. L.; Reents Jr., W. D. *J. Chem. Phys.* **1989**, *90*, 3121.
(8) Mandich, M. L.; Reents Jr., W. D.; Kolenbrander, K. D. *J. Chem. Phys.* **1990**, *92*, 437.
(9) Reents Jr., W. D.; Mandich, M. L. *J. Chem. Phys.* **1990**, *93*, 3270.
(10) Raghavachari, K. *J. Chem. Phys.* **1988**, *88*, 1688.
(11) Raghavachari, K. *J. Phys. Chem.* **1988**, *92*, 6284.
(12) Raghavachari, K. *J. Chem. Phys.* **1990**, *92*, 452.
(13) Al-Laham, M. A.; Raghavachari, K. *J. Chem. Phys.* **1991**, *95*, 2560.
(14) Olah, G. A.; Prakash, G. K. S.; Williams, R. E.; Field, L. D.; Wade, K. *Hypercarbon Chemistry*; Wiley-Interscience: New York, 1987.
(15) Hu, C. H.; Shen, M.; Schaefer III, H. F. *Chem. Phys. Lett.* **1992**, *190*, 543.
(16) Curtis, M. C.; Jackson, P. A.; Sarre, P. J.; Whitham, C. J. *Mol. Phys.* **1985**, *56*, 485.
(17) Sarre, P. J.; Walmsley, J. M.; Whitham, C. J. *Philos. Trans. R. Soc. London, A* **1988**, *324*, 233.
(18) Hall, D. I.; Levick, A. P.; Sarre, P. J.; Whitham, C. J.; Alijah, A.; Duxbury, G. *J. Chem. Soc., Faraday Trans.* **1993**, *89*, 177.
(19) Dyke, J. M.; Jonathan, N.; Morris, A.; Ridha, A.; Winter, M. J. *Chem. Phys.* **1983**, *81*, 481.
(20) Smith, D. M.; Martineau, P. M.; Davies, P. B. *J. Chem. Phys.* **1992**, *96*, 1741.
(21) Okumura, M.; Yeh, L. I.; Lee, Y. T. *J. Chem. Phys.* **1988**, *88*, 79.
(22) Yeh, L. I.; Okumura, M.; Myers, J. D.; Price, J. M.; Lee, Y. T. *J. Chem. Phys.* **1989**, *91*, 7319.
(23) Boo, D. W.; Price, J. M.; Lee, Y. T. Preprint.
(24) Price, J. M.; Crofton, M. W.; Lee, Y. T. *J. Phys. Chem.* **1991**, *95*, 2182.
(25) Johnson, M. A.; Lineberger, W. C. In *Techniques for the Study of Ion-Molecule Reactions*; Farrar, J. M., Saunders Jr., W. H., Eds.; Wiley-Interscience: New York, 1988; p 591.
(26) Proch, D.; Trickl, T. *Rev. Sci. Instrum.* **1989**, *60*, 713.
(27) Brosnan, S. J.; Byer, R. L. *IEEE J. Quantum Electron.* **1979**, *QE-15*, 415.
(28) Kubas, G. J. *Acc. Chem. Res.* **1988**, *21*, 120.

Intracluster rearrangement of protonated nitric acid: Infrared spectroscopic studies of $H^+(HNO_3)(H_2O)_n$

Yibin Cao, Jong-Ho Choi, Bernd-Michael Haas, Matthew S. Johnson, and Mitchio Okumura
A. A. Noyes Laboratory of Chemical Physics,[a] California Institute of Technology, Pasadena, California 91125

(Received 9 August 1993; accepted 21 September 1993)

Infrared spectra of clusters of protonated nitric acid and water exhibit a marked change with cluster size, indicating that an intracluster reaction occurs with sufficient solvation. In small clusters, H_2O binds to a nitronium ion core, but at a critical cluster size the NO_2^+ reacts. A lower bound of 174 kcal/mol is found for the proton affinity of HNO_3.

INTRODUCTION

The large differences between gas phase and solution phase basicities highlight the dramatic effects of solvation on ion chemistry. Strong aqueous acids such as HNO_3 can possess a proton affinity in the gas phase that is higher than that of H_2O. By clustering water molecules sequentially to a protonated nitric acid, the structure and properties of the ion will evolve towards the solvated form. Investigations of these hydrated cluster ions can provide insights into microscopic aspects of solvation.

Protonation of nitric acid occurs in the liquid phase under nearly anhydrous conditions, e.g., in neat nitric acid and in concentrated sulfuric acid, by the reaction $H^+ + HNO_3 \rightarrow NO_2^+ + H_2O$.[1] Upon addition of water, the nitronium ion (NO_2^+) rapidly undergoes the reverse reaction and is therefore not present in aqueous solution.

Experimental[2,3] and theoretical[4,5] studies have concluded that gas phase protonated nitric acid $H_2NO_3^+$ possesses several isomers. The most stable form is a weakly bound complex of NO_2^+ and H_2O and, as in nonaqueous liquids, the most basic site is on the OH group. Cacace *et al.*[3] found evidence for a second isomer, $(HO)_2NO^+$, which lies 10–20 kcal/mol higher and is formed by the protonation of a terminal oxygen atom of HNO_3. *Ab initio* calculations[5] by Lee and Rice confirmed the structures and relative stability of the two isomers, but the computed proton affinity for nitric acid is 182 ± 4 kcal/mol, in disagreement with Cacace's ICR bracketing measurement of 168 ± 3 kcal/mol and closer to an earlier measurement[2] of 176 ± 7 kcal/mol. These values lead to large differences in the binding energy of the $NO_2^+(H_2O)$ complex (5–19 kcal/mol).

The existence of hydrated $H_2NO_3^+$ was inferred by Fehsenfeld *et al.*, who studied the ion chemistry of HNO_3 in a flowing afterglow apparatus.[2] They observed rapid proton transfer from H_3O^+ to HNO_3, and attributed the decay of $H_2NO_3^+$ to its association with H_2O. However, they were unable to detect hydrated clusters of protonated nitric acid, and postulated a fast reaction $H^+(HNO_3)(H_2O) + H_2O \rightarrow H_3O^+(H_2O) + HNO_3$ that would destroy the association products and convert NO_2^+ to HNO_3. In an *ab initio* calculation, Grandinetti *et al.*[6] predicted that the lowest energy structure of $H^+(HNO_3)(H_2O)$ is $NO_2^+(H_2O)_2$. Kay *et al.* formed the clusters $H^+(HNO_3)(H_2O)_n$ ($n=1$–12) by ionization of neutral clusters in a beam[7] and attributed a minimum in the size distribution at $n=4$ to the formation of solvated ion pairs in the neutral complexes, but made no conclusions regarding the ionic clusters.

We have investigated the clusters $H^+(HNO_3)(H_2O)_n$ for $n=0$ to 4 by infrared vibrational predissociation spectroscopy. In this Communication, we present evidence for solvent-induced changes in the structure of protonated nitric acid.

EXPERIMENT

The apparatus has been described elsewhere,[8] and is briefly described here. UHP helium was seeded with HNO_3/H_2O vapor by passage over the surface of concentrated (70%) nitric acid at 0 °C. The HNO_3/H_2O/He mixture at a total stagnation pressure of 1000 Torr was then pulsed into a small channel where a high voltage pulse was applied between two electrodes to initiate a glow discharge. The resulting ions underwent many thermal collisions as the gas flowed through the channel and expanded into the vacuum, promoting cooling and clustering. The ion chemistry in our source was similar to that of high pressure discharges, producing the most stable ions. The ions were mass analyzed by a time-of-flight (TOF) mass spectrometer. A pulsed tunable infrared laser, a $LiNbO_3$ optical parametric oscillator[9] with 1.5 cm^{-1} resolution, was timed to excite clusters of a selected mass. Upon photon absorption, clusters could vibrationally predissociate. The resulting fragment ions were mass analyzed by a reflectron mass spectrometer. Infrared spectra were obtained by measuring the photofragment intensity as a function of the laser wavelength.

We typically generated $H^+(HNO_3)(H_2O)_n$ clusters with n ranging from 0 to 7, as well as $H_3O^+(H_2O)_n$ and small amounts of $NO^+(H_2O)_n$. We obtained the vibrational predissociation spectra of $H^+(HNO_3)(H_2O)_n$ clusters, with $n=0$ to 4, in the range 2650–3850 cm^{-1}.

RESULTS

The infrared spectrum of protonated nitric acid ($n=0$) had two distinct bands, one centered at 3626 cm^{-1}

TABLE I. Vibrational predissociation band centers for $H^+(HNO_3)(H_2O)_n$ in cm^{-1}.

	H_3O^+ H bonded	HNO_3, ν_1 NO–H	H_2O, ν_1 Symmetric	H_2O, ν_3 Antisymmetric
$H^+(HNO_3)$			3626	3708,3716
$H^+(HNO_3)(H_2O)$			3635	3715
$H^+(HNO_3)(H_2O)_2$			3636	3716
$H^+(HNO_3)(H_2O)_3$	~2600,~3000	3519,3550	3644	3717
$H^+(HNO_3)(H_2O)_4$	~2700,~3000	3523,3550	3644	3717,3733
H_2O monomer			3657	3756
HNO_3 monomer		3551		

and the other a doublet with maxima at 3708 and 3716 cm^{-1} (Table I). These were redshifted by less than 50 cm^{-1} from the symmetric and antisymmetric stretching bands of the water monomer. The only predissociation process observed was

$$H_2NO_3^+ \rightarrow NO_2^+ + H_2O. \quad (1)$$

The dissociation signal was very weak and exhibited a nonlinear dependence on laser intensity, indicating that the photodissociation arose from a multiphoton process.

Clusters of protonated nitric acid solvated by one or two water molecules, $H^+(HNO_3)(H_2O)_n$ ($n=1,2$), behaved like the unsolvated $H_2NO_3^+$, with a single water molecule evaporating upon vibrational excitation:

$$H^+(HNO_3)(H_2O)_n \rightarrow H^+(HNO_3)(H_2O)_{n-1} + H_2O. \quad (2a)$$

In both clusters, only two bands were observed in the OH stretch region, slightly redshifted from the water symmetric and antisymmetric stretches, respectively (Table I). The dissociation signal was much stronger than for $n=0$ and depended linearly on laser intensity. For $n=3$, two small features appeared in the 3550 cm^{-1} region.

For clusters $H^+(HNO_3)(H_2O)_n$ with $n \geq 2$, we observed the onset of a new photodissociation channel, loss of a nitric acid molecule,

$$H^+(HNO_3)(H_2O)_n \rightarrow H^+(H_2O)_n + HNO_3 \quad (2b)$$

in competition with the water loss channel (2a). Although evaporation of nitric acid was a minor channel for $n=2$ predissociation, it was a major channel for $n=3$ and the dominant channel for $n=4$. The ratio of the nitric acid channel (2b) yield to the water channel (2a) yield was 1:8 for $n=2$, and 9:1 for $n=4$. In $n=3$, the yield depended on the band excited: it was 7:1 upon excitation in the 3550 cm^{-1} region and 2:1 in the 3600–3800 cm^{-1} region.

Three new bands were observed for the clusters $H^+(HNO_3)(H_2O)_3$ and $H^+(HNO_3)(H_2O)_4$ in addition to the two H_2O bands (Fig. 1). Two were close to 3550 cm^{-1}, the OH stretching frequency of the HNO_3 monomer. The third was a broad band at 2600–2700 cm^{-1}. A similar band at 2670 cm^{-1} was observed by Lee and coworkers in their studies of $H_3O^+(H_2O)_n$ clusters and assigned to the hydrogen-bonded OH stretches of the H_3O^+ ion.[10]

DISCUSSION

We can derive qualitative structural information about these clusters from their infrared spectra and photodissociation behavior. Protonated nitric acid, $H^+(HNO_3)$, has two redshifted H_2O stretch bands and dissociates directly into NO_2^+ and H_2O. Coupled with the absence of bands near 3550 cm^{-1}, we conclude that protonated nitric acid is a weakly bound complex $NO_2^+(H_2O)$, in agreement with earlier studies. The structure calculated by Lee and Rice[5] is a highly asymmetric top for which the symmetric H_2O stretching mode would be an *a* type band and the antisymmetric mode a *b* type band. This is consistent with the observed rotational contours, a single maximum at 3626 cm^{-1} and two closely spaced maxima at 3712 cm^{-1}.

The similarity in the spectra and the photoproducts of $H^+(HNO_3)$ and its hydrated clusters ($n=1,2$) indicates that the smaller hydrates are also complexes of an NO_2^- ion core and H_2O ligands (Fig. 2). With additional ligands, the binding energy should be lower and the H_2O stretching modes less perturbed. This inference is confirmed by the stronger photodissociation signal and its linear power dependence, as well as the smaller redshift of the H_2O bands.

There is a striking difference in the properties of the larger clusters ($n=3,4$). The appearance of nitric-acidlike bands near 3550 cm^{-1} and the onset of dissociation releasing HNO_3 indicate that neutral HNO_3 exists intact in the clusters. The ~2650 cm^{-1} band and the bands in the 3600–3800 cm^{-1} region are evidence of H_3O^+ and H_2O,

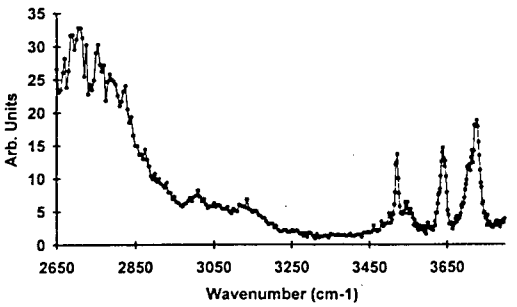

FIG. 1. Vibrational predissociation spectrum of $H^+(HNO_3)(H_2O)_4$. The ordinate is the $H_3O^+(H_2O)_3$ photofragment signal, with laser-independent background subtracted and normalized for laser intensity.

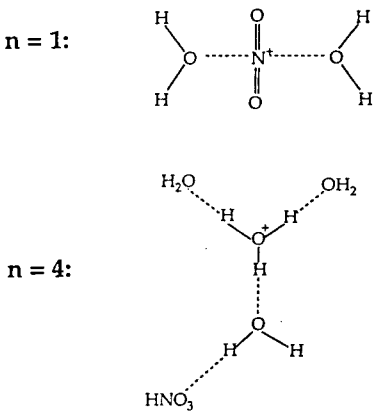

FIG. 2. The proposed structures for $H^+(HNO_3)(H_2O)$ and $H^+(HNO_3)(H_2O)_4$.

respectively. We therefore conclude that the larger clusters are complexes of an H_3O^+ core surrounded by water ligands and a neutral HNO_3.

H_2O is more strongly bound than HNO_3 due to its more favorable hydrogen bonding,[2] suggesting that the first solvation shell in the $n=4$ cluster is occupied by water ligands with HNO_3 in the second shell, as depicted in Fig. 2. In both $n=3$ and $n=4$ clusters, channel (2b) dominates because the HNO_3 ligand is more likely to predissociate.

The wavelength dependence of the branching ratio in the $n=3$ cluster is surprising. HNO_3 evaporation is approximately three times more likely upon excitation of the HNO_3 band relative to excitation of the H_2O bands. This behavior suggests that the predissociation process is mode selective. However, it is more likely that two nearly isoenergetic isomers are present, one with a hydronium ion core, $H_3O^+(H_2O)_2(HNO_3)$, and the other with a nitronium ion, $NO_2^+(H_2O)_4$. The latter would absorb only at 3600–3800 cm^{-1} and would produce only H_2O fragments. The $H_3O^+(H_2O)_2(HNO_3)$ isomer would absorb at 3550 cm^{-1} as well, but would dissociate primarily by loss of HNO_3. A mixture of the two isomers would thus appear to have wavelength-dependent branching ratios.

Our results provide a lower limit on the proton affinity of nitric acid. From the nonlinear power dependence of the predissociation, we infer that dissociation requires at least two photons, and that the binding energy of $NO_2^+(H_2O)$ is >10.6 kcal/mol. Using known thermodynamic quantities[11,12] and a revised ΔH_f° for NO_2^+,[13] we can compute ΔH_f° for $H_2NO_3^+$ and hence the proton affinity of HNO_3. We find a lower limit on the proton affinity of 174 kcal/mol, which disagrees with the currently accepted value[3] of 168 kcal/mol, but agrees well with the earlier measurement of 176 kcal/mol by Fehsenfeld *et al.*[2] and the *ab initio* value of 182 kcal/mol.[5]

We found no evidence for the formation of the higher energy isomer $(HO)_2NO^+$ or its hydrates in our source. While this ion is covalently bound and may not predissociate upon photon absorption, the hydrates should. Møller–Plesset (MP2) calculations[5] predict that the (scaled) NO–H stretching frequencies lie near 3450 cm^{-1}, but no such bands were observed in any clusters.

In conclusion, we have observed the intracluster reaction $NO_2^+ + 2H_2O \rightarrow HNO_3 + H_3O^+$ upon sufficient solvation. The driving force for overcoming the intrinsic stability of gas phase NO_2^+ is the solvent stabilization of H_3O^+. This stabilization effect has also been observed in other studies.[14,15] Our technique provides a direct spectroscopic probe of solvent-induced phenomena in clusters; other systems are currently under investigation.

Note added in proof. The binding energy of $NO_2^+(H_2O)$ was recently measured directly and found to be 14.8 kcal/mol.[16]

ACKNOWLEDGMENTS

We acknowledge the support of a National Science Foundation P.Y.I. Award No. CHEM-8957243, and the Dreyfus, Irvine, and AT&T Foundations. We thank Dr. Timothy Lee for helpful discussions.

[4] Contribution No. 8837.
[1] C. C. Addison, Chem. Rev. **80**, 21 (1980).
[2] F. C. Fehsenfeld, C. J. Howard, and A. L. Schmeltekopf, J. Chem. Phys. **63**, 2835 (1975).
[3] F. Cacace, M. Attina, G. de Petris, and M. Speranza, J. Am. Chem. Soc. **111**, 5481 (1989); **112**, 1014 (1990).
[4] M.-T. Nguyen and A. F. Hegarty, J. Chem. Soc. Perkin Trans. II, 2043 (1984).
[5] T. J. Lee and J. E. Rice, J. Phys. Chem. **96**, 650 (1992); J. Am. Chem. Soc. **114**, 8247 (1992).
[6] F. Grandinetti, L. Bencivenni, and F. Ramondo, J. Phys. Chem. **96**, 4354 (1992).
[7] B. D. Kay, V. Hermann, and A. W. Castleman, Jr., Chem. Phys. Lett. **80**, 469 (1981).
[8] Y. Cao, J.-H. Choi, B.-M. Haas, M. S. Johnson, and M. Okumura, J. Phys. Chem. **97**, 5215 (1993).
[9] S. J. Brosnan and R. L. Byer, IEEE J. Quantum Electron. **QE-15**, 415 (1979).
[10] L. I. Yeh, M. Okumura, J. D. Myers, J. M. Price, and Y. T. Lee, J. Chem. Phys. **91**, 7319 (1989); J. M. Price, Ph.D. thesis, University of California at Berkeley, 1990.
[11] D. L. Baulch, R. A. Cox, P. J. Crutzen, R. F. Hampson, Jr., J. A. Kerr, J. Troe, and R. T. Watson, J. Phys. Chem. Ref. Data **11**, 327 (1982).
[12] H. M. Rosenstock, K. Draxl, B. W. Steiner, and J. T. Herron, J. Phys. Chem. Ref. Data **6**, Suppl. No. 1 (1977).
[13] G. Bryant, Y. Jiang, and E. Grant, Chem. Phys. Lett. **200**, 495 (1992).
[14] S. Wei, W. B. Tzeng, R. G. Keesee, and A. W. Castleman, Jr., J. Am. Chem. Soc. **113**, 1960 (1991), and references therein.
[15] C. A. Deakyne, M. Mautner, C. L. Campbell, M. G. Hughes, and S. P. Murphy, J. Chem. Phys. **84**, 4958 (1986).
[16] L. S. Sunderlin and R. R. Squires, Chem. Phys. Lett. **212**, 307 (1993).

12176 Reprinted from The Journal of Physical Chemistry, 1994, 98.

Spectroscopic Studies of the Intracluster Hydration Reaction of NO_2^+

Yibin Cao, Jong-Ho Choi, Bernd-Michael Haas, and Mitchio Okumura*

Arthur Amos Noyes Laboratory of Chemical Physics,† California Institute of Technology, Pasadena, California 91125

Received: May 17, 1994⊗

Infrared spectra of $NO_2^+(H_2O)_n$ clusters formed in a pulsed discharge source were recorded by vibrational predissociation spectroscopy as a function of cluster size. A significant change in the vibrational spectra and the predissociation product yields were observed at $n = 4$, suggesting the onset of a rearrangement at this critical cluster size. For $NO_2^+(H_2O)_n$ with $n \leq 3$, the clusters possessed red-shifted H_2O bands and dissociated primarily by loss of H_2O. These were clusters of H_2O ligands bound to a nitronium ion core. At $n = 4$, we found evidence for the occurrence of an intracluster hydration reaction $NO_2^+ + 2H_2O \rightarrow HNO_3 + H_3O^+$. Vibrational excitation of the cluster led to loss of HNO_3 as the major channel, as well as loss of H_2O. New vibrational bands appeared and were assigned to solvated H_3O^+ and to HNO_3 ligands. With the H_3O^+ replacing NO_2^+ as the charge center, the clusters rearranged to form $H_3O^+(H_2O)_2(HNO_3)$. Upon addition of a fifth water molecule, the hydronium ion was further stabilized by completion of the first hydration shell, leaving HNO_3 in the second shell.

Introduction

The solvation of ions can have a profound influence on the structure and reactivity of ions. Dramatic effects can be seen when even a small number of solvent molecules bind to an ion in the gas phase. Such effects were discovered in early studies[1] of clusters composed of hydrated ions, complexes which are abundant in the ionosphere and stratosphere of earth.[2,3] Many of these are complexes of stable ions such as NO^+, O_2^+, and NO_2^+ with H_2O, but hydrates of the hydronium ion H_3O^+ are the most abundant, especially at lower altitudes. Reactions which occur within these clusters as a function of cluster size have been found to play an important role in determining their relative concentrations in and the final ion composition of the upper atmosphere.

One example of such a system is $NO_2^+(H_2O)_n$, clusters which are present in the stratosphere.[1,2] Their formation begins with the production of $NO_2^+(H_2O)$ by the proton transfer reaction of H_3O^+ with HNO_3 (an important trace species in the stratosphere). The larger clusters $NO_2^+(H_2O)_n$ are then formed in subsequent association reactions with H_2O. $NO_2^+(H_2O)$ is also the intermediate product of an ion-catalyzed reaction which converts N_2O_5 to HNO_3 in the stratosphere.[4] However, instead of becoming a major ionic species in the stratosphere, the $NO_2^+(H_2O)_n$ clusters are thought to convert back to hydrated hydronium ions $H_3O^+(H_2O)_n$ via the reaction

$$NO_2^+(H_2O)_n + H_2O \rightarrow H_3O^+(H_2O)_{n-1} + HNO_3 \quad (1)$$

The net effect of the reaction cycle involving $NO_2^+(H_2O)_n$ is to accelerate the hydration of H_3O^+ in the stratosphere. Despite the acceptance of reaction 1 in models of atmospheric ion chemistry, there has been no direct observation of this reaction.

The first laboratory studies of $NO_2^+(H_2O)_n$ clusters were flowing-afterglow experiments carried out by Fehsenfeld *et al.*[5,6] They compared the reactivity of protonated nitric acid, $H_2NO_3^+$, which was produced by direct proton transfer from H_3O^+ to HNO_3, with that of the $NO_2^+(H_2O)$ cluster, which was formed by clustering NO_2^+ with H_2O. The similarity in reaction behavior led them to infer that these two species are identical. Their conclusion was supported by *ab initio* calculations[7-9] as well as recent experiments by Cacace *et al.*[10] Cacace *et al.* also found evidence for a second isomer from isotope exchange studies and metastable ion kinetic energy (MIKE) release measurements. Sunderlin and Squires[11] recently measured the dissociation energy of the $NO_2^+(H_2O)$ complex in a flowing-afterglow triple quadrupole apparatus by energy-resolved collision-induced dissociation and found $D_0 = 14.8 \pm 2.3$ kcal/mol. Cacace *et al.* measured the gas phase equilibrium to reexamine the relative proton affinities of methyl nitrate and nitric acid.[12] From known data on protonated methyl nitrate, they obtained a somewhat larger binding enthalpy for $NO_2^+(H_2O)$ of $\Delta H_{298} = 19.6 \pm 2$ kcal/mol.

Fehsenfeld *et al.* did not detect any $NO_2^+(H_2O)_n$ clusters with $n \geq 2$ in their flow tube experiment,[6] but they assumed that $NO_2^+(H_2O)_n$ was formed because they expected that further association of H_2O with $NO_2^+(H_2O)$ was thermodynamically favored. To account for the absence of larger clusters, they postulated the occurrence of reaction 1, with $n = 2$, resulting in a steady state concentration of $NO_2^+(H_2O)_2$ clusters too low to be detected. They concluded that the rate of destruction by reaction 1 with $n = 2$ must be rapid ($k > 10^{-10}$ cm^3 s^{-1}) relative to formation by the three-body association of $NO_2^+(H_2O)$ with H_2O.

There have been limited studies of clusters with $n \geq 2$. Kay, Hermann, and Castleman[13] observed the deuterated larger clusters $D^+(D_2O)_n(DNO_3)_m$ formed by electron impact ionization of neutral mixed clusters of D_2O and DNO_3. In a theoretical study, Grandinetti *et al.*[9] predicted that a second H_2O molecule would solvate the NO_2^+ with a binding energy 3 kcal/mol less than that of the first H_2O molecule.

Zhang *et al.* have recently reported studies of the reactions of $D_3O^+(D_2O)_n$ with DNO_3.[14] In contrast to the above studies of low hydration numbers, they find that the primary products are $D_3O^+(D_2O)_nDNO_3$ with $n \geq 5$ formed by ligand switching reactions at $T \leq 180$ K. They have also observed the incorporation of additional DNO_3 as a minor channel in reactions of larger clusters. Although they cannot directly probe the

* To whom correspondence should be addressed.
† Contribution No. 8911.
⊗ Abstract published in *Advance ACS Abstracts*, October 15, 1994.

0022-3654/94/2098-12176$04.50/0

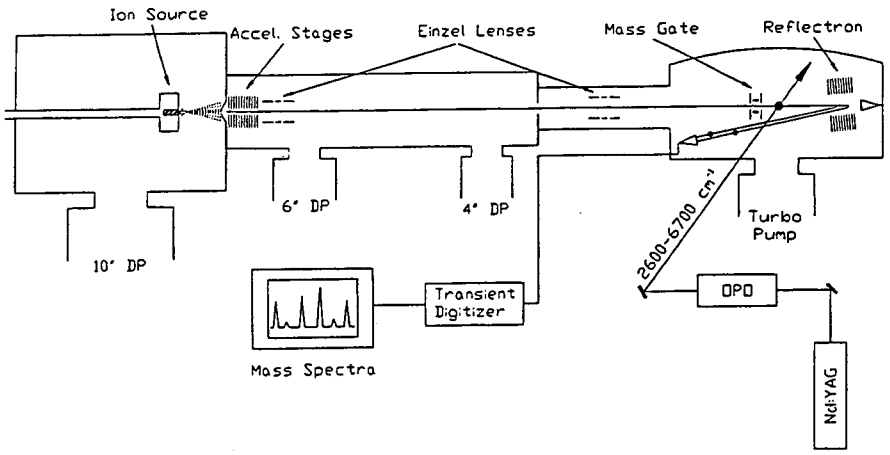

Figure 1. Schematic of the experimental apparatus for detecting infrared predissociation spectra of mass-selected cluster ions.

structure, these authors use energetics to argue that the DNO_3 binds as a ligand to the hydrated ion core.

We have presented preliminary results in an earlier communication[15] of an investigation of the $NO_2^+(H_2O)_n$ clusters for $n = 1-5$ using infrared vibrational predissociation spectroscopy. We have examined how both the vibrational spectra and the photofragment yields vary with solvation number. These experiments provide insights into the structure of these clusters and have allowed us to directly observe the formation of HNO_3 and H_3O^+ products from an intracluster reaction as a function of cluster size.

Infrared spectroscopy can provide detailed information on cluster ion structure, including vibrational frequencies and rotational constants. From such data, we can probe how solvent shells evolves upon sequential solvation. For example, using a corona discharge source Lee and co-workers[16] obtained infrared spectra of H_n^+, $H_3O^+(H_2O)_n$, and $NH_4^+(NH_3)_n$ and assigned their structures with the aid of *ab initio* calculations. Lisy *et al.*[17] have provided evidence for a filled solvation shell around Cs^+ with their infrared spectra of $Cs^+(CH_3OH)_n$. Recently, we have obtained infrared spectra of the clusters SiH_7^+ [18] and of $NO^+(H_2O)_n$.[19]

Our studies on the hydrated NO_2^+ and NO^+ clusters have revealed that addition of H_2O ligands can lead not only to growth of a solvent cage around an ion but also to structural rearrangement induced by solvation. In this paper, we present infrared spectra for all clusters $NO_2^+(H_2O)_n$, $n = 1-5$, in the 2.6–3.7 μm region and describe the experimental apparatus in detail. These experiments provide a bridge between the studies of protonated nitric acid, i.e., $NO_2^+(H_2O)$, and the later study of the larger clusters.

Experiment

Figure 1 is a schematic diagram of the apparatus employed in the experiment. $NO_2^+(H_2O)_n$ clusters were formed by pulsing a gas mixture of HNO_3 and H_2O vapor seeded in He through a pulsed discharge source. Action spectra of the ions formed in this discharge were obtained using a technique analogous to those of Lee and co-workers,[16] using an apparatus based on the ion photodissociation spectrometer pioneered by Johnson and Lineberger.[20,21] The ions extracted through a skimmer were mass-analyzed by a modified Wiley–McLaren[22] time-of-flight (TOF) mass spectrometer. A pulsed tunable infrared laser was timed to excite clusters of a selected *m/e*. Ions pumped to vibrationally excited states could predissociate if their internal energy exceeded the cluster binding energy. The resulting photofragment ions were mass-analyzed by a reflectron mass spectrometer. Infrared spectra of the clusters were obtained by measuring the photofragment intensity as a function of the laser frequency. For some clusters, more than one dissociation channel could be open; in this case, the cluster fragmentation pattern could provide additional information on the cluster structure.

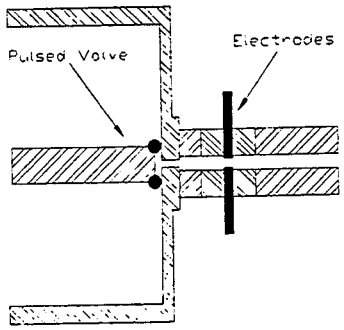

Figure 2. Schematic of the pulsed high-pressure glow discharge source. As the gas pulse enters the discharge cell, a voltage of -1.5 to -3.0 kV is applied between the Ni electrodes (<1-mm separation) to initiate the discharge. Peak discharge currents are typically $10^{-3}-10^{-2}$ A.

Ion Source. Ionic clusters were produced in a pulsed high-pressure glow discharge source, shown in Figure 2. The source consisted of a piezo-driven pulsed valve[23] with a nozzle diameter of 0.5 mm, followed by a 2-mm-long, 0.5-mm-diameter short channel and a 10-mm-long, 1-mm-diameter stainless steel grounded discharge cell. Two sharpened Ni electrodes extended into the cell and were separated by less than 1 mm. The pulsed valve was operated at a stagnation pressure of ~1000 Torr and generated gas pulses of ~200-μs duration. When the pressure inside the cell reached a maximum (~50 Torr), a thyratron was triggered to apply a high-voltage pulse (-1.5 to -3.0 kV) across the electrodes to initiate the discharge. The source conditions were optimized to produce a high-pressure glow discharge without initiating an arc discharge. The source was operated at a repetition rate of 10 Hz. The pressure in the 50 × 50 × 75 cm^3 source chamber was maintained at $(1-2) \times 10^{-4}$ Torr

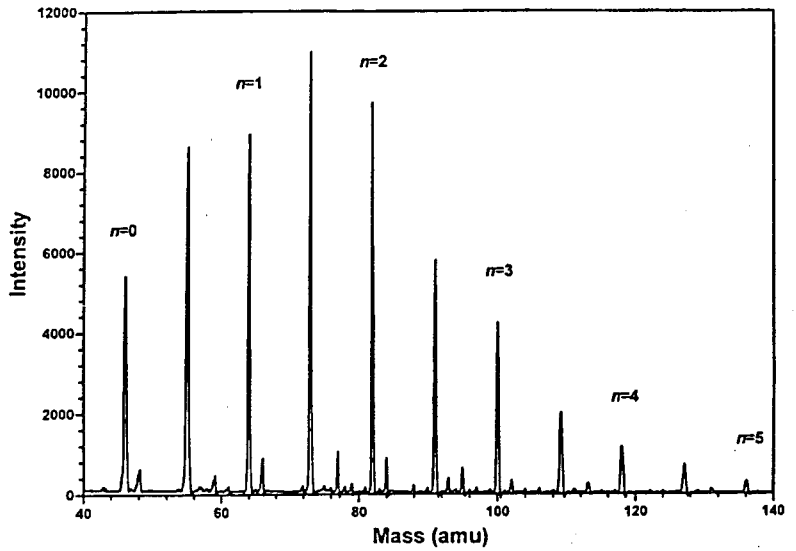

Figure 3. TOF mass spectrum of the $NO_2^+(H_2O)_n$ clusters ($n = 0-5$). The ions are formed in a pulsed discharge of nitric acid and water vapor seeded in 1000 Torr of helium. The other major species in the mass spectrum are $H_3O^+(H_2O)_n$, the hydrated hydronium ion clusters.

by a baffled 10-in. diffusion pump. Ions formed in the discharge underwent many thermal collisions as the gas flowed through the discharge cell and expanded into the vacuum, promoting cooling and clustering. The ion chemistry in our discharge source was similar to that of high-pressure discharges and typically produced the most stable ions. To make larger clusters, the channel could be extended with additional segments after the discharge cell to increase the number of collisions.

An MKS flow control system was normally used to produce the proper gas mixture in the stagnation region of the pulsed valve. However, the vapor pressure of NO_2 at room temperature was too low to allow stable operation. In the present experiment, we bypassed the MKS controller. Instead, we installed a Pyrex tube containing concentrated (70%) nitric acid at 273 K in the gas flow line and passed UHP helium gas over the liquid surface. The resulting gas mixture contained nominally 0.7 Torr of HNO_3 and 0.5 Torr of H_2O vapor (if saturated) seeded in 900−1000 Torr of the He buffer gas.

TOF Mass Spectrometer. A skimmer with a 3-mm-diameter orifice was placed approximately 4 cm away from the ion source to collimate the ion beam into the time-of-flight chamber while removing most of the gas load. Two diffusion pumps (4 and 6 in.) maintained the pressure inside the TOF chamber at $\sim 2 \times 10^{-6}$ Torr during the experiment. To maximize the ion collection volume of the TOF mass spectrometer, we pulse-extracted the ions along the expansion axis by applying a 2.6-kV pulse to a repeller plate. In this configuration, ions filled the entire extraction region instead of being confined longitudinally; therefore, the mass resolution was lower than in perpendicular extraction arrangements.

To improve the mass resolution, we modified the Wiley−McLaren TOF configuration by adding an extra acceleration stage. Specifically, a 4.4-cm-long pulsed extraction region was followed by two consecutive acceleration regions of 3.0 and 4.8 cm. These fields accelerated the ions to a final kinetic energy of 2.6 keV. Calculations of ion time-of-flight spectra revealed that, with an optimum selection of electric fields in the acceleration regions, both first- and second-order spatial focusing could be achieved simultaneously. The second-order focusing condition, not achieved in general for two-stage systems, reduces the dependence of the arrival time of an ion on its initial position in the extraction region. By carefully adjusting the voltages on the ion optics, we were able to improve the mass resolution of our apparatus by a factor of 2 or more. De Heer and Milani have presented a detailed analysis of a similar three-stage time-of-flight mass spectrometer for the special case in which the center region is field-free.[24]

After exiting the extraction/acceleration ion optics, the ions were focused with an einzel lens and then traveled field-free through the remainder of the TOF chamber before being collimated by a second einzel lens. They entered the photolysis/detection chamber, in which the pressure was maintained at $\sim 5 \times 10^{-7}$ Torr by a 500 L/s turbomolecular pump. At 1.75 m downstream from the acceleration optics, both first- and second-order spatial focusing were achieved. At this location, the ions of a selected mass were intersected by a pulsed infrared laser beam. The fragment ions were then mass-analyzed by a reflectron spectrometer, which consisted of a 13-cm-long retarding electrical field and a 30-cm-long field-free region. Details of the photofragment detection are discussed by Alexander *et al.*[21] In electrostatics, particle trajectories are invariant to mass if the ratio of kinetic energy to applied potential is fixed. If there is little recoil upon dissociation, the fragment retains the velocity of the parent and its kinetic energy is reduced to $T_f = (m_f/m_p)T_p$ with T the kinetic energy and m_f and m_p the fragment and parent masses, respectively. The fragment trajectory will follow that of the parent when the reflectron voltage is reduced to $(m_f/m_p)V_0$, where V_0 is the potential of the reflectron used to detect the parent. As Alexander *et al.* point out, fragment ions can then be unambiguously identified because their arrival time will be identical to that of the parent. When recording photofragment intensities, we set the reflectron voltage to $(m_f/m_p)V_0$ to minimize mass discrimination effects due to differences in ion trajectories.

The ions were detected by a dual chevron microchannel plate detector (Galileo Electro-Optic) with the cathode biased at between −1.5 and −2.0 kV. The signal was amplified by a Comlinear CLC 100 preamplier and recorded by a transient digitizer/signal averager (LeCroy 8818/6010). Typically, 100

scans were summed by the signal averager and then transferred via a GPIB interface to an IBM-AT computer for display and analysis.

Other parent ions could reach the detector simultaneously with the photofragment, complicating data analysis. To solve this problem, a "mass gate" was installed to select the proper parent ions immediately before they were excited by the infrared laser. The mass gate consisted of two stainless parallel steel plates 1 cm in length and 1.2 cm apart from each other, with the ion trajectory midway between them. A potential of 400 V was applied between these two plates to deflect ions passing between the plates, causing them to miss the detector. The voltage was switched off only when ions that were selected for photodissociation arrived at the mass gate. Consequently, the only ions that reached the detector were the selected ions and their fragments, and spurious signal that might come from other masses was eliminated.

Tunable IR Laser. The tunable infrared laser used to excite the clusters was a $LiNbO_3$ optical parametric oscillator (OPO). The OPO cavity, based on the design of Brosnan and Byer,[25] consisted of a 5-cm-long $LiNbO_3$ crystal, a pair of ZnSe prisms as the beam expander, a 600 line/mm grating as the rear mirror as well as a line width-narrowing element, and a broad-band reflective mirror (60% at 1.4−1.8 μm) as the output coupler. The OPO was pumped by a 10-Hz Spectra-Physics GCR-12s Nd:YAG laser which generated 350-mJ pulses at 1.06 μm. The pump beam was multipassed 4 m to achieve a nominally Gaussian transverse intensity profile and coupled into the oscillator cavity by an intracavity 45° beam splitter coated for reflectivity at 1.064 μm. By simultaneously adjusting the crystal and grating angles along an empirically determined tuning curve, the OPO was continuously tunable from 2700 to 6700 cm^{-1}. Typical OPO pulse energies were about 4−8 mJ with a line width of 1.5 cm^{-1}. A higher OPO resolution of 0.15 cm^{-1} could be achieved by inserting a 2-mm line-narrowing etalon into the cavity and scanning the etalon angle simultaneously with the crystal and grating angles. The optical path from the laser to the vacuum chamber was enclosed and continuously purged with dry air to eliminate absorption caused by ambient water vapor.

Data Acquisition. Spectra were recorded by stepping the OPO wavelength and recording the photofragment signal at each wavelength. Background, primarily caused by collision-induced dissociation in the ion optics chamber, was measured by firing the laser 10 μs before the ion arrival for an equal number of shots. Signal and background TOF spectra were alternately averaged for 100 laser shots. Fragment intensity was determined by integrating the fragment peak in the TOF spectra; the background integral was then subtracted to obtain the photodissociation signal. The data were then normalized with respect to the OPO laser intensity, which was measured by a Molectron model J25LP joulemeter. The OPO laser wavelength was calibrated during the scan by recording the rovibrational spectrum of the methane ν_3 band (taken with the OPO idler) or the hydrogen chloride first overtone band (OPO signal) in a photoacoustic cell.

Results

$n = 1$. NO_2^+ was the only photofragment ion observed from the vibrational predissociation of $H_2NO_3^+$; thus, protonated nitric acid underwent the dissociation process

$$H_2NO_3^+ \rightarrow NO_2^+ + H_2O \qquad (2)$$

However, the dissociation signal from $H_2NO_3^+$ was very weak,

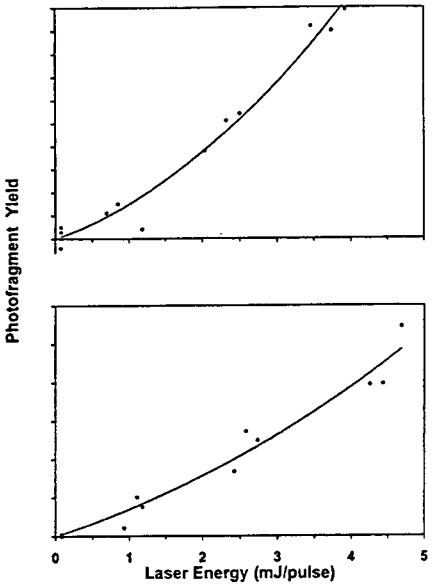

Figure 4. Dependence on laser pulse energy of the fragment signal from photodissociation of the parent ions $NO_2^+(H_2O)_n$ ($n = 1$ and 2). The lines are fits to a sum of linear and quadratic terms. The fits reveal (a) a nearly quadratic dependence for $n = 1$ and (b) a nearly linear dependence for $n = 2$.

and its dependence on laser fluence was clearly nonlinear. A quadratic dependence gave a better fit to the data than a linear dependence, but neither fit was satisfactory. The pulse energy dependence could be best fit to the sum of a linear term and a quadratic term (Figure 4a). This fit gave a significant improvement over either term alone (F-test values corresponding to $p = 0.01$ and 0.02 over linear and quadratic terms, respectively) and resulted in a reduced $\chi^2 \approx 1$. This dependence suggested that the photodissociation of $H_2NO_3^+$ was due to a combination of sequential two-photon absorption by vibrationally cold clusters and one-photon absorption by "hot" clusters.

The vibrational predissociation spectrum of $NO_2^+(H_2O)$ consisted of two prominent bands centered at 3626 and 3704 cm^{-1} (Figure 5). Partially resolved structure could be observed reproducibly in both bands. The 3626-cm^{-1} band possessed P, Q, and R subbands, while the 3704-cm^{-1} band was a doublet split by 8 cm^{-1}. Note that the frequency of the 3704-cm^{-1} band was incorrectly reported in a previous communication.[15]

$n = 2$. Vibrational excitation of $NO_2^+(H_2O)_2$ clusters also led to evaporative loss of a water molecule:

$$NO_2^+(H_2O)_n \rightarrow NO_2^+(H_2O)_{n-1} + H_2O \qquad (3)$$

The signal from $NO_2^+(H_2O)_2$ dissociation became much stronger and was more nearly linear with respect to laser intensity (Figure 4b). Again, a sum of linear and quadratic terms gave a better fit than either term alone. The statistical significance of the improvement as obtained from the F test was $p < 0.05$ and 0.005 over linear and quadratic terms, respectively. Consequently, we infer that the binding energy of $NO_2^+(H_2O)_2$ is less than that of $n = 1$ but still slightly larger than $h\nu_{IR}$ (~10.5 kcal/mol). The only two bands observed (top spectrum, Figure 6a) were both in the OH stretch region and were centered at 3635 and 3715 cm^{-1}.

$n = 3$. For $NO_2^+(H_2O)_3$, water evaporation (reaction 3)

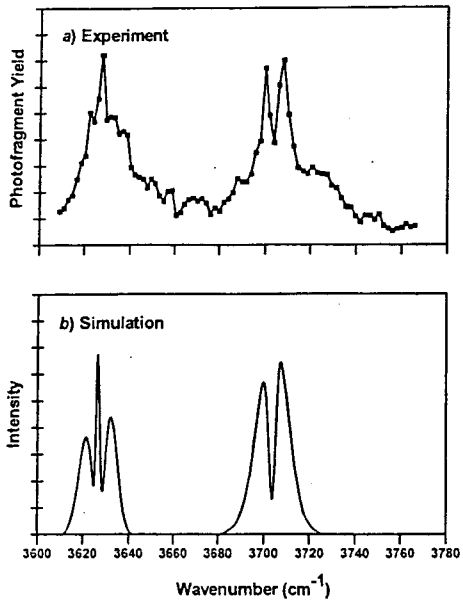

Figure 5. O−H stretching bands of the $NO_2^+(H_2O)$ cluster. (a) The predissociation spectrum obtained experimentally. (b) Simulation of the rotational band contour using rotational constants calculated from the *ab initio* structure. We used a rotational temperature of 80 K and convoluted the predicted spectrum with a Gaussian to simulate a resolution of 1.5 cm^{-1} (fwhm).

remained the dominant photodissociation channel, but a new channel opened,

$$NO_2^+(H_2O)_n \rightarrow H_3O^+(H_2O)_{n-2} + HNO_3 \qquad (4)$$

accounting for 15% of the photofragments. A linear laser fluence dependence was observed for this cluster. The infrared spectrum was almost identical to that of $NO_2^+(H_2O)_2$, with two O−H stretching bands centered at 3636 and 3716 cm^{-1} (Figure 6b). Although HNO_3 was one of the photofragments from $NO_2^-(H_2O)_3$, we found no band assignable to the O−H stretch of an HNO_3 moiety, which should be near the monomer frequency of 3550 cm^{-1}.[26]

$n = 4$. For $NO_2^+(H_2O)_4$, loss of HNO_3 (reaction 4) became the major predissociation pathway. The six bands observed in the infrared predissociation spectrum are shown in Figure 7a. In addition to the red-shifted water O−H stretching bands at 3644 and 3717 cm^{-1}, two sharp bands were found near the O−H stretch frequency of HNO_3 monomer, at 3519 and 3550 cm^{-1}. Two broad features appeared at lower frequencies, one a weak band at ~3050 cm^{-1} extending from 2900 to 3300 cm^{-1} and the other the onset of a strong broad band with a maximum located below 2700 cm^{-1}. The branching ratio between the HNO_3 loss channel and the H_2O loss channel was wavelength-dependent, with a ratio of 7:1 upon photon excitation in the 3550-cm^{-1} region and 2:1 in the 3600−3800-cm^{-1} region. The variation in relative yields can be seen by comparing the differences in the action spectra in Figure 6c,d recorded for the H_2O and HNO_3 loss channels.

$n = 5$. For $NO_2^+(H_2O)_5$ photodissociation, the HNO_3 loss channel was dominant, with a relative yield of >80%. The infrared spectrum, seen in Figure 7b with detail in Figure 6e, was similar to that of $NO_2^+(H_2O)_4$ but possessed some additional features. In the O−H stretching region of H_2O (ν > 3600

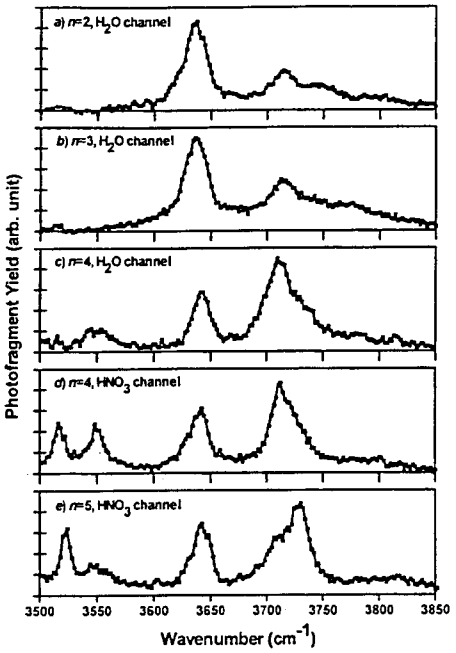

Figure 6. Vibrational predissociation spectra of $NO_2^+(H_2O)_n$ clusters (n = 2−5) in the 3500−3850-cm^{-1} region. The ordinates for the top three panels are the photofragment yield from the H_2O loss channel. In the lower two panels (n = 4 and 5), the ordinate is the photofragment yield from the HNO_3 loss channel.

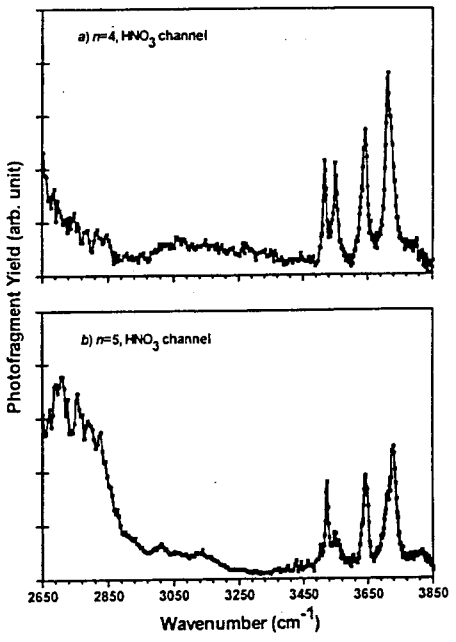

Figure 7. Vibrational predissociation spectra of $NO_2^+(H_2O)_4$ and $NO_2^+(H_2O)_5$ in the 2700−3500-cm^{-1} region. The ordinate is the photofragment yield from the HNO_3 loss channel.

cm^{-1}), three bands were observed at 3644, 3717, and 3733 cm^{-1}. In the 3500−3600-cm^{-1} region, a sharp band at 3523 cm^{-1} and a broad, weaker band at 3550 cm^{-1} were observed. The most

prominent feature in the spectrum was a strong, broad band peaked at 2700 cm^{-1}. A weaker, broad band appeared to the blue at 3050 cm^{-1}. We were unable to obtain a spectrum recorded detecting the H_2O loss channel, because the signal was too weak, but within error bars (±10%) the branching ratio was independent of wavelength.

Discussion

Protonated Nitric Acid ($n = 1$). Both experiments and *ab initio* calculations[7-9] have shown that there are two isomers of protonated nitric acid. The first structure is a weakly bound cluster of NO_2^+ and H_2O, $NO_2^+(H_2O)$, while the second isomer has a covalently bound structure $(HO)_2NO^+$, similar to that of nitric acid. We have found that $H_2NO_3^+$ behaves like an ion–molecule complex which dissociates upon excitation by two IR photons. The observed vibrational spectrum resembles that of an H_2O ligand perturbed by a charge, with bands red-shifted by 31 and 52 cm^{-1} respectively from the origins of the ν_1 and ν_3 modes of a free H_2O monomer. The observed frequencies at 3626 and 3704 cm^{-1} agree well with the (scaled) *ab initio* frequencies for $NO_2^+(H_2O)$ (3617 and 3710 cm^{-1}, respectively) computed by Lee and Rice at the CCSD(T) level of theory.[8] The observation of a quadratic fluence dependence indicates that two photons are required to dissociate the complex and places limits on the dissociation energy of $10.5 < D_0 < 21$ kcal/mol, consistent with current values which range from 14.8 to 19.6 kcal/mol.

Our results are inconsistent with identification of the cluster as the second isomer $(HO)_2NO^+$, which is calculated to be higher in energy by 20 kcal/mol. MP2 calculations by Lee and Rice[8] predict that the (scaled) NO–H stretching frequency of $(HO)_2NO^+$ is 3450 cm^{-1}. No such bands were found in the IR spectra of any clusters. This isomer may not be detected in this experiment, because it is covalently bound and thus may not predissociate. However, even if $(HO)_2NO^+$ does not undergo predissociation, its hydrate $(HO)_2NO^+(H_2O)$ should dissociate easily. Grandinetti *et al.*[9] calculate that the dissociation energy D_e of $(HO)_2NO^+(H_2O) \rightarrow (HO)_2NO^+ + H_2O$ should be similar to that of $NO_2^+(H_2O)_2$. However, we do not observe the predicted band in the predissociation spectrum of the parent ion at $m/e = 82$. We thus conclude that the isomer of $H_2NO_3^+$ present in the discharge source is the complex $NO_2^+(H_2O)$ and that $(HO)_2NO^+$ is a higher energy isomer not observed in this experiment.

The partially resolved structure in the two vibrational bands are rotational subband contours, and these can be compared to band contours predicted from rotational constants and selection rules based on the theoretical structure. From their CCSD(T) calculation, Lee and Rice[8] have found that protonated nitric acid $H_2NO_3^+$ possesses a planar structure with a nearly linear NO_2^+ bound to an H_2O ligand 2.45 Å away. This structure is a highly asymmetric rotor, with rotational constants of $A = 0.398$ cm^{-1}, $B = 0.202$ cm^{-1}, and $C = 0.134$ cm^{-1}. In the rigid rotor approximation, the symmetric stretching mode of H_2O would be an a-type transition and the antisymmetric mode a b-type transition. The predicted selection rules are consistent with the observed spectrum, which exhibits a single maximum with two shoulders (partially resolved P, Q, and R branches) in the 3626-cm^{-1} band and two closely spaced maxima (Q-branch features) in the band at 3704 cm^{-1}. We have simulated the band contours of these two transitions using the *ab initio* rotational constants and a rotational temperature of 80 K to predict the asymmetric rotor transitions[27] and then convoluting with a line width of 1.5 cm^{-1}. The temperature used here is consistent with fits to other partially resolved rotational spectra of ions produced with the same pulsed discharge source.[18,19] The calculated band contours, shown in Figure 5b, match the main features observed in the experimental spectra. In particular, the 8-cm^{-1} spacing between the two maxima in the 3704-cm^{-1} bands agrees with the simulation. Thus, the observed rotational contours are in quantitative agreement with the *ab initio* structure and provide additional confirmation that the observed isomer of $H_2NO_3^+$ is $NO_2^+(H_2O)$.

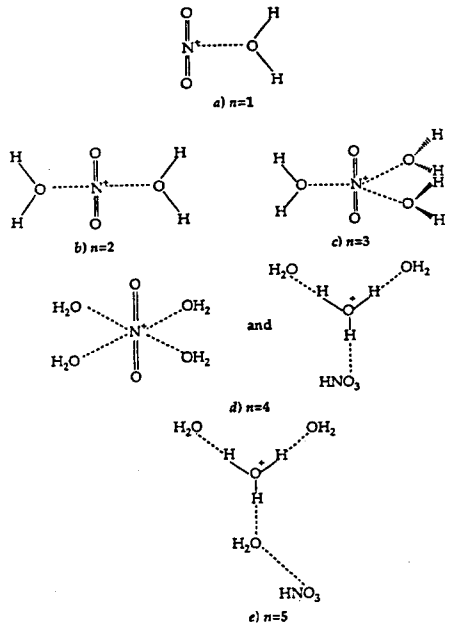

Figure 8. Proposed structures of the $NO_2^+(H_2O)_n$ clusters, for $n = 1-5$.

$NO_2^+(H_2O)_2$ and $NO_2^+(H_2O)_3$. The similarities in both the spectra and the photoproducts among $H_2NO_3^+$ and its first two hydrated clusters indicate that the $n = 2$ and $n = 3$ complexes have structures similar to $NO_2^+(H_2O)$. In particular, the absence of new O–H stretching bands rule out all of the higher energy isomers predicted by Grandinetti *et al.*[9] and instead suggests that the H_2O moieties in the clusters are in similar environments. Therefore, we propose that the first two hydrated clusters of protonated nitric acid are complexes of an NO_2^+ central ion core and (two or three) H_2O ligands, as shown in Figure 8b,c.

With additional ligands, the charge-dipole interaction between the NO_2^+ and each H_2O ligand will be weakened. The resulting lower binding energies for the larger clusters are consistent with the rise in photodissociation yield with n and the increasingly linear dependence on laser intensity. The presence of the NO_2^+ positive charge will also cause a red shift of the O–H vibrational frequencies. The magnitude of the red shift can be used to qualitatively infer the strength of the solvating interactions: the stronger the interaction, the larger the red shift. The red shifts are largest for $n = 1$ and smallest for $n = 3$. This decrease in O–H frequency shift of $NO_2^+(H_2O)_n$ is also consistent with a decrease in the binding energy with n.

$NO_2^+(H_2O)_4$ and $NO_2^+(H_2O)_5$. The significant changes in the IR spectra and photodissociation patterns upon addition of the fourth and fifth water molecules point to a major transformation in cluster structure. In contrast to the smaller clusters, $NO_2^+(H_2O)_4$ and $NO_2^+(H_2O)_5$ clusters dissociate primarily by evaporation of an HNO_3 molecule. This result suggests that HNO_3 either is formed upon vibrational excitation or exists intact

within these clusters. The sharp bands at 3519 and 3550 cm^{-1} observed in the spectrum of the $n = 4$ cluster and the sharp band at 3520 cm^{-1} in the $n = 5$ cluster are close to the O−H stretch frequency in neutral HNO_3 monomer.[26] From the appearance of these bands in the clusters $n = 4$ and $n = 5$, we infer that an HNO_3 moiety is already present in the $NO_2^+(H_2O)_4$ and $NO_2^+(H_2O)_5$ clusters. Vibrational excitation of the cluster thus leads to evaporation of this HNO_3 ligand.

The existence of HNO_3 moieties in the $NO_2^+(H_2O)_4$ and $NO_2^+(H_2O)_5$ clusters indicates that the positive charge no longer resides on an NO_2^+ core; rather, a reaction has occurred to form the hydronium ion H_3O^+. This prediction is verified by the observation of an intense broad band around 2700 cm^{-1} and a weaker broad band in the 3000−3200-cm^{-1} region in the spectra of both $NO_2^+(H_2O)_4$ and $NO_2^+(H_2O)_5$. These bands have been observed in previous IR spectroscopic studies[16,28] of $H_3O^+(H_2O)_3$ clusters and are assigned as the O−H stretching bands of the H_3O^+ ion. The large frequency shift, the broad line width, and the intensity of the band are typical of ionic OH bonds involved in strong hydrogen bonds formed between the hydronium ion and its ligands.

The observation of H_3O^+ and HNO_3 thus indicates that the following intracluster hydration reaction occurs for $n = 4$ and 5:

$$NO_2^+(H_2O)_n \rightarrow H_3O^+(H_2O)_{n-2}(HNO_3) \qquad (4)$$

In the following discussion, we sometimes replace $NO_2^+(H_2O)_4$ with $H_3O^+(H_2O)_2(HNO_3)$ to emphasize the structure and make the analogous substitution for $NO_2^+(H_2O)_5$.

The relative strengths of the intermolecular interactions between different moieties determine the structure of these clusters. The ionic hydrogen bonds that H_3O^+ forms with neutral ligands are stronger than intermolecular forces between neutral molecules. Therefore, they are the most important factors in determining the cluster structures. The binding between H_3O^+ and water ligands are particularly strong, *viz.* the large binding energies of $H_3O^+(H_2O)$ (31.6 kcal/mol) and $H_3O^+(H_2O)_2$ (19.5 kcal/mol).[29] Although the binding energies of HNO_3 with H_3O^+ or $H_3O^+(H_2O)_n$ have not been measured, ligand-switching experiments indicate that these will be considerably weaker for $n < 6$.[4,14] Consequently, we propose that the cluster $H_3O^+(H_2O)_2(HNO_3)$ consists of a central H_3O^+ ion and three immediate hydrogen-bonded ligands (two H_2O and one HNO_3), while $H_3O^+(H_2O)_3(HNO_3)$ is comprised of the central H_3O^+ ion core surrounded by water ligands in the first solvation shell with the more weakly bound HNO_3 occupying the second solvation shell.

The weak binding of HNO_3 is consistent with the observations of Zhang *et al.*[14] These authors finds that $D_3O^+(D_2O)_m$ clusters do not undergo ligand switching with DNO_3 (replacing D_2O) until $m \geq 6$. Thus, the binding energy of H_2O is larger than that of HNO_3 for the smaller clusters.

The position of the hydronium ion stretch of $H_3O^+(H_2O)_3(HNO_3)$ shown in Figure 7b is in good agreement with the band position in the hydrated hydronium ion $H_3O^+(H_2O)_3$ (2700 cm^{-1}), not the band position in $H_3O^+(H_2O)_4$ (2860 cm^{-1}).[16] Thus, the HNO_3 ligand weakly perturbs the hydrated hydronium ion core, much less so than an H_2O ligand. This spectroscopic evidence supports our contention that the HNO_3 ligand is weakly bound to the solvated ion core and is most likely in the second shell.

Given these considerations, we can assign the other vibrational bands observed in the spectra of $n = 4$ and 5. We begin by inspecting the H_2O stretch bands in the 3600−3800-cm^{-1} region shown in Figure 6. These bands are qualitatively different from the corresponding bands of the smaller clusters $NO_2^+(H_2O)_n$ ($n = 1-3$). Specifically, they are sharper bands and exhibit a ν_3:ν_1 intensity ratio of ~2:1. A similar ratio was found for the H_2O stretch bands of $H_3O^+(H_2O)_n$. Second, the emergence of a third band in the 3600−3800-cm^{-1} (free OH stretch) region of the spectrum of $n = 5$, a shoulder at 3717 cm^{-1}, cannot be explained if all three neutral H_2O moieties occupy chemically equivalent positions in the $H_3O^+(H_2O)_3(HNO_3)$ cluster. Price *et al.* have observed similar spectra in $H_3O^+(H_2O)_n$ for $n \geq 4$ and identified a shoulder at 3713 cm^{-1} as the free O−H stretching band of a "first shell" neutral H_2O which is hydrogen-bonded to a "second shell" neutral ligand.[16] The appearance of this distinct, reproducible shoulder at 3717 cm^{-1} in our spectrum of $H_3O^+(H_2O)_3(HNO_3)$ provides clear evidence that one of the first shell H_2O molecules is hydrogen-bonded to a molecule in the second shell, most likely the neutral HNO_3.

The H_2O bound both to H_3O^+ and to the second shell HNO_3 will possess a donor OH stretching band that is broader and red-shifted. We therefore assign the broader band at 3550 cm^{-1} to this mode. This band is quite similar in appearance and position to the 3545-cm^{-1} ν_1 mode of the donor molecule in the neutral dimer $(H_2O)_2$.[30] An alternative assignment is suggested by earlier work on hydrated hydronium ions. Price has assigned the analogous donor band of a first shell H_2O bound to the second shell H_2O in the complex $H_3O^+(H_2O)_4$ to a broad band at 3200 cm^{-1}. The magnitude of the donor band red shift will depend on the strength and ionic character of this hydrogen bond.

The O−H stretch mode (ν_1) of a neutral HNO_3 monomer occurs at 3550 cm^{-1}. In the $n = 4$ cluster, two bands are observed (Figures 6 and 7a), one at 3550 cm^{-1} and the second sharper band at 3519 cm^{-1}. This observation can be explained if there are two ways for HNO_3 to hydrogen bond to H_3O^+, one by a terminal O atom and the second by the O atom on the hydroxy group. The 3550-cm^{-1} band can be assigned to the former, because the OH group is essentially unperturbed, and the O−H stretch frequency will be nearly identical to that of the free HNO_3. We then conclude that hydrogen bonding by the hydroxy group red-shifts the HNO_3 O−H stretch to 3519 cm^{-1}. In the $n = 5$ cluster, our assignment of the 3523-cm^{-1} band to HNO_3 suggests that most of the nitric acid forms hydrogen bonds with the OH group as the hydrogen-bond acceptor. *Ab initio* calculations would be helpful in confirming these assignments by providing predicted vibrational frequency shifts for different conformations of HNO_3 hydrogen-bonded to H_2O or H_3O^+.

Thermochemistry. Our experiment confirms the occurrence of an intracluster reaction 4 proposed by Fehsenfeld *et al.*[6] converting $NO_2^+ + H_2O$ to HNO_3 and H_3O^+. Figure 9 illustrates the effects of solvation on the energetics of the NO_2^+ hydration reaction:

$$NO_2^+(H_2O)_{n-1} + H_2O \rightarrow NO_2^+(H_2O)_n \rightarrow H_3O^+(H_2O)_{n-2} + HNO_3 \qquad (5)$$

Each curve is a reaction path for a given solvation number n. The leftmost column gives the reactants $NO_2^+(H_2O)_{n-1} + H_2O$ with the vertical position given by the binding energy for another H_2O. The reaction products $H_3O^+(H_2O)_{n-2} + HNO_3$ are given in the rightmost column. The reaction proceeds through an intermediate complex $NO_2^+(H_2O)_n$ formed by association of the reactants. If an intracluster reaction can occur, a complex of the products, $H_3O^+(H_2O)_{n-2}(HNO_3)$, may be formed. We expect a free energy barrier for such a rearrangement. If we

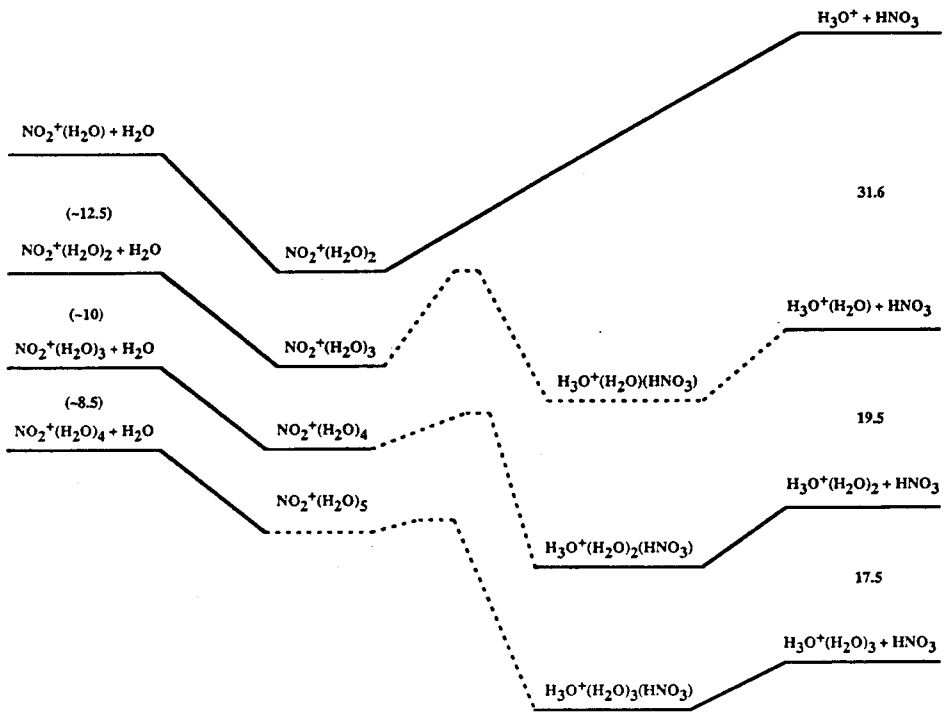

Figure 9. Reaction paths for $NO_2^+(H_2O)_{n-1} + H_2O \rightarrow NO_2^+(H_2O)_n \rightarrow H_3O^+(H_2O)_{n-1} + HNO_3$. Each reaction pathway for a cluster n is lower relative to the $n-1$ pathway by the hydration enthalpies. Numbers are in kcal/mol; those in parentheses are estimates only. Dashed lines indicate postulated barriers and intermediates. The binding energy for $NO_2^+(H_2O)$ is taken as $D_0 = 14.8$ kcal/mol, from ref 11.

TABLE 1: Literature Values for the Cluster Binding Enthalpies in kcal/mol for $X^+(H_2O)_n \rightarrow X^+(H_2O)_{n-1} + H_2O$, Where $X^+ = H_3O^+$ or NO_2^+

	$-\Delta H^\circ_{n-1,n}$	
n	$NO_2^+(H_2O)_n$	$H_3O^+(H_2O)_n$[a]
1	14.8 ± 2.3[b]	31.6
	19.6 ± 2[c]	
	17.3 ± 2[d]	
2	(12.5)[e]	19.5
3	(10)[e]	17.5
4	(8.5)[e]	15.3
5		13.0

[a] Reference 29. [b] Reference 11. [c] Reference 12. [d] Reference 8. [e] Values in parentheses are estimates extrapolated from a binding energy for $n = 1$ of 14.8 kcal/mol.

have spectral evidence for such a complex, the well is indicated by a solid line; if the complex is hypothesized, it is given by a dashed line. In no cases are the energies of these complexes or the activation barrier heights known.

Literature values of the heats of formation at $T = 0$ K for the species involved in the reaction are[31-33] $\Delta H_f^\circ(NO_2^+) = 229.7$ kcal/mol, $\Delta H_f^\circ(H_2O) = -57.1$ kcal/mol, $\Delta H_f^\circ(HNO_3) = -29.8$ kcal/mol, and $\Delta H_f^\circ(H_3O^+) = 143$ kcal/mol.

The binding enthalpies $-\Delta H^\circ_{n-1,n}$ for $NO_2^+(H_2O)_n$ and $H_3O^+(H_2O)_n$ given in the literature are given in Table 1. Kebarle and co-workers[29] have measured the association enthalpies for $H_3O^+(H_2O)_n$. There are several values for the binding enthalpy of $NO_2^+(H_2O)$. We have used the value $\Delta H^\circ_{0,1} = -14.8 \pm 2.3$ kcal/mol at $T = 0$ K that Sunderlin and Squires determined from a direct experimental measurement. The clustering enthalpies for $NO_2^+(H_2O)_n$ with $n > 1$ are not accurately known, and the values listed in Table 1 are only estimates extrapolated from the $\Delta H^\circ_{0,1}$ obtained by Sunderlin and Squires.

For $n = 2$, reaction 5 is the direct proton transfer reaction from $H_2NO_3^+$ to H_2O and is endothermic by 12.3 kcal/mol. We have observed that $NO_2^+(H_2O)_2$ is an intermediate complex along the reaction coordinate. Fehsenfeld *et al.*[6] find that the reverse reaction, proton transfer from H_3O^+ to HNO_3, is very fast ($k = 1.6 \times 10^{-9}$ cm^3 s^{-1}), indicating that there is no activation barrier.

The $n = 3$ system is close to thermoneutral, and its energetics are the most sensitive to the initially assumed binding energy. For this cluster size, reaction 5 is shown in Figure 9 as exothermic by 6.5 kcal/mol based on our extrapolation in Table 1 from the $\Delta H_{0,1}$ determined by Sunderlin and Squires. If the theoretical value of $\Delta H_{0,1} = -17.3$ kcal/mol is used to obtain $\Delta H_f(H_2NO_3^+)$, the reaction would still be exothermic by 2 kcal/mol. The most recent value for $\Delta H_{0,1}$ of 19.6 ± 2 kcal/mol obtained by Cacace *et al.* leads to a reaction that is thermoneutral or slightly endothermic. Fehsenfeld *et al.*[6] predict that this reaction occurs at a fast rate ($k > 10^{-10}$ cm^3 s^{-1}), which implies that little or no activation barrier is present along the reaction pathway.

We have observed only a complex of an NO_2^+ ion with three H_2O ligands. The interaction between the products $H_3O^+(H_2O)$ and HNO_3 can lead to another stable adduct, $H_3O^+(H_2O)(HNO_3)$, but no HNO_3 stretch has been observed, suggesting that the cluster is not of this form. The absence of $H_3O^+(H_2O)(HNO_3)$ indicates that this complex is higher in energy than $NO_2^+(H_2O)_3$. In Figure 9, we have depicted the HNO_3 complex as slightly higher in energy than the hydrated NO_2^+ form. The resulting binding energy of HNO_3 to $H_3O^+(H_2O)$ is somewhat low ($\approx$5 kcal/mol). If the binding energy were more in line

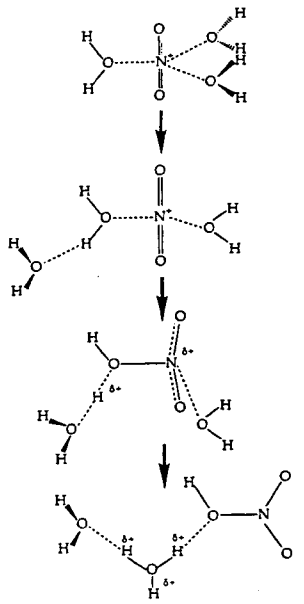

Figure 10. Proposed solvent rearrangement occurring after excitation of $NO_2^+(H_2O)_3$ with an IR photon, leading to formation of HNO_3 and the hydrated hydronium ion $H_3O^+(H_2O)$.

with those of other molecules binding to this ion, this complex would lie lower in energy, and the $NO_2^+(H_2O)_3$ energy would then also have to be lower. Thus, our data indirectly suggest that the binding enthalpies listed in Table 1 are somewhat low.

We have found that absorption of an infrared photon by $NO_2^+(H_2O)_3$ cluster leads to a yield of ~15% for the products $HNO_3 + H_3O^+(H_2O)$. Given the absence of an HNO_3 stretch in the vibrational spectrum, we infer that the HNO_3 is not originally present in the cluster but rather is formed by an intracluster reaction induced by absorption of the photon. The relatively low yield of the energetically favored product suggests that there is a free energy barrier for the reaction to proceed. We expect such a barrier to be present, because a significant amount of charge relocation and solvent reorganization must occur. Charge must move from the N atom on the nitronium ion to three H atoms on a newly formed hydronium ion, a process which must be induced by solvent rearrangement as illustrated in Figure 10. Given the lower proton affinity of H_2O, such a transfer of charge is unlikely unless at least one water molecule has moved from solvating the NO_2^+, creating an energetic penalty for initially desolvating the ion as well. Thus, the dissociation of vibrationally excited $n = 3$ clusters can be understood as a statistical unimolecular decay process in which the channel with a loose transition state dominates over one with a tight transition state. The H_2O evaporation channel is then favored because it involves direct bond fission.

A single IR photon will deposit approximately the same internal energy (10 kcal/mol) as an activated $NO_2^+(H_2O)_3$ complex formed from the thermal association of $NO_2^+(H_2O)_2 + H_2O$ prior to stabilization by a third body. This coincidence suggests that the reaction efficiency (the fraction of bimolecular ion-dipole collisions that lead to reaction) will be comparable to the photoproduct yield. We have observed a similar a correspondence in a related system, the nitrosonium hydrate cluster $NO^+(H_2O)_4$.[19] We therefore predict for $NO_2^+(H_2O)_3$ that the rate constant for reaction 2 will be 15% of the ion-dipole collision rate, or $k \approx 5 \times 10^{-11}$ cm^3 s^{-1}. While this value is somewhat below the lower limit set by Fehsenfeld *et al.*,[6] the reaction was not directly observed in those experiments, and the limit was set solely to explain the absence of $n = 2$ clusters.

For $n = 4$, reaction 5 is significantly exothermic, with $\Delta H_r = -16.2$ kcal/mol. Since our crude estimate of binding energy of the fourth H_2O in $NO_2^+(H_2O)_4$ is $\Delta H_f^\circ \sim -8$ kcal/mol, the $NO_2^+(H_2O)_4$ cluster lies higher in energy than the product channel of $H_3O^+(H_2O)_2 + HNO_3$. Therefore, the global potential minimum on the reaction pathway is the cluster formed from the association of products, $H_3O^+(H_2O)_2(HNO_3)$. This cluster is the conformer observed in our experiment. However, the existence of the minor H_2O dissociation channel suggests that both clusters, $H_3O^+(H_2O)_2(HNO_3)$ and $NO_2^+(H_2O)_4$, might be present in our experiment since one IR photon could not provide enough energy for $H_3O^+(H_2O)_2(HNO_3)$ to reach the reactant channel $NO_2^+(H_2O)_3 + H_2O$.

The wavelength dependence of the branching ratio in the $n = 4$ cluster is consistent with the coexistence of two isomers. HNO_3 evaporation is ~3 times more likely upon excitation of the HNO_3 band relative to excitation of the H_2O bands. This behavior could be due to the existence of two isomers for the $n = 4$ cluster. In the latter case, one isomer, an $NO_2^+(H_2O)_4$ cluster composed of reactants, would absorb in the OH stretch region only at 3600−3800 cm^{-1} and would produce only H_2O fragments. A second isomer, the $H_3O^+(H_2O)_2(HNO_3)$ cluster formed from reaction products, would absorb at 3550 cm^{-1} as well and would dissociate primarily by loss of HNO_3. A mixture of the two isomers would appear to have wavelength-dependent branching ratios. Alternatively, the wavelength dependence could be due to mode-specific predissociation. In this case, excitation of the HNO_3 bands would lead to preferential loss of HNO_3. Excitation of the H_2O would lead to more favorable H_2O evaporation, even though the HNO_3 is more weakly bound.

In $n = 5$, the reaction is exothermic by 25.7 kcal/mol. Addition of the fifth water would result in a complex which still lies above the product channel in energy. The high exothermicity may lead to a barrier which is lower than the entrance channel; this hypothesis would account for the hydration reaction going to completion, i.e., all clusters formed by association of products. The branching ratio is independent of wavelength, suggesting that only this complex is present, but dissociates with loss of either HNO_3 or H_2O to $H_3O^+(H_2O)_3$ or to $H_3O^+(H_2O)_2HNO_3$, respectively.

Conclusion

Size-selected studies of the vibrational predissociation spectra of the clusters $NO_2^+(H_2O)_n$ clusters provide a means for demonstrating the influence of solvent molecules on chemical reactions. We find direct evidence for the intracluster reaction $NO_2^+ + 2H_2O \rightarrow HNO_3 + H_3O^+$, which occurs upon the solvation of the nitronium ion by a critical number of solvent molecules in the clusters. The driving force for the reaction, which must overcome the intrinsic stability of gas phase NO_2^+, is the solvent stabilization of H_3O^+. We find evidence for the onset of the cluster reaction

$$NO_2^+(H_2O)_{n-1} + H_2O \rightarrow H_3O^+(H_2O)_{n-2} + HNO_3$$

at $n = 3$, consistent with the hypothesis of Fehsenfeld *et al.*; however, we do not observe the formation of products within the cluster, $H_3O^+(H_2O)_{n-2}(HNO_3)$, until $n = 4$.

Acknowledgment. We acknowledge the support of an National Science Foundation PYI Award, CHEM-8957243, a

Newly Appointed Faculty Award from the Camille and Henry Dreyfus Foundation, and support from the Irvine and AT&T Foundations. B.M.H. acknowledges support of a Deutsche Forschungsgemeinshaft Fellowship. We thank M.-F. Jagod of the Oka group at the University of Chicago for providing us with ASMWIRP, an asymmetric rotor spectral simulation program.

References and Notes

(1) Fehsenfeld, F. C.; Ferguson, E. E. *J. Geophys. Res.* **1969**, *74*, 2217. Linerberger, W. C.; Puckett, L. J. *Phys. Rev.* **1969**, *187*, 286.
(2) Ferguson, E. E.; Fehsenfeld, F. C.; Albritton, D. L. In *Gas Phase Ion Chemistry*; Bowers, M. T., Ed.; Academic Press: New York, 1979; Vol. I, Chapter 2.
(3) Brasseur, G.; Solomon, S. *Aeronomy of the Middle Atmosphere*; D. Reidel Publishing: Dordrecht, 1986.
(4) Böhringer, H.; Fahey, D. W.; Fehsenfeld, F. C.; Ferguson, E. E. *Planet. Space Sci.* **1983**, *31*, 185.
(5) Fehsenfeld, F. C.; Ferguson, E. E. *J. Chem. Phys.* **1973**, *59*, 6272.
(6) Fehsenfeld, F. C.; Howard, C. J.; Schmeltekopf, A. L. *J. Chem. Phys.* **1975**, *63*, 2835.
(7) Nguyen, M.-T.; Hegarty, A. F. *J. Chem. Soc., Perkin Trans. 2* **1984**, 2043.
(8) Lee, T. J.; Rice, J. E. *J. Phys. Chem.* **1992**, *96*, 650; *J. Am. Chem. Soc.* **1992**, *114*, 8247.
(9) Grandinetti, F.; Bencivenni, L.; Ramondo, F. *J. Phys. Chem.* **1992**, *96*, 4354.
(10) Cacace, F.; Attina, M.; de Petris, G.; Speranza, M. *J. Am. Chem. Soc.* **1989**, *111*, 5481; **1990**, *112*, 1014.
(11) Sunderlin, L. S.; Squires, R. R. *Chem. Phys. Lett.* **1993**, *222*, 333.
(12) Cacace, F.; Attinà, M.; De Petris, G.; Speranza, M., preprint.
(13) Kay, B. D.; Hermann, V.; Castleman, A. W., Jr. *Chem. Phys. Lett.* **1981**, *80*, 469.
(14) Zhang, X.; Mereand, E. L.; Castleman, A. W., Jr. *J. Phys. Chem.* **1994**, *98*, 3554.
(15) Cao, Y.; Choi, J.-H.; Haas, B.-M.; Johnson, M. S.; Okumura, M. *J. Chem. Phys.* **1993**, *99*, 9307. The frequencies for the two subbands in the ν_3 mode of the $n = 1$ complex were incorrectly reported as 3708 and 3716 cm^{-1} in Table I. The correct frequencies are 3700 and 3708 cm^{-1}, with the band centered at 3704 cm^{-1} (see text).
(16) Okumura, M.; Yeh, L. I.; Lee, Y. T. *J. Chem. Phys.* **1988**, *91*, 7319. Yeh, L. I.; Okumura, M.; Myers, J. D.; Price, J. M.; Lee, Y. T. *J. Chem. Phys.* **1989**, *91*, 7319. Okumura, M.; Yeh, L. I.; Myers, J. D.; Lee, Y. T. *J. Phys. Chem.* **1990**, *94*, 3416. Price J. M. Ph.D. Thesis, University of California at Berkeley, 1990. Price, J. M.; Crofton, M. W.; Lee, Y. T. *J. Phys. Chem.* **1991**, *95*, 2182.
(17) Liu, W.-L.; Lisy, J. M. *J. Chem. Phys.* **1988**, *89*, 605.
(18) Cao, Y.; Choi, J.-H.; Haas, B.-M.; Johnson, M. S.; Okumura, M. *J. Phys. Chem.* **1993**, *97*, 5215.
(19) Choi, J. H.; Kuwata, K. T.; Haas, B. M.; Cao, Y.; Johnson, M. S.; Okumura, M. *J. Chem. Phys.* **1994**, *100*, 7153.
(20) Johnson, M. A.; Lineberger, W. C. In *Techniques for the Study of Ion-Molecule Reactions*; Farrar, J. M., Saunders, W. H., Jr., Eds.; Wiley-Interscience: New York, 1988.
(21) Alexander, M. L.; Levinger, N. E.; Johnson, M. A.; Ray, D.; Lineberger, W. C. *J. Chem. Phys.* **1988**, *88*, 6200.
(22) Wiley, W. C.; MacLaren, I. H. *Rev. Sci. Instrum.* **1955**, *26*, 1150.
(23) Proch, D.; Trickl, T. *Rev. Sci. Instrum.* **1989**, *60*, 712.
(24) De Heer, W. A.; Milani, P. *Rev. Sci. Instrum.* **1991**, *62*, 670.
(25) Brosnan, S. J.; Byer, R. L. *IEEE J. Quantum Electron.* **1979**, *QE-15*, 415.
(26) McGraw, G. E.; Bernitt, D. L.; Hisatsune, I. C. *J. Chem. Phys.* **1965**, *42*, 237.
(27) Program ASMWIRP developed at the University of Chicago. Jagod, M.-F., private communication.
(28) Schwarz, H. A. *J. Chem. Phys.* **1977**, *67*, 5525.
(29) Cunningham, A. J.; Payzant, J. D.; Kebarle, P. *J. Am. Chem. Soc.* **1972**, *94*, 7627. Lau, Y. K.; Ikuta, S.; Kebarle, P. *J. Am. Chem. Soc.* **1982**, *104*, 1462.
(30) Page, R. H.; Frey, J. G.; Shen, Y. R.; Lee, Y. T. *Chem. Phys. Lett.* **1984**, *106*, 373.
(31) Baulch, D. L.; Cox, R. A.; Crutzen, P. J.; Hampson, Jr., R. F.; Kerr, J. A.; Troe, J.; Watson, R. T. *J. Phys. Chem. Ref. Data* **1982**, *11*, 327.
(32) Rosenstock, H. M.; Draxl, K.; Steiner, B. W.; Herron, J. T. *J. Phys. Chem. Ref. Data* **1977**, *6* (Suppl. 1). Lias, S. G.; Bartmess, J. E.; Liegman, J. F.; Holmes, J. L.; Levin, R. D.; Mallard, W. G. *J. Phys. Chem. Ref. Data* **1982**, *17* (Suppl. 1).
(33) Bryant, G.; Jiang, Y.; Grant, E. *Chem. Phys. Lett.* **1992**, *200*, 495.